Journal of Applied Mechanics

JUNE, 1942

VOL. 9, NO. 2

Partially Plastic Thick-Walled Cylinder Theory

By M. C. STEELE,[1] URBANA, ILL.

Previous theories for partially plastic thick-walled cylinders under internal pressure are reviewed. A quantitative comparison is given for (*a*) compressibility versus incompressibility of material, and (*b*) von Mises' versus Tresca's theory of failure. The former reveals that deflections at the outside and bore surfaces agree closely, although considerable percentage differences may be found in the axial stresses and strains. Large differences (except for the axial stress) are found in comparing the two theories of failure. Based on the comparison and available experimental evidence, a theory is presented in closed form to include the Hencky stress-strain relations, incompressibility, and Ludwik's strain-hardening function.

Nomenclature

The following nomenclature is used in the paper:

$d\sigma$; $d\epsilon$ = principal stress increment; principal strain increment

σ; ϵ = principal stress; principal strain

$\sigma_\theta, \sigma_r, \sigma_z$ } = principal stresses and strains in hoop, radial, and axial directions, respectively
$\epsilon_\theta, \epsilon_r, \epsilon_z$ }

ϵ_e; ϵ_p = elastic component of strain; plastic component of strain

$\bar{\sigma}$; $\bar{\epsilon}$ = effective stress; effective strain

σ_e = tensile yield stress

$s\left(=\frac{\sigma_e}{2}\right)$ = yield shear stress in tension

τ; γ = maximum shear stress; maximum shear strain

γ_e = maximum shear strain at yield

r_e = internal radius

$r = y\, r_e$ = variable radius

$r_n = n\, r_e$ = plastic-elastic boundary radius

$r_1 = k\, r_e$ = outside radius

λ, $d\lambda$, β = plastic flow functions

P = internal pressure

G; E = modulus of rigidity; elasticity

m = strain-hardening parameter

ν = Poisson's ratio

$(\epsilon_\theta)_o, (\epsilon_\theta)_i$ = circumferential strains at outside and bore surfaces, respectively

Introduction

The partial overstraining of thick-walled cylinders by internal uniform pressure has claimed the attention of several prominent investigators. Table 1 lists some of the contributions and illustrates differences in basic assumptions. The rigorous mathematical solutions require numerical procedures for their completion. In general, the solutions are so complex that little practical use may be made of them by design engineers.

The mathematician's approach to the problem under consideration is fundamentally different from that of the engineer. The former is interested in an accurate knowledge of the stresses and strains in terms of the applied load or loads for all points in an idealized body. In general, the engineer seeks an estimation of the variation of factors with applied loads, which are of significance only in the functional design of the part. The rigorous solution due to Hill, Lee, and Tupper (1)[2] shows that in Nadai's (2) approximate solution, the axial stresses are in error by as much as 66⅔ per cent. This factor may or may not be of interest to the engineer. For materials exhibiting flat-topped (well-defined yield point) stress-strain curves, or small amounts of strain-hardening, the engineer is interested in deformations rather than stresses. In the case of the thick-walled cylinder, interest lies in deflections of bore and outside surfaces for specific internal pressures. An accurate knowledge of the stresses would be required only if rupture theories were to be considered before the deflections become the governing feature in design. The axial stress is small, in general, compared to the other two principal stresses, and a considerable percentage error in the axial stresses may be tolerated if their effect on the bore and outside deflections is small.

The necessity for accurate solutions to the thick-walled cylinder is not denied. Indeed, history has shown that present-day elastic mechanics of materials could not have been so soundly formulated without the solutions of the theory of elasticity on which to base it. It is believed that a similar evolution must take place in the case of plasticity if the advantages it has to offer are to be understood and used widely by industry. The thick-walled cylinder under internal pressure has been widely treated by the methods of the mathematical theory of plasticity, and the author feels particularly fortunate in having these solutions at his disposal for an attempt at formulating the problem on a "plastic mechanics of materials" basis.

It is thus the purpose of this paper to examine the causes leading to complexities in the analyses listed in Table 1, and by a partial elimination of them, to present a theory which, it is hoped, will be of use to design engineers.

Outline of Solutions

Table 1 will be better understood by outlining the requirements for a solution for the stresses and strains in a partially plastic thick-walled cylinder subjected to internal pressure. They are as follows:

(*a*) *Radial Equilibrium*

$$\frac{\partial(y\sigma_r)}{\partial y} = \sigma_\theta \qquad [1]$$

[1] Research Assistant Professor, Department of Theoretical and Applied Mechanics, University of Illinois.

Contributed by the Applied Mechanics Division and presented at the Annual Meeting, Atlantic City, N. J., November 25–30, 1951, of The American Society of Mechanical Engineers.

Discussion of this paper should be addressed to the Secretary, ASME, 29 West 39th Street, New York, N. Y., and will be accepted until July 10, 1952, for publication at a later date. Discussion received after the closing date will be returned.

Note: Statements and opinions advanced in papers are to be understood as individual expressions of their authors and not those of the Society. Manuscript received by ASME Applied Mechanics Division, June 11, 1951. Paper No. 51—A-25.

[2] Numbers in parentheses refer to the Bibliography at the end of the paper.

TABLE 1 PARTIALLY PLASTIC THICK-WALLED-CYLINDER THEORIES

Author	Plastic stress-strain law	Compressibility: Plastic domain	Compressibility: Elastic domain	Flow condition	Axial boundary	Type of solution
Hill, Lee, and Tupper (1)	Prandtl-Reuss	Comp	Comp	Tresca	$\epsilon_z = 0$	Numerical
Hill, Lee, and Tupper (15)	Prandtl-Reuss	Comp	Comp	Tresca	Closed ends	Numerical
MacGregor, Coffin, and Fisher (12)	Hencky	Comp	Comp	von Mises	Open ends	Numerical
Sokolovsky (16)	Hencky	Comp	Comp	von Mises	$\epsilon_z = 0$	Numerical
Sokolovsky (16)	Hencky	Comp	Comp	von Mises[a]	$\epsilon_z = 0$	Numerical
Sokolovsky (16)	Hencky	Incomp	Comp	von Mises	$\epsilon_z = 0$	Closed form
Sokolovsky (16)	Hencky	Incomp	Comp	von Mises[a]	$\epsilon_z = 0$	Numerical
Hodge and White (10)	Prandtl-Reuss	Comp	Comp	von Mises	$\epsilon_z = 0$	Numerical
Hodge and White (10)	Hencky	Comp	Comp	von Mises	$\epsilon_z = 0$	Numerical
Allen and Sopwith (11)	Hencky	Comp	Comp	Tresca	Either $\epsilon_z = 0$, or closed ends, or open ends	Closed form
Cook (17)	Hencky	Incomp	Comp	Tresca with upper and lower yield	Closed ends	Closed form[b]
Nadai (2)	Hencky	Incomp	Comp	von Mises	$\epsilon_z = 0$	Closed form
Steele (13)	Hencky	Incomp	Comp	Tresca	Either $\epsilon_z = 0$, or closed ends, or open ends	Closed form
Steele (theory of this paper)	Hencky	Incomp	Comp or incomp	Tresca[a]	Either $\epsilon_z = 0$, or closed ends, or open ends	Closed form

[a] Inclusion of strain-hardening; nonasterisked solutions assume material to flow according to function defining theory of failure.
[b] Solution dependent on experimental measurements which Cook made on closed-ended cylinders.

(b) Strain Compatibility

$$\frac{\partial(y\epsilon_\theta)}{\partial y} = \epsilon_r \quad \ldots\ldots [2]$$

(c) Boundary Conditions

$$\left.\begin{aligned} &\sigma_r = -P, \; y = 1 \\ &\sigma_r = 0, \quad y = k \end{aligned}\right\}$$

Either

$$\epsilon_z = 0$$

or

$$\int_1^k \sigma_z y \, dy = 0 \text{ (open ends)}$$

or

$$\int_1^k \sigma_z y \, dy = \frac{P}{2} \text{ (closed ends)} \quad \ldots\ldots [3]$$

It should be noted that a comparison of the theories in Table 1 is hampered by inconsistency among authors in the selected axial boundary. Choosing the axial strain as zero is convenient mathematically and is popular for the more rigorous solutions. It is a condition, however, not found in practice where cylinders have either open or closed ends. Solutions for $\epsilon_z = 0$ and closed ends do not differ greatly, but the difference is larger for open-ended cylinders.

(d) Plane Sections to Remain Plane

$$\epsilon_z \text{ is independent of } r \quad \ldots\ldots [4]$$

(e) Continuity Across Elastic-Plastic Interface. Continuous displacement implies continuous ϵ_θ and ϵ_z. Equilibrium demands continuous σ_r. Conditions at the elastic-plastic boundary may be deduced from these. For example, if incompressibility of plastic material only is assumed, then ϵ_r cannot be continuous. Also, if the tensile stress-strain relation is discontinuous (e.g., upper and lower yield points), then σ_θ must be discontinuous when Tresca's yield condition is used.

(f) Plastic Stress-Strain Relations. One of two plastic stress-strain relations replaces the well-known Hooke's law for elastic bodies. The Prandtl-Reuss (3) relations provide the basis for the "incremental strain" or "flow" type of theory. They take the form

$$E d\epsilon_1 = d\sigma_1 - \nu d(\sigma_2 + \sigma_3) + d\lambda \left[\sigma_1 - \frac{1}{2}(\sigma_2 + \sigma_3)\right] . \quad [5]$$

(plus two similar equations for the other two principal strain increments).

The Hencky (4) relations describe the "total strain" or "deformation" theory. They may be written

$$E\epsilon_1 = \sigma_1 - \nu(\sigma_2 + \sigma_3) + \lambda \left[\sigma_1 - \frac{1}{2}(\sigma_2 + \sigma_3)\right] . . [6]$$

(plus two similar equations for the other two principal strains).

The basic differences in Equations [5] and [6] have been described adequately elsewhere (4). It is well established that the incremental theory is the more correct, and that if the principal axes of stress remain fixed in direction, and the principal stress ratios are constant, the Prandtl-Reuss and Hencky relations yield the same result. Frequently, even though the conditions on stress axes and ratios are not strictly maintained, solutions using Equation [6] vary only a small amount from those solved by the Prandtl-Reuss relations. This is the case for partially plastic thick-walled cylinders subjected to internal uniform pressure only, and the small inaccuracy in using the Hencky relations is compensated for by certain advantages of mathematical convenience.

(g) Compressibility of Plastic Material. The total strain in an overstrained material is composed of an elastic and a plastic component; thus

$$\epsilon = \epsilon_e + \epsilon_p \quad \ldots\ldots [7]$$

It is observed from experiments on metals that there is no change in volume due to the plastic component of strain. Thus volume changes during plastic deformation are elastic; hence

$$\epsilon_1 + \epsilon_2 + \epsilon_3 = \frac{1 - 2\nu}{E}(\sigma_1 + \sigma_2 + \sigma_3) \quad \ldots\ldots [8]$$

If the stresses and strains obey Equation [8], the material is said to be compressible. If the plastic component of strain is predominant

$$\epsilon_1 + \epsilon_2 + \epsilon_3 \cong 0 \quad [9]$$

When Equation [9] is used, the material is said to be incompressible. In the cylinder problem under consideration the plastic material is restrained by an outer elastic hoop. The plastic strains are thus comparable in magnitude to the elastic ones, and errors are introduced if Equation [9] is used. The inclusion of compressibility, however, considerably complicates a solution. It is seen from Table 1 that there is only one solution in closed form observing compressibility of the plastic material.

(*h*) *Flow Condition.* The theories of failure due to Tresca (maximum shear stress) and von Mises (maximum energy of distortion) are well known. They are usually stated as

$$\sigma_1 - \sigma_3 = \sigma_y = 2s \quad [10]$$

where

$$\sigma_1 \geq \sigma_2 \geq \sigma_3$$

and

$$(\sigma_1 - \sigma_2)^2 + (\sigma_2 - \sigma_3)^2 + (\sigma_3 - \sigma_1)^2 = 2\,\sigma_e^2 \quad [11]$$

All the cylinder theories incorporating strain-hardening make use of a generalization of Equation [11]. The "effective stress" and "effective strain" are defined as

$$\left.\begin{aligned} \bar{\sigma} &= \frac{\sqrt{2}}{2}\sqrt{(\sigma_1 - \sigma_2)^2 + (\sigma_2 - \sigma_3)^2 + (\sigma_3 - \sigma_1)^2} \\ \bar{\epsilon} &= \frac{\sqrt{2}}{3}\sqrt{(\epsilon_1 - \epsilon_2)^2 + (\epsilon_2 - \epsilon_3)^2 + (\epsilon_3 - \epsilon_1)^2} \end{aligned}\right\} \quad [12]$$

and it is assumed that $\bar{\sigma} = f(\bar{\epsilon})$ for all combinations of stress. Hill (5) has pointed out the limitations of this assumption. As for the case of the Hencky stress-strain relations, however, this strain-hardening function has approximate application in many instances and in particular to the problem under consideration. It is not common to make use of an extension of Equation [10] for strain-hardening material. Ludwik (6) in 1909 stated that the maximum shearing stress as a function of the maximum shearing strain described the subsequent flow of a ductile material in the strain-hardening range. Little use has been made of this assumption. Tests on low-carbon steel thin cylinders[3] under combined stress have shown that von Mises' theory closely describes failure and subsequent flow condition. In steel with a drop in stress at the yield point, Morrison (7) states that initiation of yield is due to a critical maximum shear stress but that plastic flow continues in accordance with von Mises' criterion.

Experimental work by Steele and Young (8) on low-carbon steel, and Macrae (9) on nickel-gun-steel thick-walled cylinders under internal fluid pressure, contradict the findings of the previous paragraph from thin-walled cylinder tests. Strains were found to agree closely with theories based on the Tresca condition and were in definite disagreement with von Mises' criterion. It is of importance that experimental results lay on the side of the strain curves computed using Tresca's condition, remote from the curves based on von Mises' theory. Steele and Young attributed this to the mechanism of flow in steels containing a flat-topped portion at yield in a tension test. They showed that the theoretical assumption that a partially plastic thick cylinder consists of two regions, both containing isotropic material and separated by a circular boundary, is incorrect. By polishing the ends of cylinders it was shown that the overstrained portion consists mostly of elastic material separated by a small number of thin, spiral, wedge regions of plastic material.

[3] Bibliography (2), chapter 17.

A comparison will be effected in the next section of this paper among certain of the theories listed in Table 1. Previous comparisons, with one exception (10), have involved several variables, e.g., axial boundary, compressibility, theory of failure, and so forth, and the effects of the individual variable have been masked. It is proposed to adopt a standard set of conditions and examine the effect of compressibility and theory of failure on the significant stresses and strains. In addition, the effect of making Poisson's ratio 0.5 rather than the normal value (0.3 for steel) is discussed for theories which assume incompressibility of the plastic material.

Comparison of Theories[4]

Hodge and White (10) have given a quantitative comparison of the Reuss stress-strain relations and the Hencky relations for cylinders in plane strain, and composed of compressible material obeying von Mises' flow condition. Their results show that the two theories yield almost identical values for the stresses and strains. It is realized that this cannot be generalized strictly to the cases of open and closed cylinders. No solution is known to the author which includes the incremental theory, compressibility, and von Mises' flow condition for closed or open-ended cylinders. Incremental solutions using Tresca's theory all yield the same values for hoop and radial stresses since the equilibrium equations may be integrated directly (for zero strain-hardening); the solution for these stresses is statically determinate. It is difficult to estimate the errors involved in the computed strains by using the Hencky stress-strain relations for open-ended cylinders rather than the Prandtl-Reuss equations, but there seems at present no alternative to the selection of the former relations for the basis of a practical solution.

A quantitative comparison follows to examine the effect of (*a*) compressibility, and (*b*) theory of failure. The basis of the comparison is as follows:

1 Hencky (total strain) plastic stress-strain relations.

2 Material exhibits idealized, flat-topped tensile stress-strain curve.

3 Open-ended cylinders.

4 Diameter ratio (k) = 2.

5 Stresses plotted for cylinders yielded halfway through the wall ($n = 1.5$).

The comparison is effected with reference to three theories, viz., those of (*a*) Allen and Sopwith (11), (*b*) MacGregor, Coffin, and Fisher (12), and (*c*) Steele (13). Information on these theories may be obtained from Table 1. It is seen that if Allen and Sopwith's, and Steele's work are compared, the effect of compressibility may be estimated with all other variables standardized. Similarly, if Allen and Sopwith's theory is compared with MacGregor, Coffin, and Fisher's solution, the differences in the stresses and strains for the von Mises and Tresca flow condition are found.

Figs. 1, 2, and 3 show plots for these three theories of the principal stresses and strains at the outside and bore surfaces.

With regard to compressibility versus incompressible (plastic material) solutions for the stresses, it is seen that the only difference lies in the axial direction. In Steele's solution a discontinuity arises at the plastic-elastic boundary when Poisson's ratio for elastic material is taken as 0.3, since

$$\epsilon_\theta + \epsilon_r + \epsilon_z = \frac{1 - 2\nu}{E}(\sigma_\theta + \sigma_r + \sigma_z)$$

on the elastic side, and

$$\epsilon_\theta + \epsilon_r + \epsilon_z = 0$$

[4] The comparison presented here is included in a PhD thesis submitted by the author to the University of Glasgow, Scotland, in April, 1951 (see Bibliography 13).

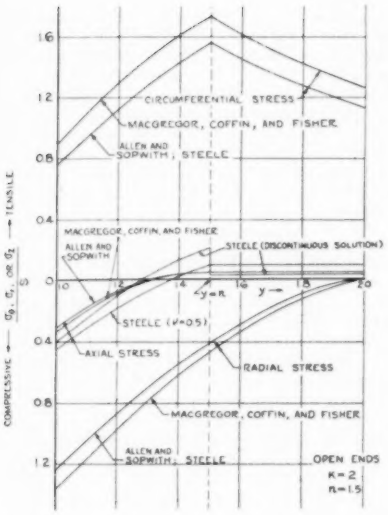

FIG. 1 RADIAL, CIRCUMFERENTIAL, AND AXIAL STRESSES FOR THEORIES OF (a) ALLEN AND SOPWITH ($\nu = 0.3$); (b) MACGREGOR, COFFIN, AND FISHER ($\nu = 0.3$); (c) STEELE ($\nu = 0.3$ AND 0.5)

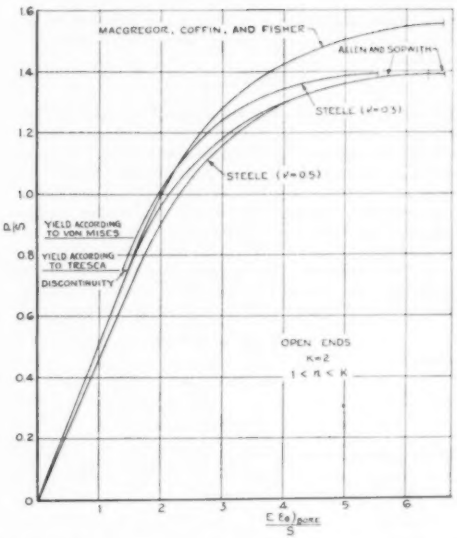

FIG. 3 BORE CIRCUMFERENTIAL STRAINS FOR THEORIES OF (a) ALLEN AND SOPWITH ($\nu = 0.3$); (b) MACGREGOR, COFFIN, AND FISHER ($\nu = 0.3$); (c) STEELE ($\nu = 0.3$ AND 0.5)

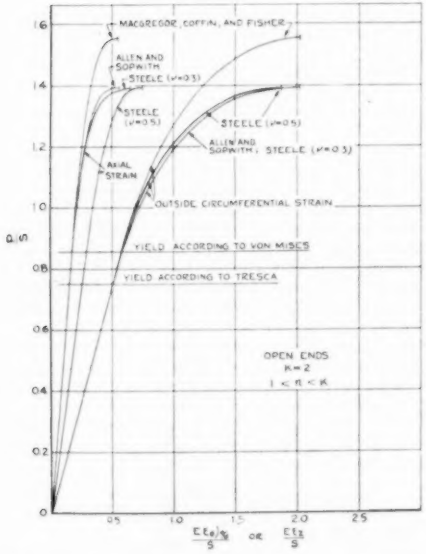

FIG. 2 OUTSIDE CIRCUMFERENTIAL (TENSILE) AND AXIAL (COMPRESSIVE) STRAINS FOR THEORIES OF (a) ALLEN AND SOPWITH ($\nu = 0.3$); (b) MACGREGOR, COFFIN, AND FISHER ($\nu = 0.3$); (c) STEELE ($\nu = 0.3$ AND 0.5)

on the plastic side. This would be considered serious if an accurate knowledge of the axial stresses is required. However, as pointed out in the introduction, the deflections of outside and bore surfaces of the cylinder are of greater interest to the engineer, and Figs. 2 and 3 show that the percentage differences here are small. Indeed the plots for outside circumferential strain for Allen and Sopwith's, and Steele's theories cannot be differentiated on the scale used. The largest percentage difference is noticed in the axial strain which has little effect on the circumferential strain.

To eliminate the physically unrealistic discontinuities in axial stress and bore circumferential strain, it has been suggested by Nadai[5] and Prager (14) that the elastic material should be considered incompressible also, i.e., $\nu = 0.5$. The stresses and strains for $\nu = 0.5$ are shown plotted in Figs. 1, 2, and 3, and it is seen that the curves show closer agreement with the more correct theory of Allen and Sopwith. Largest differences again occur in axial stress and strain, but the outside and bore circumferential strains vary at the most by 3 per cent for a specified applied load once the plastic region has extended to a depth of one half the wall thickness or greater. Thus it is contended that a solution based on incompressibility in both the plastic and elastic domains will be of value to the engineer, since he is interested in factors which are not affected seriously by such radical assumptions. It should be emphasized that the foregoing is not a general statement applicable to all problems in plasticity, but one suitable for a plastic mechanics-of-materials solution for this specific problem.

Theories of failure are compared by two solutions (Allen and Sopwith, and MacGregor, Coffin, and Fisher) which may be classed as rigorously correct. The plots in Figs. 1, 2, and 3 show

[5] Bibliography (2), p. 460.

large differences in the computed stresses and strains[6] (with the exception of the axial stress), and decision as to which theory to use depends on the experimental behavior of the cylinder material. It was pointed out in the introduction that tests performed on thick-walled cylinders by Steele and Young, and Macrae, gave results at variance with von Mises' theory and this was attributed to the mechanism of yielding. It is further reasoned that von Mises' theory may be operative within the wedge regions of overstrain, but the integrated effect of such regions on observed strains at the outside and bore surfaces is more closely in agreement with Tresca's theory. Evidently some new theory must be devised to estimate the over-all effects of wedge regions of overstrain in an elastic material, but so far this has proved exceedingly difficult.

Most gun steels have a short flat-topped portion to the tensile stress-strain curve before strain-hardening becomes operative. It is suggested that the flat-topped portion gives rise to the wedge type of yielding in members in which a stress gradient exists. Further, for geometrically similar cylinders made of different materials and exhibiting varying lengths for the flat-topped portion in a tension test, the amount of strain-hardening within wedges will be dependent on the length of the flat portion and the strain-hardening characteristics of the material. Experiments have shown (Steele and Young) that for mild steel, which has a long flat portion, compared to the strain at critical yield, cylinder outside and bore circumferential strains may be described approximately by Tresca's theory (zero strain-hardening). Therefore it is suggested that the plastic mechanics-of-materials solution should be based on Tresca's theory as extended by Ludwik to describe the strains existing in a cylinder of strain-hardening material. Such a theory in closed form is given in the next section including also the simplifying assumption of incompressibility of plastic and elastic material.

Theory

Assumptions

$$\frac{\epsilon_\theta - \epsilon_r}{\sigma_\theta - \sigma_r} = \frac{\epsilon_r - \epsilon_z}{\sigma_r - \sigma_z} = \frac{\epsilon_z - \epsilon_\theta}{\sigma_z - \sigma_\theta} = \beta \quad \ldots\ldots [13]$$

β is a function of the radius only for any stage in plastic flow. Equation [13], together with the compressibility condition, satisfies the Hencky relations (Equation [6])

$$\epsilon_\theta + \epsilon_r + \epsilon_z = 0 \quad \ldots\ldots [14]$$

(Incompressibility)

$$\sigma_\theta - \sigma_r = 2f(\gamma) \quad \ldots\ldots [15]$$

(Ludwik's strain-hardening function)

For linear strain-hardening, Fig. 4

$$\tau = s + mG(\gamma - \gamma_e) = s(1 - m) + mG\gamma \quad \ldots\ldots [16]$$

When $m = 0$, $\tau = s$ as for zero strain-hardening.

For an incompressible material and ϵ_z = const at any stage in plastic flow, compatibility relations are satisfied by

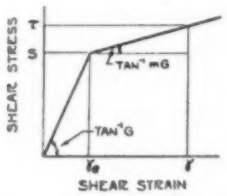

Fig. 4 Linear Strain-Hardening Diagram

$$\left.\begin{aligned} \epsilon_r &= -\frac{\epsilon_z}{2} - \frac{c}{r^2} \\ \epsilon_\theta &= -\frac{\epsilon_z}{2} + \frac{c}{r^2} \end{aligned}\right\} \quad \ldots\ldots [17]$$

where c is a constant of integration.

Now

$$\gamma = \epsilon_\theta - \epsilon_r = \frac{2c}{r^2} = \frac{2c}{r_0^2 y^2}$$

At elastic-plastic boundary, $y = u$, $\gamma = s/G$

$$\gamma = \frac{su^2}{Gy^2} \quad \ldots\ldots [18]$$

From Equations [16] and [18]

$$\tau = s(1 - m) + \frac{smu^2}{y^2} \quad \ldots\ldots [19]$$

Radial equilibrium of an element gives

$$y\frac{\partial \sigma_r}{\partial y} = \sigma_\theta - \sigma_r \quad \ldots\ldots [20]$$

In the elastic domain, Lamé's solution (98) for Equation [20] gives

$$\left.\begin{aligned} \sigma_r &= A + \frac{B}{y^2} \\ \sigma_\theta &= A - \frac{B}{y^2} \end{aligned}\right\} \quad \ldots\ldots [21]$$

where A and B are constants of integration.

In the plastic domain

$$y\frac{\partial \sigma_r}{\partial y} = \sigma_\theta - \sigma_r = 2\tau = 2s(1 - m) + \frac{2smu^2}{y^2}$$

On integration

$$\left.\begin{aligned} \sigma_r &= s(1 - m)\log y^2 - \frac{smu^2}{y^2} + D \\ \sigma_\theta &= s(1 - m)\log y^2 + 2 + \frac{smu^2}{y^2} + D \end{aligned}\right\} \quad \ldots\ldots [22]$$

where D is a constant of integration.

Boundary Conditions:

1 $\sigma_r = 0$ at $y = k$

2 σ_r is continuous at plastic-elastic boundary.

3 σ_θ is continuous at plastic-elastic boundary.

[6] It should be noted that the Mises-Tresca comparison is based on the assumption that the two laws agree for a tension test. This follows the customary engineering treatment for theories of failure. However, the constants for the two flow conditions could be chosen equally well so that they agree for any other stress system; and if, for example, the values in pure shear (thin-walled tube under pure torsion) were made to agree exactly, the difference between the two theories for the stresses and strains in the particular problem under consideration probably would be small.

Hence in elastic domain $(n < y < k)$

$$\left.\begin{aligned}\frac{\sigma_r}{s} &= n^2\left(\frac{1}{k^2}-\frac{1}{y^2}\right)\\ \frac{\sigma_\theta}{s} &= n^2\left(\frac{1}{k^2}+\frac{1}{y^2}\right)\end{aligned}\right\} \quad \ldots\ldots\ldots [23]$$

and in plastic domain $(1 < y < n)$

$$\left.\begin{aligned}\frac{\sigma_r}{s} &= (1-m)\log\left(\frac{y}{n}\right)^2 - \frac{(k^2-n^2)}{k^2} - m\left(\frac{n^2}{y^2}-1\right)\\ \frac{\sigma_\theta}{s} &= (1-m)\log\left(\frac{y}{n}\right)^2 + \frac{(k^2+n^2)}{k^2} + m\left(\frac{n^2}{y^2}-1\right)\end{aligned}\right\} \quad .[24]$$

at $y = 1$, $\sigma_r = -P$, hence

$$\frac{P}{s} = (1-m)\log n^2 + \frac{k^2-n^2}{k^2} + m(n^2-1) \ldots [25]$$

The strain at the outside diameter is obtained from the elastic equations

$$E\epsilon_\theta = \sigma_\theta - \nu(\sigma_z)$$

substituting for σ_θ and σ_z

$$\frac{(E\epsilon_\theta)_{o/d}}{s} = \frac{2n^2}{k^2}(1-\nu^2) - \nu\frac{E\epsilon_z}{s} \quad \ldots\ldots [26]$$

Plastic Strains. From Equation [13]

$$\frac{\epsilon_\theta - \epsilon_r}{\sigma_\theta - \sigma_r} = \frac{\gamma}{2\tau} = \beta$$

Substituting for γ and τ from Equations [18] and [19], respectively

$$\beta = \frac{n^2}{2G(1-m)y^2 + 2Gmn^2} \quad \ldots\ldots [27]$$

Also

$$\epsilon_\theta - \epsilon_r = \gamma = \frac{sn^2}{Gy^2}$$

and from Equation [14], $\epsilon_\theta + \epsilon_r = -\epsilon_z$; hence

$$\left.\begin{aligned}\epsilon_\theta &= \frac{sn^2}{2Gy^2} - \frac{\epsilon_z}{2}\\ \epsilon_r &= -\frac{sn^2}{2Gy^2} - \frac{\epsilon_z}{2}\end{aligned}\right\} \quad \ldots\ldots [28]$$

In particular, the bore circumferential strain is given by

$$\frac{(E\epsilon_\theta)_{bore}}{s} = (1+\nu)n^2 - \frac{1}{2}\frac{E\epsilon_z}{s} \quad \ldots\ldots [29]$$

where

$$G = \frac{E}{2(1+\nu)}$$

From Equation [13]

$$\sigma_z = \frac{\epsilon_z}{\beta} - \frac{\epsilon_\theta}{\beta} + \sigma_\theta$$

in the plastic domain. Substituting for ϵ_θ, β, and σ_θ

$$\frac{\sigma_z}{s} = \frac{3\left[(1-m)\frac{y^2}{n^2}+m\right]}{2(1+\nu)}\left(\frac{E\epsilon_z}{s}\right) + (1-m)\log\left(\frac{y}{n}\right)^2 + \frac{n^2}{k^2} \quad \ldots\ldots [30]$$

also

$$\frac{\sigma_z}{s} = \frac{E\epsilon_z}{s} + \frac{2\nu n^2}{k^2}$$

in the elastic region from the elastic equations.

The end condition gives

$$\int_1^k \sigma_z\, y\, dy = 0 \text{ (open ends)}; \quad \frac{P}{2} \text{ (closed ends)} \ldots [31]$$

Assuming open ends

$$\int_1^k \sigma_z\, y\, dy = s\int_1^n \left\{\frac{3\left[(1-m)\frac{y^2}{n^2}+m\right]}{2(1+\nu)}\frac{E\epsilon_z}{s} + (1-m)\log\left(\frac{y}{n}\right)^2 + \frac{n^2}{k^2}\right\} y\, dy + s\int_n^k \left(\frac{E\epsilon_z}{s} + \frac{2\nu n^2}{k^2}\right) y\, dy = 0$$

From which

$$\frac{E\epsilon_z}{s} = -\left\{\frac{(1-m)\log n^2 - (n^2-1)\left[1-m-\frac{n^2}{k^2}\right] + \frac{2\nu n^2}{k^2}(k^2-n^2)}{\frac{3(1-m)(n^4-1)}{4(1+\nu)n^2} + k^2 - n^2 + \frac{3m(n^2-1)}{2(1+\nu)}}\right\} \quad \ldots\ldots [32]$$

Summarizing the formulas: In the elastic domain $(n < y < k)$

$$\frac{\sigma_r}{s} = n^2\left(\frac{1}{k^2}-\frac{1}{y^2}\right)$$

$$\frac{\sigma_\theta}{s} = n^2\left(\frac{1}{k^2}+\frac{1}{y^2}\right)$$

$$\frac{\sigma_z}{s} = \frac{E\epsilon_z}{s} + \frac{2\nu n^2}{k^2}$$

$$\frac{(E\epsilon_\theta)_{o/d}}{s} = \frac{2n^2}{k^2}(1-\nu^2) - \nu\frac{E\epsilon_z}{s}$$

In the plastic domain $(1 < y < n)$

$$\frac{\sigma_r}{s} = (1-m)\log\left(\frac{y}{n}\right)^2 - \frac{(k^2-n^2)}{k^2} - m\left(\frac{n^2}{y^2}-1\right)$$

$$\frac{\sigma_\theta}{s} = (1-m)\log\left(\frac{y}{n}\right)^2 + \frac{(k^2+n^2)}{k^2} + m\left(\frac{n^2}{y^2}-1\right)$$

$$\frac{\sigma_z}{s} = \frac{3\left[(1-m)\frac{y^2}{n^2}+m\right]}{2(1+\nu)}\frac{E\epsilon_z}{s} + (1-m)\log\left(\frac{y}{n}\right)^2 + \frac{n^2}{k^2}$$

$$\frac{(E\epsilon_\theta)_{bore}}{s} = (1+\nu)n^2 - \frac{1}{2}\frac{E\epsilon_z}{s}$$

where

$$\frac{E\epsilon_z}{s} = -\left[\frac{(1-m)\log n^2 - (n^2-1)\left[1-m-\frac{n^2}{k^2}\right] + \frac{2\nu n^2}{k^2}(k^2-n^2)}{\frac{3}{4}\frac{(1-m)(n^4-1)}{(1+\nu)n^2} + k^2 - n^2 + \frac{3m(n^2-1)}{2(1+\nu)}}\right]$$

also

$$\frac{P}{s} = (1-m)\log n^2 + \frac{(k^2-n^2)}{k^2} + m(n^2-1)$$

Curves for σ_r/s, σ_θ/s and σ_z/s are given in Fig. 5 for various values of the strain-hardening parameter m.

Figs. 6 and 7 show plots of

$$\frac{(E\epsilon_\theta)_{o/d}}{s} \quad \text{and} \quad \frac{(E\epsilon_\theta)_{\text{bore}}}{s}$$

respectively, for various values of m and for $1 \leq n \leq k$.

Conclusions

Previous partially plastic thick-walled-cylinder theories are highly mathematical and not suitable for use in design offices. A search for assumptions leading to a simplified theory for design may be made from the point of view that engineers are interested in certain significant factors—for the most part in deflections of outside and bore surfaces for specific applied pressures. It is shown that on the assumption of incompressibility of both elastic and plastic materials, a solution for the significant factors in de-

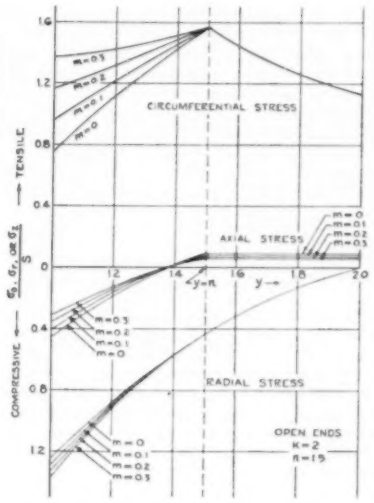

Fig. 5 Radial, Circumferential, and Axial Stresses for Various Values of Strain-Hardening Parameter m

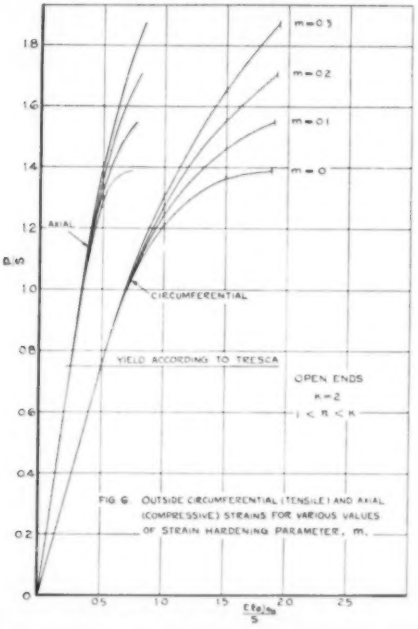

Fig. 6 Outside Circumferential (Tensile) and Axial (Compressive) Strains for Various Values of Strain-Hardening Parameter m

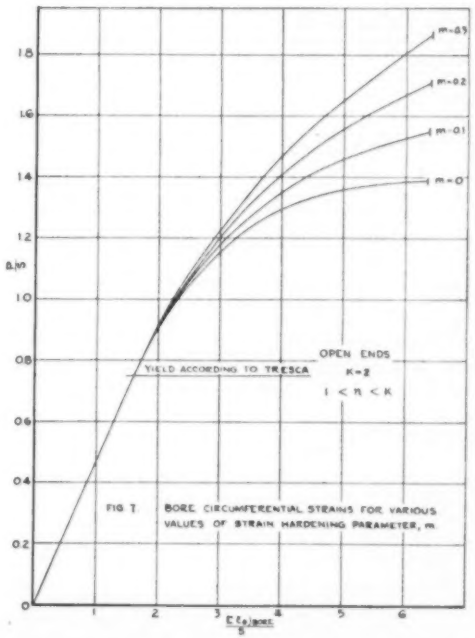

Fig. 7 Bore Circumferential Strains for Various Values of Strain-Hardening Parameter m

sign is in close agreement with a more rigorous mathematical theory based upon compressibility. Experimental work on mild-steel thick-walled cylinders under internal fluid pressure disagrees with von Mises' (maximum-energy-of-distortion) theory of failure and more closely supports that due to Tresca (maximum shear stress). On the basis of the foregoing conclusions, an extension of Tresca's theory to cover strain-hardening, incompressibility, and Hencky stress-strain relations, is considered a sound basis on which to furnish a "plastic" mechanics-of-materials solution. Such a theory is presented in closed form, i.e., the values of stresses and strains for specific applied pressures may be obtained without resort to lengthy numerical integration procedures.

Acknowledgments

The author wishes to express his indebtedness to the Department of Theoretical and Applied Mechanics, University of Illinois, of which Prof. F. B. Seely is the head, for the facilities provided for the research. Thanks are extended to Prof. J. O. Smith for his interest in the work and to Dr. C. K. Liu and Mr. John Young for their assistance with computations and figures.

The work was performed as part of a contract sponsored by the Wright-Patterson Air Force Base, Dayton, Ohio, Contract AF 33 (038)-15677.

Bibliography

1 "The Theory of Combined Plastic and Elastic Deformation With Particular Reference to a Thick Tube Under Internal Pressure," by R. Hill, E. H. Lee, and S. J. Tupper, Proceedings of the Royal Society of London, series A, vol. 191, 1947, p. 278.

2 "Theory of Flow and Fracture of Solids," by A. Nadai, McGraw-Hill Book Company, Inc., New York, N. Y., vol. 1, second edition, 1950, pp. 460–465.

3 "The Mathematical Theory of Plasticity," by R. Hill, Clarendon Press, Oxford, England, first edition, 1950, pp. 38–43.

4 Ibid., pp. 45–48.

5 Ibid., pp. 23–33

6 "Elemente der Technologischen Mechanik," by P. Ludwik, Julius Springer, Berlin, Germany, first edition, 1909.

7 "The Criterion of 'Yield' of Gun Steels," by J. L. M. Morrison, Proceedings of The Institution of Mechanical Engineers, vol. 159, 1948, pp. 81–94.

8 "An Experimental Investigation of Overstraining in Mild Steel Thick-Walled Cylinders by Internal Fluid Pressure," by M. C. Steele and J. Young, presented at the Fall Meeting, Minneapolis, Minn., Sept. 25–28, 1951, of The American Society of Mechanical Engineers.

9 "Overstrain of Metals," by A. E. Macrae, His Majesty's Stationery Office, London, England, first edition, 1930.

10 "A Quantitative Comparison of Flow and Deformation Theories of Plasticity," by P. G. Hodge, Jr., and G. N. White, Jr., Graduate Division of Applied Mathematics, Brown University, Office of Naval Research Contract N7onr-358, Technical Report No. 29.

11 "The Stresses and Strains in a Partly-Plastic Thick Tube Under Internal Pressure and End Load," by D. N. DeG. Allen and D. G. Sopwith, Proceedings of the Royal Society of London, series A, vol. 205, 1951, pp. 69–83.

12 "Partially-Plastic Thick-Walled Tubes," by C. W. MacGregor, L. F. Coffin, Jr., and J. C. Fisher, *Journal of The Franklin Institute*, vol. 245, 1948, p. 135.

13 "On the Overstraining of Thick-Walled Cylinders Under Internal Fluid Pressure and Under Interference Fit Pressure," by M. C. Steele, PhD thesis, University of Glasgow, Scotland, April, 1951.

14 "Theory of Plasticity" (mimeographed lecture notes), by W. Prager, Brown University, Providence, R. I., 1942.

15 "Plastic Flow in a Closed-End Tube With Internal Pressure," by R. Hill, E. H. Lee, and S. J. Tupper, Ministry of Supply Armament Research Department, Theoretical Research Report 11/46. To appear in Proceedings of First U. S. National Congress of Applied Mechanics, Chicago, Ill., 1951.

16 "Theory of Plasticity" (in Russian), by W. W. Sokolovsky, Moscow, USSR, 1946, chapt. 3.

17 "The Stresses in Thick-Walled Cylinders of Mild Steel Overstrained by Internal Pressure," by G. Cook, Proceedings of The Institution of Mechanical Engineers, vol. 126, 1934, p. 407.

18 "Advanced Mechanics of Materials," by F. B. Seely, John Wiley & Sons, Inc., New York, N. Y., 9th printing, 1948, p. 62.

On the Stresses in a Notched Strip

By CHIH-BING LING,[1] TAIWAN, CHINA

In a previous paper by the author (1),[2] a theoretical solution for a notched strip under longitudinal tension is given. The result demands the solution of an infinite system of linear equations. A considerable amount of labor is involved in solving such a system. It seems, however, that the labor can be diminished by adapting to the solution a process known as the promotion of rank. In this paper such a process is described and then applied to solve the problem of a notched strip under transverse bending. The solution of this problem seems also to be new. The numerical results obtained are compared graphically with the experimental results available.

Introduction

THE stresses in a strip containing a pair of symmetrical semicircular notches, under the action of tension along its length, were investigated theoretically by the present author in a recent paper (1). The stress function in question is constructed by combining linearly two sets of even biharmonic functions, in addition to a basic stress function which represents the given stress system in an unnotched strip of the same width. Each of the two sets of biharmonic functions gives no stress at infinity of the strip and, in addition, gives no normal or tangential stresses along both edges of the strip, except at the centers of the notches which are singularities. The remaining boundary conditions at the edges of the notches are satisfied by adjusting properly the coefficients of superposition. This leads to an infinite system of linear equations. The stresses at any point in the strip are calculated readily, provided that the infinite system is solved in some way.

The solution of such an infinite system usually presents some practical difficulty. If it happens that the system is in favorable form, the method of successive approximations may be used to advantage. Otherwise, the crude method of elimination of unknowns has to be resorted to in which the infinite system is first reduced to a finite system by neglecting those coefficients which are after a certain number of terms. In the particular system mentioned, both methods have been used simultaneously, each for the solution of one set of coefficients. Consequently, considerable labor has been involved in thus solving the system.

It seems, however, that the amount of labor can be diminished by adapting to the solution a process known as the "promotion of rank." This process was formerly used by Love in investigating certain elastic and electric problems (2, 3) and it appears that it can be adapted, with due extensions, to the present problem. By this process, the two sets of biharmonic functions χ_{2s}, χ_{2s}' as defined in the previous paper are replaced by two sets of new functions, say, ω_{2s}, ω_{2s}' which are formed by linear combinations of the former. The new functions involve two different sets of parametric coefficients which can be determined pair by pair.

In this paper such a process will be described in general terms and then, to fulfill an announcement made in the previous paper, will be applied to solve the transverse bending problem, i.e., the problem in which the notched strip is under the action of a constant transverse bending moment in the plane of the strip. Such a solution also seems to be new. Finally, comparison will be made to show the accuracy of the experimental results available.

Process of Promotion of Rank[3]

As in the previous paper (1), dimensionless variables will be used. The rectangular co-ordinates (x, y) are expressed as ratios to a typical length b or the half-width of the strip. The polar co-ordinates (r, θ) are defined by

$$\left.\begin{aligned} &x + iy + i = i\, r\, e^{i\theta} \\ \text{or} \quad &r \sin\theta = x, \quad r\cos\theta = 1 + y = \eta \text{ (say)} \end{aligned}\right\} \quad \ldots\ldots [1]$$

such that the pole is at the center of the lower notch and the strip is bounded by lines $y = \pm 1$ as shown in Fig. 1. The radius of the lower notch will be denoted by λ, also as a ratio to b. In the symmetrical case considered presently, the radius of the upper notch is also equal to λ.

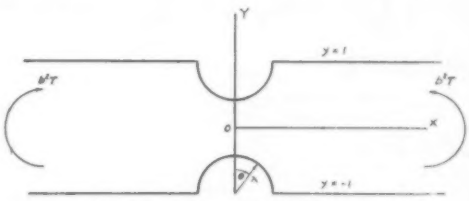

Fig. 1 The Notched Strip

Suppose now that the normal and tangential stresses $\widehat{rr}$ and $\widehat{r\theta}$ at the edge of the lower notch, derived from any one of the two sets of biharmonic functions χ_{2s}, χ_{2s}', are expanded into Fourier series between $\theta = -\pi/2$ and $\pi/2$. Denote such edge stresses by $\widehat{rr}_1$ and $\widehat{r\theta}_1$. If the biharmonic functions are even in x, we may write such stresses derived from χ_{2s} by

$$\widehat{rr}_1 = \frac{1}{b^2}\sum_{s=0}^{\infty} a_{2k,2s}\cos 2s\theta, \quad \widehat{r\theta}_1 = \frac{1}{b^2}\sum_{s=1}^{\infty} c_{2k,2s}\sin 2s\theta \ldots [2]$$

and those derived from χ_{2s}' by

$$\widehat{rr}_1 = \frac{1}{b^2}\sum_{s=0}^{\infty} a_{2k,2s}'\cos 2s\theta, \quad \widehat{r\theta}_1 = \frac{1}{b^2}\sum_{s=1}^{\infty} c_{2k,2s}'\sin 2s\theta \ldots [3]$$

where $a_{2k,2s}$, $a_{2k,2s}'$, . . . are dimensionless quantities depending only on λ. Here, in both cases, $\widehat{rr}_1$ begins with terms independent of θ, and $\widehat{r\theta}_1$ begins with terms in $\sin 2\theta$. We may describe the two sets of functions χ_{2s}, χ_{2s}' as being of rank zero. The

---

[1] Senior Research Officer, Aeronautical Research Laboratory.

[2] Numbers in parentheses refer to the Bibliography at the end of the paper.

For presentation at the National Conference of the Applied Mechanics Division, State College, Pa., June 19-21, 1952, of The American Society of Mechanical Engineers.

Discussion of this paper should be addressed to the Secretary, ASME, 29 West 39th Street, New York, N. Y., and will be accepted until July 10, 1952, for publication at a later date. Discussion received after the closing date will be returned.

Note: Statements and opinions advanced in papers are to be understood as individual expressions of their authors and not those of the Society. Manuscript received by ASME Applied Mechanics Division, December 6, 1950. Paper No. 52—APM-5.

process of promotion of rank consists in replacing them by two sets of new functions ω_2, ω_4, . . . and ω_2', ω_4', . . . of ranks equal to their suffixes, that is to say, such that $\widehat{rr_1}$ derived from them begins with terms in $\cos 2\theta$, $\cos 4\theta$, . . . and $r\widehat{\theta_1}$ begins with terms in $\sin 4\theta$, $\sin 6\theta$, . . . , respectively. For the sake of completeness, we shall write ω_0, ω_0' in place of χ_0, χ_0'. We form ω_2, ω_2' by the rule

$$\left.\begin{aligned}\omega_2 &= \chi_2 - p_{2,0}\omega_0 - p_{2,0}'\omega_0' \\ \omega_2' &= \chi_2' - q_{2,0}\omega_0 - q_{2,0}'\omega_0'\end{aligned}\right\} \quad \ldots\ldots\ldots [4]$$

where $p_{2,0}$, $q_{2,0}$, . . . are coefficients to be adjusted so that $\widehat{rr_1}$ derived from ω_2, ω_2' may contain no term independent of θ and at the same time $r\widehat{\theta_1}$ may contain no term in $\sin 2\theta$. These conditions lead to two pairs of relations

$$\left.\begin{aligned}a_{2,0} - p_{2,0}a_{0,0} - p_{2,0}'a_{0,0}' &= 0 \\ c_{2,2} - p_{2,0}c_{0,2} - p_{2,0}'c_{0,2}' &= 0\end{aligned}\right\} \quad \ldots\ldots\ldots [5]$$

and

$$\left.\begin{aligned}a_{2,0}' - q_{2,0}a_{0,0} - q_{2,0}'a_{0,0}' &= 0 \\ c_{2,2}' - q_{2,0}c_{0,2} - q_{2,0}'c_{0,2}' &= 0\end{aligned}\right\} \quad \ldots\ldots\ldots [6]$$

so that they determine $p_{2,0}$, $p_{2,0}'$ and $q_{2,0}$, $q_{2,0}'$ simultaneously. We write the stresses $\widehat{rr_1}$ and $\widehat{r\theta_1}$ derived from ω_2 as

$$\widehat{rr_1} = \frac{1}{b^2}\sum_{s=1}^{\infty} b_{2,2s}\cos 2s\theta, \quad \widehat{r\theta_1} = \frac{1}{b^2}\sum_{s=2}^{\infty} d_{2,2s}\sin 2s\theta \quad \ldots [7]$$

and those derived from ω_2' as

$$\widehat{rr_1} = \frac{1}{b^2}\sum_{s=1}^{\infty} b_{2,2s}'\cos 2s\theta, \quad \widehat{r\theta_1} = \frac{1}{b^2}\sum_{s=2}^{\infty} d_{2,2s}'\sin 2s\theta \quad \ldots [8]$$

where, for $s \geqslant 1$

$$\left.\begin{aligned}b_{2,2s} &= a_{2,2s} - p_{2,0}a_{0,2s} - p_{2,0}'a_{0,2s}' \\ b_{2,2s}' &= a_{2,2s}' - q_{2,0}a_{0,2s} - q_{2,0}'a_{0,2s}'\end{aligned}\right\} \quad \ldots\ldots\ldots [9]$$

and, for $s \geqslant 2$

$$\left.\begin{aligned}d_{2,2s} &= c_{2,2s} - p_{2,0}c_{0,2s} - p_{2,0}'c_{0,2s}' \\ d_{2,2s}' &= c_{2,2s}' - q_{2,0}c_{0,2s} - q_{2,0}'c_{0,2s}'\end{aligned}\right\} \quad \ldots\ldots\ldots [10]$$

Again, for the sake of completeness, $b_{0,2s}$, $b_{0,2s}'$, $d_{0,2s}$, $d_{0,2s}'$ are written for $a_{0,2s}$, $a_{0,2s}'$, $c_{0,2s}$, $c_{0,2s}'$, respectively. In general, we write

$$\left.\begin{aligned}\omega_{2k} &= \chi_{2k} - \sum_{n=0}^{k-1}(p_{2k,2n}\omega_{2n} + p_{2k,2n}'\omega_{2n}') \\ \omega_{2k}' &= \chi_{2k}' - \sum_{n=0}^{k-1}(q_{2k,2n}\omega_{2n} + q_{2k,2n}'\omega_{2n}')\end{aligned}\right\} \quad \ldots\ldots [11]$$

Also, we write the stresses $\widehat{rr_1}$ and $\widehat{r\theta_1}$ derived from ω_{2k} as

$$\widehat{rr_1} = \frac{1}{b^2}\sum_{s=k}^{\infty} b_{2k,2s}\cos 2s\theta, \quad \widehat{r\theta_1} = \frac{1}{b^2}\sum_{s=k+1}^{\infty} d_{2k,2s}\sin 2s\theta \quad \ldots [12]$$

and those derived from ω_{2k}' as

$$\widehat{rr_1} = \frac{1}{b^2}\sum_{s=k}^{\infty} b_{2k,2s}'\cos 2s\theta, \quad \widehat{r\theta_1} = \frac{1}{b^2}\sum_{s=k+1}^{\infty} d_{2k,2s}'\sin 2s\theta \quad [13]$$

The coefficients $p_{2k,2s}$, $p_{2k,2s}'$, . . . are determined successively by the set of k-pairs of equations

$$\left.\begin{aligned}&\left.\begin{aligned}a_{2k,0} - p_{2k,0}b_{0,0} - p_{2k,0}'b_{0,0}' &= 0 \\ c_{2k,2} - p_{2k,0}d_{0,2} - p_{2k,0}'d_{0,2}' &= 0\end{aligned}\right\} \\ &\left.\begin{aligned}a_{2k,2} - p_{2k,0}b_{0,2} - p_{2k,0}'b_{0,2}' - p_{2k,2}b_{2,2} - p_{2k,2}'b_{2,2}' &= 0 \\ c_{2k,4} - p_{2k,0}d_{0,4} - p_{2k,0}'d_{0,4}' - p_{2k,2}d_{2,4} - p_{2k,2}'d_{2,4}' &= 0\end{aligned}\right\} \\ &\quad \ldots\quad\ldots\quad\ldots \\ &\quad \ldots\quad\ldots\quad\ldots \\ &\left.\begin{aligned}a_{2k,2k-2} - \sum_{s=0}^{k-1}(p_{2k,2s}b_{2s,2k-2} + p_{2k,2s}'b_{2s,2k-2}') &= 0 \\ c_{2k,2k} - \sum_{s=0}^{k-1}(p_{2k,2s}d_{2s,2k} + p_{2k,2s}'d_{2s,2k}') &= 0\end{aligned}\right\}\end{aligned}\right\} \quad [14]$$

Similarly, $q_{2k,2s}$, $q_{2k,2s}'$, . . . are determined by

$$\left.\begin{aligned}&\left.\begin{aligned}a_{2k,0}' - q_{2k,0}b_{0,0} - q_{2k,0}'b_{0,0}' &= 0 \\ c_{2k,2}' - q_{2k,0}d_{0,2} - q_{2k,0}'d_{0,2}' &= 0\end{aligned}\right\} \\ &\left.\begin{aligned}a_{2k,2}' - q_{2k,0}b_{0,2} - q_{2k,0}'b_{0,2}' - q_{2k,2}b_{2,2} - q_{2k,2}'b_{2,2}' &= 0 \\ c_{2k,4}' - q_{2k,0}d_{0,4} - q_{2k,0}'d_{0,4}' - q_{2k,2}d_{2,4} - q_{2k,2}'d_{2,4}' &= 0\end{aligned}\right\} \\ &\quad \ldots\quad\ldots\quad\ldots \\ &\quad \ldots\quad\ldots\quad\ldots \\ &\left.\begin{aligned}a_{2k,2k-2}' - \sum_{s=0}^{k-1}(q_{2k,2s}b_{2s,2k-2} + q_{2k,2s}'b_{2s,2k-2}') &= 0 \\ c_{2k,2k}' - \sum_{s=0}^{k-1}(q_{2k,2s}d_{2s,2k} + q_{2k,2s}'d_{2s,2k-2}') &= 0\end{aligned}\right\}\end{aligned}\right\} \quad [15]$$

The coefficients $b_{2k,2s}$, $d_{2k,2s}$, . . . are given, for $s \geqslant k$, by

$$\left.\begin{aligned}b_{2k,2s} &= a_{2k,2s} - \sum_{n=0}^{k-1}(p_{2k,2n}b_{2n,2s} + p_{2k,2n}'b_{2n,2s}') \\ b_{2k,2s}' &= a_{2k,2s}' - \sum_{n=0}^{k-1}(q_{2k,2n}b_{2n,2s} + q_{2k,2n}'b_{2n,2s}')\end{aligned}\right\} \quad [16]$$

and, for $s \geqslant k+1$, by

$$\left.\begin{aligned}d_{2k,2s} &= c_{2k,2s} - \sum_{n=0}^{k-1}(p_{2k,2n}d_{2n,2s} + p_{2k,2n}'d_{2n,2s}') \\ d_{2k,2s}' &= c_{2k,2s}' - \sum_{n=0}^{k-1}(q_{2k,2n}d_{2n,2s} + q_{2k,2n}'d_{2n,2s}')\end{aligned}\right\} \quad [17]$$

In the previous paper (1) the required stress function is constructed in the form

$$\chi = \chi_{00} + b^2T\sum_{k=0}^{\infty}(A_{2k}\chi_{2k} + B_{2k}\chi_{2k}') \quad \ldots\ldots [18]$$

Now, by means of the two sets of new functions, it will be constructed in the following form instead

$$\chi = \chi_{00} + b^2T\sum_{k=0}^{\infty}(C_{2k}\omega_{2k} + D_{2k}\omega_{2k}') \quad \ldots\ldots [19]$$

For similar reasons, the factor b^2T is introduced to render the parametric coefficients C_{2k} and D_{2k} dimensionless. Besides, $\widehat{rr_1}$ and $r\widehat{\theta_1}$ at the edge of the lower notch, derived from the basic stress function χ_{00}, will be denoted, in general, between the range $\theta = -\pi/2$ and $\pi/2$, by

$$\widehat{rr}_1 = T\sum_{s=0}^{\infty}{}' b_{2s}\cos 2s\theta, \quad \widehat{r\theta}_1 = T\sum_{s=1}^{\infty} d_{2s}\sin 2s\theta \ldots [20]$$

Note that χ_∞ is here tacitly assumed to be even in x. The boundary condition of no traction at the edge of the lower notch requires that $\widehat{rr}_1 = \widehat{r\theta}_1 = 0$ when derived from χ. It leads to

$$\left.\begin{aligned} &b_0 + C_0 b_{0,0} + D_0 b_{0,0}' = 0\\ &b_2 + C_0 b_{0,2} + D_0 b_{0,2}' + C_2 b_{2,2} + D_2 b_{2,2}' = 0\\ &\qquad\cdots \qquad\cdots \qquad\cdots\\ &b_{2s} + \sum_{k=0}^{s}(C_{2k} b_{2k,2s} + D_{2k} b_{2k,2s}') = 0 \end{aligned}\right\} \ldots [21]$$

and

$$\left.\begin{aligned} &d_2 + C_0 d_{0,2} + D_0 d_{0,2}' = 0\\ &d_4 + C_0 d_{0,4} + D_0 d_{0,4}' + C_2 d_{2,4} + D_2 d_{2,4}' = 0\\ &\qquad\cdots \qquad\cdots \qquad\cdots\\ &d_{2s+2} + \sum_{k=0}^{s}(C_{2k} d_{2k,2s+2} + D_{2k} d_{2k,2s+2}') = 0 \end{aligned}\right\} \ldots [22]$$

The parametric coefficients C_{2k} and D_{2k} can now be determined successively pair by pair.

It is noted that the foregoing process, as it stands, is applicable to cases in which the strip is notched symmetrically by two semi-circular notches of equal radii under the action of a basic stress function which is even in x but may be either even or odd in y. For, in such cases, the boundary condition of no traction at the edge of the upper notch will be satisfied automatically if the same condition at the edge of the lower notch is satisfied.

It is noted further that by this process additional parametric coefficients, if required, can be computed without affecting previous computations. This property is sometimes of distinct advantage in numerical computations.

When the parametric coefficients are thus evaluated it is then a straightforward matter to calculate the stress at any point in the strip.

Transverse-Bending Problem

The foregoing process of promotion of rank will be applied to solve the transverse-bending problem for the notched strip as shown in Fig. 1. The basic stress function of an unnotched strip under a constant transverse-bending moment b^2T in the plane of the strip is given by

$$\chi_\infty = -\frac{1}{4}Tb^2y^3 \ldots [23]$$

Note that this stress system is even in x but odd in y. The two sets of biharmonic functions χ_{2k}, χ_{2k}', which possess such properties can be derived from the Howland (4) integrals χ_2 and χ_3 by a similar process as described in the previous paper (1). The functions thus obtained are shown in the following, each of which gives no stress at infinity and also no normal or tangential stresses along both edges of the strip, except at the centers of the notches $(0, \pm 1)$ which are singularities. For $k \geqslant 0$

$$\chi_{2k} = 2\int_0^\infty m^{2k}\frac{my\cosh my - (1 + m\tanh m)\sinh my}{\sinh 2m - 2m}\cosh m\cos mx\,dm$$

$$= \int_0^\infty m^{2k}(1 + m\eta)e^{-m\eta}\cos mx\,dm - \int_0^\infty m^{2k}\frac{2m\sinh m\eta - 2m^2\eta e^{-m\eta} + (1 + e^{-2m})(\sinh m\eta - m\eta\cosh m\eta)}{\sinh 2m - 2m}\times \cos mx\,dm \ldots [24]$$

$$\chi_{2k}' = 2\int_0^\infty m^{2k}\frac{y\cosh my - \coth m\sinh my}{\sinh 2m - 2m}\times \sinh m\cos mx\,dm$$

$$= \int_0^\infty m^{2k}\eta e^{-m\eta}\cos mx\,dm - \int_0^\infty m^{2k}\frac{2\sinh m\eta - 2m\eta e^{-m\eta} - \eta(1 - e^{-2m})\sinh m\eta}{\sinh 2m - 2m}\times \cos mx\,dm \ldots [25]$$

where $\eta = 1 + y$ as defined in Equation [1]. It is not difficult to show that these functions can be expressed in terms of the polar co-ordinates as follows: for $k \geqslant 0$

$$\chi_{2k} = \frac{(2k+3)\cos(2k+1)\theta}{(2k+1)r^{2k+1}} + \frac{\cos(2k+3)\theta}{r^{2k+1}} - \sum_{n=1}^{\infty}\left({}^{n}\alpha_{2k}r^{2n}\cos 2n\theta - \frac{2n-1}{2n+1}{}^{n+1}\alpha_{2k}r^{2n+1}\cos(2n+1)\theta\right) - \sum_{n=0}^{\infty}({}^{n+2}\alpha_{2k}r^{2n+2}\cos 2n\theta - {}^{n+1}\alpha_{2k}r^{2n+2}\cos(2n+1)\theta) \ldots [26]$$

$$\chi_{2k}' = \frac{\cos 2k\theta}{r^{2k}} + \frac{\cos(2k+2)\theta}{r^{2k}} - \left(\begin{matrix}\text{four similar series in which}\\ {}^{n}\alpha_{2k}\text{ is replaced by }{}^{n}\beta_{2k}\end{matrix}\right) \ldots [27]$$

where, for $n \geqslant 1$

$$\left.\begin{aligned} {}^{n}\alpha_{2k} &= \binom{2n+2k}{2k+1}\frac{(2n+2k+1)I_{2n+2k+1}}{2^{2n+2k}}\\ {}^{n+1}\alpha_{2k} &= \binom{2n+2k+1}{2k+1}\times\frac{(2n+2k+2)I_{2n+2k+2} + I_{2n+2k+1} + J_{2n+2k+1}}{2^{2n+2k+1}}\\ {}^{n}\beta_{2k} &= \binom{2n+2k-1}{2k}\times\frac{(2n+2k)I_{2n+2k} - I_{2n+2k-1} + J_{2n+2k-1}}{2^{2n+2k-1}}\\ {}^{n+1}\beta_{2k} &= \binom{2n+2k}{2k}\frac{(2n+2k+1)I_{2n+2k+1}}{2^{2n+2k}} \end{aligned}\right\} \ldots [28]$$

in which, for $s \geq 3$

$$I_s = \frac{2^s}{s!}\int_0^\infty \frac{m^s dm}{\sinh 2m - 2m} = \frac{1}{2(s!)}\int_0^\infty \frac{m^s dm}{\sinh m - m}$$
$$J_s = \frac{2^s}{s!}\int_0^\infty \frac{m^s e^{-2m} dm}{\sinh 2m - 2m} = \frac{1}{2(s!)}\int_0^\infty \frac{m^s e^{-m} dm}{\sinh m - m} \quad \ldots [29]$$

While for $s \leq 2$, special definitions are needed for the integrals in ${}^2\beta_0$

$$I_1 = 2\int_0^\infty \left[\frac{m}{\sinh 2m - 2m} - \frac{3(1+m)}{4m^2}e^{-m}\right] dm$$
$$I_2 = 2\int_0^\infty \left[\frac{m^2}{\sinh 2m - 2m} - \frac{3}{4m}e^{-m}\right] dm \quad \ldots [30]$$
$$J_1 = 2\int_0^\infty \left[\frac{me^{-2m}}{\sinh 2m - 2m} - \frac{3(1-m)e^{-m}}{4m^2}\right] dm$$

Here, for the sake of simplicity, the factors $(2k+1)!/2$ and $(2k)!/2$ have been removed from χ_{2k} and χ_{2k}', respectively.

By using the well-known formulas for the stresses in terms of the stress function $\widehat{rr_1}$ and $\widehat{r\theta_1}$ at the edge of the lower notch, $r = \lambda$, are readily derived from χ_{2k} and χ_{2k}'. They are then expanded into Fourier series between $\theta = -\pi/2$ and $\pi/2$ as required by the range of the notch. The factors $(2k+2)/\lambda^{2k+2}$ and $(2k+1)/\lambda^{2k+2}$ are further removed from χ_{2k} and χ_{2k}', respectively. By comparing the resulting expansions with Equations [2] and [3], we have, for $s \geq 1$

$$a_{2k,2s} = 2s\,{}^{2s}\alpha_{2k}' + (2s-2)\,{}^{2s+2}\alpha_{2k}'$$
$$- \frac{16(-1)^{k+s}(2k+3)(4s^2+2k+1)}{\pi[(2k+2s+2)^2-1][(2k-2s+2)^2-1]}$$
$$+ \frac{16}{\pi}\sum_{n=1}^{\infty}\frac{(-1)^{n+s}(2n-1)(4s^2-2n-1)}{[(2n+2s)^2-1][(2n-2s)^2-1]}\,{}^{2n+1}\alpha_{2k}'$$
$$e_{2k,2s} = -2s\,({}^{2s}\alpha_{2k}' + {}^{2s+2}\alpha_{2k}')$$
$$- \frac{16(-1)^{k+s}2s(2k+2)(2k+3)}{\pi[(2k+2s+2)^2-1][(2k-2s+2)^2-1]}$$
$$- \frac{16}{\pi}\sum_{n=1}^{\infty}\frac{(-1)^{n+s}2s(2n-1)2n}{[(2n+2s)^2-1][(2n-2s)^2-1]}\,{}^{2n+1}\alpha_{2k}' \quad \ldots [31]$$
$$a_{2k,2s}' = -2k\delta_{k,s} - (2k+4)\,\delta_{k+1,s}$$
$$+ 2s\,{}^{2s}\beta_{2k}' + (2s-2)\,{}^{2s+2}\beta_{2k}'$$
$$+ \frac{16}{\pi}\sum_{n=1}^{\infty}\frac{(-1)^{n+s}(2n-1)(4s^2-2n-1)}{[(2n+2s)^2-1][(2n-2s)^2-1]}\,{}^{2n+1}\beta_{2k}'$$
$$e_{2k,2s}' = -2k\delta_{k,s} - (2k+2)\,\delta_{k+1,s} - 2s\,({}^{2s}\beta_{2k}' + {}^{2s+2}\beta_{2k}')$$
$$- \frac{16}{\pi}\sum_{n=1}^{\infty}\frac{(-1)^{n+s}2s(2n-1)2n}{[(2n+2s)^2-1][(2n-2s)^2-1]}\,{}^{2n+1}\beta_{2k}'$$

and in particular, for $s = 0$

$$a_{2k,0} = -2\,{}^2\alpha_{2k}' - \frac{8(-1)^k}{\pi(2k+1)(2k+3)}$$
$$- \frac{8}{\pi}\sum_{n=1}^{\infty}\frac{(-1)^n}{4n^2-1}\,{}^{2n+1}\alpha_{2k}'$$
$$a_{2k,0}' = -2\,{}^2\beta_{2k}' - \frac{8}{\pi}\sum_{n=1}^{\infty}\frac{(-1)^n}{4n^2-1}\,{}^{2n+1}\beta_{2k}'$$

where $\delta_{k,s} = 1$ or 0, according as $k = s$, or $k \neq s$; and

$${}^n\alpha_{2k}' = \frac{n-1}{2k+2}\,{}^n\alpha_{2k}\lambda^{n+2k+1},\quad {}^n\beta_{2k}' = \frac{n-1}{2k+1}\,{}^n\beta_{2k}\lambda^{n+2k} \quad \ldots [32]$$

Table 1 reproduces the values of I_s and J_s which were computed by Howland (5). Their asymptotic values are

$$I_s = 1,\quad J_s = \frac{1}{2^{s+1}} \quad \ldots [33]$$

As shown in the Table, I_s agrees with the asymptotic value when $s > 20$, and J_s becomes negligible in comparison with I_s when $s > 15$. With these values, ${}^n\alpha_{2k}$ and ${}^n\beta_{2k}$ can be computed readily. There is then no difficulty in calculating $a_{2k,2s}$, $c_{2k,2s}$, $a_{2k,2s}'$, $c_{2k,2s}$ by Equations [31] for any given value of λ.

TABLE 1 VALUES OF I_s AND J_s

s	I_s	J_s
1	0.32084	0.43608
2	1.66676	...
3	2.03867	0.46072
4	1.35327	...
5	1.15685	0.03242
6	1.07671	...
7	1.03924	0.00539
8	1.02051	...
9	1.01086	0.00114
10	1.00577	...
11	1.00310	0.00026
12	1.00168	...
13	1.00088	0.00006
14	1.00046	...
15	1.00025	0.00002
16	1.00013	...
17	1.00007	0.00000
18	1.00004	...
19	1.00002	0.00000
20	1.00001	...

Two different values of λ will be investigated, namely, $\lambda = 1/4$ and $1/2$. The next step is to form two sets of new functions ω_{2k}, ω_{2k}' by finding successively $p_{2k,2s}$, $p_{2k,2s}'$, $q_{2k,2s}$, $q_{2k,2s}'$ and then $b_{2k,2s}$, $b_{2k,2s}'$, $d_{2k,2s}$, $d_{2k,2s}'$. The coefficients b_{2s}, d_{2s} shown in the following are obtained by expanding $\widehat{rr_1}$ and $\widehat{r\theta_1}$ derived from χ_{00} in Equation [23] into Fourier series in the range $\theta = -\pi/2$ and $\pi/2$. For $s \geq 1$

$$b_{2s} = -\frac{3}{4}\delta_{1,s} + \frac{6(-1)^s(4s^2-3)\lambda}{\pi(4s^2-1)(4s^2-9)}$$
$$d_{2s} = \frac{3}{4}\delta_{1,s} - \frac{12(-1)^s 2s\lambda}{\pi(4s^2-1)(4s^2-9)} \quad \ldots [34]$$

and, in particular, for $s = 0$

$$b_0 = \frac{3}{4} - \frac{\lambda}{\pi}$$

For the sake of brevity, only the values of the coefficients in the case $\lambda = 1/2$ will be shown in Table 2 for reference. The coefficients C_{2k}, D_{2k} now can be determined successively pair by pair from Equations [21] and [22] without difficulty. Table 3 shows these results, together with those in the limiting case $\lambda = 0$.

When T is positive, the maximum tensile stress occurs at the "crown" of the lower notch, i.e., at the point $(r, \theta) = (\lambda, 0)$, while the maximum compressive stress occurs at the crown of the upper notch. They are numerically equal in the present symmetrical case.

By virtue of the boundary condition $\widehat{rr_1} = 0$, the stress $\widehat{\theta\theta_1}$ along the edge of the notch may be computed from the sum $(\widehat{rr_1} + \widehat{\theta\theta_1})$. The contributions from various functions to the maximum stress $\widehat{\theta\theta}_m$ which occurs at the crown of the lower notch are thus given by the following:

TABLE 2 VARIOUS COEFFICIENTS IN THE CASE $\lambda = 1/4$

$2s$	$2k = 0$	$2k = 2$	$2k = 4$	$2k = 6$	$2k = 8$	$2k = 10$	$2k = 12$
			Coefficient $a_{2k,2s}$				
0	—1.07960	0.16153	—0.07312	0.04041	—0.02572	0.01781	—0.01306
2	—4.76868	—1.68016	0.34085	—0.14541	0.08085	—0.05144	0.03562
4	—2.39699	—7.65687	—2.51728	0.49191	—0.20516	0.11128	—0.06928
6	0.62763	—3.33721	—10.21996	—3.36890	0.65913	—0.27526	0.14892
8	—0.29128	0.79711	—4.20437	—12.76222	—4.22046	0.82969	—0.34796
10	0.17629	—0.38415	0.97871	—5.06139	—15.30440	—5.07186	1.00088
12	—0.11807	0.23310	—0.46982	1.15646	—5.91541	—17.84750	—5.92292
			Coefficient $a_{2k,2s}'$				
0	—0.54503	—0.02432	—0.00126	—0.00005	0.00000	0.00000	0.00000
2	—3.26142	—1.95312	0.00387	0.00032	0.00002	0.00000	0.00000
4	0.01997	—5.95943	—3.99269	0.00109	0.00013	0.00001	0.00001
6	0.05175	0.01012	—7.99712	—5.99938	0.00011	0.00001	0.00000
8	—0.01978	0.00160	0.00097	—9.99974	—7.99995	0.00000	0.00000
10	0.01391	0.00048	0.00007	0.00005	—11.99998	—10.00000	0.00000
12	—0.00954	—0.00016	0.00008	0.00002	0.00001	—14.00000	—12.00000
			Coefficient $c_{2k,2s}$				
2	—4.29864	—1.95338	0.45157	—0.21175	0.12436	—0.08231	0.05866
4	—1.25986	—6.48933	—2.88403	0.68344	—0.32838	0.19782	—0.13379
6	0.17655	—2.06410	—8.97658	—3.76124	0.87874	—0.42168	0.25528
8	—0.07269	0.37815	—2.92573	—11.50423	—4.62521	1.06199	—0.50613
10	0.03345	—0.14936	0.55913	—3.78428	—14.04075	—5.48311	1.24002
12	—0.01889	0.07598	—0.22708	0.73523	—4.63956	—16.58080	—6.33790
14	0.01163	—0.04455	0.11913	—0.30368	0.90935	—5.49285	—19.12299
			Coefficient $c_{2k,2s}'$				
2	—2.47185	—2.03114	—0.00297	—0.00028	—0.00002	0.00000	0.00000
4	—0.07729	—4.04054	—4.00725	—0.00097	—0.00011	—0.00001	0.00000
6	—0.02048	—0.00868	—6.00287	—6.00062	—0.00011	—0.00001	0.00000
8	0.00156	—0.00223	—0.00089	—8.00024	—8.00005	—0.00001	0.00000
10	—0.00184	—0.00003	—0.00012	—0.00006	—10.00001	—10.00000	0.00000
12	0.00098	—0.00015	—0.00005	—0.00002	—0.00001	—12.00000	—12.00000
14	—0.00064	+0.00007	+0.00001	0.00000	0.00000	0.00000	—14.00000
			Coefficient $p_{2k,2s}$				
0	1	—4.49444	1.31051	—0.66100	0.40329	—0.27287	0.19726
2	0	1	3.96956	—1.32120	0.72930	—0.47341	0.33479
4	0	0	1	2.44249	—0.85383	0.49280	—0.33084
6	0	0	0	1	2.10502	—0.75907	0.45075
8	0	0	0	0	1	1.95212	—0.71904
10	0	0	0	0	0	1	1.86234
12	0	0	0	0	0	0	1
			Coefficient $p_{2k,2s}'$				
0	0	8.60626	—2.46172	1.23517	—0.75163	0.50786	—0.36679
2	0	0	—5.81655	2.00542	—1.11908	0.73009	—0.51775
4	0	0	0	—3.31924	1.24476	—0.73517	0.49886
6	0	0	0	0	—2.76190	1.08764	—0.66450
8	0	0	0	0	0	—2.53636	1.03353
10	0	0	0	0	0	0	—2.41213
12	0	0	0	0	0	0	0
			Coefficient $q_{2k,2s}$				
0	0	—3.21414	0.00457	—0.00009	—0.00003	0.00000	0.00000
2	0	0	3.57693	—0.00955	—0.00002	0.00001	0.00000
4	0	0	0	2.47414	0.00004	—0.00001	0.00000
6	0	0	0	0	—2.26836	0.00002	0.00000
8	0	0	0	0	0	2.18651	0.00000
10	0	0	0	0	0	0	2.14275
12	0	0	0	0	0	0	0
			Coefficient $q_{2k,2s}'$				
0	1	6.41127	—0.00678	0.00028	0.00006	0.00000	0.00000
2	0	1	—4.88315	0.00097	0.00004	—0.00001	0.00000
4	0	0	1	—2.94774	—0.00009	0.00000	0.00000
6	0	0	0	1	—2.53191	—0.00006	0.00000
8	0	0	0	0	1	—2.36893	0.00000
10	0	0	0	0	0	1	—2.28169
12	0	0	0	0	0	0	1

(Continued on page 6)

Function	Contribution to $\widehat{\theta\theta}_m$
χ_∞/T	$3(1-\lambda)/2$
$b^2\chi_{2k}$	$-4-4\sum_{n=1}^{\infty}(^{2n}\alpha_{2k}' - {}^{2n+1}\alpha_{2k}')$
$b^2\chi_{2k}'$	$-4-4\sum_{n=1}^{\infty}(^{2n}\beta_{2k}' - {}^{2n+1}\beta_{2k}')$

Consequently, by Equations [11], the contributions from ω_{2k} and ω_{2k}' are readily computed. Table 4 shows such contributions from $(C_{2k}\omega_{2k} + D_{2k}\omega_{2k}')$. The convergence of the values in each case is clearly indicated. The resulting maximum stresses are thus as follows

λ	$1/2$	$1/4$	0
$\widehat{\theta\theta}_m$:	8.06	4.87	4.60

Now, let K be the stress-concentration factor of the notched strip under transverse bending. This factor is here defined as the ratio of the maximum stress at the minimum section of the strip to the stress at the same point in a uniform strip of the same width as the minimum section, the strip being under the same transverse bending moment; thus

$$K = \frac{2(1-\lambda)^2}{3}\widehat{\theta\theta}_m \qquad [35]$$

The following results are obtained

λ:	0,	$1/4$,	$1/2$,	1
K:	3.07	1.83	1.34	1

It appears that this factor decreases with increase of λ and becomes unity as λ tends to unity. The limiting value at $\lambda = 1$ can be visualized readily from physical consideration of the strip.

TABLE 2 (*continued*)

$2s$	$2k = 0$	$2k = 2$	$2k = 4$	$2k = 6$	$2k = 8$	$2k = 10$	$2k = 12$
			Coefficient $b_{2k,2s}$				
0	−1.07960	...	...	...	...	...	...
2	−4.76868	4.95592	...	...	...	...	...
4	−2.39699	−18.60187	−5.70583	...	...	...	...
6	0.62763	−0.96173	2.76527	−2.09422	...	...	...
8	−0.29128	−0.34180	−7.21314	−3.17175	−1.33946	...	...
10	0.17629	0.28846	2.41671	−7.12279	−5.52370	−0.99168	...
12	−0.11807	−0.21546	−1.33580	2.10470	−7.92352	−7.40310	−0.78937
			Coefficient $b_{2k,2s}'$				
0	−0.54503	...	...	...	...	...	...
2	−3.26142	3.62951	...	...	...	...	...
4	0.01997	−13.79172	−4.79045	...	...	...	...
6	0.05175	1.69563	3.72042	−1.87634	...	...	...
8	−0.01978	−0.80780	−2.71985	−0.17026	−1.23630	...	...
10	0.01391	0.47792	1.30131	−2.14359	−1.25029	−0.93133	...
12	−0.00954	−0.31849	−0.78398	0.99419	−2.25702	−2.02185	−0.75006
			Coefficient $d_{2k,2s}$				
2	−4.29864	...	...	...	...	...	...
4	−1.25986	−11.48652	...	...	...	...	...
6	0.17655	−1.09435	−0.90040	...	...	...	...
8	−0.07269	0.03802	−4.40767	−4.68357	...	...	...
10	0.03345	0.01682	1.13779	−5.02322	−6.56414	...	...
12	−0.01889	−0.01735	−0.52162	1.22510	−5.98644	−8.21121	...
14	0.01163	0.01323	0.29147	−0.55672	1.44263	−6.97985	−9.78817
			Coefficient $d_{2k,2s}'$				
2	−2.47185	...	...	...	...	...	...
4	−0.07729	−7.59438	...	...	...	...	...
6	−0.02048	0.69008	1.28035	...	...	...	...
8	0.00156	−0.24587	−1.33716	−1.03640	...	...	...
10	−0.00184	0.11928	0.52202	−1.27644	−1.83737	...	...
12	0.00098	−0.06715	−0.26579	0.50712	−1.49496	−2.45205	...
14	−0.00064	0.04155	0.15553	−0.26271	0.59768	−1.73846	−3.01040

TABLE 3 VALUES OF C_{2k} AND D_{2k}

	$\lambda = 1/2$		$\lambda = 1/4$		$\lambda = 0$	
$2k$	C_{2k}	D_{2k}	C_{2k}	D_{2k}	C_{2k}	D_{2k}
0	3.6550	−6.1558	1.1200	−1.8426	0.8836	−1.4250
2	−0.0887	−0.4191	−0.0693	−0.1953	−0.1156	−0.0636
4	0.0967	−0.3939	0.0616	−0.2301	0.0726	−0.2671
6	−0.0411	0.1090	−0.0421	0.1243	−0.0403	0.1134
8	0.0354	−0.0960	0.0270	−0.0691	0.0230	−0.0560
10	−0.0235	0.0562	−0.0173	0.0399	−0.0136	0.0295
12	0.0163	−0.0364	0.0112	−0.0237	0.0081	−0.0159

TABLE 4 CONTRIBUTION TO $\widehat{\omega\theta}_m$ FROM $(C_{2k}\omega_{2k} + D_{2k}\omega_{2k}')$

$2k$	$\lambda = \frac{1}{2}$	$\lambda = \frac{1}{4}$	$\lambda = 0$
0	11.867	3.302	2.166
2	−5.890	−0.371	−0.082
4	1.460	0.984	1.163
6	−0.191	−0.218	−0.188
8	0.095	0.067	0.051
10	−0.037	−0.023	−0.015
12	0.013	0.007	0.003

The other limiting value 3.07 at $\lambda = 0$ agrees with the corresponding value in the tension problem. Fig. 2 shows the results graphically, where the experimental values available are also plotted for comparison (6, 7).

Acknowledgment

The author wishes to thank Mr. C. P. Tsai for his help in performing the numerical computations.

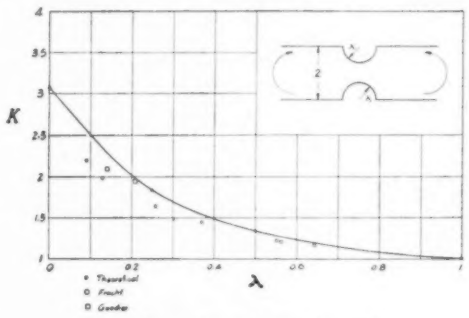

FIG. 2 STRESS-CONCENTRATION FACTOR K

BIBLIOGRAPHY

1 "Stresses in a Notches Strip Under Tension," by C. B. Ling, JOURNAL OF APPLIED MECHANICS, Trans. ASME, vol. 69, 1947, pp. A-275–280.

2 "Biharmonic Analysis, Especially in a Rectangle, and Its Applications to the Theory of Elasticity," by A. E. H. Love, Proceedings of the London Mathematical Society, Series 2, vol. 29, 1929, pp. 189–242. An abstract of lecture under the same title is also in the *Journal of the London Mathematical Society*, vol. 3, 1928, pp. 144–156.

3 "Electrostatic Problems Related to a Perforated Strip," by A. E. H. Love, *Quarterly Journal of Mathematics*, Oxford Series, vol. 9, 1938, pp. 246–258.

4 "Stress Systems in an Infinite Strip," by R. C. J. Howland, Proceedings of the Royal Society of London, vol. 124, 1929, pp. 89–119.

5 "Biharmonic Analysis in a Perforated Strip," by R. C. J. Howland and A. C. Stevenson, *Philosophical Transactions*, vol. 232, 1934, pp. 155–222.

6 "Factors of Stress Concentration Photoelastically Determined," by M. M. Frocht, JOURNAL OF APPLIED MECHANICS, Trans. ASME, vol. 57, 1935, p. A-67.

7 "An Extension of the Photoelastic Method of Stress Measurement to Plates in Transverse Bending," by J. N. Goodier, JOURNAL OF APPLIED MECHANICS, Trans. ASME, vol. 63, 1941, pp. A-27–29.

An Alternative Formulation of the Laws of Mechanics

By H. M. TRENT,[1] WASHINGTON, D. C.

The author proposes a set of laws of mechanics which are duals of those of Newton. These laws are based upon the concept of the continuity of transmitted forces around closed loops. They are particularly useful in those engineering problems where only knowledge of forces is of interest, since the laws lead directly to equations in which forces are the dependent variables.

TWO hundred and sixty-three years have elapsed since Newton enunciated his celebrated laws of motion. During this time, many of the world's greatest scientists have studied the consequences of these laws and have applied them to innumerable macroscopic systems. In view of these well-known facts it may seem heresy to suggest that the laws of mechanics can be formulated in an alternative fashion. On the other hand, as will be seen, the proposed reformulation makes use of hints appearing in books and articles by a number of writers in the field of mechanics, among whom may be mentioned D'Alembert, Appell, and Firestone. Such a reformulation seems worth attempting for two practical reasons: (*a*) because dynamical equations formulated in a different order can be particularly useful in the engineering sciences, and (*b*) because a new point of view on an old subject helps to clear up obscure points.

Newtonian Mechanics

It is well known that Newton's laws in the usually stated form, due actually to Euler, apply to the dynamics of particles; a particle being defined as a body in which rotations and deformations are insignificant in the problem under consideration. Studies of the invariant properties of the laws show that if they are valid for one set of reference axes, they are valid for a second set of axes if, and only if, there is no relative acceleration between the two sets. Hence Newton's laws are valid only for a very special set of reference axes which are often called "inertial axes." The demonstration that any given choice of reference axes is indeed inertial presents one of the most difficult problems in Newtonian mechanics even to this day. Be that as it may, any acceleration of a particle measured relative to a set of inertial axes is called an "absolute acceleration." This concept of an absolute acceleration plays a principal role in the laws of classical mechanics.

Let a mechanical system be defined as a collection of particles which, in general, interact on each other. We admit the possibility that excitations may be applied to the system by external devices. One of the great triumphs of Newtonian mechanics is that the absolute motions of the particles within a system can be computed from only a knowledge of the externally applied forces and the nature of the interactions. On the other hand, if a knowledge of the internal forces is desired, the motions of each particle either must be computed or be known by some other means. Since, in many practical cases, a knowledge of internal forces is of primary interest, it seems unfortunate that these forces cannot be calculated directly from a knowledge of external excitations and the natures of interactions. This deficiency will be removed by the methods presented in the following discussion.

Newton's laws are nodal in character since they specify what happens at a point in the system. This characteristic is most easily understood in terms of D'Alembert's principle. Let a particle of mass m be acted on by n-forces, f_1, f_2, f_3, $-f_n$. Then by the second law of motion

$$\sum_{i=1}^{n} f_i = ma \qquad [1]$$

where a is the absolute acceleration of the particle.

With D'Alembert, define a force f_I so that $f_I = -ma$. We have then

$$\sum_{i=1}^{n} f_i + f_I = 0 \qquad [2]$$

The force f_I, is usually called an "inertial force" and we have the principle, due to D'Alembert, that the sum of all forces including the inertial force acting on a particle (point) is equal to zero. Applications of this principle are so well known that they need no further comment. The important point is the analogy between this principle and Kirchhoff's current law which may be written: the sum of all currents entering a junction point is zero.

Let us pursue this analogy further. Those familiar with modern electric network analysis are aware that a knowledge of the applied excitations and the nature of each element in a system together with Kirchhoff's current law is sufficient for an analysis of the network. This so-called nodal analysis yields a set of simultaneous equations in which voltage drops are the dependent variables. Should a knowledge of the currents flowing through elements be desired, a second calculation must be made. Suppose, however, primary interest centers on the currents flowing through elements. Is it necessary first to compute voltage drops? The answer is "no," for there is an alternative procedure—the "mesh analysis." In this kind of analysis use is made of Kirchhoff's voltage law which states that the sum of the voltage drops around any closed path is equal to zero. This is a circuital concept and one which focuses attention on the continuity of currents in a network. Dependent variables are now circuital currents and voltage drops are computed, if at all, as a second step. The important point for our purpose is that a shift from a nodal to a circuital basis actually changes the nature of the dependent variables used in the formulation.

Returning to the mechanical system, we ask ourselves, by analogy, the following question, "If we shift from Newton's laws, which are nodal in character, to a circuital basis, will the order in which motion and forces are computed be reversed?"

---

[1] Head, Applied Mathematics Branch, Mechanics Division, Naval Research Laboratory.

Contributed by the Applied Mechanics Division and presented at the Annual Meeting, Atlantic City, N. J., November 25-30, 1951, of The American Society of Mechanical Engineers.

Discussion of this paper should be addressed to the Secretary, ASME, 29 West 39th Street, New York, N. Y., and will be accepted until July 10, 1952, for publication at a later date. Discussion received after the closing date will be returned.

Note: Statements and opinions advanced in papers are to be understood as individual expressions of their authors and not those of the Society. Manuscript received by ASME Applied Mechanics Division, February 5, 1951. Paper No. 51—A-30.

The answer is "yes," as will be explained in the remainder of this paper.

Circuital Formulation of Mechanics

The concept of force, rather than that of absolute acceleration, plays a principal role in a circuital formulation of mechanics. The dynamical properties of a particle, or any interaction between particles, shall be specified in terms of its ability to transmit a force. As an example of an interaction, consider an idealized spring, i.e., one having negligible mass, which need not be linear. If an external force f_A pushes on the left end of a horizontal spring, we can expect the right end to exert an equal push f_T in the same direction on another element. It is natural to call the first of these an "applied" and the other a "transmitted" force. We have then

$$f_A = f_T \quad [3]$$

a statement that forces are transmitted unchanged through an idealized spring. We see that the function of a spring, or indeed of any interaction, is to transmit a force unchanged. The relative motion between the ends of the spring can be expressed in terms of the magnitude of the transmitted force. For example, consider a simple linear spring and let r_1, r_2 be the positions of its ends. From the well-known properties of a spring, we have

$$\frac{dr_1}{dt} - \frac{dr_2}{dt} = \epsilon \frac{df}{dt} \quad [4]$$

where ϵ is the compressibility of the spring. The ability to express the relative motion between the terminals of any interaction in terms of the transmitted force is basic to the circuital method.

Consider next the ability of a particle to transmit a force. For simplicity, assume that the particle is acted on by a push from the left f_1, and that it transmits a push to the right f_2, on another element. It is clear that

$$f_1 - f_2 = ma \quad [5]$$

Here, f_1 can be called an applied and f_2 a transmitted force. Conventionally, we would say that the applied force is equal to the transmitted force only if the particle has no absolute acceleration. However, in analogy with the assumption of D'Alembert, let us postulate that ma is equivalent to a force f_D, which we shall call the "D'Alembert force." Equation [5] then becomes

$$f_1 = f_2 + f_D \quad [6]$$

and if f_D is taken as a transmitted force, we again have a principle of the continuity of forces.

Hereafter, it will be assumed that the D'Alembert force is a real transmitted force. It has one quality analogous to that of a Maxwell displacement current; it assures the continuity of forces through a particle just as the displacement current assures continuity of current through a condenser.

There is one essential difference between the forces f_2 and f_D in Equation [6]. Conceptually at least, f_2 is measurable by a dynamometer, but f_D is not. Its existence can be inferred only from other observations.

One additional continuity idea is necessary to complete the picture. Consider a system of n-particles with interactions between pairs of particles. Let there be $m (m \leqslant n)$ external forces applied to the system, and let F_i represent one of these forces. It is well known that

$$\sum_{K=1}^{n} m_K a_K = \sum_{i=1}^{m} F_i \quad [7]$$

The left-hand side of this equation is simply the sum of the D'Alembert forces. If it is assumed that Equation [7] is another expression of the continuity of forces, and if the D'Alembert forces are considered as applied forces, then the relation implies that the D'Alembert forces are applied to some point and that the external forces are transmitted away from the same point. In other words, the D'Alembert forces all join at a common point and then divide to form the external forces, F_i. This interpretation is consistent with the mechanics of the situation and hence may be employed without error in all further considerations.

We now give a simple interpretation of the point where the D'Alembert forces join. Let this point be called O. It was stated before that the force transmitted by an interaction can be expressed in terms of the relative velocity between its terminals, Equation [4], for example. In like fashion, we shall express any D'Alembert force in terms of the relative velocity between the particle from which it originates and the point O where it terminates. We have

$$f_D = ma \quad [8]$$

If this equation is integrated with respect to time, there results

$$v = \frac{1}{m} \int f_D \, dt + C \quad [9]$$

Let us identify the constant C with the velocity of the point O and call it v_o. Then

$$v - v_o = \frac{1}{m} \int f_D \, dt \quad [10]$$

Clearly, the point O is associated with an inertial reference since a in Equation [8] is an absolute acceleration. It will be shown later by an example that this point need not be identified physically; it is necessary only to postulate its existence and include it in any schematic representation of the system. The foregoing discussion shows that a particle is really a two-terminal device like a spring on a dashpot. One terminal is physically at the particle and is accessible for physical connections. The other terminal is at an inertial reference but is inaccessible, and the D'Alembert force is transmitted from one terminal to the other.

Applying the Theory

We now seek to incorporate the foregoing ideas into a set of assumptions and postulates which will yield a circuital type of mechanics. The principal concept used in this formulation is the ability of an interaction or a particle to transmit a force in a specified direction. It will be assumed that all forces, with the exception of D'Alembert forces, are measurable—at least conceptually. Three postulates are now stated as follows:

1 Any measurable force transmitted by a particle is equal to that applied unless the particle has an absolute acceleration.

2 The excess of the measurable force applied to a particle over that transmitted is proportional to the absolute acceleration of the particle and in the same direction.

3 In any system, forces are transmitted continuously around closed circuits.

The first two postulates are obvious duals of Newton's first two laws of motion. They could be stated in other ways; the form used has been selected in order to bring out this duality. The first postulate furnishes an answer to the old problem of whether a given choice of axes is indeed inertial or not. The second postulate leads directly to a definition of the D'Alembert force which serves to maintain continuity of forces through a particle. The

third postulate brings out the circuital nature of the formulation.

In order to analyze any system, it is necessary to have three additional items of information: (*a*) It is necessary to know the nature of any excitations applied to the system. Typical cases are generators which specify either a transmitted force or a relative motion. (*b*) It must be possible to express the relative motion across any interaction in terms of the transmitted force. As pointed out before, the velocity of a particle relative to inertial co-ordinates always can be specified in terms of the D'Alembert force. (*c*) The kinematic necessity that any sum of cyclic relative velocities around a closed loop is equal to zero must be recognized. This principle, which is analogous to Kirchhoff's voltage law, is basic to the solution of mechanical problems by the circuital method.

In order to show how to obtain a circuital type of formulation, integrodifferential equations for a simple mechanical system will be developed. Consider three rigid bodies which are all moving along the same line, say, the y-axis. Let their positions at any instant be y_1, y_2, and y_3. There is a velocity generator between the first and second body which specifies the motion of the second body relative to the first, $V(t)$. In addition, there is a linear spring and a linear dashpot acting between the second and third body. The bodies, being rigid, will be treated as particles.

The first step in the formulation is to construct a schematic diagram showing the connections between the members of the system. This diagram must show paths for the D'Alembert forces and their union at an inertial reference. It can take the form shown in Fig. 1 where the paths taken by the D'Alembert

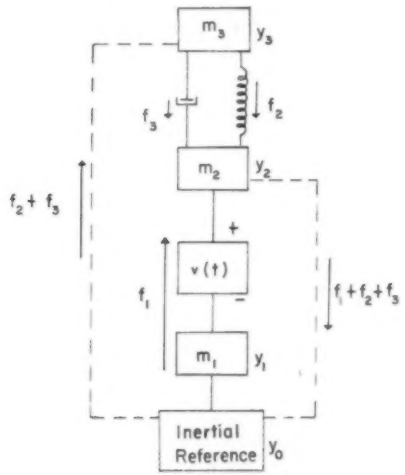

FIG. 1 SCHEMATIC DIAGRAM OF REACTION-TYPE VIBRATION

forces are shown as dotted lines which have been separated for ease in reading the drawing. A practical embodiment of such a system might be a reaction-type vibrator in which m_1 is the eccentric mass, m_2 is the platform being vibrated, $V(t)$ is the prescribed motion of the platform relative to the eccentric mass, and the platform is supported on the earth (m_3) by means of a spring which includes some viscosity.

The diagram contains three geometrically independent loops or meshes, which means that the equations for the system must involve three forces as dependent variables. It is now necessary to select these forces and to assign them to independent closed loops. Such a selection is usually made so that forces of greatest interest appear as unknowns. Let these be (1) the force delivered by the generator to m_2; (2) the force transmitted by the spring to m_2; and (3) the force transmitted by the dashpot. A choice of loops consistent with these interests is indicated in Fig. 1.

The next step in the formulation is to write expressions for the sums of the relative velocities around each loop. These are

$$\left.\begin{aligned}
&\text{Loop 1}\ \left(\frac{dy_1}{dt}-\frac{dy_2}{dt}\right)+\left(\frac{dy_2}{dt}-\frac{dy_s}{dt}\right)+\left(\frac{dy_0}{dt}-\frac{dy_1}{dt}\right)=0\\
&\text{Loop 2}\ \left(\frac{dy_3}{dt}-\frac{dy_2}{dt}\right)+\left(\frac{dy_2}{dt}-\frac{dy_0}{dt}\right)+\left(\frac{dy_0}{dt}-\frac{dy_3}{dt}\right)=0\\
&\text{Loop 3}\ \left(\frac{dy_3}{dt}-\frac{dy_2}{dt}\right)+\left(\frac{dy_2}{dt}-\frac{dy_0}{dt}\right)+\left(\frac{dy_0}{dt}-\frac{dy_3}{dt}\right)=0
\end{aligned}\right\}\quad\ldots[11]$$

As pointed out before, each relative velocity appearing in Equations [11] can be expressed in terms of transmitted forces. These relations are easily seen to be

$$\left.\begin{aligned}
\frac{dy_1}{dt}-\frac{dy_2}{dt}&=-V(t)\\
\frac{dy_2}{dt}-\frac{dy_0}{dt}&=\frac{1}{m_2}\int(f_1+f_2+f_3)dt\\
\frac{dy_0}{dt}-\frac{dy_1}{dt}&=\frac{1}{m_1}\int f_1dt\\
\frac{dy_3}{dt}-\frac{dy_2}{dt}&=\epsilon\frac{df_2}{dt}=Bf_2\\
\frac{dy_0}{dt}-\frac{dy_3}{dt}&=\frac{1}{m_3}\int(f_2+f_3)dt
\end{aligned}\right\}\quad\ldots\ldots[12]$$

where ϵ is the compressibility of the spring and B is the reciprocal of the coefficient of viscosity of the dashpot. If these expressions are substituted in Equations [11] the following dynamical equations are obtained

$$\left.\begin{aligned}
&\left(\frac{1}{m_1}+\frac{1}{m_2}\right)\int f_1dt+\frac{1}{m_2}\int f_2dt+\frac{1}{m_3}\int f_3dt=V(t)\\
&\frac{1}{m_2}\int f_1dt+\epsilon\frac{df_2}{dt}+\left(\frac{1}{m_2}+\frac{1}{m_3}\right)\int f_2dt+\left(\frac{1}{m_2}+\frac{1}{m_3}\right)\int f_3dt=0\\
&\frac{1}{m_2}\int f_1dt+\left(\frac{1}{m_2}+\frac{1}{m_3}\right)\int f_2dt+Bf_2+\left(\frac{1}{m_2}+\frac{1}{m_3}\right)\int f_3dt=0
\end{aligned}\right\}\quad\ldots[13]$$

With a little experience it is easy to go from the schematic diagram directly to equations like Equations [13] by simple inspection.

Conclusion

It is clear that the circuital type of formulation has led directly to dynamical relations involving only excitations and transmitted forces. Again it is emphasized that no direct specifications of an inertial reference are required—only an admission that one exists. Should relative motions be desired, they can be obtained by inserting the values of f_1 and f_2 into Equations [12].

Two remarks are in order in this connection: (1) Any velocity of a particle relative to the inertial reference can be computed only to within an additive constant since the initial values of the indefinite integrals are not known in general. On the other hand, absolute accelerations can be computed exactly, and if observed values of acceleration with respect to arbitrarily selected co-ordinates do not agree with the computed values, then indeed the co-ordinates selected are not inertial. (2) The computed values of any relative velocity across an interaction will be observed in practice if it is referred to co-ordinates which are not rotating. This is a much less restrictive requirement.

In conclusion, then, there are alternative ways in which a mechanical system can be analyzed—one based on Newton's laws, which leads naturally to equations in kinematical variables, the other, a circuital type of analysis which leads to equations in force variables. The most efficient one to use in any given case depends upon the nature of the system and on the results desired. It does appear that the circuital method is the natural one to use when interest is focused primarily on internal forces.

A Variational Principle for the Mesh-Type Analysis of a Mechanical System

By R. A. TOUPIN,[1] WASHINGTON, D. C.

The mesh-type equations for a dynamical system consisting of *N*-mass points are derived from the Newtonian form of the equations of motion. The appropriate Lagrangian for a variational principle is established for these equations.

As pointed out by Trent,[2] there are alternative methods of analyzing a mechanical system. Frequently the interest is primarily in the solution for the internal forces of a mechanical system, the actual motion of the components being of secondary concern. The usual procedure, however, is to solve the problem first for the detailed motion of the system and then to compute the internal forces by means of some functional relation between the kinematical variables and the internal forces of the system. The Newtonian formulation of the equations of motion leads directly to this procedure. It is possible, however, to derive a set of equations, sufficient in number, to determine the internal forces directly without recourse to the kinematical solution. These equations follow from the Newtonian form of the equations of motion. Further, it is possible to give an analytical development of the new system quite analogous to the ordinary exposition in analytical mechanics.

The Mesh Equations

Consider a dynamical system consisting of N-mass points subject only to interaction forces. Let f^i be the ith component of the force acting on m due to the presence of m. The Newtonian equations of motion for such a system are the $3N$ equations.

$$m\ddot{x}^i - f^i = 0 \qquad [1]$$

where

$$f^i = \sum_\lambda f^i_{\mu\lambda} \qquad [2]$$

Ordinarily, the f^i are some specified functions of ξ^i, the relative position vector of the two particles, or in the general case, a function of ξ^i and the time explicitly

$$f^i_{\mu\nu} = f^i(\xi^i_{\mu\nu}, \dot{\xi}^i_{\mu\nu}, t); \quad \xi^i_{\mu\nu} \equiv x^i_\mu - x^i_\nu \qquad [3]$$

Newton's third law requires that

$$f^i_{\mu\nu} = -f^i_{\nu\mu} \qquad [4]$$

The usual procedure is to substitute the Functions [3] into [1] and [2], and obtain differential equations for the x^i_μ. The mesh equations for the system can be obtained as follows:

Integrating Equation [1] once yields

$$\dot{x}^i_\mu - \frac{1}{m_\mu}\int f^i dt = 0 \qquad [5]$$

The constant of integration is fixed by the initial conditions. If we define

$$I^i_\mu \equiv \int f^i_\mu dt = \int \sum_\lambda f^i_{\mu\lambda}\, dt = \sum_\lambda I^i_{\mu\lambda} \qquad [6]$$

Then Equation [5] may be written in the form

$$\dot{x}^i_\mu - \frac{1}{m_\mu}\sum_\lambda I^i_{\mu\lambda} = 0 \qquad [7]$$

Now form the differences $\dot{\xi}^i_{\mu\nu} = \dot{x}^i_\mu - \dot{x}^i_\nu$ by combining Equation [7] two at a time

$$\frac{1}{m_\mu}\sum_\lambda I^i_{\mu\lambda} - \frac{1}{m_\nu}\sum_\lambda I^i_{\nu\lambda} = \dot{\xi}^i_{\mu\nu} \qquad [8]$$

There are $3N(N-1)$ quantities $I^i_{\mu\nu}$, but due to their antisymmetric property, only $3N(N-1)/2$ are independent. We shall take as the independent variables those having $\mu > \nu$. We now assume that the Functions [3] may be inverted to yield equations of the form

$$\xi^i_{\mu\nu} = \xi^i_{\mu\nu}(I^i_{\mu\nu}, t) \qquad [9]$$

We do not discuss the general class of functions for which this is possible. But for the usual functions occurring in mechanics, the Inversion [9] is readily obtained. Substituting Equation [9] into [8] yields the mesh equations for the system. It also should be pointed out that here we have considered a system of mass points subject only to interaction forces. Classical mechanics separates the treatment of external and internal forces of such a system. In the formalism developed here, external forces can be introduced by choosing the system so as to include the sources of the external fields. The mass of such a source can then be regarded as infinite in the final equations.

If we define the scalar function T

$$T \equiv \sum_{\mu,i}\frac{1}{2m_\mu}\left(\sum_\lambda I^i_{\mu\lambda}\right)^2 \qquad [10]$$

it is easy to verify that the left-hand side of Equation [8] is given by

[1] Applied Mathematics Branch, Naval Research Laboratory.

[2] "An Alternative Formulation of the Laws of Mechanics," by H. M. Trent, Journal of Applied Mechanics (submitted for publication).

Contributed by the Applied Mechanics Division and presented at the Annual Meeting, Atlantic City, N. J., November 25-30, 1951, of The American Society of Mechanical Engineers.

Discussion of this paper should be addressed to the Secretary, ASME, 29 West 39th Street, New York, N. Y., and will be accepted until July 10, 1952, for publication at a later date. Discussion received after the closing date will be returned.

Note: Statements and opinions advanced in papers are to be understood as individual expressions of their authors and not those of the Society. Manuscript received by ASME Applied Mechanics Division, February 5, 1951. Paper No. 51—A-19.

$$\frac{1}{m_\mu}\sum_\lambda I^i_{\mu\lambda} - \frac{1}{m_\nu}\sum_\lambda I^i_{\nu\lambda} = \frac{\partial T}{\partial \dot{I}^i_{\mu\nu}} \quad [11]$$

The mesh equations take the form

$$\frac{\partial T}{\partial \dot{I}^i_{\mu\nu}} = \xi^i_{\mu\nu} \quad [12]$$

The relative velocities play the role of generalized forces in Lagrangian mechanics. If the forces are conservative, we may define a potential function W such that

$$f^i_{\mu\nu} = -\frac{\partial W}{\partial \xi^i_{\mu\nu}} \quad [13]$$

By means of Legendre's dual transformation[3] we obtain the function G

$$G = -\sum_{\mu\nu,i} f^i_{\mu\nu}\,\xi^i_{\mu\nu} - W \quad [14]$$

From the properties of this transformation it follows that

$$\xi^i_{\mu\nu} = -\frac{\partial G}{\partial f^i_{\mu\nu}} = -\frac{\partial G}{\partial \dot{I}^i_{\mu\nu}} \quad [15]$$

Equation [12] can then be written in the form

$$\frac{\partial T}{\partial I^i_{\mu\nu}} + \frac{d}{dt}\left(\frac{\partial G}{\partial \dot{I}^i_{\mu\nu}}\right) = 0 \quad [16]$$

If frictional forces of the linear type

$$f^i_{\mu\nu} = -\eta \dot{\xi}^i_{\mu\nu}$$

also occur, we may define the function $\mathfrak{F}$ analogous to the ordinary Rayleigh dissipation function

$$\mathfrak{F} \equiv \sum_{\mu\nu,i} \frac{1}{2\eta}(\dot{I}^i_{\mu\nu})^2 \quad [17]$$

and the mesh equations become

$$\frac{\partial T}{\partial I^i_{\mu\nu}} + \frac{d}{dt}\left(\frac{\partial G}{\partial \dot{I}^i_{\mu\nu}}\right) + \frac{\partial \mathfrak{F}}{\partial \dot{I}^i_{\mu\nu}} = 0 \quad [18]$$

Since T is a function of the $I^i_{\mu\nu}$ only and G a function of $\dot{I}^i_{\mu\nu}$ only, then for conservative systems we define the Lagrangian function

$$L(I^i_{\mu\nu}, \dot{I}^i_{\mu\nu}) \equiv T - G \quad [19]$$

Equation [16] now takes the form

$$\frac{\partial L}{\partial I^i_{\mu\nu}} - \frac{d}{dt}\left(\frac{\partial L}{\partial \dot{I}^i_{\mu\nu}}\right) = 0 \quad [20]$$

which are the Euler-Lagrange equations of the variational principle with fixed end points

$$\delta \int L\,dt = 0 \quad [21]$$

The Cyclic Nature of Impulse

The most general length-preserving transformation from one Cartesian co-ordinate system to another is of the form

$$x^{*i} = \sum_k c_k{}^i x^k + x_I{}^i; \quad \sum_i c_k{}^i c_s{}^i = \delta_{ks} \quad [22]$$

The Newtonian equations of motion are not covariant under the transformation, Equation [22], unless

$$\dot{c}_k{}^i = 0; \quad \ddot{x}_I{}^i = 0 \quad [23]$$

in which case the transformation is called Galilean. It is interesting to note that Equations [8] do not require the second of the Conditions [23] for their covariance. They remain valid in a co-ordinate system that is moving with arbitrary translatory motion relative to an inertial system. It is this property that allows the following interpretation of the mesh-type equations:

Substitution of Equations [7] into [8] yields the identical relations

$$\dot{\xi}^i_{\mu\nu} - \dot{x}^i_\mu + \dot{x}^i_\nu = 0 \quad [24]$$

If we make the co-ordinate transformation

$$x^{*i} = \sum_k c_k{}^i\, x^k + x_I{}^i; \quad \dot{c}_k{}^i = 0 \quad [25]$$

Equation [24] takes the form

$$\dot{\xi}^{*i}_{\mu\nu} + (\dot{x}_I{}^i - \dot{x}^{*i}_\mu) + (\dot{x}^{*i}_\nu - \dot{x}_I{}^i) = 0 \quad [26]$$

The vector $x_I{}^i$ is the position vector of the origin O_I of the unstarred, inertial system, and Equation [26] is simply the cyclic sum of the relative velocities of the points m_μ, m_ν, and O_I. Dropping the asterisks, Equation [8] is now formally reproduced by the substitutions

$$\left.\begin{aligned} \dot{x}_I{}^i - \dot{x}^i_\mu &= -\frac{1}{m_\mu}\sum_\lambda I^i_{\mu\lambda} \\ \dot{x}^i_\nu - \dot{x}_I{}^i &= \frac{1}{m_\nu}\sum_\lambda I^i_{\nu\lambda} \end{aligned}\right\} \quad [27]$$

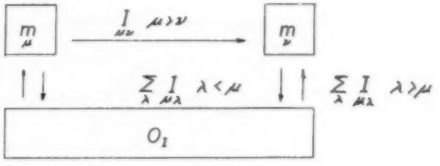

Fig. 1

where the independent variables in the summands are the $I^i_{\mu\nu}$, $\mu > \nu$. With this convention the significance of Equations [27] can be seen with the aid of Fig. 1. The $I^i_{\mu\nu}$, $\mu > \nu$, act as though they were cyclically transmitted around the closed path $m_\nu \rightarrow m_\mu \rightarrow O_I$

Acknowledgment

The equations discussed in this paper were proposed by Trent, including the interpretation of the cyclic properties of impulse and force. It is hoped that the derivation given here will further clarify their connection with the Newtonian equations of motion for a system of particles and lead to possible generalization. The author wishes to thank Dr. Trent for the suggestion of this work and for the many helpful and interesting discussions.

[3] "The Variational Principles of Mechanics," by C. Lanczos, University of Toronto Press, Toronto, Ont., Canada, 1949, p. 161.

The Limit Design of a Transversely Loaded Square Grid[1]

BY JACQUES HEYMAN,[2] PROVIDENCE, R. I.

An earlier paper[3] discussed the derivation of a breakdown criterion for beams subjected to combined bending and torsion. The present paper deals with the limit design of grids, formed by two sets of parallel beams intersecting at right angles, subjected to transverse loading at the joints. This form of loading introduces both bending and twisting moments in the beams, and modes of failure under these combined actions are investigated. Exact solutions are determined for some simple grids, but general methods are demonstrated which lead to upper and lower bounds on the collapse load.

Space Frames

As in the previous paper,[3] the type of space frame to be investigated has members which lie all in the same plane, all loads acting perpendicularly to this plane. Thus bending moments whose axes lie perpendicular to the plane and shear forces in the plane are zero. Any member of the frame is then acted upon by shear forces parallel to the applied loads and by two moments whose axes lie in the plane, that is, a bending moment M and a torque T. It is assumed that the shear force plays no part in causing breakdown at a hinge; this usually will be the case, but attention would have to be paid to examples in which exceptionally large shear forces were encountered.

The customary structural assumption is made that deformations are small compared with the over-all dimensions of the frame, so that it is admissible to satisfy the equilibrium conditions in the undeformed rather than in the deformed configuration.

It was shown in the previous paper[3] that a plastic hinge would be formed in a box beam carrying a bending moment M and a torque T when

$$M^2 + \frac{4}{3} T^2 = M_0^2 \quad [1]$$

where M_0 is the limit moment (full plastic moment) in pure bending. Later in the present paper, the slightly more general criterion

$$M^2 + \alpha T^2 = M_0^2 \quad [2]$$

will be used, where α is a (known) number and corresponds to the shape of cross section employed. In the work immediately following, however, α will be taken as unity in order to simplify the calculations, so that

$$M^2 + T^2 = M_0^2 \quad [3]$$

The methods proposed are in no way affected by this restriction on α.

For plane frames (no twisting), the bending moment M at any section must satisfy

$$|M| \leq M_0 \quad [4]$$

and Equation [3] implies that the corresponding restriction for space frames is

$$M^2 + T^2 \leq M_0^2 \quad [5]$$

In accordance with other work,[4,5] the weight per unit length of a beam with limit moment M_0 will be taken as directly proportional to M_0, so that for a frame consisting of N beams, the material consumption is given to some scale by

$$W = \sum_{i=1}^{N} M_i l_i \quad [6]$$

where M_i and l_i are the limit moment and length, respectively, of the ith beam.

The Square Grid

Consider a square opening of side length L as shown in Fig. 1.

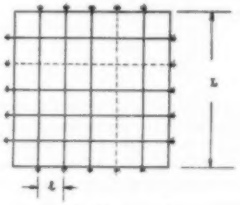

Fig. 1 Type of Grid

This opening might correspond to a section between bulkheads and decks in a ship, or to part of the flat roof of a building. The problem is to cover this opening with a grid of beams in order to support a load P uniformly distributed over the area. For the sake of simplicity, the load will be taken as split into equal concentrated loads of value p acting at the joints of the grid. If

[1] The conclusions presented here were obtained in the course of research conducted under contract N7onr-358 sponsored jointly by the Office of Naval Research and the Bureau of Ships.

[2] Research Associate, Graduate Division of Applied Mathematics, Brown University, and Fellow of Peterhouse, Cambridge, England.

[3] "The Limit Design of Space Frames," by Jacques Heyman, Journal of Applied Mechanics, Trans. ASME, vol. 73, 1951, pp. 157–162.

For presentation at the Annual Conference of the Applied Mechanics Division, The Pennsylvania State College, State College, Pa., June 19–21, 1952, of The American Society of Mechanical Engineers.

Discussion of this paper should be addressed to the Secretary, ASME, 29 West 39th Street, New York, N. Y., and will be accepted until July 10, 1952, for publication at a later date. Discussion received after the closing date will be returned.

Note: Statements and opinions advanced in papers are to be understood as individual expressions of their authors and not those of the Society. Manuscript received at ASME Headquarters, August 11, 1950. Paper No. 52—APM-2.

[4] "Minimum Weight Design of Plane Frames," by Jacques Heyman, *Quarterly of Applied Mathematics*, vol. 8, 1951, pp. 373–381.

[5] "Limit Design of Continuous Beams for Minimum Weight," by Jacques Heyman, Technical Report A11-47, April, 1950, from the Graduate Division of Applied Mathematics, Brown University, to the Office of Naval Research under Contract N7onr-358.

there are n equally spaced beams spanning in either direction, then there will be n^2 joints, so that

$$P = n^2 p \quad [7]$$

In addition, the elementary span length will be denoted by l, so that

$$(n + 1)l = L \quad [8]$$

The general problem will be approached through the investigation of very simple grids consisting of a small number of beams. For all the grids under discussion, it is assumed that the equally spaced parallel beams have equal limit moments which may, however, be different from the limit moments of the beams spanning at right angles. This restriction, as will be seen, does not affect the generality of the proposed methods.

Single Beam Spanning Each Way

Consider a grid formed of two beams of section moments M_1 and M_2 arranged symmetrically in the opening and intersecting at the center at right angles. The ends A and B of the beams are encastré, so that the limit moments may be reached at those points, and the joint O is perfectly rigid, allowing bending moment and torque to be transmitted from one beam to the other. The load $p = P$ acts at the joint O. It is easy to see that the mode of failure of this symmetrical grid corresponds to the mechanism of one degree of freedom shown in Fig. 2. The eight hinges (shown

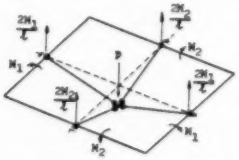

Fig. 2 Collapse Mode of Single-Beam Grid

as dots) are all formed under pure bending, so that the problem is in fact one of plane failure in this instance.

By considering the vertical equilibrium

$$p = 4\frac{M_1}{l} + 4\frac{M_2}{l} \quad [9]$$

This value for p may also be derived from the principle of virtual work. If the deflection of the center O of the grid is δ, then the angle change at each of the eight hinges is δ/l. Now the plastic work done in a hinge is equal to the angle change multiplied by the limit moment at that hinge, and equating this to the work done by the load p

$$p\delta = 4M_1\left(\frac{\delta}{l}\right) + 4M_2\left(\frac{\delta}{l}\right) \quad [10]$$

which leads directly to Equation [9]. The material consumption in the grid is given from Equation [6] by

$$W = L(M_1 + M_2) \quad [11]$$

Hence, using Equation [9] and remembering that $L = 2l$

$$W = \frac{1}{8}PL^2$$

or

$$\frac{W}{P} = \frac{1}{8}L^2 \quad [12]$$

The ratio of W/P is a measure of the material consumption per unit load, and it will be noticed that this expression is independent of M_1 and M_2. This means that considering the problem as one of design, any values of M_1 and M_2 so chosen that the grid fails under a unit load will lead to a material consumption that is constant. In particular, if $M_1 = M_2 = M_0$

$$M_0 = \frac{1}{16}PL \quad [13]$$

Two Beams Spanning Each Way

The mode of failure of the 2×2 beam grid shown in Fig. 3 again introduces no twisting moments. The loads $p = {}^1/_4P$ act at

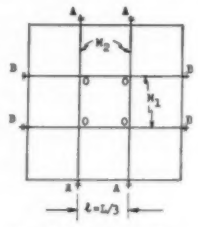

Fig. 3 Two-Beam Grid

the joints O, and hinges are formed at the two ends of the beams AO, BO. (The beams forming the square OOOO are also subjected to the limit moments M_1 and M_2.) Vertical equilibrium or virtual work gives

$$4p = 4\left(\frac{2M_1}{l} + \frac{2M_2}{l}\right)$$

i.e.

$$PL = 24(M_1 + M_2) \quad [14]$$

The material consumption is given by

$$W = 2L(M_1 + M_2) \quad [15]$$

or

$$\frac{W}{P} = \frac{1}{12}L^2 \quad [16]$$

and in particular, if $M_1 = M_2 = M_0$

$$M_0 = \frac{1}{48}PL \quad [17]$$

It will be noticed that the material consumption per unit load is reduced in the ratio ${}^8/_{12}$ when compared with the previous case.

Three Beams Spanning Each Way

With a 3×3 beam grid, twisting moments are introduced in the collapse, and use must be made not only of the breakdown criterion (Equation [3]), but also of the orthogonal flow relationship which may be derived from it.[3] If the plastic change in bending angle at a hinge is denoted by β, and the plastic change in twist at the same hinge by θ, then the flow relationship corresponding to Equation [3] is

$$\frac{M}{T} = \frac{\beta}{\theta} \quad [18]$$

It will be useful at this stage to derive expressions for the moment and torque in terms of the changes in angle at a hinge. Solving Equations [3] and [18] simultaneously

$$\left.\begin{aligned} M &= \frac{\beta}{\sqrt{\theta^2+\beta^2}}M_0 \\ T &= \frac{\theta}{\sqrt{\theta^2+\beta^2}}M_0 \end{aligned}\right\} \quad \ldots\ldots\ldots\ldots\ldots [19]$$

In addition, the total plastic work done at the hinge is $(M\beta + T\theta)$, since M and T remain constant during collapse, so that

$$\text{Plastic work at hinge} = M_0\sqrt{\theta^2+\beta^2} \ldots\ldots\ldots [20]$$

The three-beam grid is shown in Fig. 4. The elementary span length is $l = {}^1/_4L$, and the load at each of the joints is $p = {}^1/_9P$. It may be shown that minimum material consumption is achieved for such a grid when beams of equal section span in either direction. For this reason it will be assumed that $M_1 = M_2 = M_0$, so that Equations [3] and [18] apply at every hinge in the grid. Owing to symmetry, it will be necessary to consider only the portion of the grid enclosed by the dashed line in Fig. 4.

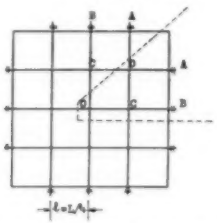

FIG. 4 THREE-BEAM GRID

An exact analysis may be made for this rather simple grid, and the collapse load is given by

$$p_c = 2.32\frac{M_0}{l} \ldots\ldots\ldots\ldots\ldots [21]$$

However, it is possible to find close bounds on this value p_c of the collapse load by the use of two principles, which perhaps are best illustrated by examples of their application.

Suppose collapse of the grid occurs in a way similar to the previous case, that is, beams AD and BC develop hinges at both ends while the central portion of the grid behaves as a rigid body. Then, by virtual work

$$9p = 24\left(\frac{M_0}{l}\right)$$

or

$$p = \frac{8}{3}\frac{M_0}{l} \ldots\ldots\ldots\ldots\ldots [22]$$

Equation [22] was derived from the fact that, during collapse, the work done by the external forces on the structure is equal to the work dissipated in the hinges. Now this is true only if the assumed mode of collapse is the mode that actually will occur; if the assumed mode is not correct, it has been shown by Drucker, Greenberg, and Prager,[6,7] that the load determined by equating the internal and external work *is always greater than the true collapse load*. This kinematic principle gives a valuable method for determining an *upper bound* on the collapse load. A mechanism (of one or more degrees of freedom) is constructed by the insertion of yield hinges at arbitrary locations of the structure, and the work done by the external loads during a small displacement equated to the work dissipated in the hinges. The load determined by this equation is then greater than the true collapse load. Thus, for the example cited, it is known from Equation [22] that the true collapse load p_c is less than ${}^8/_3(M_0/l)$ (or equal to this value, if the assumed mode happens to be correct).

In order to find a lower bound for p_c, the frame may be examined statically under the load $p = {}^6/_5(M_0/l)$. The various torques, shears, and bending moments are shown in Fig 5 where

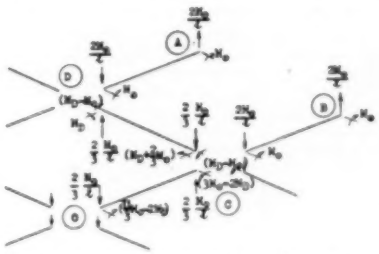

FIG. 5 STATICAL ANALYSIS OF THREE-BEAM GRID

the single redundancy of the central portion of the frame has been introduced as the unknown bending moment M_D. It will be seen that the moment at O is

$$\left(\frac{11}{3}M_0 - 2M_D\right)$$

while the moment at the end C of the beam CD is

$$\left(\frac{2}{3}M_0 + M_D\right)$$

Suppose the yield criterion is exceeded at both these critical points in the same ratio k, that is

$$\left.\begin{aligned} \left(\frac{11}{3}M_0 - 2M_D\right) &= kM_0 \\ \left(\frac{2}{3}M_0 + M_D\right)^2 + (M_D - M_0)^2 &= k^2M_0^2 \end{aligned}\right\} \quad \ldots [23]$$

These simultaneous equations are satisfied by $M_D = M_0$, and this value of M_D gives the bending moment distribution shown in Fig. 6, from which the "worst" bending moment ${}^5/_3(M_0)$ occurs at the two critical points considered.

Now, suppose all the values in Fig. 8 to be multiplied by the factor ${}^3/_5$; a bending-moment distribution results that is an equilibrium with a load of

$$\frac{3}{5}\left(\frac{8}{3}\right)\frac{M_0}{l} = \frac{8}{5}\frac{M_0}{l} \ldots\ldots\ldots\ldots [24]$$

and which *nowhere violates the yield condition*. Such a distribution has been termed *statically admissible*, and it has been shown,[6,7] that the load in equilibrium with such a distribution *is always less than the true collapse load*. The principle thus gives a method for determining a *lower bound* on the collapse load; if, for any given load, a distribution of moment, torque, and shear

[6] "On Limit Design of Beams and Frames," by H. J. Greenberg and W. Prager, Proceedings of the ASCE, Separate No. 59, February, 1951.

[7] "The Safety Factor of an Elastic-Plastic Body in Plane Strain," by D. C. Drucker, H. J. Greenberg, and W. Prager, JOURNAL OF APPLIED MECHANICS, Trans. ASME, vol. 73, 1951, pp. 371–378.

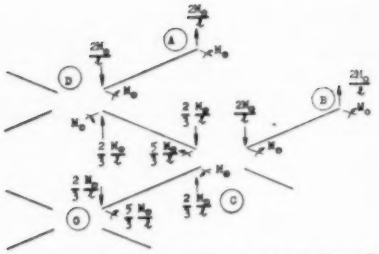

FIG. 6 EQUILIBRIUM DISTRIBUTION FOR THREE-BEAM GRID

force can be determined that is in equilibrium with the load and which nowhere violates the yield condition, then this load is less than the true collapse load of the structure. This statically admissible distribution need not be the distribution that would actually occur under the given load; any distribution that satisfies the equilibrium conditions may be used.

For the present example, combination of the principles leads to (from Equations [22] and [24])

$$\left.\begin{aligned} &\frac{8}{3}\frac{M_0}{l} \geq p_c \geq \frac{8}{5}\frac{M_0}{l} \\ \text{or} \\ &p_c = 2.135\,\frac{M_0}{l} \pm 25 \text{ per cent} \end{aligned}\right\} \quad \ldots\ldots\ldots [25]$$

In order to improve these bounds, extra yield hinges must be inserted at the two critical points. At first sight it would seem that the resulting mechanism shown in Fig. 7 (drawn looking from the center of the grid along OB), has four independent de-

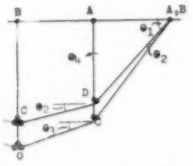

FIG. 7 GENERAL COLLAPSE MODE OF THREE-BEAM GRID

grees of freedom. This is in fact the case, if the mechanism is considered purely in a kinematic sense; however, if both of Equations [3] and [18] are applied at each hinge, and statical equilibrium is attained throughout the grid, it is found that only one arbitrary parameter is needed to specify completely the collapse mode. This approach is the basis of the exact solution which leads to the collapse load in Equation [21]; the equations are complicated and tedious to solve. However, exact values of the angles θ_2, θ_3, and θ_4 in Fig. 7 were determined in terms of the one arbitrary degree of freedom specified by θ_1.

The advantage of the kinematic method of determining an upper bound on the collapse load is that no reference is made to equilibrium conditions. Suppose, for example, the mechanism in Fig. 7 is specified by assigning arbitrary values for the deflections of the joints D, C, and O. Then the changes in angle and hence the work done at each hinge may be determined, and the total work dissipated in the hinges equated to the work done by the loads p in deflecting the joints. This equation will give a value of p in excess of the true collapse load p_c, whatever collapse configuration is assumed. If now the frame is examined statically under the load p, it will be found, in general, that it is impossible to satisfy equilibrium conditions at the joints, the total load at each joint being either in excess of or less than p. This implies that extra (positive or negative) forces are required at the joints in order to produce the originally assumed collapse configuration. The significance of these extra forces is best appreciated by actually performing a calculation for the three-beam grid.

Suppose as a first trial that the deflections of the joints D, C, and O are given by

$$\delta_D = 0.56,\ \delta_C = 0.75,\ \delta_0 = 1.00 \quad \ldots\ldots\ldots [26]$$

that is, joints ADC and BCO lie on parabolas. The deflection of the central joint has been taken arbitrarily as unity, since a mechanism of one arbitrary degree of freedom is necessary for collapse.

Table 1 sets out the location of the hinges, the total number of hinges in the grid, the angle changes and work done at each hinge, and the corresponding moments and torques. (For clarity, the span l and limit moment M_0 do not appear in the table.)

TABLE 1 GRID DATA

Hinge	No.	β	θ	$\sqrt{\theta^2+\beta^2}$	Moment	Torque
B	4	0.75	0	0.750	1.00	0
A	8	0.56	0.11*	0.571	0.98	0.19
D	8	0.37	0.08*	0.378	0.98	0.21
CD	8	0.19	0.06	0.199	0.95	0.30
CB	4	0.50	0	0.500	1.00	0
O	4	0.25	0	0.250	1.00	0

It will be noticed that the rotation $\theta_4 = 0.11$ of beam AD is not directly determinate in terms of the deflections of the joints. The value was estimated by introducing a statical consideration. Since, for equilibrium, the torques at A and D on beam AD must be equal, the bending moments must also be equal since hinges occur at both points (Equation [3]). Equation [8] then gives the ratio β/θ the same at both points, and the asterisked values in Table 1 satisfy this condition approximately. (It should be emphasized that this extra statical condition is not necessary for the application of the method and gives only a slight improvement in the value for the upper bound; any values of twist at A and D that total 0.19, the slope of beam DC, may be used.)

The total work done in all the hinges is $15.18(M_0/l)$, and equating this to the work done by the loads at the joints, $p(\delta_0 + 4\delta_C + 4\delta_D)$

$$p_c \leq p = \frac{15.18}{6.24}\frac{M_0}{l} = 2.43\,\frac{M_0}{l} \quad \ldots\ldots\ldots [27]$$

The statical analysis of the frame is shown in Fig. 8. The number in a circle at each joint gives the total load at that joint; for example, it appears that a load of $4.06(M_0/l)$ is necessary at the joint D to produce the deflection 0.75 assumed. This load is nearly double the actual load that should act, indicating that the assumed deflection was too large and should be reduced. In the

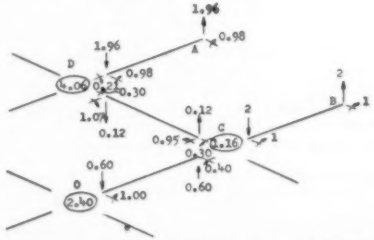

FIG. 8 STATICAL ANALYSIS CORRESPONDING TO TABLE 1

same way, the total load at joint C is less than the actual load, so that the deflection should be increased. A better bound for the collapse load should be obtained by making these changes in deflection.

In working more complicated examples, it is found that the process of adjusting deflections bears a marked resemblance to a relaxation process, and that a reduction in the out-of-balance force at one joint induces increased errors at the neighboring joints. In fact, for this example, a simple trial shows that reduction of the deflection of joint D immediately requires a reduction in the deflection of joint C instead of an increase at the latter joint. Suppose, then, that for a second trial, deflections

$$\delta_D = 0.30,\ \delta_C = 0.60,\ \delta_b = 1.00 \quad [28]$$

are assumed; that is, joints ADC lie on a straight line, so that no hinge is formed at D. This gives the value of the load

$$p = 2.33\,\frac{M_0}{l} \quad [29]$$

and the slight out-of-balance forces at the joints indicate that the deflection of D is now too small, while the deflection of C is too large. The changes may be made and the process repeated, but a lower bound should be determined on the collapse load before further work is carried out. If small changes are made in the bending moments, torques, and shear forces, an equilibrium system may be constructed for the grid under the load given by Equation [29]. It is found on examination that these changes cause the yield condition to be violated at some of the assumed hinges, the worst violation being in the ratio 1.016. Thus a lower bound may be determined by reducing the load in the ratio 1/1.016, leading to the continued inequality

$$2.29\,\frac{M_0}{l} \leq p_i \leq 2.33\,\frac{M_0}{l} \quad [30]$$

or

$$p_c = 2.31\,\frac{M_0}{l} \pm 1 \text{ per cent} \quad [31]$$

and these bounds are certainly close enough for any practical purpose.

Before dealing with the analysis of more complicated grids, a summary may be made of the proposed procedure, based upon the results obtained in the foregoing:

1 Insert yield hinges at a large number of points in the grid, producing a mechanism of many degrees of freedom. The hinges should be placed at all the sections at which it is suspected actual hinges might occur in the collapse.

2 Assign arbitrary (but reasonable) deflections to the joints of the grid, and determine the corresponding changes in angle at each hinge. Equating the work dissipated in the hinges to the work done by the external loads gives a value of the load which is in excess of the true collapse load.

3 Calculate the out-of-balance forces at each joint that are necessary to produce the assumed deflections. If the out-of-balance force acts in the same direction as the actual load at a joint, the deflection of that joint was estimated as too large, and vice versa.

4 Adjust the deflections, and calculate a new upper bound for the collapse load.

5 At any stage, if the out-of-balance forces are small, and it is suspected that the upper bound is a good estimate of the collapse load, a statical analysis may be made. Adjustments are made in the various shears and bending and twisting moments in order to produce an equilibrium system, from which a lower bound may be determined.

It is not recommended that a statical analysis be made in the first few trials, as this usually involves more labor than does the determination of a good upper bound.

More Complicated Grids

In order to obtain some information of the possible saving in material when a grid formed of a large number of beams is used, grids were analyzed, composed of four, five, and nine beams spanning in either direction. The section moments of the two sets of beams were again made equal, and the procedure outlined in the foregoing was used to determine bounds on the collapse load and hence on the material consumption per unit load. These dimensionless material consumptions are plotted in Fig. 9. Bounds were obtained for the nine-beam grid to within ±5 per cent, which is probably close enough for any design purpose. However, the out-of-balance forces were still quite large at this stage, and the next step to reduce the upper bound was clearly defined. The arrangement of hinges chosen to determine the upper bound is shown for a quarter of the grid in Fig. 10.

The rate of saving of material is greatly reduced as the number of beams is increased, as may be seen from Fig. 9; a full investigation of the economy effected by using a large number of beams

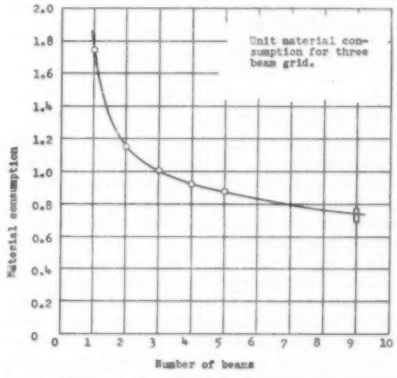

Fig. 9 Material Consumptions for Different Grids

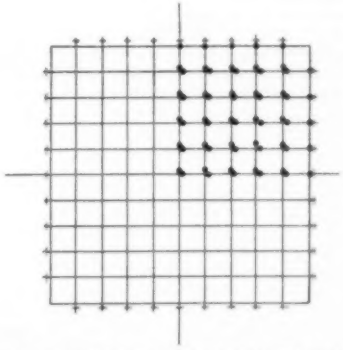

Fig. 10 General Collapse Mode of Nine-Beam Grid

would have to be based upon such factors as the cost of fabricating a complicated grid and the increased costs of erection. For example, the use of a nine-beam rather than a three-beam grid would give a saving of about 25 per cent in raw material; however, this economy might be completely lost in the increased cost of welding 81 as against 9 joints.

More General Breakdown Criterion

In conclusion of the present work, the more general criterion

$$M^2 + \alpha T^2 = M_0^2 \quad [32]$$

will be applied to both three and four-beam grids. In order to obtain some measure of the material consumption, it should be noted from Equation [32] that the variation of α does not affect the value of the moment to cause breakdown when no torque is present. On the other hand, the value of the breakdown torque in pure twisting is given by

$$T = \frac{M_0}{\sqrt{\alpha}} \quad [33]$$

Thus the variation of α implies that the torque to cause breakdown is varied, while the limit moment in pure bending is held constant. In particular, for $\alpha = 0$, the section is infinitely strong against twisting, which would imply an infinite amount of material in the cross section. For this reason the material consumption will be expressed as

$$W = {}^1/_2\Sigma (M_i + T_i)l_i$$
$$= {}^1/_2\Sigma M_i l_i \left(1 + \frac{1}{\sqrt{\alpha}}\right) \quad [34]$$

where M_i and T_i are the breakdown moments for the ith beam under pure bending and torque, respectively. It should be pointed out that Equation [34] is completely arbitrary, and is one of several that reduce to Equation [6] when $\alpha = 1$. However, it will serve to give some idea of the material consumption involved.

Exact solutions for both three and four-beam grids were obtained for a range of values of α, and the dimensionless material consumptions (compared with the material consumption for a three-beam grid with $\alpha = 1$) are plotted in Fig. 11. The general shape of the curves indicates that a section weak in torsion will give the most economical material consumption. However, it has been pointed out that Equation [34] is arbitrary, and a detailed investigation of the amount of material necessary to produce a given torsional limit must be carried out before any definite conclusions may be drawn.

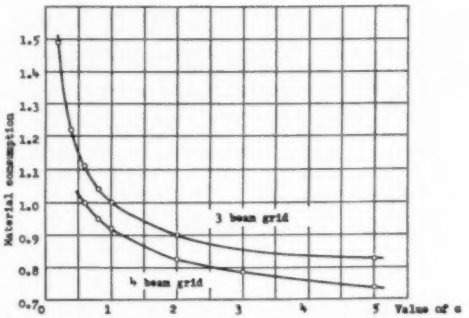

Fig. 11 Material Consumptions for Different Breakdown Conditions

Summary

This paper describes and analyzes the type of square grid that might be employed to support transverse loads, and a method is proposed which leads to arbitrarily close bounds on the collapse load of such a grid. Although discussion has been made only of grids formed by the intersection of regularly spaced beams, rectangular, or indeed grids of any shape, may be investigated using identical methods of solution.

In effect, the determination of an upper bound on the collapse load is an extension of the kinematic principle of Greenberg and Prager,[8] but applied to states which are not necessarily in equilibrium with the applied loads. Equating the internal and external work still gives an upper bound on the collapse load, however. For the grid problems, hinges are assumed (generally in a greater number than that required for collapse), and a collapse configuration is arbitrarily specified, from which the internal and external work can be calculated.

Since more hinges may be assumed than are required to form a mechanism of one degree of freedom, the resulting bending-moment distribution will not be an equilibrium state; if the kinematic solution is reasonably good, slight adjustments may be made in order to obtain a statically admissible equilibrium solution, from which a lower bound may be determined.

The conclusions that may be drawn from the minimum material consumption investigation must be regarded as tentative. It was shown that a grid consisting of a large number of beams is the most economical in the consumption of raw material, but the increased costs of fabrication may more than overcome this saving. In addition, no accurate estimate was made of the material required in a cross section in order that given bending and torsional limit moments might be sustained. In fact, it is likely that with the advent of limit design methods, new structural sections will be designed in order to achieve the greatest economy.

Acknowledgment

The author is indebted to Prof. W. Prager and Dr. D. C. Drucker for their valuable criticism and advice in the preparation of this paper.

Heat-Exchanger Tube-Sheet Design—2 Fixed Tube Sheets

By K. A. GARDNER,[1] MASSILLON, OHIO

It is shown that "fixed" tube sheets may be designed in exactly the same manner as "floating" tube sheets with the same boundary restraint, provided that a fictitious uniform "equivalent design pressure" is used in the calculations instead of the actual hydrostatic pressure. This equivalent pressure is evaluated in terms of tube-side pressure, shell-side pressure, differential thermal expansion, and the condition of boundary restraint. The design factors for all tube sheets presented in an earlier paper[2] are shown to be well represented by very simple expressions when the fundamental design parameter x_a becomes large.

Nomenclature

The following nomenclature is used in this paper:

a = radius of tube sheet over which hydrostatic pressure acts, in.
ber x = real part of Bessel function, $I_0(x\sqrt{i})$
bei x = imaginary part of Bessel function, $I_0(x\sqrt{i})$
ber′ x = $d(\text{ber } x)/dx$
bei′ x = $d(\text{bei } x)/dx$
c = width of annular expansion joint diaphragms, in.
C = arbitrary constant
d = outside diameter of tube, in.
D = flexural rigidity of tube sheet = $Eh^3\eta_e/12(1-\nu^2)$, in-lb
e = base of Napierian logarithms = 2.718
E = modulus of elasticity, psi
f = fraction of total tube-sheet area on which pressure acts directly
$F_q, F_v, F_w, F_\theta, F_M$ = dimensionless factors for obtaining effective pressures, deflection, slope, and radial bending moment of tube sheets
h = tube sheet thickness, in.
H = arbitrary constant
k = tube-bundle modulus = $Nt(d-t)E_t/a^2L$, psi per in.
K = $2E_sI_sa/E_tNt(d-t)$ (Equation [17]), dimensionless
L = tube length, in.
m = distance tube-sheet edges move with respect to each other under load, in.
M_r = radial bending moment, in-lb per in.
M_a = peripheral bending moment, in-lb per in.
n_d = number of diaphragms per expansion joint
N = number of tubes in tube sheet
p = hydrostatic pressure, psi (without subscript represents equivalent design pressure, see Equations [9] and [16])
P = tube pitch (spacing between centers), in.
q = local effective pressure at radius r, psi
r = radius, in.
t = thickness, in. (without subscript represents tube-wall thickness)
T = temperature, deg F
w = tube-sheet deflection, in.
W_t = tube load, lb per tube
x = βr, dimensionless (see Equation [40])
α = linear coefficient of thermal expansion, (deg F)$^{-1}$
β = $(2k/D)^{1/4}$, in.
η_e = flexural efficiency, dimensionless
η_σ = ligament efficiency, dimensionless
θ = tube-sheet slope at radius r, radians
ν = Poisson's ratio
σ = stress, psi

Subscripts:

a = at periphery of tube sheet
c = at critical radius of tube sheet
d = diaphragm of expansion joint
r = radial
s = shell
t = tube

Introduction

In an earlier paper[2] the author presented an analysis of the deflection and bending moments in the circular tube sheets of heat exchangers of the "internal floating head" type. For exchangers in which two tube sheets are connected by the tubes expanded or welded into them (as distinguished from U-tube or bayonet-tube exchangers), it was shown that the tube-sheet deflection equations are those of plates on an elastic foundation, this foundation being the "tube bundle" itself. It was stated in the conclusions of the paper that the same method of analysis could be applied to tube sheets "integral with the supporting member . . . . . ," and it is the purpose of the present paper to derive design equations for such conditions. It will also be shown that the results are applicable, as a special case, to "externally packed floating head" exchangers.

A fixed or "integral" tube-sheet type of exchanger is shown diagrammatically in Fig. 1. This is the simplest and cheapest type of shell-and-tube exchanger, and while it suffers from the disadvantages of inaccessability of the outer tube surface for cleaning and from differential thermal-expansion stresses, it is adequate for many performance conditions where these factors are of little consequence. The addition of an expansion joint in the shell overcomes the thermal-stress problem, although the floating-head type offers the same advantage and others as well. Fig. 1 also shows one type of externally packed floating-

[1] Assistant Chief Engineer, The Griscom-Russell Company. Mem. ASME.

[2] "Heat-Exchanger Tube-Sheet Design," by K. A. Gardner, Trans. ASME, Journal of Applied Mechanics, vol. 70, 1948, p. 377.

Contributed by the Applied Mechanics Division and presented at the Annual Meeting, Atlantic City, N. J., November 25–30, 1951, of The American Society of Mechanical Engineers.

Discussion of this paper should be addressed to the Secretary, ASME, 29 West 39th Street, New York, N. Y., and will be accepted until July 10, 1952, for publication at a later date. Discussion received after the closing date will be returned.

Note: Statements and opinions advanced in papers are to be understood as individual expressions of their authors and not those of the Society. Manuscript received by ASME Applied Mechanics Division, June 11, 1951. Paper No. 51—A-38.

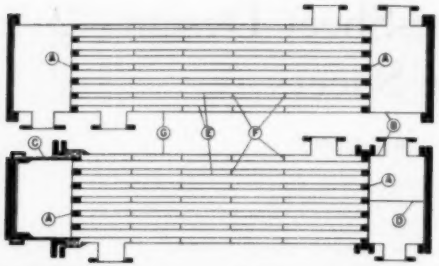

A Tube sheet
B Stationary head (channel)
C Floating head
D Head partition
E Tubes
F Baffles and tube supports
G Shell

FIG. 1 INTEGRAL TUBE-SHEET HEAT EXCHANGER, AND BELOW EXTERNALLY PACKED FLOATING-HEAD EXCHANGER

head exchanger which, for purposes of tube-sheet computation, is identical with an integral tube-sheet exchanger with a perfectly flexible expansion joint in the shell. As in the previous paper, only circular tube sheets with uniform tube distribution, supported only at the periphery, will be considered.

METHOD OF ATTACK

The nomenclature and fundamental assumptions of the original paper[2] are used. These assumptions are as follows:

1 The mean neutral deflection surface of a uniformly perforated plate under load may be considered congruent with that of a homogeneous plate of the same radius, identically loaded, whose flexural rigidity D is a fraction η_w of that of the original undrilled plate.

2 The tube-sheet element associated with a single tube is so small compared to the total tube-sheet area that it may be considered of differential size and hence the external forces exerted on the tube sheet by the tubes may be treated as continuously varying.

3 The entire surface of the tube sheet over which the pressure acts may be treated as uniformly perforated.

The first two assumptions make it possible to treat a drilled tube sheet as though it were a solid plate of some lesser thickness on a uniform elastic foundation. The last ignores the band of undrilled plate at the periphery which, in any event, is practically nonexistent in fixed-tube-sheet exchangers. Malkin[3] has, in effect, proved that assumption (1) is valid for tube sheets drilled on a triangular layout and has, furthermore, derived expressions which permit evaluation of the deflection efficiency η_w; however, he also shows that this assumption is, at best, an empirical approximation for square tube layouts. (See the author's discussion following Malkin's paper.[3])

The force exerted by a single tube on the tube-sheet element associated with it is determined by the change in its length (corrected for thermal expansion), its original length, its cross-sectional metal area, and its modulus of elasticity; thus

$$W_t = \frac{\pi t(d-t)E_t}{L}(m - \alpha_t T_t L - 2w) \quad [1]$$

where

α_t = coefficient of thermal expansion of tubes, (deg F)$^{-1}$
T_t = average metal temperature of tubes, deg F

and the other symbols are as used before. Thus deflections w are considered positive when the two tube sheets bend toward each other and the value of W_t, if positive, represents a tensile force in the tube and, if negative, a compressive force. The dimension m is the distance the outer edges of the two tube sheets move away from each other under the combined effects of pressure and thermal expansion. The load W_t, considered as uniformly distributed over its associated tube-sheet element, and combined with the hydrostatic pressures on both sides of the tube sheet, results in a net effective pressure on that element of

$$q = (f_t p_t - f_s p_s) + k(m - \alpha_t T_t L - 2w), \text{ psi} \quad [2]$$

where

p_t = hydrostatic pressure on tube side, psi
p_s = hydrostatic pressure on shell side, psi
f_t = fraction of tube side face of tube sheet, including tube ends, on which tube side pressure acts directly

$$= 1 - \frac{N}{4}\left(\frac{d-2t}{a}\right)^2$$

f_s = fraction of shell-side face of tube sheet on which shell-side pressure acts directly

$$= 1 - \frac{N}{4}\left(\frac{d}{a}\right)^2$$

$$k = \frac{Nt(d-t)E_t}{a^2 L}, \text{ lb per cu in.}$$

Equation [2] is identical in form with the expression derived in the original paper for internal-floating-head exchangers. Therefore the fundamental differential equation and its general solutions are the same, namely

$$x^4\frac{d^4q}{dx^4} + 2x^3\frac{d^3q}{dx^3} - x^2\frac{d^2q}{dx^2} + x\frac{dq}{dx} + x^4 q = 0 \quad [3]$$

$$q = C(\text{ber } x + H \text{ bei } x) \quad [4]$$

$$w = \frac{C}{\beta^4 D}[(\text{ber } x_a - \text{ber } x) + H(\text{bei } x_a - \text{bei } x)] \quad [5]$$

$$\theta = \frac{-C}{\beta^3 D}(\text{ber}' x + H \text{ bei}' x) \quad [6]$$

$$M_r = \frac{C}{\beta^2}\left\{[\text{bei } x + \frac{(1-\nu)}{x}\text{ber}' x] - H[\text{ber } x - \frac{(1-\nu)}{x}\text{bei}' x]\right\} \quad [7]$$

in which, for simplicity in nomenclature, C has replaced A_{sf} of the original paper, H has replaced B_{sf}/A_{sf}, and

$$x = \beta r = (2k/D)^{1/4} r \quad [8]$$

There are three boundary conditions available for determination of the three arbitrary constants, m, C, and H:

1 The balance of forces on either tube sheet (see Fig 2) is given by

$$\pi a^2 p = \pi a^2 p_t - \frac{2\pi a E_t t_s}{L}(m - \alpha_s T_s L)$$

or

$$p = p_t - \frac{2E_t t_s}{aL}(m - \alpha_s T_s L) \quad [9]$$

[3] "Notes on a Theoretical Basis for the Design of Tube Sheets of Triangular Layout," by I. Malkin, Paper No. 50—A-120, presented at the Annual Meeting, New York, N. Y., November 26–December 1, 1950, of THE AMERICAN SOCIETY OF MECHANICAL ENGINEERS.

in which p is the average effective pressure acting on the tube sheet face, i.e.

$$p = \frac{1}{\pi a^2}\int_0^a 2\pi r q dr = \frac{2C\ \text{bei}'\ x_a}{x_a}\left(1 - H\frac{\text{ber}'\ x_a}{\text{bei}'\ x_a}\right) \quad [10]$$

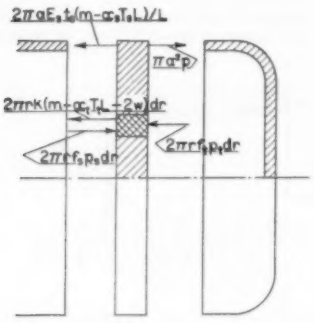

FIG. 2 BALANCE OF FORCES ON INTEGRAL TUBE SHEET

2 The deflection w at the periphery is equal to zero

$$0 = (f_t p_t - f_s p_s) + k(m - \alpha_t T_t L) - q_a$$

or

$$pF_q = (f_t p_t - f_s p_s) + k(m - \alpha_t T_t L) \quad [11]$$

in which F_q is the ratio of maximum to the average effective pressure, as used in the original paper, i.e.

$$F_q = \frac{q_a}{p} = \frac{x_a}{2}\frac{\text{bei}\ x_a}{\text{bei}'\ x_a}\left[\frac{\dfrac{\text{ber}\ x_a}{\text{bei}\ x_a} + H}{1 - H\dfrac{\text{ber}'\ x_a}{\text{bei}'\ x_a}}\right] \quad [12]$$

3 The condition of peripheral restraint can be expressed generally as the ratio of the slope to the radial bending moment at that point; thus

$$\frac{M_a}{\theta_a} = -\beta D\left\{\frac{\left[\text{bei}\ x_a + \dfrac{(1-\nu)}{x_a}\text{ber}'\ x_a\right] - H\left[\text{ber}\ x_a - \dfrac{(1-\nu)}{x_a}\text{bei}'\ x_a\right]}{\text{ber}'\ x_a + H\ \text{bei}'\ x_a}\right\} \quad [13]$$

Simultaneous solution of Equations [9], [11], and [13] yields

$$m = \alpha_t T_t L + \frac{aL}{2E_s t_s}(p_t - p) \quad [14]$$

$$C = p\left[\frac{x_a}{2\ \text{bei}'\ x_a\left(1 - H\dfrac{\text{ber}'\ x_a}{\text{bei}'\ x_a}\right)}\right] \quad [15]$$

in which

$$p = \frac{p_t + K[(f_t p_t - f_s p_s) - kL(\alpha_t T_t - \alpha_s T_s)]}{(1 + KF_q)} \quad [16]$$

$$K = \frac{2E_s t_s}{akL} = \frac{2E_s t_s a}{E_t N t(d-t)} \quad [17]$$

and

$$H = -\left\{\frac{\text{ber}'\ x_a + \left(\dfrac{\beta D\theta_a}{M_a}\right)\left[\text{bei}\ x_a + \dfrac{(1-\nu)}{x_a}\text{ber}'\ x_a\right]}{\text{bei}'\ x_a - \left(\dfrac{\beta D\theta_a}{M_a}\right)\left[\text{ber}\ x_a - \dfrac{(1-\nu)}{x_a}\text{bei}'\ x_a\right]}\right\} \quad [18]$$

EFFECT OF AN EXPANSION JOINT

The parameter K is actually the ratio of the effective elastic modulus of the shell to that of the tube bundle, i.e., it is the ratio of the force required to produce a given strain in the shell to the force necessary to produce the same strain in the tube bundle. It is thus the measure of the ability of the shell (relative to the tube bundle) to resist movement of the two tube-sheet edges with respect to each other. This ability is reduced by the introduction of an expansion joint into the shell. Although there is little general agreement on the design of expansion joints, a paper by Feely and Goryl[4] may be used to approximate the effect on K for the type of joint which consists essentially of a series of annular diaphragms welded together alternately at their inner and outer circumferences. Ignoring deflection due to pressure, the effective value of K may be obtained by multiplying the value from Equation [17] by

$$\frac{1}{\left[1 + n_d\dfrac{t_s}{L}\left(\dfrac{c}{t_d}\right)^3\dfrac{E_s}{E_d}\right]}$$

where c is the width of the annuli, t_d and E_d are the thickness and modulus, respectively, of the diaphragms, and n_d is the total number of diaphragms in the expansion joint (normally a minimum of 2). The additional deflection due to internal pressure and the rotation of the junction between the shell and the diaphragms still further reduces the effective value of K.

An externally packed floating head, Fig. 1, is for purposes of tube-sheet computation, a perfect expansion joint and for exchangers so constructed the value of K is zero. There is, of course, a resistance to sliding friction through the packing gland but this effect is negligible compared to the elastic resistance of metals.

EQUIVALENT DESIGN PRESSURE

The value of K for the internal floating-head type of exchanger covered by the earlier paper[2] is obviously zero since there is no shell resistance to the relative movement of the edges of the two tube sheets. The average effective pressure p is, therefore, equal (by Equation [16]) to the actual tube-side hydrostatic pressure p_t, and, with this substitution, all the equations of the previous paper are reproduced.

The important conclusion may now be drawn, and the main point of this paper made, that the effective pressure, deflection, slope, bending moment, and so forth, of integral or fixed tube sheets are all identical to the corresponding quantities for floating tube sheets of the same diameter, identically supported (as characterized by M_a/θ_a) for which the "equivalent tube-side design pressure" is the value given by Equation [16] rather than p_t. This is true because the value of C in all the design equations is simply scaled down in the ratio p/p_t.

Since the conditions of operation of most heat exchangers do not preclude the possibility that the full hydrostatic pressure on

[4] "Stress Studies on Piping Expansion Bellows," by F. J. Feely, Jr., and W. M. Goryl, JOURNAL OF APPLIED MECHANICS, Trans. ASME, vol. 72, 1950, p. 135.

one side may be exerted in the absence of any pressure on the other side, it will not often be possible to design on the basis of Equation [16] as it stands, i.e., on the basis of the differential pressure. Rather, the larger of the two following values usually must be used

$$p = \frac{p_t(1 + Kf_t) - KkL(\alpha_t T_t - \alpha_s T_s)}{(1 + KF_q)} \quad [16a]$$

$$p = \frac{-K[f_s p_s + kL(\alpha_t T_t - \alpha_s T_s)]}{(1 + KF_q)} \quad [16b]$$

which, in the absence of thermal effects, become

$$p = p_t \left(\frac{1 + Kf_t}{1 + KF_q} \right) \quad [16c]$$

$$p = -p_s \frac{Kf_s}{(1 + KF_q)} \quad [16d]$$

Ignoring thermal effects for the moment, it is apparent that the equivalent design pressure for a fixed-tube-sheet exchanger must always be less than either shell- or tube-side hydrostatic pressure, since f_s and f_t by their nature are always less than unity, F_q is always greater than unity, and K is always positive. It is also obvious that with $K = 0$, a condition closely approximated by fire-tube boilers and heat exchangers with shell expansion joints or outside packed floating heads, the design pressure is entirely independent of the shell-side pressure, no matter how high it may be, and is, in fact, equal to the tube-side pressure exactly as in an internal-floating-head exchanger.

On the other hand, if K is large the equivalent design pressure approaches $p_t f_t/F_q$ or $p_s f_s/F_q$, whichever is greater; this has a maximum value of approximately one half the actual pressure and may be considerably less, depending on the value of F_q. Between these two extremes perhaps the most remarkable features of Equations [16c] and [16d] is the fact that the tube-side pressure is usually the controlling factor in fixed tube-sheet design, even though the shell-side pressure may be many times as high.

The effect of differential thermal expansion becomes quite impressive when considered as an equivalent hydrostatic pressure; thus

$$p = -KkL \left(\frac{\alpha_t T_t - \alpha_s T_s}{1 + KF_q} \right) \quad [16e]$$

If no expansion joint is used, $Kkl = 2E_s t_s/a$, which normally has a value of about 10^6; since α and $(1 + KF_q)$ are of the orders 10^{-6} and 1, respectively, the equivalent pressures are of the order of magnitude, $\pm 10(T_t - T_s)$. Thus a difference between shell and tube metal temperatures of only 50 deg F could produce effects equivalent to 500 psi pressure. It should be noted that the equivalent pressure found in this way is less than that obtained on the common assumption that all tubes are stretched or compressed exactly the same amount; on this basis

$$p = -KkL \left(\frac{\alpha_t T_t - \alpha_s T_s}{1 + K} \right) \quad [19]$$

However, it is the "maximum local" effective pressure, not the average, which determines the possibility of damaged tubes or tube joints, and this quantity is higher in the ratio $F_q(1 + K)/(1 + KF_q)$ than would be obtained on the simpler basis.

Boundary Restraint

By definition, the slope at the periphery is negative if the tube-side face of the tube sheet is concave at that point, and the external bending moment is also negative if it tends to produce such concavity. Since the moment exerted by the restraining influence of the shell (and sometimes the stationary head) always opposes the deflection, the dimensionless parameter $(\beta D\theta_a/M_a)$ occurring in Equation [18], which is a measure of the degree of boundary restraint, is always negative in fixed-tube-sheet exchangers unless some other external bending moment is present in addition to that produced by the shell. (See Fig. 3, for definition sketch.) Thus, for simply supported

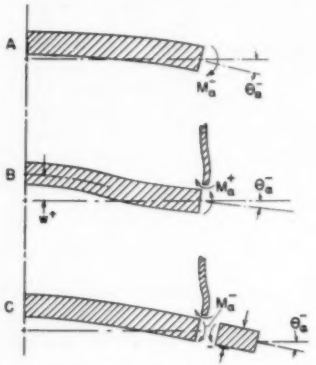

Fig. 3 Definition Sketch for Signs of Deflections, Edge Slopes, and Moments
(B and C show effects of shell only and of shell and flange bolting, respectively.)

plates, this parameter equals minus infinity (since $M_a = 0$), for perfectly clamped sheets it equals zero and, in the absence of any other restraint than the resistance to deflection and bending of the shell, other values lie between these extremes.

However, in cases where the tube sheet is extended to form a flange for the tube fluid heads, a negative external bending moment is applied which may be sufficient to make $(\beta D\theta_a/M_a)$ positive. The effect of these externally applied bending moments is rather complex, since it depends, among other things, upon whether the equivalent design pressure is positive or negative and whether the value of x_a is greater or less than 2.65 (the tube-sheet stress may be alleviated rather than intensified); even in their absence, the complication of the combined effects of discontinuity stresses due to shell and head pressures and differential thermal expansion between shell, tube sheet, and head makes the determination of boundary restraint an uncertain factor in the estimation of tube-sheet stresses.

In view of the foregoing, therefore, it is suggested that the designer be guided by his judgment and experience in determining the relative fixity of the tube-sheet periphery as between clamped and simply supported.

Asymptotic Expressions for Design Factors

In the previous paper,[2] the maximum effective pressure, deflection, slope, radial bending moment and stress were given in the following terms

$$q_{max} = pF_q \quad [20]$$

$$w_{max} = \frac{pa^4}{D} F_w \quad [21]$$

$$\theta_{max} = \frac{pa^3}{D} F_\theta \quad [22]$$

TABLE 1 DESIGN FACTORS

	$F_q = \frac{q}{p}$		$F_w = \frac{Dw_{max}}{pa^2}$		$F_\theta = \frac{D\theta_{max}}{pa^2}$		$F_M = \frac{(M_r)_{max}}{pa^2}$		$F_c = \frac{q_c}{p}$	
x_a	Simple	Clamped	Simple	Clamped	Simple	Clamped	Simple	Clamped	Simple	Clamped
0	1.0000	1.0000	0.0636	0.01563	—0.0957	—0.02405	—0.2063	0.125	1.000	1.000
1.0		1.0046	0.0628	0.01554	—0.0947	—0.0239	—0.2025	0.1245	0.966	0.980
1.5			0.060				—0.1914		0.812	
2.0	1.396	1.079	0.0531	0.01445	—0.0825	—0.0218	—0.1648	0.1200	0.545	0.845
2.5			0.043							
3.0	2.253	1.317	0.0316	0.01112	—0.0546	—0.0175	—0.0884	0.1056	—0.306	0.407
3.5										
4.0	3.086	1.636	0.0150	0.00691	—0.0321	—0.0111	—0.0610	0.08560	—0.740	—0.0875
4.5									—0.727	
5.0			0.00719	0.00378	—0.0210	—0.00719	—0.0490	0.06945	—0.626	—0.323
5.5										
6.0	4.54	2.39	0.00390	0.00206	—0.0144	—0.00487	—0.0405	0.0581	—0.516	—0.276
6.5										
7.0			0.00240			—0.00354	—0.0345	0.0500	—0.530	—0.210
8.0	5.97	3.095	0.00159		—0.00799			0.04387	—0.564	—0.205
8.5										
9.0			0.00110				—0.02665	0.03913	—0.602	—0.214
9.5										
10.0	7.39	3.790	0.000803		—0.00510		—0.02384	0.0352	—0.640	—0.224

$$(M_r)_{max} = pa^2F_M \quad [23]$$

$$(\sigma_r)_{max} = \frac{6p}{\eta_\sigma}\left(\frac{a}{h}\right)^2 F_M \quad [24]$$

Values of these design factors were tabulated and graphed in most cases over the range, $x_a = 0$ to 10. For convenience' sake they are repeated here in Table 1.

With the considerable reductions of equivalent design pressures which can be achieved for fixed-tube-sheet exchangers by the use of Equations [16], [16a], and so forth, the necessary tube-sheet thicknesses decrease and the values of x_a frequently will be found to exceed 10. Fortunately, for larger values of x_a, the special Bessel functions employed in this analysis are well represented by single terms of asymptotic expansions as shown in the Appendix, and the expressions for the various design factors become quite simple.

For clamped plates, as $x_a \to \infty$

$$F_q \to \frac{1}{4}(1 + \sqrt{2}x_a) \quad [25]$$

$$F_w \to \frac{\sqrt{2}(1 + e^{-\pi})}{4x_a^2} \quad [26]$$

$$F_\theta \to \frac{-\sqrt{2}e^{-\pi/4}}{4x_a^2} \quad [27]$$

$$F_M \to \frac{\sqrt{2}}{4x_a} \quad [28]$$

For simply supported plates, as $x_a \to \infty$

$$F_q \to \frac{1}{4}(1 + 2\sqrt{2}x_a) \quad [29]$$

$$F_w \to \frac{\sqrt{2}(1 + e^{-3\pi/4})}{2x_a^2} \quad [30]$$

$$F_\theta \to \frac{-1}{2x_a^2} \quad [31]$$

$$F_M \to \frac{-e^{-\pi/4}}{2x_a} \quad [32]$$

The error in these approximations at $x_a = 10$ ranges from 0 to 1 per cent for clamped plates and from 1 to 4 per cent for simply supported plates, the maximum in the latter case occurring in F_M with an approximate value of —0.0228 as compared to the calculated value of —0.0238.

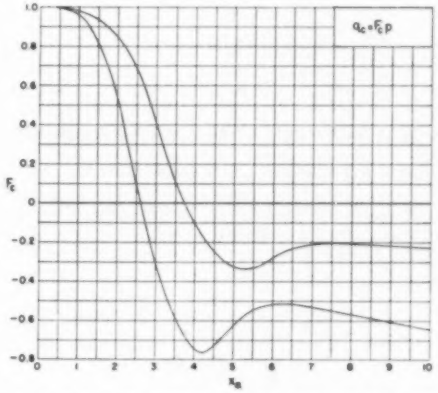

FIG. 4 VARIATION OF EFFECTIVE PRESSURE AT RADIUS OF MAXIMUM DEFLECTION WITH x_a; UPPER CURVE, CLAMPED; LOWER CURVE, SIMPLE

TUBE-COMPRESSION DESIGN FACTOR

The load on any tube, from Equations [1] and [2] is given by

$$W_t = \frac{\pi a^2}{N}[q - (f_t p_t - f_s p_s)] \quad [33]$$

in which q is the local effective pressure at the tube-sheet radius at which the tube is located. The maximum load, as can be seen by examination of Fig. 8 of the previous paper,[2] occurs at the periphery and its value is

$$W_{to} = \frac{\pi a^2}{N}[pF_q - (f_t p_t - f_s p_s)] \quad [34]$$

In ordinary floating-head-type exchangers, this is a compressive load if the higher pressure is on the shell side and a tensile load if on the tube side. In the type of exchanger under consideration here, however, the outermost tubes are always in tension regardless of which pressure is higher, unless the thermal-expansion effect is sufficiently great to overcome the pressure effect. This can be appreciated better if the expression for the equivalent pressure, p, is substituted in Equation [34] thus

$$W_{to} = \frac{\pi a^2}{N}\left[\frac{p_t(F_q - f_t) + f_s p_s - F_q KkL(\alpha_t T_t - \alpha_s T_s)}{1 + KF_q}\right] \quad [34a]$$

This can become negative only if

$$F_q K k L(\alpha_t T_t - \alpha_s T_s) > p_t(F_q - f_t) + f_s p_s$$

so that if an expansion joint or an outside packed floating head is used, or the left-hand member is small for any other reason, the outermost tubes must always be in tension.

Insufficient attention was paid in the original paper[2] to the fact that the criterion governing the ability of the tube bundle to develop the support attributed to it in this method of analysis may be the failure of some ring of tubes under a critical buckling load. Even though the numerical value of the tensile load in the outermost tubes may far exceed the compressive load at some point in the interior of the bundle, it is possible that the latter may be the governing value. Therefore an additional design factor giving the maximum negative effect pressure is needed; thus, by defmition

$$q_c = pF_c \quad \ldots\ldots\ldots\ldots\ldots\ldots\ldots\ldots [35]$$

and the corresponding tube load is

$$W_{tc} = \frac{\pi a^2}{N}[pF_c - (f_t p_t - f_s p_s)] \quad \ldots\ldots\ldots\ldots [36]$$

This factor is tabulated in Table 1 and shown graphically in Fig. 4.

For values of x_a above 10, F_c is approximated by

$$F_c \rightarrow \frac{-e^{-\pi}}{4}\frac{(1+\sqrt{2}x_a)}{\sqrt{1-\dfrac{\pi\sqrt{2}}{x_a}}} \qquad \text{(clamped)} \quad \ldots\ldots\ldots [37]$$

and

$$F_c \rightarrow \frac{-\sqrt{2}e^{\frac{-3\pi}{4}}}{8}\frac{(1+2\sqrt{2}\,x_a)}{\sqrt{1-\dfrac{3\pi\sqrt{2}}{4x_a}}} \text{ (simply supported)} \ldots [38]$$

Flexural Efficiency

In order to utilize any of the foregoing it is necessary to be able to evaluate x_a, which is defined as

$$x_a = a\left(\frac{2k}{D}\right)^{1/4} = \left[24(1-\nu^2)\frac{E_t}{\eta_w E}\frac{Nt(d-t)}{aL}\left(\frac{a}{h}\right)^2\right]^{1/4} \ldots [39]$$

In this the "deflection efficiency" or "flexural efficiency," η_w, is the only term not defined quantitatively. It is suggested that the following values be used pending experimental evaluation of more accurate values

$$\eta_w = 0.35\left[1 - 0.908\left(\frac{d}{P}\right)^2\right] \quad \text{for triangular pitch} \ldots [40a]$$

$$\eta_w = 0.25\left[1 - 0.785\left(\frac{d}{P}\right)^2\right] \quad \text{for square pitch} \ldots\ldots [40b]$$

Reference should be made to Malkin's paper,[2] and the discussion by the present author for the justification of these expressions.

Example

Calculate the necessary tube-sheet thickness for an integrally welded steel heat exchanger, 20 in. ID, with 260 $^3/_4$-in. 18 BWG steel tubes 12 ft long on 1-in. triangular pitch, and 5 semi-support plates on 27-in. centers. The shell thickness is $^3/_8$ in., the elastic modulus for all parts is 30×10^6 psi, the allowable design stress for all parts is 12,000 psi, and the coefficient of thermal expansion is 6.7×10^{-6} per deg F.

The design conditions are as follows:

Tube-side pressure, 150 psi; metal temperature, 300 F[5]
Shell-side pressure, 400 psi; metal temperature, 290 F[5]

The fundamental constants are as follows

$$f_t = 1 - \frac{260}{4}\left(\frac{0.652}{10}\right)^2 = 0.723$$

$$f_s = 1 - \frac{260}{4}\left(\frac{0.75}{10}\right)^2 = 0.635$$

$$k = \frac{260 \times 0.049 \times 0.701 \times 30 \times 10^6}{100 \times 144} = 1.86 \times 10^4$$

$$\eta_w = 0.35\left[1 - 0.906\left(\frac{0.75}{1}\right)^2\right] = 0.171$$

$$K = \frac{2 \times 30 \times 10^6 \times 0.375}{10 \times 1.86 \times 10^4 \times 144} = 0.84$$

$$D = \frac{30 \times 10^6 \times 0.171}{12 \times 0.91} \times h^3 = 0.469h^3 \times 10^6$$

$$x_a = 10\left(\frac{2 \times 1.86 \times 10^4}{0.469h^3 \times 10^6}\right)^{1/4} = 5.3/h^{3/4}$$

The equivalent design pressure may be written in terms of the effects of tube-side pressure, shell-side pressure, and thermal expansion; thus

$$p = \frac{150(1 + 0.84 \times 0.723) - 0.84 \times 0.635 \times 400 - 0.84 \times 1.86 \times 10^4 \times 144 \times 6.7 \times 10^{-6} \times 10}{1 + 0.84F_q}$$

$$= \frac{241 - 213 - 151}{1 + 0.84F_q}$$

Even though the value of F_q is not known at this point, it will be helpful to tabulate the values of $(1 + 0.84F_q)p$ in terms of all possibilities of pressure failure; a check ($\surd$) indicates which effects are considered to act:

Tube pressure	Shell pressure	Thermal expansion	$p(1 + 0.84F_q)$
$\surd$	..	..	+241
..	$\surd$	..	−213
..	..	$\surd$	−151
$\surd$	$\surd$	$\surd$	−123
$\surd$	$\surd$	..	+28
$\surd$	..	$\surd$	+90
..	$\surd$	$\surd$	−364

Obviously, the worst condition will be the simultaneous action of the shell pressure and thermal expansion in the absence of tube pressure. (In many cases, loss of shell pressure would affect the equivalent thermal-expansion pressure but, for purposes of illustration, this will be assumed not to occur here.)

Some assumption as to the tube-sheet thickness must now be made and checked; the maximum value of p would occur if F_q were unity and would be equal to $-364/1.84 = 198$ psi. Using the ordinary TEMA formula for this case[2,6]

$$h = 10\sqrt{198/12000} = 1.285 \text{ in.}$$

---

[5] These temperatures are so nearly the same that thermal expansions would not normally be even considered. However, this very fact, taken together with the results that follow, emphasizes the equivalent-pressure effect of thermal expansion.

[6] "Standards of Tubular Exchanger Manufacturer's Association," Second edition, New York, N. Y., 1949, pp. 13 and 28.

which suggests a thickness of 1.25 in. as a starting point. On this basis

$$x_a = 5.3/(1.25)^{3/4} = 4.49$$
$$F_q = 1.8 \text{ (clamped) or } 3.5 \text{ (simply supported)}$$
$$F_M = 0.077 \text{ (clamped) or } 0.055 \text{ (simply supported)}$$

The equivalent design pressure thus becomes

$$p = \frac{-364}{2.51} = -145 \text{ (clamped) or } \frac{-364}{3.94} = -93 \text{ (simply supported)}$$

Although there is some uncertainty as to the value of the ligament efficiency, a value of 0.3 will be used on the assumption that it lies somewhere between $(P - d)/P = 0.25$ and $(P - d + 2t)/P = 0.35$; the maximum radial bending stress is therefore

$$\sigma = \frac{6 \times 0.077 \times 145}{0.3}\left(\frac{10}{1.25}\right)^2 = 14{,}300 \text{ psi (clamped)}$$

or

$$\sigma = \frac{6 \times 0.055 \times 93}{0.3}\left(\frac{10}{1.25}\right)^2 = 6450 \text{ psi (simply supported)}$$

At this point the designer's judgment is called into play, for the thickness is more than ample if the tube sheet may be considered simply supported, but not enough if it must be considered clamped. The following facts may be taken into consideration:

(*a*) It is certain that a $^3/_4$-in. shell cannot rigidly clamp a $1^1/_4$-in. plate; there will be some rotation of the junction.

(*b*) The normal operating condition (assuming no failure of tube pressure) has an equivalent design pressure of —67 psi and a bending stress of 6600 psi even if the tube sheet is fully clamped.

(*c*) Even if yielding of the tube sheet should occur (which is very unlikely owing to the safety factor in the 12,000 psi allowable stress), the equivalent thermal-expansion pressure would be partially relieved, and the condition of boundary restraint would approach simple support as a result.

Assuming that the exchanger is not to operate in a cycling service, i.e., that it would operate under fairly steady conditions for months at a time, the author would be persuaded by these considerations that the $1^1/_4$-in. tube-sheet thickness is ample and might even be further decreased, provided that no other part would thereby become overstressed.

With a $^3/_4$-in. tube sheet, $x_a = 6.58$, $F_q = 5.0$, and $F_M = 0.037$ (both simply supported); the equivalent design pressure becomes $-346/5.2 = -67$ and the stress

$$\sigma = \frac{6 \times 0.037 \times 67}{0.3}\left(\frac{10}{0.75}\right)^2 = 8800 \text{ psi}$$

Inasmuch as good heat-exchanger tube-expanding practice does not permit much thinner tube sheets for $^3/_4$-in. tubes, the remaining calculations will be based upon the $^3/_4$-in. tube-sheet thickness.

The ability of the tubes to contribute the support attributed to them must next be investigated. The load per tube in the outermost ring of tubes is given by Equation [34], and in the tubes at maximum tube-sheet deflection, by Equation [36]; thus, with $F_q = 5.0$ (simply supported) or 2.6 (clamped), and $F_s = -0.52$ (simply supported) or —0.23 (clamped)

$$W_{ta} = \frac{\pi \times 100}{260}[5.0 \times p - 0.723 \times 150 + 0.635 \times 400]$$
$$= 1.21(5p - 109 + 254) \text{ (simply supported)}$$

or

$$W_{ta} = 1.21(2.6p - 109 + 254) \text{ (clamped)}$$

and

$$W_{te} = 1.21(-0.52p - 109 + 254) \text{ (simply supported)}$$

or

$$W_{te} = 1.21(-0.23p - 109 + 254) \text{ (clamped)}$$

Three separate terms have been left within the parentheses to indicate the separate contributions of the equivalent design pressure, tube-side pressure, and shell-side pressure, respectively. With the aid of these equations and the table of equivalent design pressures previously made, a similar table of tube loads can be made up as follows:

Tube pressure	Shell pressure	Thermal expansion	W_{ta} Simple	W_{ta} Clamped	W_{te} Simple	W_{te} Clamped
√	..	..	+149	+108	—157	—153
..	√	..	+ 59	+ 97	+333	+328
..	..	√	—176	—149	+ 18	+ 13
√	√	√	+ 33	+ 56	+193	+189
√	√	..	+208	+204	+175	+175
√	..	√	— 27	— 41	—139	—139
..	√	√	—116	— 52	+351	+341

By inspection it can be seen that the maximum tensile load would occur at the point of maximum tube-sheet deflection if the tube pressure failed, but the other effects were still felt, and that the maximum compressive load would occur in the outermost ring of tubes if both pressures failed but the fluid streams remained at temperature. The same conclusions could be reached more rapidly if Equation [34*a*] were used and Equation [36] were thrown into the same form, but there is some instructive value in the foregoing tabulation.

The maximum direct tensile stress would be

$$\sigma_t = \frac{351}{\pi \times 0.049(0.75 - 0.049)} = 3250 \text{ psi}$$

There is no bending stress in the tube at this point since the tube-sheet slope is zero at the radius of maximum deflection.

Considered as columns, the tubes have a maximum unsupported span of 45 in. from the tube sheet to the second support plate and could be considered as built-in at the tube-sheet end and "pinned" at the support plate as a conservative assumption. The critical load for such a column, by Euler's formula, is

$$W_t = \left(\frac{3\pi}{2 \times 45}\right)^2 \times 30 \times 10^6 \times \frac{\pi}{4}(\overline{0.375^4} - \overline{0.326^4})$$
$$= 2190 \text{ lb}$$

Even if the entire tube length were used, considering both ends built-in but ignoring the support plates entirely, the critical load would be

$$W_t = \left(\frac{2\pi}{144}\right)^2 \times 30 \times 10^6 \times \frac{\pi}{4}(\overline{0.375^4} - \overline{0.326^4}) = 384 \text{ lb}$$

as compared to the maximum possible load of 351 lb. Therefore there is no danger of failure of tube support either by buckling or by direct tension.

In problems of this kind there is always the possibility that the shell may not be able to take its share of the load without failure, so this point requires investigation also. From the equation preceding Equation [9], it will be observed that the tensile force acting axially through the shell is

$$\frac{2\pi a E_s t_s}{L}(m - \alpha_s T_s L)$$

and that this is equal to

$$\pi a^2(p_i - p)$$

Therefore the direct longitudinal stress in the shell is

$$\sigma_s = \frac{a}{2t_s}(p_i - p)$$

From the table of equivalent design pressures it will be seen that the largest possible negative value of p is $-364/(1 + 0.84 \times 2.6) = -115$ but that this occurs in the absence of any tube pressure; the largest negative value with tube pressure presumed acting is $-123/(1 + 0.84 \times 2.6) = -39$. The maximum possible tensile stress in the shell is accordingly

$$\sigma_s = \frac{10}{\frac{2}{3} \times 0.375}(150 + 39) = 2520 \text{ psi}$$

which is well below the allowable value.

Summary and Conclusions

Subject to the same assumptions and restrictions as postulated in the previous paper[2] fixed tube sheets may be designed in exactly the same way as the tube sheets of floating-head exchangers by merely substituting an equivalent design pressure (Equation [16]) for the actual hydrostatic pressure. This equivalent design pressure is a function of the shell-side and tube-side hydrostatic pressures and of the differential free thermal expansion between the shell and the tubes. For the purposes of this paper, a fixed-tube-sheet exchanger need only be considered as one in which the shell pressure can be exerted only on one side of the floating head; thus externally packed floating-head exchangers come within this classification as a special case, as do fire-tube boilers.

Since the equivalent design pressure is normally considerably less than either hydrostatic pressure, thinner tube sheets are possible than with floating-head exchangers; this means, in general, that higher values of the characteristic parameter x_a are encountered in design. The expressions based upon the asymptotic expansion of the Bessel functions result in considerable simplification of the basic design factors as shown by Equations [25] to [32], inclusive.

It is recognized that all the results of this paper and its predecessor[2] are somewhat conservative owing to the neglect of the counteracting bending moment of the tubes. This effect was recognized in the original paper in so far as its effect on the tubes themselves was concerned but the reaction on the tube sheet was ignored as negligible. This effect will be investigated in a subsequent paper.

Acknowledgment

The author gratefully acknowledges the encouragement of L. E. Sebald, late vice-president (Engineering), The Griscom-Russell Company, in the work which is summarized in this and previous papers. He also wishes to thank O. W. Heimberger, Chief Engineer, The Griscom-Russell Company, for permission to publish this paper.

Appendix

The Bessel functions employed in this paper may be represented by the asymptotic expansions given in the following

$$\text{ber } x = \frac{e^\delta}{\sqrt{2\pi x}} \cos \gamma$$

$$\text{bei } x = \frac{e^\delta}{\sqrt{2\pi x}} \sin \gamma$$

where

$$\delta = \frac{x}{\sqrt{2}} + \frac{1}{8\sqrt{2}x} - \frac{25}{384\sqrt{2}x^3} - \cdots$$

$$\gamma = \frac{x}{\sqrt{2}} - \frac{\pi}{8} - \frac{1}{8\sqrt{2}x} - \frac{1}{16x^2} - \frac{25}{384\sqrt{2}x^3} + \cdots$$

For large values of the argument, these reduce to

$$\text{ber } x \cong \frac{e^{x/\sqrt{2}}}{\sqrt{2\pi x}} \cos\left(\frac{x}{\sqrt{2}} - \frac{\pi}{8}\right)$$

$$\text{bei } x \cong \frac{e^{x/\sqrt{2}}}{\sqrt{2\pi x}} \sin\left(\frac{x}{\sqrt{2}} - \frac{\pi}{8}\right)$$

and the use of these expressions and their derivatives leads to the results given in Equations [25] through [32], [37], and [38].

Inasmuch as many of the expressions encountered involve ratios of these Bessel functions, the following will also be helpful

$$\frac{\text{ber } x}{\text{bei } x} \cong \cot\left(\frac{x}{\sqrt{2}} - \frac{\pi}{8}\right) = \frac{1 + \cot\left(\frac{x}{\sqrt{2}} + \frac{\pi}{8}\right)}{1 - \cot\left(\frac{x}{\sqrt{2}} + \frac{\pi}{8}\right)}$$

$$\frac{\text{ber}' x}{\text{bei}' x} \cong \cot\left(\frac{x}{\sqrt{2}} + \frac{\pi}{8}\right)$$

$$\frac{\text{bei } x}{\text{bei}' x} \cong \frac{\sqrt{2}}{\left[1 + \cot\left(\frac{x}{\sqrt{2}} - \frac{\pi}{8}\right)\right]} = \frac{\sqrt{2}}{2}\left[1 - \cot\left(\frac{x}{\sqrt{2}} + \frac{\pi}{8}\right)\right]$$

Bending and Buckling of an Elastically Restrained Circular Plate

By H. REISMANN,[1] FORT WORTH, TEXAS

This paper considers the effect of an elastic boundary restraint upon the deflection, moments, and critical (buckling) loads of a circular plate. The solutions given are based on the classical theory of plates and are exact within the assumptions underlying this theory. They include, as particular limiting cases, the known solutions for the simply supported and rigidly clamped edge. The physical significance of the results obtained is discussed in detail with particular emphasis upon the degree of restraint along the clamped edge.

Nomenclature

The following nomenclature is used in the paper:

a = plate radius
b = radius of load circle
r = radial co-ordinate
θ = angular co-ordinate
$\rho = r/a$ = dimensionless radial co-ordinate
$\delta = b/a$ = load position parameter
w = deflection of median surface
F = magnitude of concentrated load
$M_r, M_\theta, M_{r\theta}$ = radial, tangential, and twisting moment
Q_r, Q_θ = radial and tangential shearing forces
$\sigma_r, \sigma_\theta, \tau_{r\theta}$ = radial, tangential, and shearing stresses
D = flexural rigidity of plate $= \dfrac{Eh^3}{12(1-\nu^2)}$
E = Young's modulus
h = plate thickness
ν = Poisson's ratio
k = restraining constant
q = load intensity
Re = "real part of"
Im = "imaginary part of"

$$\nabla^2 = \frac{\partial^2}{\partial r^2} + \frac{1}{r}\frac{\partial}{\partial r} + \frac{1}{r^2}\frac{\partial^2}{\partial \theta^2}$$

Introduction and Statement of Problem

The problem of the circular plate has been discussed by numerous authors for various loading and boundary conditions. The solution corresponding to a rigidly clamped circular plate under a concentrated load at the center was first obtained by Poisson (1).[2] Clebsch (2) gave a solution in form of an infinite series for the case where the concentrated load is applied at an arbitrary point, while Michell (3) obtained the solution of the same problem in closed form. A series solution for the simply supported circular plate under an arbitrarily located concentrated load was given by Foeppl (4). The problem of radially symmetrical buckling of a circular plate under radial compressive forces uniformly distributed around the edge of the plate was first treated by G. H. Bryan (5) for both simple and rigidly clamped boundary supports.

It is the object of this investigation (*a*) to determine the deflection and moments of a circular plate under a concentrated load acting perpendicular to the median plane of the plate, the point of application of the load being arbitrary, and (*b*) to find the critical loads necessary to cause radially symmetrical buckling of a circular plate under a uniform distribution of radial compressive forces acting at the circular boundary in the median plane of the plate. In both cases (*a*) and (*b*) we shall assume the boundary of the plate to be elastically restrained against rotation according to a linear law; i.e., the slope of a line normal to the boundary and tangent to the median plane at the boundary is taken proportional to the radial moment.

The results obtained are of practical significance since neither rigidly clamped nor simply supported boundary conditions can be realized fully under actual physical conditions, and thus any case encountered in practice must lie somewhere between the two limiting cases of the problems under consideration.

Formulation and Solution

Transverse Bending With Elastic Boundary Restraint. According to the classical small-deflection theory, the transverse deflections of the median plane of the plate are characterized by

$$\nabla^4 w = \frac{q}{D} \qquad [1]$$

where q and D are the load intensity and flexural rigidity, respectively. The bending moments, shears, and stresses are related to the deflections w by means of the following equations which, for our purposes, we refer to polar co-ordinates (6)

$$\left.\begin{aligned} M_r &= -D\left[\frac{\partial^2 w}{\partial r^2} + \nu\left(\frac{1}{r}\frac{\partial w}{\partial r} + \frac{1}{r^2}\frac{\partial^2 w}{\partial \theta^2}\right)\right] \\ M_\theta &= -D\left[\nu\frac{\partial^2 w}{\partial r^2} + \frac{1}{r}\frac{\partial w}{\partial r} + \frac{1}{r^2}\frac{\partial^2 w}{\partial \theta^2}\right] \\ M_{r\theta} &= (1-\nu)D\left(\frac{1}{r}\frac{\partial^2 w}{\partial r \partial \theta} - \frac{1}{r^2}\frac{\partial w}{\partial \theta}\right) \end{aligned}\right\} \qquad [2]$$

$$\left.\begin{aligned} Q_r &= -D\frac{\partial}{\partial r}(\nabla^2 w) \\ Q_\theta &= -D\frac{1}{r}\frac{\partial}{\partial \theta}(\nabla^2 w) \end{aligned}\right\} \qquad [3]$$

---

[1] Senior Structures Engineer, Consolidated Vultee Aircraft Corporation; formerly, Research Engineer, Armour Research Foundation.

For presentation at the National Conference of the Applied Mechanics Division, State College, Pa., June 19–21, 1952, of The American Society of Mechanical Engineers.

Discussion of this paper should be addressed to the Secretary, ASME, 29 West 39th Street, New York, N. Y., and will be accepted until July 10, 1952, for publication at a later date. Discussion received after the closing date will be returned.

Note: Statements and opinions advanced in papers are to be understood as individual expressions of their authors and not those of the Society. Manuscript received by ASME Applied Mechanics Division, July 12, 1951. Paper No. 52—APM-7.

[2] Numbers in parentheses refer to the Bibliography at the end of the paper.

$$\left.\begin{aligned} \sigma_r &= \frac{12z}{h^3} M_r \\ \sigma_\theta &= \frac{12z}{h^3} M_\theta \\ \tau_{r\theta} &= -2Gz \frac{\partial}{\partial r}\left(\frac{1}{r}\frac{\partial w}{\partial \theta}\right) \end{aligned}\right\} \quad \ldots\ldots\ldots\ldots [4]$$

Without loss of generality we may assume the point of application of the concentrated load F to lie on the x-axis of the system of co-ordinates with origin at O as shown in Fig. 1. Thus a point P on the plate is determined uniquely by its polar co-ordinates r and θ where $0 \leq r \leq a$ and $0 \leq \theta < 2\pi$.

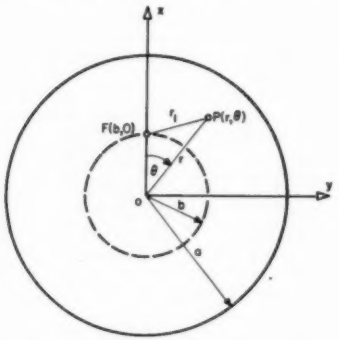

FIG. 1 ECCENTRICALLY LOADED CIRCULAR PLATE

In the particular problem under consideration the deflections along the circular boundary $r = a$ must vanish, and the inclination of the median surface with respect to a horizontal plane is proportional to the radial moment, or

$$\left.\begin{aligned} w(a, \theta) &= 0 \\ kD\left[\frac{\partial w}{\partial r}\right]_{a,\theta} &= aM_r(a, \theta) \end{aligned}\right\} \quad \ldots\ldots\ldots [5]$$

where k is a dimensionless restraining constant varying from zero to infinity. In particular, $k = 0$ corresponds to a simple support, while $k \to \infty$ represents the case of a rigidly clamped boundary.

The problem then consists of determining a function $w(r, \theta)$ which is biharmonic throughout the region $0 \leq r \leq a$ with the exception of the point of application of the concentrated load where it must possess an appropriate singularity. This function must, moreover, conform to the boundary conditions of Equations [5]. To solve the problem formulated we follow the approach used by Symonds (7) and assume a solution in the form

$$w(r, \theta) = w_1 + w_2 \quad \ldots\ldots\ldots\ldots [6]$$

where w_1 is a particular solution of Equation [1] and w_2 is the general solution of the homogeneous equation

$$\nabla^4 w = 0 \quad \ldots\ldots\ldots\ldots [7]$$

The particular solution w_1 is biharmonic with the exception of the load point where it has the required singularity. The solution w_2 contains an infinity of initially arbitrary constants and is biharmonic in the circular region of the plate $0 \leq r \leq a$. Upon superposition of w_1 and w_2 it is possible to adjust the constants so that $w(r, \theta)$ satisfies Equations [1] and [5].

A particular solution of Equation [1] is

$$\frac{8\pi D}{F} w_1 = r_1^2 \log r_1 \quad \ldots\ldots\ldots\ldots [8]$$

where w_1 is the deflection at P due to a load F at a distance r_1 from P as shown in Fig. 1. It is the singular part of the deflection function of a plate of infinite extent under a concentrated load.

The function w_1 may be expanded into an infinite trigonometric series. With the notation indicated in Fig. 1

$$r_1^2 = r^2 + b^2 - 2br\cos\theta \quad \ldots\ldots\ldots\ldots [9]$$

With reference to Fig. 1, let

$$\left.\begin{aligned} \overline{OP} &= z = re^{i\theta} \\ \overline{OF} &= z_0 = b \\ \overline{PF} &= z_0 - z = r_1 e^{i\phi} \end{aligned}\right\} \quad \ldots\ldots\ldots\ldots [10]$$

where z and z_0 are the complex numbers characterizing the vectors $\overline{OP}$ and $\overline{OF}$, respectively.

Hence for $r > b$

$$\left.\begin{aligned} r_1^2 \log r_1 &= (r^2 + b^2 - 2br\cos\theta)\, Re\,[\log(z - z_0)] \\ &= (r^2 + b^2)\log r + b^2 - \left(rb + \frac{1}{2}\frac{b^3}{r} + 2rb\log r\right)\cos\theta \\ &\quad + b^2 \sum_{n=2}^{\infty}\left[\frac{1}{n(n-1)}\left(\frac{b}{r}\right)^{n-2} - \frac{1}{n(n+1)}\left(\frac{b}{r}\right)^{n}\right]\cos n\theta \end{aligned}\right\} \quad [11a]$$

Similarly, for $r < b$

$$\left.\begin{aligned} r_1^2 \log r_1 &= (r^2 + b^2 - 2br\cos\theta)\, Re\,[\log(z_0 - z)] \\ &= (b^2 + r^2)\log b + r^2 - \left(br + \frac{1}{2}\frac{r^3}{b} + 2br\log b\right)\cos\theta \\ &\quad + b^2 \sum_{n=2}^{\infty}\left[\frac{1}{n(n-1)}\left(\frac{r}{b}\right)^{n} - \frac{1}{n(n+1)}\left(\frac{r}{b}\right)^{n+2}\right]\cos n\theta \end{aligned}\right\} \quad [11b]$$

The general solution of the biharmonic Equation [7] in polar co-ordinates is

$$\left.\begin{aligned} w_2 &= R_0 + R_1\cos\theta + \sum_{n=2}^{\infty} R_n \cos n\theta \\ \text{where} \\ R_0 &= A_0 + B_0 r^2 + C_0 \log r + D_0 r^2 \log r \\ R_1 &= A_1 r + B_1 r^3 + C_1 r^{-1} + D_1 r \log r \\ R_n &= A_n r^n + B_n r^{-n} + C_n r^{n+2} + D_n r^{-n+2} \end{aligned}\right\} \quad \ldots [12]$$

It represents the deflection of a circular plate subjected to loads at the boundary only.

Since the deflections, slopes, and moments must remain finite at $r = 0$

$$C_0 = D_0 = C_1 = D_1 = B_n = D_n = 0$$

The remaining constants are determined by applying to the solution, Equation [6], the boundary conditions Equations [5], and making use of Equations [12] as well as the series expansions Equations [11] of the particular solution. We obtain identities in θ giving rise to a system of six independent equations in six unknowns.

Introducing $\rho = r/a$, $\delta = b/a$ as dimensionless radial coordinate and load position parameter respectively, and solving, we obtain the following solution

$$\left.\begin{aligned}
\frac{8\pi D}{F} A_0 &= -a^2\delta^2 \log a - a^2\delta^2 - a^2 T \\
\frac{8\pi D}{F} B_0 &= T - \log a \\
\frac{8\pi D}{F} A_1 &= 2a\delta \log a + a\delta U \\
\frac{8\pi D}{F} B_1 &= \frac{1}{2}\frac{1}{a}\delta^4 + \frac{1}{a}\delta - \frac{1}{a}\delta U \\
\frac{8\pi D}{F} A_n &= \frac{b^2}{a^n}(W_n - V_n) \\
\frac{8\pi D}{F} C_n &= \frac{\delta^2}{a^n} V_n
\end{aligned}\right\} \quad \ldots\ldots [13]$$

where for convenience

$$\left.\begin{aligned}
T &= \frac{k^{-1}[\delta^2(1-\nu) - (3+\nu)] - (1+\delta^2)}{2[k^{-1}(1+\nu)+1]} \\
U &= \frac{k^{-1}\left[\delta^2\left(\frac{5}{4}+\nu\right)+2\right]+\delta^2}{k^{-1}(3+\nu)+1} \\
V_n &= \delta^{n-2} \left\{\frac{k^{-1}\left[\frac{\delta^2(1-\nu)}{(n+1)} + \frac{(1+\nu)}{n}\right] + \left[\frac{1}{n} - \frac{\delta^2}{(n+1)}\right]}{k^{-1}(2n+\nu+1)+1}\right\} \\
W_n &= \frac{\delta^n}{n(n+1)} - \frac{\delta^{n-2}}{n(n-1)}
\end{aligned}\right\} \quad \ldots [14]$$

The foregoing constants together with Equations [6], [8], [9], and [12] yield the equation of the elastic surface

$$\left.\begin{aligned}
\frac{8\pi D}{a^2 F} w(\rho,\theta) &= \tfrac{1}{2}(\rho^2 + \delta^2 - 2\delta\rho\cos\theta)\log(\rho^2 + \delta^2 - 2\delta\rho\cos\theta) \\
&+ T(\rho^2 - 1) - \delta^2 + \delta\rho\left[U(1-\rho^2) + \rho^2\left(\frac{1}{2}\delta^2 + 1\right)\right]\cos\theta \\
&+ \delta^2 \sum_{n=2}^{\infty} \rho^n [V_n(\rho^2 - 1) + W_n]\cos n\theta
\end{aligned}\right\} \quad \ldots [15]$$

Substituting Equation [15] into Equations [2] we obtain the moments

$$\left.\begin{aligned}
-\frac{8\pi}{F} M_r(\rho,\theta) &= 2 + 2(1+\nu)T + 2(3+\nu)\delta\rho\left(\frac{1}{2}\delta^2 + 1 - U\right)\cos\theta \\
&+ \frac{2(\nu-1)\delta^2\sin\theta}{(\rho^2+\delta^2-2\delta\rho\cos\theta)} + (1+\nu)\log[e(\rho^2+\delta^2-2\delta\rho\cos\theta)] \\
&+ (1-\nu)\frac{\delta^2}{\rho^2}\sum_{n=2}^{\infty}(n)(n-1)\rho^n W_n \cos n\theta
\end{aligned}\right\} \quad [16a]$$

$$\left.\begin{aligned}
&+ \delta^2 \sum_{n=2}^{\infty} [n^2(1-\nu) + n(3+\nu) + 2(\nu+1) \\
&\qquad - (1-\nu)(n)(n-1)\rho^{-2}](\rho^n V_n \cos n\theta)
\end{aligned}\right\} \quad [16a]\ cont.$$

$$\left.\begin{aligned}
-\frac{8\pi}{F} M_\theta(\rho,\theta) &= 2\nu + 2(1+\nu)T + 2(3\nu+1)\delta\rho\left(\frac{1}{2}\delta^2 + 1 - U\right)\cos\theta \\
&+ \frac{2(1-\nu)\delta^2\sin\theta}{(\rho^2+\delta^2-2\delta\rho\cos\theta)} + (1+\nu)\log[e(\rho^2 + \delta^2 - 2\delta\rho\cos\theta)] \\
&+ (\nu-1)\frac{\delta^2}{\rho^2}\sum_{n=2}^{\infty}(n)(n-1)\rho^n W_n\cos n\theta \\
&+ \delta^2 \sum_{n=2}^{\infty} [n^2(1+\nu) + n(3\nu-1) + 2(\nu-1) \\
&\qquad - (1-\nu)(n)(n-1)\rho^{-2}](\rho^n V_n \cos n\theta)
\end{aligned}\right\} \quad [16b]$$

$$\left.\begin{aligned}
\frac{8\pi}{(1-\nu)F} M_{r\theta}(\rho,\theta) &= \frac{2\delta(\rho - \delta\cos\theta)\sin\theta}{(\rho^2+\delta^2-2\delta\rho\cos\theta)} - \rho\delta[\delta^2 + 2(1-U)]\sin\theta \\
&- \frac{\delta^2}{\rho^2}\sum_{n=2}^{\infty}(n)(n-1)\rho^n W_n \sin n\theta \\
&- \delta^2 \sum_{n=2}^{\infty} n[(n+1) - (n-1)\rho^{-2}]\rho^n V_n \sin n\theta
\end{aligned}\right\} \quad [16c]$$

The infinite trigonometric series in Equations [15] and [16] involving W_n may be summed by methods described in the Appendix.

Buckling With Elastic Boundary Restraints. The circular plate under consideration is assumed to be subjected to uniform pressure $-\sigma_r$ at its edge. The plane-stress system therefore will be one of uniform compression throughout the plate, and the possible radially symmetric equilibrium positions of the median plane characterized by

$$w = w(r) \quad \ldots\ldots [17]$$

must satisfy the differential equation

$$D\nabla^4 w = -h\sigma_r \nabla^2 w \quad \ldots\ldots [18]$$

where, because of the assumption of radial symmetry

$$\nabla^2(\quad) = \frac{1}{r}\frac{d}{dr}\left[r\frac{d}{dr}(\quad)\right] \quad \ldots\ldots [19]$$

Thus Equation [18] assumes the form

$$\frac{1}{r}\frac{d}{dr}\left(r\left\{\frac{d}{dr}\left[\frac{1}{r}\frac{d}{dr}\left(r\frac{dw}{dr}\right)\right]\right\}\right) = -\alpha^2\frac{1}{r}\frac{d}{dr}\left(r\frac{dw}{dr}\right) \quad \ldots\ldots [20]$$

where

$$\alpha^2 = \frac{h\sigma_r}{D}$$

Integrating Equation [20] once, we obtain

$$\frac{d}{dr}\left[\frac{1}{r}\frac{d}{dr}\left(r\frac{dw}{dr}\right)\right] = -\alpha^2\frac{dw}{dr} + \frac{c}{r} \quad \ldots\ldots [21]$$

where c is an arbitrary constant. However, for the case of a full plate the integration constant c must vanish since

$$\left(\frac{dw}{dr}\right)_{r=0} = 0$$

It is now convenient to introduce the slope

$$-\phi = \frac{dw}{dr}$$

into Equation [21] as a new variable. Carrying out the indicated differentiation we obtain

$$r^2\frac{d^2\phi}{dr^2} + r\frac{d\phi}{dr} + (\alpha^2r^2 - 1)\phi = 0 \quad \ldots\ldots [22]$$

We shall require a solution of Equation [22] which satisfies the boundary conditions

$$\frac{D}{a}k\phi(a) = D\left(\frac{d\phi}{dr} + \nu\frac{\phi}{r}\right)_{r=a} \quad [23]$$

i.e., the inclination of the median surface with respect to a horizontal plane is proportional to the radial moment.

Equation [22] is recognized as Bessel's differential equation, the general solution of which is given by

$$\phi = C_1J_1(\alpha r) + C_2Y_1(\alpha r) \quad \ldots\ldots [24]$$

where J_1 and Y_1 represent the Bessel function of the first and second kind, respectively, both of the first order, and C_1 and C_2 are arbitrary constants.

Regularity conditions at $r = 0$ require that $C_2 = 0$, and substitution of the solution, Equation [24] into the boundary condition Equation [23] results in

$$\alpha aJ_0(\alpha a) = (k + 1 - \nu)J_1(\alpha a) \quad \ldots\ldots [25]$$

Thus Equation [24] represents a nontrivial solution of Equation [22] only for certain discrete values of $\alpha a = u$ which are roots of the transcendental Equation [25], and the critical (buckling) stress $(\sigma_r)_{cr}$ is obtained from

$$(\sigma_r)_{cr} = \frac{Du^2}{ha^2} \quad \ldots\ldots [26]$$

where $u = u(k)$, i.e., the critical stress may be considered as a function of the degree of constraint along the boundary.

Discussion of Results

The graphs shown in Figs. 2, 3, 4, and 5 exhibit the effect of the degree of constraint on the deflections and moments of an elastically clamped circular plate for which $\delta = 0.5$ and $\nu = 0.3$.

Deflection profiles along a diameter passing through the load point are shown in Fig. 2. Deflections corresponding to different degrees of constraint are illustrated, namely, those where $k = 0$ (simple support), $k = 1$ (elastic clamp), and $k \to \infty$ (rigid clamp). It is apparent that for identical loads the range of deflection profiles for elastically clamped plates is bounded by the profiles of the simply supported and rigidly clamped plate.

Fig. 3 shows the variation of the radial bending moment along a diameter passing through the load point. Here again we consider the cases $k = 0$, $k = 1$, and $k \to \infty$. Values of the radial moment of elastically clamped plates lie between those of a rigidly clamped and simply supported plate for corresponding points. Because of the singularity of the solution at the point of application of the concentrated load at $\delta = 0.5$, moments directly under the load tend to infinity. This was to be expected because the assumptions of the theory of bending of thin plates do not hold near the point of application of a concentrated load.

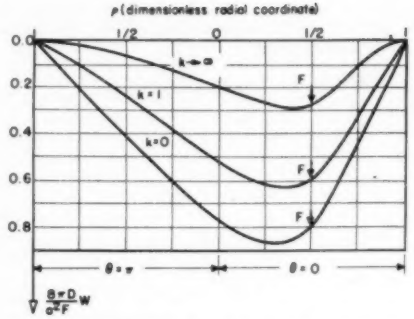

Fig. 2 Deflection Profiles Along Diameter Passing Through Load Point
($\delta = 0.5$, $\nu = 0.3$.)

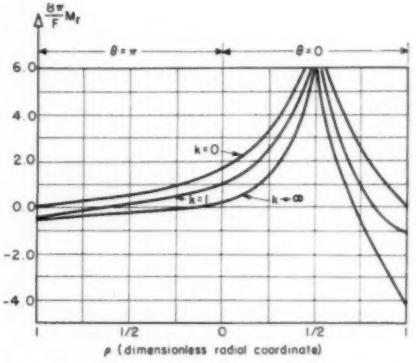

Fig. 3 Radial Bending Moments Along Diameter Passing Through Load Point
($\delta = 0.5$, $\nu = 0.3$.)

Fig. 4 indicates the distribution of radial moments along the circular boundary. As before, the three cases $k = 0$, $k = 1$, and $k \to \infty$ are considered, and one may conclude that the maximum radial moment at the boundary will occur at the point of the edge which is closest to the point of application of the load. Moreover, this location is independent of the degree of constraint. Here again, values of moments of an elastically clamped plate lie between those of a simply supported and rigidly clamped plate.

Fig. 5 permits study of the effect of the restraining constant on the maximum radial bending moment at the boundary. This moment is largest for $k \to \infty$ corresponding to a rigidly clamped plate, and decreases rapidly with k. The case of a simply supported edge is approached asymptotically and is characterized by $k = M_r = 0$.

Finally, Fig. 6 shows the dependence of the critical (buckling) stress $(\sigma_r)_{cr}$ on the restraining constant k in dimensionless form. This graph is obtained from a plot of Equation [26] which, in turn, required a solution of the transcendental Equation [25] for a continuous spectrum of the values of the restraining constant k. The known limiting cases are obtained for $k = 0$ and $k \to \infty$, the case of simple and rigidly clamped boundary supports, respec-

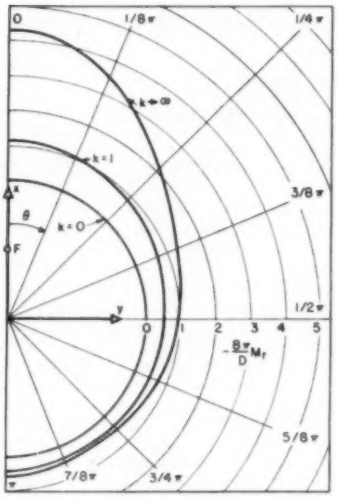

FIG. 4 RADIAL PLOT OF RADIAL BENDING MOMENTS ALONG BOUNDARY
($\delta = 0.5$, $\nu = 0.3$.)

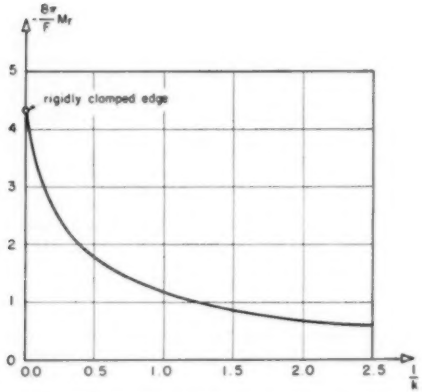

FIG. 5 MAXIMUM RADIAL BENDING MOMENT AT BOUNDARY AS A FUNCTION OF RESTRAINING CONSTANT
($\delta = 0.5$, $\nu = 0.3$, $\rho = 1$, $\theta = 0$.)

tively. It is seen that the critical stress $(\sigma_r)_{cr}$ is highest for a rigidly clamped plate and decreases rapidly with a decrease in the restraining constant. As $k \to 0$ the buckling stress approaches asymptotically the known value for the case of a simply supported plate. Only the first mode of buckling was considered.

ACKNOWLEDGMENT

The author wishes to thank Dr. E. Sternberg for many valuable suggestions in the preparation of this paper.

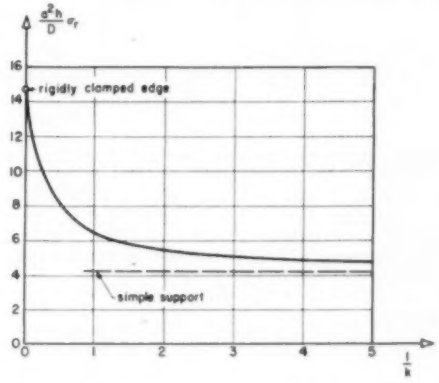

FIG. 6 CRITICAL STRESS AS A FUNCTION OF RESTRAINING CONSTANT
(First buckling mode, $\nu = 0.3$.)

BIBLIOGRAPHY

1 "Sur le Mouvement des Corps Elastiques," by S. D. Poisson. Memoirs de l'Academie Royale des Sciences de L'Institut de France, vol. 8, 1829, p. 545.

2 "Theorie der Elasticitaet Fester Koerper," by A. Clebsch, B. G. Teubner, Leipzig, Germany, 1862.

3 "The Flexure of a Circular Plate," by J. H. Michell, Proceedings of the London Mathematical Society, vol. 34, 1902, p. 223.

4 "Die Biegung einer Kreisfoermigen Platte," by A. Foeppl, *Sitzungsberichte Bayerische Akademie Wiss.*, vol. 42, 1912, p. 164.

5 "Stability of a Plane Plate Under Thrusts in Its Own Plane, by G. H. Bryan, Proceedings of the London Mathematical Society, vol. 22, 1891, p. 54.

6 "Theory of Plates and Shells," by S. Timoshenko, McGraw-Hill Book Company, Inc., New York, N. Y., 1940.

7 "Concentrated Force Problems in Plane Strain, Plane Stress, and Transverse Bending of Plates," by P. S. Symonds, JOURNAL OF APPLIED MECHANICS, Trans. ASME, vol. 68, 1946, p. A-183.

Appendix

To facilitate numerical evaluation of the results, the following infinite series involving W_n appearing in Equations [15] and [16] were summed (7). In the following discussion let $z = \Omega e^{i\theta}$ where $|z| < 1$. Then

$$\left.\begin{aligned}\sum_{n=2}^{\infty} \frac{\Omega^n}{n(n+1)} \cos n\theta &= Re\left[1 - \frac{1}{2}z + \left(\frac{1}{z} - 1\right)\log(1-z)\right] \\ \sum_{n=2}^{\infty} \frac{\Omega^n}{n(n-1)} \cos n\theta &= Re\left[z + (1-z)\log(1-z)\right]\end{aligned}\right\} \quad \ldots [27]$$

where Re denotes real part of. Similarly

$$\left.\begin{aligned}\sum_{n=2}^{\infty} \Omega^n \cos n\theta &= Re\left(\frac{1}{1-z} - 1 - z\right) \\ \sum_{n=2}^{\infty} \Omega^n \sin n\theta &= Im\left(\frac{1}{1-z} - 1 - z\right)\end{aligned}\right\} \quad \ldots [28]$$

where Im denotes imaginary part of. Furthermore

$$\left.\begin{aligned}\sum_{n=2}^{\infty}\frac{(n-1)}{(n+1)}\Omega^n\cos n\theta &= Re\left[1-\frac{1}{z}+\frac{1}{z(1-z)}+\frac{2}{z}\log(1-z)\right]\\ \sum_{n=2}^{\infty}\frac{(n-1)}{(n+1)}\Omega^n\sin n\theta &= Im\left[1-\frac{1}{z}+\frac{1}{z(1-z)}+\frac{2}{z}\log(1-z)\right]\end{aligned}\right\}\quad\ldots[29]$$

Combining Equations [27], [28], and [29] and letting $\Omega = \delta\rho$, we obtain

$$\sum_{n=2}^{\infty}\rho^n W_n\cos n\theta = 1-\frac{\rho}{\delta}\left(\frac{1}{2}\delta^2+1\right)\cos\theta+\frac{1}{2\delta}\left[\frac{1}{\rho}(1+\rho^2)\cos\theta+\frac{1}{\delta}(1+\delta^2)\right]\log(\delta^2\rho^2+1-2\delta\rho\cos\theta)+\left(\rho+\frac{1}{\delta\rho}\right)\sin\theta\,\arcsin\left[\frac{\delta\rho\sin\theta}{(\delta^2\rho^2+1-2\delta\rho\cos\theta)^{1/2}}\right]$$

$$\sum_{n=2}^{\infty}(n)(n-1)\rho^n W_n\cos n\theta = 1+\frac{1}{\delta^2}+\frac{1}{\delta\rho}(\rho^2-1)\cos\theta+\frac{\frac{1}{\delta\rho}(\rho^2+1)\cos\theta-\frac{1}{\delta^2}-\cos 2\theta}{(1+\delta^2\rho^2-2\delta\rho\cos\theta)}+\frac{1}{\delta\rho}\cos\theta\log(1+\delta^2\rho^2-2\delta\rho\cos\theta)+\frac{2}{\delta\rho}\sin\theta\,\arcsin\left[\frac{\delta\rho\sin\theta}{(1+\delta^2\rho^2-2\delta\rho\cos\theta)^{1/2}}\right]$$

$$\sum_{n=2}^{\infty}(n)(n-1)\rho^n W_n\sin n\theta = \frac{1}{\delta\rho}(\rho^2+1)\sin\theta+\frac{\sin 2\theta-\frac{1}{\delta\rho}(\rho^2+1)\sin\theta}{(1+\delta^2\rho^2-2\delta\rho\cos\theta)}-\frac{1}{\delta\rho}\sin\theta\log(1+\delta^2\rho^2-2\delta\rho\cos\theta)+\frac{2}{\delta\rho}\cos\theta\,\arcsin\left[\frac{\delta\rho\sin\theta}{(1+\delta^2\rho^2-2\delta\rho\cos\theta)^{1/2}}\right]$$

Gas Cooling of a Porous Heat Source[1]

By LEON GREEN, JR.,[2] DOWNEY, CALIF.

A limiting case of solid-fluid heat transfer is examined, in which a gas passes through a porous wall of high specific surface with heat generation within the solid material. Dimensionless temperature profiles in the wall are presented in terms of the rate of heat generation, rate of flow, and thermal properties of the gas and solid. The pressure drop across the wall is approximated by using an average wall temperature and assuming isothermal conditions. Temperature profiles, pressure drops, and pumping-power/power-output ratios are calculated for the hypothetical case of a heated graphite wall cooled by helium. It is found that the thermal dependence of the gas viscosity produces a minimum in the pressure-drop versus flow-rate curve, and it appears that favorable pumping-power/power-output ratios can be obtained by the use of high pressures. The problem of temperature stability in a gas-cooled porous solid is pointed out and the need for experimental work emphasized. Use of the sweat-cooling technique for high-pressure, high-temperature ducts is suggested.

Nomenclature

The following nomenclature is used in the paper:

- b = gas constant = R/M, (in./deg R)
- c_p = specific heat of gas, (Btu/lb deg F)
- g = gravitational acceleration, (in./sec^2)
- G = weight flow rate of gas, (lb/in.^{2} sec)
- k_g = thermal conductivity of gas, (Btu/in. sec deg F)
- k_s = apparent (bulk) thermal conductivity of solid, (Btu/in. sec deg F)
- l = thickness of wall, in.
- M = molecular weight of gas, (lb/lb mol)
- p = fluid pressure, psi
- q = rate of heat generation in wall, (Btu/in.^{3} sec)
- Q = rate of heat removal from wall (Btu/in.^{2} sec)
- R = universal gas constant $\left(10.73 \frac{\text{lb}}{\text{in.}^2} \times \frac{\text{ft}^3}{\text{lb mol}} \times \frac{1}{\text{deg R}}\right)$
- T = temperature, deg F or deg R
- W = power required for pumping of fluid (Btu/in.^{2} sec)
- x = length variable
- α = viscous resistance coefficient of porous material (in.$^{-2}$)
- β = inertial resistance coefficient of porous material (in.$^{-1}$)
- μ = dynamic viscosity of gas (lb sec/in.^{2})
- ρ = specific weight of gas, pcf

[1] This paper is based on studies carried out under Contract AT-11-1-GEN-8 for the Atomic Energy Commission.

[2] Research Engineer, North American Aviation, Inc. Now Devel. Engr., Solid Engine & Chemical Divisions, Aerojet Engineering Corp., Azusa, Calif. Jun. ASME.

Contributed by the Applied Mechanics Division and presented at the Annual Meeting, Atlantic City, N. J., November 25–30, 1951, of The American Society of Mechanical Engineers.

Discussion of this paper should be addressed to the Secretary, ASME, 29 West 39th Street, New York, N. Y., and will be accepted until July 10, 1952, for publication at a later date. Discussion received after the closing date will be returned.

Note: Statements and opinions advanced in papers are to be understood as individual expressions of their authors and not those of the Society. Manuscript received by ASME Applied Mechanics Division, July 6, 1951. Paper No. 51—A-32.

Introduction

The possibility of using porous construction to achieve efficient heat removal from a power-producing solid, although not a new idea, has recently been emphasized by Tsien (1).[3] Such construction would reconcile high power density with small temperature differences in the solid and the coolant fluid. The purpose of the present paper is to study a limiting case of heat removal from a porous wall by a gaseous coolant when the surface per unit volume of the porous structure is high enough that the temperature of the fluid at any point in its path may be considered to be substantially the same as that of the adjacent solid. Studies of sweat-cooled porous metals (2) indicate that this assumption is not unreasonable.

Temperature Distribution

The assumptions involved in the temperature-distribution problem are summarized as follows:

1 In the porous wall, gas temperature and solid temperature are approximately equal.

2 The gas flow and heat flow are steady and one-dimensional. Convective effects neglected by this assumption will alter the temperature distribution in the approaching gas at low flow rates but should not influence greatly the conditions prevailing within the wall.

3 All heat conduction in the wall takes place in the solid.

4 The thermal conductivities of the solid and gas and the specific heat of the gas are constant.

The one-dimensional flow of a gas at weight flow rate G through a porous wall of thickness l is shown in Fig. 1. If the rate of heat generation per unit volume in the wall is q, a heat balance on an element of volume in the wall (see Fig. 2) leads to the equation

$$\text{Wall:} \quad \frac{d_2T}{dx^2} - \frac{G\,c_p}{k_s}\frac{dT}{dx} + \frac{q}{k_s} = 0 \qquad [1]$$

A similar balance on a volume element in the approaching gas gives

$$\text{Gas:} \quad \frac{d^2T}{dx^2} - \frac{G\,c_p}{k_g}\frac{dT}{dx} = 0 \qquad [2]$$

subject to the conditions that at

$$x = -\infty,\ T = T_0 \qquad [3]$$

$$x = 0,\ T = T_1 \qquad [4]$$

and

$$k_g \left.\frac{dT}{dx}\right|_{\text{gas}} = k_s \left.\frac{dT}{dx}\right|_{\text{wall}} \qquad [5]$$

at

$$x = l,\ T = T_0 + \frac{ql}{G\,c_p} = T_2 \qquad [6]$$

solutions of Equations [1] and [2] are as follows

[3] Numbers in parentheses refer to the Bibliography at the end of the paper.

$$\text{Wall: } (0 \leq x \leq l) \quad \frac{T - T_0}{\frac{ql}{G c_p}} = \frac{x}{l} + \frac{1 - e^{-\frac{G c_p l}{k_s}\left(1 - \frac{x}{l}\right)}}{\frac{G c_p l}{k_s}} \quad \ldots [7]$$

$$\text{Gas: } (-\infty \leq x \leq 0) \quad \frac{T - T_0}{\frac{ql}{G c_p}} = \frac{1 - e^{-\frac{G c_p l}{k_s}}}{\frac{G c_p l}{k_s}} e^{\frac{G c_p l}{k_g}\left(\frac{x}{l}\right)} \quad \ldots [8]$$

Fig. 3 presents curves of the dimensionless temperature distribution in the wall as given by Equation [7] for different values of the parameter $(G\ c_p l/k_s)$. As expected, it is seen that uniformity of the wall temperature (desirable from the thermal stress viewpoint) is promoted by a high thermal conductivity in the solid. Manipulation of Equation [7] gives a relative temperature-uniformity index independent of the rate of power production in the form of the ratio

$$\frac{T_1 - T_0}{T_2 - T_0} = \frac{1 - e^{-\frac{G c_p l}{k_s}}}{\frac{G c_p l}{k_s}} \quad \ldots [9]$$

which approaches unity with decreasing flow rate as shown in

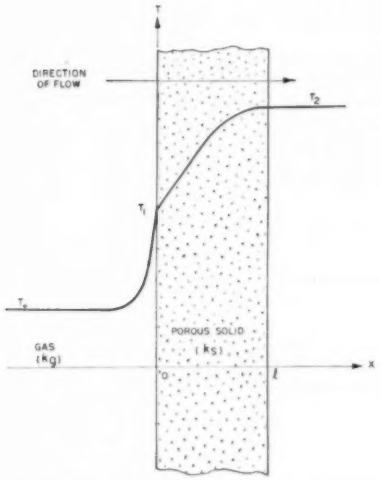

Fig. 1 Temperature Distribution in a Gas in One-Dimensional Flow Through a Porous Wall Generating Heat

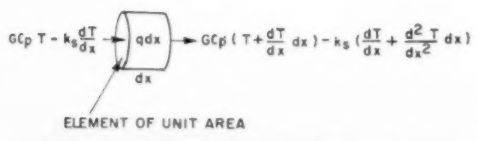

Fig. 2 Heat Balance on a Volume Element in Wall

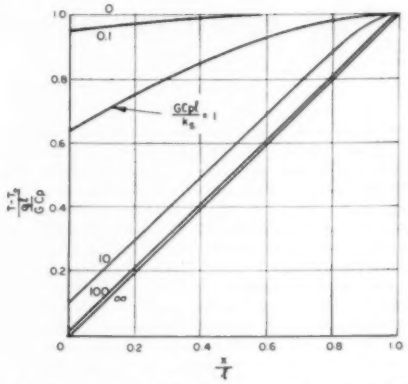

Fig. 3 Dimensionless Temperature Distribution in Porous Wall for Different Values of the Parameter $(G\ C_p l/k_s)$

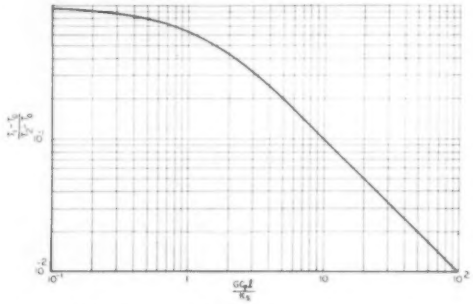

Fig. 4 Temperature Uniformity Ratio Versus $G\ C_p l/k_s$

Fig. 4. The absolute temperature difference across the wall, however, increases with decreasing flow rate, reaching a maximum value of

$$\lim_{G \to 0} \quad (T_2 - T_1) = \frac{ql^2}{2\,k_s} \quad \ldots [10]$$

For calculation of the pressure drop across the wall (as discussed in the following) it is convenient to use an average wall temperature

$$T_{avg} = \frac{1}{l} \int_0^l T\,dx \quad \ldots [11]$$

which with use of Equation [7] may be expressed in the form

$$\frac{T_{avg} - T_0}{\frac{ql}{G c_p}} = \frac{1}{2} + \frac{\frac{G c_p l}{k_s} - 1 + e^{-\frac{G c_p l}{k_s}}}{\left(\frac{G c_p l}{k_s}\right)^2} \quad \ldots [12]$$

This average temperature index is presented as a function of $(G\ c_p l/k_s)$ in Fig. 5. Since the index varies only between 0.5 and 1.0, the average wall temperature is, roughly, inversely proportional to the flow rate, as would be expected.

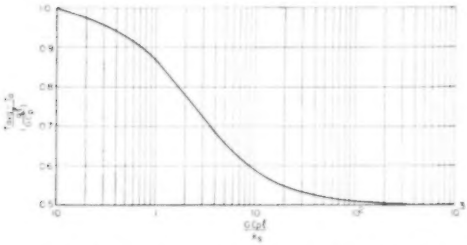

FIG. 5 AVERAGE TEMPERATURE INDEX VERSUS $G\ C_p l/k_s$

FLOW RESISTANCE

Experiments with porous metals (3) have shown that the pressure gradient in a perfect gas in steady, isothermal flow through a moderately fine-grained porous medium can be expressed by a quadratic equation of the type

$$-\frac{d\,(p^2)}{dx} = \alpha\,(2\,b\,T\mu)\,G + \beta\left(\frac{2\,b\,T}{g}\right)G^2 \ldots\ldots [13]$$

where $b = R/M$ is the specific gas constant, μ is the dynamic viscosity, and the coefficients α and β are length parameters characteristic of the structure of the porous material itself and are called the viscous and inertial resistance coefficients of the material, respectively. The viscous coefficient α, with dimensions (L^{-2}), characterizes the flow resistance of the material in the regime of "creeping" flow, where inertia forces are negligible. The inertial coefficient β, of dimension (L^{-1}), provides a measure of the additional resistance due to microscopic accelerations of the fluid within the interstices of the material.

A commonly encountered correlation of pressure-drop versus flow-rate data for porous media is formulated in terms of a Reynolds number and friction factor based upon the so-called "equivalent capillary diameter," calculated by invoking an analogy between the laws of Darcy and Poiseuille, which are valid only for low-velocity flows. This analogy would explain the deviation from Darcy's law at higher flow rates by the onset of turbulence within the pores which are visualized as straight, parallel capillaries. The porous-metal flow studies (3), however, showed that a single length parameter is not always sufficient to correlate pressure-drop versus flow-rate curves over a large range of flow rates, curves which in general are not "parallel" and may even cross one another in some cases of sufficiently different porous structures.

The necessity of having two independent length parameters for characterization of a porous medium of arbitrary complexity considerably reduces the advantage of the dimensionless friction-factor versus Reynolds number presentation. Although a Reynolds number and friction factor for a porous structure of a geometry defying description may be defined by writing Equation [13] in dimensionless groups (3), no convenience in calculations is achieved by so doing. With the introduction of heat generation within the solid material, as in the present problem, the complications involved in dimensionless representation are so great that its use is not justified, and greater simplicity is achieved by direct calculation of the pressure drops from Equation [13] in the foregoing form.

An exact solution of the pressure-drop problem would require integration of Equation [13] across the thickness of the heated wall, substituting at each point the proper temperature from Equation [7] and the corresponding value of the dynamic viscosity of the coolant gas. (This procedure, of course, assumes that the coefficients α and β are independent of temperature.[4]) For thin walls of high thermal conductivity, however, a simpler calculation using the average wall temperature from Equation [12] is sufficiently accurate.

HELIUM FLOW THROUGH A GRAPHITE WALL

As a specific example of gas cooling of a heat-producing porous solid, calculations of the anticipated performance of a porous graphite heater for helium gas have been made. Graphite as a heater material for use with inert gases is of interest because it has been found to exhibit remarkable mechanical properties at temperatures of incandescence (4, 5, 6). The hypothetical heater wall thickness is taken as 0.5 in. and the material is assumed to be National Carbon Company Grade 30 commercial porous graphite, pertinent properties of which are presented in Table 1. The high-temperature viscosity of helium, yielded by an intrepid extrapolation of the data of Akin and Norris (7), is shown in Fig. 6.

TABLE 1 SOME PROPERTIES OF GRADE 30 POROUS GRAPHITE[a]

Thermal conductivity,[b] Btu/in. deg F	9.3×10^{-4}
Tensile strength,[b] psi	80
Compressive strength,[b] psi	520
Viscous resistance coefficient,[c] $in.^{-2}$	8.4×10^{5}
Inertial resistance coefficient,[c] $in.^{-1}$	4.9×10^{3}

[a] National Carbon Company.
[b] From National-Acheson Handbook.
[c] Calculated from water-flow data obtained by M. R. Hatfield (8)

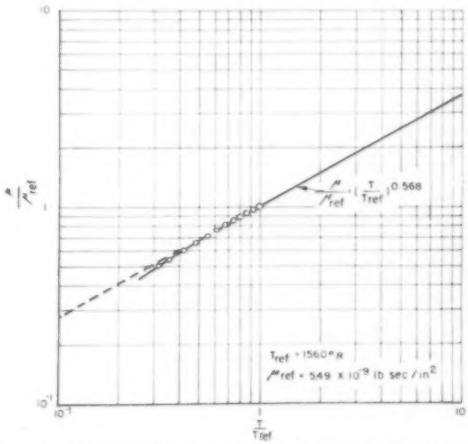

FIG. 6 THERMAL DEPENDENCE OF THE DYNAMIC VISCOSITY OF HELIUM, EXTRAPOLATED FROM THE DATA OF AKIN AND NORRIS (7)

Calculated temperature profiles in the wall described, and in the approaching gas are shown in Fig. 7 for a rate of heat generation of 10 Btu/in.³ sec and for several different weight flow rates. Fig. 8 presents curves of the pressure-square gradient across the wall versus flow rate (assuming an inlet temperature of 500 R) for heat-generation rates of 0, 0.1, 1.0, and 10 Btu/in.³ sec. The curves are terminated at the point where the wall temperature reaches the sublimation temperature of graphite (roughly, 6400 F at atmospheric pressure). The most striking feature of

[4] Flow experiments with porous metals at temperatures up to 1200 F support this assumption.

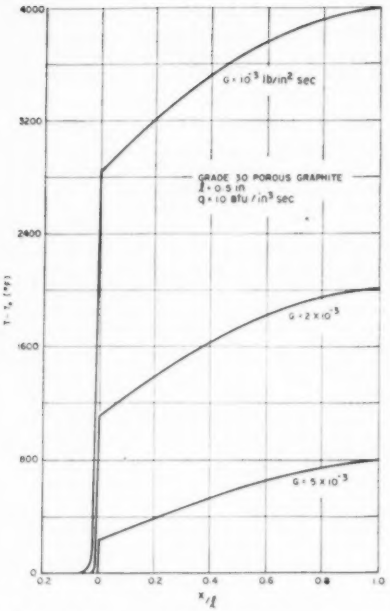

FIG. 7 TYPICAL TEMPERATURE PROFILES IN GAS AND POROUS WALL

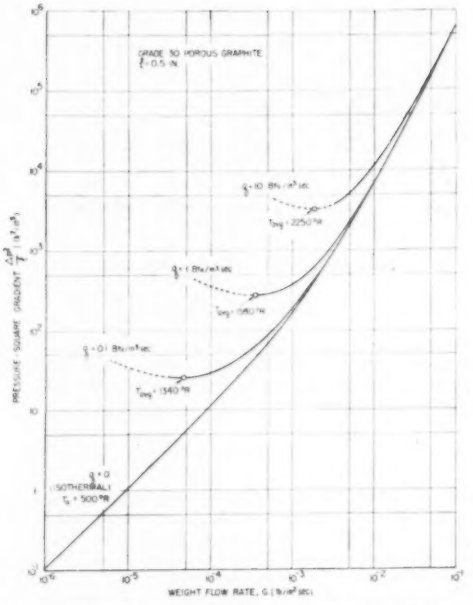

FIG. 8 PRESSURE-SQUARE GRADIENT IN POROUS WALL VERSUS WEIGHT FLOW RATE FOR DIFFERENT RATES OF HEAT GENERATION (Dashed portion indicates region where gas viscosity was calculated by extrapolation.)

these curves is that the flow rate is a double-valued function of the flow resistance, owing to the increase of the gas viscosity with temperature, and operation of the heater at the minimum point for greatest efficiency is indicated. The most extreme case ($q = 10$ Btu/in.^{3} sec) is investigated further in Fig. 9 which gives the pressure drop across the wall for inlet pressures of 5, 10, and 20 atm, respectively, thus emphasizing the advantage of operating the heater at high pressures. Because of the relative weakness of the porous structure (see Table 1), a small pressure difference across the wall is imperative.

A figure of merit commonly applied to heat exchangers is the ratio of the power required for the pumping of the fluid to the power removed as thermal energy. Since the pumping power used in forcing a perfect gas through the wall is

$$W = -G \int \frac{dp}{\rho} = bT_{avg} G \ln \frac{p_1}{p_2} \quad [14]$$

and the heat-removal rate is

$$Q = G c_p (T_2 - T_0) \quad [15]$$

the figure of merit becomes

$$\frac{W}{Q} = \frac{bT_{avg}}{c_p (T_2 - T_0)} \ln \frac{p_1}{p_2} \quad [16]$$

or for small pressure drops relative to the average absolute pressure

$$\frac{W}{Q} = \frac{bT_{avg}}{c_p (T_2 - T_0)} \frac{(p_1 - p_2)}{p_{avg}} \quad [17]$$

This ratio is plotted in Fig. 10 as a function of flow rate for the same case as in Fig. 9. It appears that in a high-pressure system the W/Q ratio may be reduced to a value low enough to permit useful power production from the heated gas. Gilliland (9) has shown analytically that the W/Q ratio for a gaseous heat-transfer system varies inversely as the square of the system pressure, and this prediction is obeyed by the data in Fig. 10, as is shown in Fig. 11, which indicates that a pressure of 40 atm would be required to reduce the W/Q ratio for the present case to 0.1 per cent.

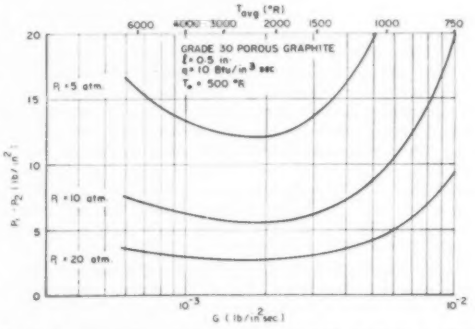

FIG. 9 PRESSURE DROP ACROSS WALL VERSUS FLOW RATE FOR THE CASE OF $q = 10$ BTU/IN.^{3} SEC AND FOR DIFFERENT INLET PRESSURES

It must be emphasized that the foregoing results do not show

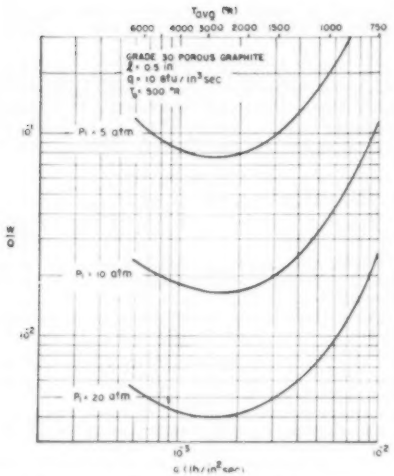

FIG. 10 PUMPING-POWER/POWER-OUTPUT RATIO VERSUS FLOW RATE FOR DIFFERENT INLET PRESSURES

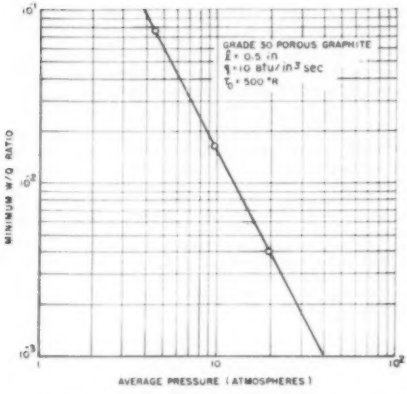

FIG. 11 MINIMUM W/Q RATIO VERSUS AVERAGE PRESSURE

conclusively that low W/Q ratios with gaseous coolants can be achieved with certainty merely by using porous construction. In preliminary experiments by the author,[5] however, using a nitrogen-cooled, electrically heated, porous-wall Ni-Fe tubular heat exchanger with a power density of 0.088 Btu/in.³ sec, W/Q ratios from 0.2 to 2.0 (depending upon the flow rate) were obtained. Since the mean pressure in the system (which exhausted to the atmosphere) averaged about 2 atm, it may be presumed that a system pressure of about 20 atm could effect a W/Q ratio of the order of 1 per cent. It may certainly be concluded that the idea appears attractive enough to justify an experimental investigation of its possibilities.

[5] Unpublished work conducted at the Jet Propulsion Laboratory of the California Institute of Technology, 1948.

TEMPERATURE STABILITY

The curves in Figs. 8, 9, 10, and 11 immediately suggest operation of the porous heater at the point of minimum pressure drop. If for some reason nonoptimum operation is desired, a choice of two alternative positions (high-temperature, low-flow, or low-temperature, high-flow) is available for each value of the pressure difference established across the wall. The order of commencing the coolant circulation and the power generation then determines which position is attained.

Instability of the wall temperature, however, may arise from the temperature dependence of the gas viscosity. Should a hot spot in the wall exist owing to some inhomogeneity of the porous material, for instance, the increased viscosity would tend to cut down the flow at the point, thus increasing the local temperature and aggravating the situation. The wall temperature conceivably could increase in this fashion until failure occurred. In the foregoing experiments by the author, no such instability was noted, but in this case the power density was low, operation was well into the high-flow, low-temperature region, and a considerable amount of heat was conducted out through the electrodes. Because of the difficulty in analyzing the temperature-stability problem in the porous heat source, it appears that an experimental approach would be more fruitful. It may be presumed, however, that stability will be promoted by high thermal conductivity in the porous solid, high heat capacity in the gas, and high flow rate. Stability considerations indeed may require operation on the high-flow side of the optimum point, where the flow resistance is dominated by the quadratic, nonviscous term of Equation [13]. Experimental work will be required to resolve this problem.

CONCLUSION

The foregoing discussion has explored the problem of heat removal from a porous heat source by a gaseous coolant. Consideration of the specific case of a helium-cooled graphite wall showed that efficient operation from the point of view of pumping power would require the use of a system under a pressure of at least several atmospheres. The use of such high pressures at the extreme temperature desired poses a serious problem of ducting or containment of the system, since the creep of most materials at such temperatures prohibits their use. In this connection the "sweat-cooling" technique proposed by Duwez (10) for use in the cooling of rocket motors appears to offer interesting possibilities. A section of a high-pressure, high-temperature, sweat-cooled duct is idealized in Fig. 12. Analysis (11, 12) and experiment (13, 14) have shown that effective cooling of the wall can be achieved by a relatively small flow of coolant, as is indicated in Fig. 13.

Since the effectiveness of the porous-wall cooling method (in cases with a temperature gradient along the wall) has been found to be greatest for wall materials of low thermal conductivity (11), the use of ungraphitized carbon is indicated for the present proposed application. For a stream temperature of 4000 F, for instance, a coolant flow (from a reservoir at 100 F) rate of only 0.2 per cent of the main stream rate would reduce the inner wall surface temperature to about 2450 F. The presence of the porous shield probably would eliminate the need for high-temperature materials in the outer casing. In this scheme the hot inner duct would be subject to only a small compressive stress required by the pressure difference driving the coolant, thus minimizing the creep problem, and the high pressure would be contained by the cool outer casing. Sweat-cooled ducts as applied to a gas turbine (the coolant air being taken from the compressor) have been

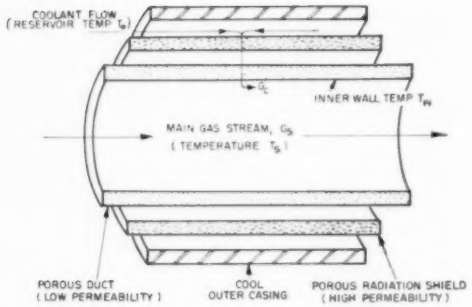

FIG. 12 SCHEMATIC SECTION OF A HIGH-PRESSURE SWEAT-COOLED DUCT

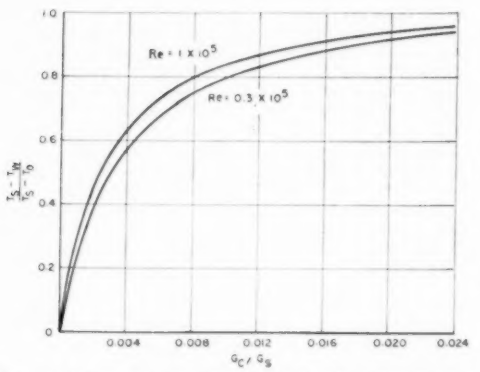

FIG. 13 EFFECT OF SWEAT COOLING ON WALL TEMPERATURE FOR TWO DIFFERENT MAIN-STREAM REYNOLDS NUMBERS
[After Rannie (11).]

studied by Moore and Grootenhuis (15), and it is reported that the power loss may approach 1 per cent at low coolant flows. It is possible that the sweat-cooling technique may make feasible the operation of a gaseous system at temperatures and pressures high enough to exploit the compactness and high permissible power density peculiar to a porous heat source.

ACKNOWLEDGMENT

The author wishes to acknowledge helpful discussions with Prof. Pol Duwez of the California Institute of Technology, at whose suggestion the foregoing analysis was made. The numerical calculations were made by Miss Barbara Lemke.

BIBLIOGRAPHY

1 "Rockets and Other Thermal Jets Using Nuclear Energy," by H. S. Tsien, contained in *The Science and Engineering of Nuclear Power*, Addison-Wesley Press, Inc., Cambridge, Mass., vol. II, 1949, p. 124.

2 "Heat Transfer in Sweat-Cooled Porous Metals," by S. Weinbaum and H. L. Wheeler, Jr., *Journal of Applied Physics*, vol. 20, 1949, p. 113.

3 "Fluid Flow Through Porous Metals," by L. Green, Jr., and P. Duwez, JOURNAL OF APPLIED MECHANICS, Trans. ASME, vol. 73, 1951, p. 39.

4 "Some Mechanical Properties of Graphite at Elevated Temperatures," by C. R. Malmstrom, R. D. Keen, and L. Green, Jr., *Journal of Applied Physics*, vol. 22, 1951, p. 593.

5 "The Thermal Dependence of the Elastic Moduli of Polycrystalline Graphite," by F. E. Faris, L. Green, Jr., and C. A. Smith, to be published in the *Journal of Applied Physics*.

6 "The Behavior of Graphite Under Alternating Stress," by L. Green, Jr., JOURNAL OF APPLIED MECHANICS, Trans. ASME, vol. 73, 1951, p. 345.

7 "Thermodynamic Properties of Helium at High Pressures and Temperatures," by S. W. Akin and R. H. Norris, G. E. General Engineering and Consulting Laboratory, April 23, 1947.

8 "Fluid Flow Through Porous Carbon," by M. R. Hatfield *Industrial and Engineering Chemistry*, vol. 31, 1939, p. 1419.

9 "Heat Transfer," by E. R. Gilliland, contained in *The Science and Engineering of Nuclear Power*, Addison-Wesley Press, Inc., Cambridge, Mass., vol. I, 1947, p. 342.

10 "Experimental Study of Cooling by Infiltration of a Fluid Through a Porous Material," by P. Duwez, Sixth International Congress for Applied Mechanics, Paris, France, 1946.

11 "A Simplified Theory of Porous Wall Cooling," by W. D. Rannie, Progress Report 4-50, Jet Propulsion Laboratory, California Institute of Technology, Pasadena, Calif., November 24, 1947.

12 "Some Observations on the Mechanism of Sweat Cooling," by P. Grootenhuis and N. P. W. Moore, Seventh International Congress for Applied Mechanics, vol. 3, 1948, p. 106.

13 "Experimental Study of Cooling by Injection of a Fluid Through a Porous Material," by P. Duwez and H. L. Wheeler, Jr., *Journal of the Aeronautical Sciences*, vol. 15, 1948, p. 509.

14 "Cooling by Forcing a Fluid Through a Porous Plate in Contact With a Hot Gas Stream," by M. Jakob and I. B. Fieldhouse, Heat Transfer and Fluid Mechanics Institute, 1949.

15 "Sweat Cooling," by N. P. W. Moore and P. Grootenhuis, *The Engineer*, vol. 189, 1950, p. 230.

The Marcus Method Applied to Solution of Uniformly Loaded and Clamped Rectangular Plate Subjected to Forces in Its Plane

By C. C. CHANG[1] AND H. D. CONWAY,[2] ITHACA, N. Y.

This paper presents a solution to the small-deflection problem of the uniformly loaded rectangular plate with all edges clamped, when the latter are subjected to uniform tensile or compressive forces in the plane of the plate. Since an exact solution to the problem is hardly possible, the Marcus method was used for the approximate solution of the biharmonic equation, subject to the conditions of zero slope and deflection at the boundary. Deflections and moments are presented for a square plate with four particular values of tensile end load, and for the rectangular plate with seven length-breadth ratios and with one value of compressive end load.

Introduction

THE problem of the uniformly loaded rectangular plate subjected to forces in its plane is frequently encountered in the design of such structures as a ship's bottom plating. If the edges of the plate may be assumed free from bending moment, an exact solution to the small-deflection problem is easily obtained in the form of Fourier series using the Levy method (1).[3] The results of such calculations and when a pair of opposite edges are subjected to uniform tensile or compressive forces have already been presented (2). Results for the case in which all edges are subjected to uniform tensile forces have also been given (3).

We now consider the problem when all edges are clamped and subjected to uniform tensile or compressive forces. With the usual nomenclature, the differential equation to be solved is

$$\nabla^4\omega = \frac{\partial^4\omega}{\partial x^4} + 2\frac{\partial^4\omega}{\partial x^2\partial y^2} + \frac{\partial^4\omega}{\partial y^4} = \frac{q}{D} + \frac{P}{D}\left(\frac{\partial^2\omega}{\partial x^2} + \frac{\partial^2\omega}{\partial y^2}\right) \quad [1]$$

where a positive value for the load P per unit length denotes tension and vice versa. Taking the co-ordinate origin at the center of the plate, the boundary conditions are

$$\left.\begin{aligned} \omega &= \frac{\partial\omega}{\partial x} = 0 \text{ at } x = \pm a/2 \\ \omega &= \frac{\partial\omega}{\partial y} = 0 \text{ at } y = \pm b/2 \end{aligned}\right\} \quad [2]$$

where a and b denote the lengths of the sides of the plate. Having determined the function ω, the bending and twisting moments per unit length of plate are

$$\left.\begin{aligned} M_x &= -D\left(\frac{\partial^2\omega}{\partial x^2} + \nu\frac{\partial^2\omega}{\partial y^2}\right) \\ M_y &= -D\left(\frac{\partial^2\omega}{\partial y^2} + \nu\frac{\partial^2\omega}{\partial x^2}\right) \\ M_{xy} &= D(1-\nu)\frac{\partial^2\omega}{\partial x\partial y} \end{aligned}\right\} \quad [3]$$

Since an exact solution to the problem is hardly possible, use is made of the Marcus method (4) for obtaining an approximate solution to Equation [1]. This method has recently been used by E. G. Odley (5) in his analysis of clamped rectangular plates subjected to hydrostatic pressure. It is apparent from Odley's paper that the Marcus method gives results which are sufficiently accurate for most practical purposes. The main value of the method is that the meeting of specified boundary conditions presents little difficulty.

We assume that a solution to Equation [1] may be written in the form

$$\omega = KXY \quad [4]$$

where K is a parameter and X and Y are, respectively, functions of x and y only. Adopting the nondimensional co-ordinates

$$\xi = 2x/a;\ \eta = 2y/b$$

and substituting Equation [4] in Equation [1], the intensity q_1 is found to be

$$q_1 = 16KD\left[\frac{Y}{a^4}\frac{d^4X}{d\xi^4} + \frac{2}{a^2b^2}\frac{d^2X}{d\xi^2}\frac{d^2Y}{d\eta^2} + \frac{X}{b^4}\frac{d^4Y}{d\eta^4}\right] - 4PK\left[\frac{Y}{a^2}\frac{d^2X}{d\xi^2} + \frac{X}{b^2}\frac{d^2Y}{d\eta^2}\right] \quad [5]$$

If the function X of x were known, a determination of the function Y of y could be made as follows:

From Equation [5], the load p_x on a strip of the plate of unit width is

$$p_x = 2\int_0^{a/2} q_1 dx = \frac{16KD}{a^3}\left[\frac{a^4}{b^4}C_x\frac{d^4Y}{d\eta^4} + \left(2\frac{a^2}{b^2}B_x - \frac{Pa^4}{4Db^2}C_x\right)\frac{d^2Y}{d\eta^2} + \left(A_x - \frac{Pa^2}{4D}B_x\right)Y\right] \quad [6]$$

where

$$A_x = \int_0^1 \frac{d^4X}{d\xi^4}d\xi,\ B_x = \int_0^1 \frac{d^2X}{d\xi^2}d\xi,\ C_x = \int_0^1 X d\xi$$

However, the actual load on this strip is qa and, after writing the following expression for K

---

[1] Formerly Graduate Student at Cornell University.

[2] Professor of Mechanics, Cornell University. Jun. ASME.

For presentation at the National Conference of the Applied Mechanics Division, The Pennsylvania State College, State College, Pa., June 19–21, 1952, of The American Society of Mechanical Engineers.

[3] Numbers in parentheses refer to the Bibliography at the end of the paper.

Discussion of this paper should be addressed to the Secretary, ASME, 29 West 39th Street, New York, N. Y., and will be accepted until July 10, 1952, for publication at a later date. Discussion received after the closing date will be returned.

Note: Statements and opinions advanced in papers are to be understood as individual expressions of their authors and not those of the Society. Manuscript received by ASME Applied Mechanics Division, May 14, 1951. Paper No. 52—APM-1.

$$K = \frac{qa^4}{4(4DA_x - Pa^2B_x)}$$

we obtain

$$\frac{d^4Y}{d\eta^4} + 2\frac{b^2}{a^2}\left[\frac{B_x}{C_x} - \frac{Pa^2}{8D}\right]\frac{d^2Y}{d\eta^2} + \frac{b^4}{a^4}\left[\frac{A_x}{C_x} - \frac{Pa^2}{4D}\frac{B_x}{C_x}\right](Y - 1) = 0 \quad \ldots\ldots [7]$$

There are two forms of solution to this equation which are required for our problems. For

$$\left[\frac{B_x}{C_x} - \frac{Pa^2}{8D}\right]^2 < \left[\frac{A_x}{C_x} - \frac{Pa^2}{4D}\frac{B_x}{C_x}\right]$$

the solution is

$$Y = 1 - (A \sin \phi_x\eta \sinh \psi_x\eta + B \sin \phi_x\eta \cosh \psi_x\eta + C \cos \phi_x\eta \sinh \psi_x\eta + D \cos \phi_x\eta \cosh \psi_x\eta) \quad \ldots\ldots [8]$$

where

$$\phi_x = \frac{b}{a}\sqrt{\frac{1}{2}\left[\sqrt{\left[\frac{A_x}{C_x} - \frac{Pa^2}{4D}\frac{B_x}{C_x}\right]^2 + \left(\frac{B_x}{C_x} - \frac{Pa^2}{8D}\right)^2} + \left[\frac{A_x}{C_x} - \frac{Pa^2}{4D}\frac{B_x}{C_x}\right]\right]},$$

$$\psi_x = \frac{b}{a}\sqrt{\frac{1}{2}\left[\sqrt{\left[\frac{A_x}{C_x} - \frac{Pa^2}{4D}\frac{B_x}{C_x}\right]^2 + \left(\frac{B_x}{C_x} - \frac{Pa^2}{8D}\right)^2} - \left[\frac{A_x}{C_x} - \frac{Pa^2}{4D}\frac{B_x}{C_x}\right]\right]}$$

while for

$$\left[\frac{B_x}{C_x} - \frac{Pa^2}{8D}\right]^2 > \left[\frac{A_x}{C_x} - \frac{Pa^2}{4D}\frac{B_x}{C_x}\right]$$

the solution is

$$Y = 1 - (A' \cos \phi_x'\eta + B' \sin \phi_x'\eta + C' \sin \psi_x'\eta + D' \cos \psi_x'\eta) \quad \ldots\ldots [9]$$

where

$$\phi_x' = \frac{b}{a}\sqrt{\left[\frac{B_x}{C_x} - \frac{Pa^2}{8D}\right] + \sqrt{\left[\frac{B_x}{C_x} - \frac{Pa^2}{8D}\right]^2 - \left[\frac{A_x}{C_x} - \frac{Pa^2}{4D}\frac{B_x}{C_x}\right]}};$$

$$\psi_x' = \frac{b}{a}\sqrt{\left[\frac{B_x}{C_x} - \frac{Pa^2}{8D}\right] - \sqrt{\left[\frac{B_x}{C_x} - \frac{Pa^2}{8D}\right]^2 - \left[\frac{A_x}{C_x} - \frac{Pa^2}{4D}\frac{B_x}{C_x}\right]}}$$

If the function Y of y was known instead of X, similar calculations would yield the load p_y on a strip of the plate of unit width and perpendicular to the former strip

$$p_y = 2\int_0^{b/2} q_1\,dy = \frac{16KD}{b^3}\left[\frac{b^4}{a^4}C_y\frac{d^4X}{d\xi^4} + \left(2\frac{b^2}{a^2}B_y - \frac{Pb^4}{4Da^2}C_y\right)\frac{d^2X}{d\xi^2} + \left(A_y - \frac{Pb^2}{4D}B_y\right)X\right] \quad \ldots [10]$$

where

$$A_y = \int_0^1 \frac{d^4Y}{d\eta^4}\,d\eta, \quad B_y = \int_0^1 \frac{d^2Y}{d\eta^2}\,d\eta, \quad C_y = \int_0^1 Y d\eta$$

Writing

$$K = \frac{qb^4}{4(4DA_y - Pb^2B_y)}$$

we obtain

$$\frac{d^4X}{d\xi^4} + 2\frac{a^2}{b^2}\left[\frac{B_y}{C_y} - \frac{Pb^2}{8D}\right]\frac{d^2X}{d\xi^2} + \frac{a^4}{b^4}\left[\frac{A_y}{C_y} - \frac{Pb^2}{4D}\frac{B_y}{C_y}\right](X - 1) = 0 \quad \ldots\ldots [11]$$

As before, there are two forms of solution of this equation which are required for our problems. For

$$\left[\frac{B_y}{C_y} - \frac{Pb^2}{8D}\right]^2 < \left[\frac{A_y}{C_y} - \frac{Pb^2}{4D}\frac{B_y}{C_y}\right]$$

the solution is

$$X = 1 - (A'' \sin \phi_y\xi \sinh \psi_y\xi + B'' \sin \phi_y\xi \cosh \psi_y\xi + C'' \cos \phi_y\xi \sinh \psi_y\xi + D'' \cos \phi_y\xi \cosh \psi_y\xi) \quad \ldots [12]$$

where

$$\phi_y = \frac{a}{b}\sqrt{\frac{1}{2}\left[\sqrt{\left[\frac{A_y}{C_y} - \frac{Pb^2}{4D}\frac{B_y}{C_y}\right]^2 + \left(\frac{B_y}{C_y} - \frac{Pb^2}{8D}\right)^2} + \left[\frac{A_y}{C_y} - \frac{Pb^2}{4D}\frac{B_y}{C_y}\right]\right]},$$

$$\psi_y = \frac{a}{b}\sqrt{\frac{1}{2}\left[\sqrt{\left[\frac{A_y}{C_y} - \frac{Pb^2}{4D}\frac{B_y}{C_y}\right]^2 + \left(\frac{B_y}{C_y} - \frac{Pb^2}{8D}\right)^2} - \left[\frac{A_y}{C_y} - \frac{Pb^2}{4D}\frac{B_y}{C_y}\right]\right]}$$

while for

$$\left[\frac{B_y}{C_y} - \frac{Pb^2}{8D}\right]^2 > \left[\frac{A_y}{C_y} - \frac{Pb^2}{4D}\frac{B_y}{C_y}\right]$$

the solution is

$$X = 1 - (A''' \cos \phi_y'\xi + B''' \sin \phi_y'\xi + C''' \sin \psi_y'\xi + D''' \cos \psi_y'\xi) \quad \ldots [13]$$

where

$$\phi_y' = \frac{a}{b}\sqrt{\left[\frac{B_y}{C_y} - \frac{Pb^2}{8D}\right] + \sqrt{\left[\frac{B_y}{C_y} - \frac{Pb^2}{8D}\right]^2 - \left[\frac{A_y}{C_y} - \frac{Pb^2}{4D}\frac{B_y}{C_y}\right]}},$$

$$\psi_y' = \frac{a}{b}\sqrt{\left[\frac{B_y}{C_y} - \frac{Pb^2}{8D}\right] - \sqrt{\left[\frac{B_y}{C_y} - \frac{Pb^2}{8D}\right]^2 - \left[\frac{A_y}{C_y} - \frac{Pb^2}{4D}\frac{B_y}{C_y}\right]}}$$

Observing that, from considerations of symmetry and edge clamping

$$B_x = \int_0^1 \frac{d^3X}{d\xi^3}\,d\xi = \left[\frac{dX}{d\xi}\right]_0^1 = 0$$

$$B_y = \int_0^1 \frac{d^3X}{d\eta^3}\,d\eta = \left[\frac{dX}{d\eta}\right]_0^1 = 0$$

the ϕ and ψ are reduced to the forms

$$\phi_x = \frac{b}{a}\sqrt{\frac{1}{2}\sqrt{\frac{A_x}{C_x}} - \frac{Pa^2}{16D}}; \quad \psi_x = \frac{b}{a}\sqrt{\frac{1}{2}\sqrt{\frac{A_x}{C_x}} + \frac{Pa^2}{16D}} \quad \ldots [14]$$

$$\phi_x' = \frac{b}{a}\sqrt{-\frac{Pa^2}{8D} + \sqrt{\left(\frac{Pa^2}{8D}\right)^2 - \frac{A_x}{C_x}}};$$

$$\psi_x' = \frac{b}{a}\sqrt{-\frac{Pa^2}{8D} - \sqrt{\left(\frac{Pa^2}{8D}\right)^2 - \frac{A_x}{C_x}}} \quad \ldots [15]$$

$$\phi_y = \frac{a}{b}\sqrt{\frac{1}{2}\sqrt{\frac{A_y}{C_y}} - \frac{Pb^2}{16D}}; \quad \psi_y = \frac{a}{b}\sqrt{\frac{1}{2}\sqrt{\frac{A_y}{C_y}} + \frac{Pb^2}{16D}} \quad \ldots [16]$$

$$\phi_y' = \frac{a}{b}\sqrt{-\frac{Pb^2}{8D} + \sqrt{\left(\frac{Pb^2}{8D}\right)^2 - \frac{A_y}{C_y}}};$$

$$\psi_y' = \frac{a}{b}\sqrt{-\frac{Pb^2}{8D} - \sqrt{\left(\frac{Pb^2}{8D}\right)^2 - \frac{A_y}{C_y}}} \quad \ldots [17]$$

The values of the constants, obtained from the boundary conditions, are then

$$\left.\begin{aligned} A &= \frac{\phi_x \sin\phi_x \cosh\psi_x - \psi_x \cos\phi_x \sinh\psi_x}{\phi_x \sinh\psi_x \cosh\psi_x + \psi_x \sin\phi_x \cos\phi_x} \\ B &= C = 0 \\ D &= \frac{\psi_x \sin\phi_x \cosh\psi_x + \phi_x \cos\phi_x \sinh\psi_x}{\phi_x \sinh\psi_x \cosh\psi_x + \psi_x \sin\phi_x \cos\phi_x} \end{aligned}\right\} \quad [18]$$

$$\left.\begin{aligned} A' &= \frac{-\psi_x' \sin\psi_x'}{\phi_x' \sin\phi_x' \cos\psi_x' - \psi_x' \cos\phi_x' \sin\psi_x'} \\ B' &= C' = 0 \\ D' &= \frac{\phi_x' \sin\phi_x'}{\phi_x' \sin\phi_x' \cos\psi_x' - \psi_x' \cos\phi_x' \sin\psi_x'} \end{aligned}\right\} \quad [19]$$

$$\left.\begin{aligned} A'' &= \frac{\phi_y \sin\phi_y \cosh\psi_y - \psi_y \cos\phi_y \sinh\psi_y}{\phi_y \sinh\psi_y \cosh\psi_y + \psi_y \sin\phi_y \cos\phi_y} \\ B'' &= C'' = 0 \\ D'' &= \frac{\psi_y \sin\phi_y \cosh\psi_y + \phi_y \cos\phi_y \sinh\psi_y}{\phi_y \sinh\psi_y \cosh\psi_y + \psi_y \sin\phi_y \cos\phi_y} \end{aligned}\right\} \quad [20]$$

$$\left.\begin{aligned} A''' &= \frac{-\psi_y' \sin\psi_y'}{\phi_y' \sin\phi_y' \cos\psi_y' - \psi_y' \cos\phi_y' \sin\psi_y'} \\ B''' &= C''' = 0 \\ D''' &= \frac{\phi_y' \sin\phi_y'}{\phi_y' \sin\phi_y' \cos\psi_y' - \psi_y' \cos\phi_y' \sin\psi_y'} \end{aligned}\right\} \quad [21]$$

From Equation [12]

$$\left.\begin{aligned} C_x &= 1 - \frac{A''}{\phi_y''^2 + \psi_y''^2}(-\phi_y \cos\phi_y \sinh\psi_y \\ &+ \psi_y \sin\phi_y \cosh\psi_y) - \frac{D''}{\phi_y''^2 + \psi_y''^2}(\phi_y \sin\phi_y \cosh\psi_y \\ &+ \psi_y \cos\phi_y \sinh\psi_y) \\ A_x &= -A''[\psi_y(\psi_y''^2 - 3\phi_y''^2)\sin\phi_y \cosh\psi_y \\ &+ \phi_y(3\psi_y''^2 - \phi_y''^2)\cos\phi_y \sinh\psi_y] \\ &-D''[\psi_y(\psi_y''^2 - 3\phi_y''^2)\cos\phi_y \sinh\psi_y \\ &- \phi_y(3\psi_y''^2 - \phi_y''^2)\sin\phi_y \cosh\psi_y] \end{aligned}\right\} \quad [22]$$

or, from Equation [13]

$$\left.\begin{aligned} C_x &= 1 - \frac{A'''}{\phi_y'''}\sin\phi_y' - \frac{D'''}{\psi_y'''}\sin\psi_y' \\ A_x &= -A'''\phi_y'^2 \sin\phi_y' - D'''\psi_y'^2 \sin\psi_y' \end{aligned}\right\} \quad [23]$$

Also, from Equation [8]

$$\left.\begin{aligned} C_y &= 1 - \frac{A}{\phi_x^2 + \psi_x^2}(-\phi_x \cos\phi_x \sinh\psi_x \\ &+ \psi_x \sin\phi_x \cosh\psi_x) - \frac{D}{\phi_x^2 + \psi_x^2}(\phi_x \sin\phi_x \cosh\psi_x \\ &+ \psi_x \cos\phi_x \sinh\psi_x) \\ A_y &= -A[\psi_x(\psi_x^2 - 3\phi_x^2)\sin\phi_x \cosh\psi_x \\ &+ \phi_x(3\psi_x^2 - \phi_x^2)\cos\phi_x \sinh\psi_x] \\ &-D[\psi_x(\psi_x^2 - 3\phi_x^2)\cos\phi_x \sinh\psi_x \\ &- \phi_x(3\psi_x^2 - \phi_x^2)\sin\phi_x \cosh\psi_x] \end{aligned}\right\} \quad [24]$$

or, from Equation [9]

$$\left.\begin{aligned} C_y &= 1 - \frac{A'}{\phi_x'}\sin\phi_x' - \frac{D'}{\psi_x'}\sin\psi_x' \\ A_y &= -A\phi_x'^2 \sin\phi_x' - D'\psi_x'^2 \sin\psi_x' \end{aligned}\right\} \quad [25]$$

In order to apply the Marcus method, a function X_0 is chosen to satisfy the boundary conditions. A suitable one for the present case is

$$X_0 = 1 - 2\xi^2 + \xi^4$$

A complementary function Y_1 is then found either from Equation [8] or from Equation [9]. Using this value of Y_1 and either Equation [12] or Equation [13], a new function X_1 is obtained. The procedure is repeated until successive values of X and Y are respectively the same. Numerical calculations for a particular case are given in the Appendix for illustrative purposes.

Results

In order to illustrate how the Marcus method may be used to solve Equation [1], numerical details for a particular case are given in the Appendix. When making numerical calculations, it is useful to introduce a nondimensional parameter P/P_E, where $P_E = 4\pi^2 D/b^2$; a value of Poisson's ratio of 0.3 was used throughout.

The functions X and Y depend only on the length-breadth ratio a/b and on P/P_E. It is then possible to write the deflection at any point in the form

$$\omega = \alpha \frac{qb^4}{Eh^3}$$

where α is a constant, dependent on a/b, P/P_E and the location of the point.

For uniform tensile end loads ($P > 0$), particular cases of square plates ($a/b = 1$) have been worked out for $P/P_E = 0$, 1, 2, and 3. Expressions for the deflections are listed in Table 1(a), and values of the constant α for the center deflections are given in Table 1(b). For tensile end loads, the center deflections are also the maximum deflections.

For uniform compressive end loads ($P < 0$), the expressions for the deflections for $P/P_E = -1/2$ and for various values of a/b are listed in Table 2(a). Values of α for intervals along the x-axis are given in Table 2(b). For values of a/b greater than 2, the maximum deflections do not occur at the center, while for $a/b > 5$, the major portion of the deflected surface is cylindrical. As might be expected, the maximum deflection for the cylindrical surface converges to the value

$$\omega_{max} = 0.05647 \frac{qb^4}{Eh^3}$$

which refers to a uniformly loaded and clamped strip of length b with a compressive end load of $P = -1/2 P_E$.

Having obtained the deflections, the bending moments may be obtained from Equations [3]. They may be represented in the forms

$$M_x = \beta q b^2; \quad M_y = \gamma q b^2$$

where β and γ are constants which depend on the values of a/b and P/P_E and the location of the point at which the moments are to be evaluated. The values of β and γ for the cases of compressive and tensile end load mentioned previously are tabulated in Table 3 for a quarter of the plate and for a value of Poisson's ratio of 0.3.

For the cases of tensile end load, the maximum moment is observed to act at the centers of the edges. However, for $P/P_E =$

TABLE 1 DEFLECTIONS FOR CASE OF TENSILE END LOAD ($P > 0$)

$a/b = 1, \xi = 2x/a, \eta = 2y/b, P_E = 4\pi^2 D/b^2$

(*a*) Deflection Equations

$P/P_E = 0$

$$w = \frac{b^4}{37.956}\frac{q}{16D}[1 - 0.34895 \sin 2.0871\xi \sinh 2.0871\xi - 0.10118 \cos 2.0871\xi \cosh 2.0871\xi]$$
$$[1 - 0.34893 \sin 2.0872\eta \sinh 2.0872\eta - 0.10113 \cos 2.0872\eta \cosh 2.0872\eta]$$

$P/P_E = 1$

$$w = \frac{b^4}{67.603}\frac{q}{16D}[1 - 0.15501 \sin 1.8296\xi \sinh 2.8779\xi - 0.14362 \cos 1.8296\xi \cosh 2.8779\xi]$$
$$[1 - 0.15501 \sin 1.8291\eta \sinh 2.8775\eta - 0.14378 \cos 1.8291\eta \cosh 2.8775\eta]$$

$P/P_E = 2$

$$w = \frac{b^4}{94.482}\frac{q}{16D}[1 - 0.035157 \sin 1.3922\xi \sinh 3.4362\xi - 0.16764 \cos 1.3922\xi \cosh 3.4362\xi]$$
$$[1 - 0.035172 \sin 1.3923\eta \sinh 3.4363\eta - 0.16761 \cos 1.3923\eta \cosh 3.4363\eta]$$

$P/P_E = 3$

$$w = \frac{b^4}{119.80}\frac{q}{16D}[1 + 0.20524 \sin 0.58071\xi \sinh 3.8912\xi - 0.18339 \cos 0.58071\xi \cosh 3.8912\xi]$$
$$[1 + 0.20506 \sin 0.58102\eta \sinh 3.8912\eta - 0.18337 \cos 0.58102\eta \cosh 3.8912\eta]$$

(*b*) Center Deflections (at $\xi = \eta = 0$)

$$w_{\text{center}} = \alpha \frac{qb^4}{Eh^3}$$

$P/P_E =$	0	1	2	3
$\alpha =$	0.0145	0.00740	0.00500	0.00379

TABLE 2 DEFLECTIONS FOR CASE OF COMPRESSIVE END LOAD ($P < 0$)

$P/P_E = -1/2, P_E = 4\pi^2 D/b^2, \xi = 2x/a, \eta = 2y/b$

(*a*) Deflection Equations

$a/b = 1$

$$w = \frac{b^4}{20.862}\frac{q}{16D}[1 - 0.64750 \sin 2.1127\xi \sinh 1.4128\xi - 0.063956 \cos 2.1127\xi \cosh 1.4128\xi]$$
$$[1 - 0.64750 \sin 2.1127\eta \sinh 1.4128\eta - 0.063956 \cos 2.1127\eta \cosh 1.4128\eta]$$

$a/b = 1.5$

$$w = \frac{b^4}{8.1900}\frac{q}{16D}[1 - 0.25617 \sin 2.9631\xi \sinh 1.7967\xi + 0.28427 \cos 2.9631\xi \cosh 1.7967\xi]$$
$$[1 - 1.48555 \sin 1.7114\eta \sinh 0.67956\eta - 0.4506 \cos 1.7114\eta \cosh 0.67956\eta]$$

$a/b = 2$

$$w = \frac{b^4}{5.9403}\frac{q}{16D}[1 + 0.053404 \sin 3.9085\xi \sinh 2.3253\xi + 0.21845 \cos 2.9085\xi \cosh 2.3253\xi]$$
$$[1 - 2.61053 \sin 1.6172\eta \sinh 0.38489\eta - 0.57449 \cos 1.6172\eta \cosh 0.38489\eta]$$

$a/b = 2.5$

$$w = \frac{b^4}{4.6946}\frac{q}{16D}[1 + 0.12339 \sin 4.8593\xi \sinh 2.8621\xi + 0.050193 \cos 4.8593\xi \cosh 2.8621\xi]$$
$$[1 + 2.29179 \cos 1.7499\eta - 2.94397 \cos 1.3684\eta]$$

$a/b = 3$

$$w = \frac{b^4}{3.7967}\frac{q}{16D}[1 + 0.065464 \sin 5.8091\xi \sinh 3.3969\xi - 0.041652 \cos 5.8091\xi \cosh 3.3969\xi]$$
$$[1 + 0.82488 \cos 1.9340\eta - 1.53688 \cos 1.0928\eta]$$

$a/b = 4$

$$w = \frac{b^4}{2.7813}\frac{q}{16D}[1 - 0.020708 \sin 7.7142\xi \sinh 4.4755\xi - 0.016254 \cos 7.7142\xi \cosh 4.4755\xi]$$
$$[1 + 0.44479 \cos 2.0459\eta - 1.22842 \cos 0.86530\eta]$$

$a/b = 5$

$$w = \frac{b^4}{2.1949}\frac{q}{16D}[1 - 0.002868 \sin 9.6210\xi \sinh 5.5569\xi - 0.0084428 \cos 9.6210\xi \cosh 5.5569\xi]$$
$$[1 + 0.31557 \cos 2.0939\eta - 1.14246 \cos 0.74170\eta]$$

(*b*) Deflections of Center Lines ($\eta = 0$)

$$w = \alpha \frac{qb^4}{Eh^3}$$

	$\xi =$	0	0.2	0.4	0.6	0.8	1.0
$a/b = 1$	$\alpha =$	0.02866	0.02643	0.02027	0.01178	0.00371	0
$a/b = 1.5$	$\alpha =$	0.05878	0.05486	0.04345	0.02647	0.00879	0
$a/b = 2$	$\alpha =$	0.05956	0.05818	0.05179	0.03642	0.01387	0
$a/b = 2.5$	$\alpha =$	0.05310	0.05535	0.05716	0.04722	0.02058	0
$a/b = 3$	$\alpha =$	0.04961	0.05298	0.05932	0.05538	0.02734	0
$a/b = 4$	$\alpha =$	0.05223	0.05193	0.05553	0.06162	0.03989	0
$a/b = 5$	$\alpha =$	0.05427	0.05336	0.05267	0.06045	0.05036	0

TABLE 3 DISTRIBUTION OF MOMENTS IN A QUARTER OF PLATE

$P_E = 4\pi^2 D/b^2$, $\xi = 2x/a$, $\eta = 2y/b$

I—Tensile End Load, $a/b = 1$

(a) $P/P_E = 0$. Values of β in $M_x = \beta qb^2$

1.0	−0.01631	−0.01522	−0.01207	−0.00740	−0.00250	0
0.8	−0.00269	−0.00247	−0.00205	−0.00205	−0.00363	−0.00635
0.6	0.00897	0.00846	0.00646	0.00157	−0.00612	−0.02467
0.4	0.01719	0.01619	0.01244	0.00367	−0.01286	−0.04023
0.2	0.02189	0.02061	0.01583	0.00483	−0.01618	−0.05073
0	0.02339	0.02203	0.01692	0.00515	−0.01735	−0.05437*
η/ξ	0	0.2	0.4	0.6	0.8	1.0

(b) $P/P_E = 1$. Values of β in $M_x = \beta qb^2$

1.0	−0.01115	−0.01054	−0.00868	−0.00566	−0.00208	0
0.8	−0.00091	−0.00075	−0.00041	−0.00040	−0.00185	−0.00694
0.6	0.00498	0.00500	0.00467	0.00267	−0.00365	−0.01887
0.4	0.00797	0.00798	0.00743	0.00427	−0.00554	−0.02896
0.2	0.00928	0.00932	0.00871	0.00499	−0.00680	−0.03515
0	0.00963	0.00968	0.00907	0.00518	−0.00723	−0.03719*
η/ξ	0	0.2	0.4	0.6	0.8	1.0

(c) $P/P_E = 2$. Values of β in $M_x = \beta qb^2$

1.0	−0.00904	−0.00857	−0.00705	−0.00433	−0.00052	0
0.8	−0.00099	−0.00090	−0.00067	−0.00037	−0.00031	−0.00175
0.6	0.00324	0.00332	0.00334	0.00237	−0.00192	−0.01443
0.4	0.00495	0.00510	0.00518	0.00370	−0.00314	−0.02351
0.2	0.00555	0.00577	0.00594	0.00428	−0.00385	−0.02857
0	0.00570	0.00593	0.00614	0.00444	−0.00407	−0.03016*
η/ξ	0	0.2	0.4	0.6	0.8	1.0

(d) $P/P_E = 3$. Values of β in $M_x = \beta qb^2$

1.0	−0.00783	−0.00748	−0.00637	−0.00441	−0.00177	0
0.8	−0.00004	0.00005	0.00028	0.00035	−0.00072	−0.00590
0.6	0.00273	0.00285	0.00303	0.00249	−0.00115	−0.01470
0.4	0.00365	0.00383	0.00413	0.00343	−0.00173	−0.02126
0.2	0.00391	0.00413	0.00454	0.00382	−0.00212	−0.02494
0	0.00395	0.00420	0.00464	0.00392	−0.00225	−0.02610*
η/ξ	0	0.2	0.4	0.6	0.8	1.0

II—Compressive End Load, $P/P_E = -1/2$

(a) $a/b = 1$. Values of β in $M_x = \beta qb^2$

1.0	−0.00297	−0.00274	−0.00210	−0.00122	−0.00038	0
0.8	0.01202	0.01154	0.01014	0.00757	0.00372	−0.00128
0.6	0.02829	0.02762	0.02519	0.01995	0.01053	−0.00407
0.4	0.04201	0.04137	0.03863	0.03159	0.01726	−0.00700
0.2	0.05097	0.05042	0.04767	0.03962	0.02202	−0.00913
0	0.05406*	0.05356	0.05084	0.04247	0.02372	−0.00990
η/ξ	0	0.2	0.4	0.6	0.8	1.0

(b) $a/b = 1.5$. Values of β in $M_x = \beta qb^2$

1.0	−0.04501	−0.04201	−0.03327	−0.02027	−0.00673	0
0.8	−0.02083	−0.01934	−0.01536	−0.01057	−0.00779	−0.01086
0.6	0.00811	0.00791	0.00610	−0.00027	−0.01417	−0.03575
0.4	0.03466	0.03294	0.02580	0.00865	−0.02204	−0.06326
0.2	0.05307	0.05032	0.03948	0.01467	−0.02819	−0.08396
0	0.05964	0.05652	0.04435	0.01679	−0.03049	−0.09159*
η/ξ	0	0.2	0.4	0.6	0.8	1.0

(c) $a/b = 1.5$. Values of γ in $M_y = \gamma qb^2$

1.0	−0.15004*	−0.14003	−0.11091	−0.06757	−0.02244	0
0.8	−0.08098	−0.07555	−0.05985	−0.03683	−0.01351	−0.00326
0.6	−0.01093	−0.01010	−0.00804	−0.00610	−0.00625	−0.01072
0.4	0.04831	0.04526	0.03576	0.01967	0.00094	−0.01898
0.2	0.08770	0.08209	0.06490	0.03673	0.00227	−0.02519
0	0.10148	0.09497	0.07510	0.04268	0.00335	−0.02747
η/ξ	0	0.2	0.4	0.6	0.8	1.0

(d) $a/b = 2$. Values of β in $M_x = \beta qb^2$

1.0	−0.04478	−0.04374	−0.03893	−0.02738	−0.01042	0
0.8	−0.02441	−0.02316	−0.01923	−0.01304	−0.00777	−0.01063
0.6	−0.00272	−0.00240	0.00421	0.00456	−0.00752	−0.03509
0.4	0.01615	0.01979	0.02574	0.02094	−0.00846	−0.06230
0.2	0.02897	0.03364	0.04075	0.03243	−0.00951	−0.08290
0	0.03349	0.03855	0.04611	0.03655	−0.00995	−0.09051*
η/ξ	0	0.2	0.4	0.6	0.8	1.0

(e) $a/b = 2$. Values of γ in $M_y = \gamma qb^2$

1.0	−0.14927*	−0.14581	−0.12979	−0.09128	−0.03476	0
0.8	−0.08328	−0.08115	−0.07182	−0.05036	−0.02002	−0.00319
0.6	−0.01533	−0.01430	−0.01136	−0.00751	−0.00563	−0.01052
0.4	0.04277	0.04298	0.04069	0.02947	0.00629	−0.01869
0.2	0.08182	0.08153	0.07582	0.05445	0.01417	−0.02487
0	0.09555	0.09509	0.08817	0.06325	0.01692	−0.02715
η/ξ	0	0.2	0.4	0.6	0.8	1.0

(f) $a/b = 2.5$. Values of β in $M_x = \beta qb^2$

1.0	−0.03956	−0.04123	−0.04259	−0.03518	−0.01533	0
0.8	−0.02328	−0.02334	−0.02200	−0.01663	−0.00908	−0.01099
0.6	−0.00747	−0.00474	0.00210	0.00685	−0.00309	−0.03645
0.4	0.00566	0.01133	0.02417	0.02907	0.00185	−0.06491
0.2	0.01434	0.02218	0.03952	0.04478	0.00510	−0.08648
0	0.01737	0.02601	0.04500	0.05042	0.00623	−0.09445*
η/ξ	0	0.2	0.4	0.6	0.8	1.0

(g) $a/b = 2.5$. Values of γ in $M_y = \gamma qb^2$

1.0	−0.13188	−0.13746	−0.14197*	−0.11727	−0.05112	0
0.8	−0.07482	−0.07781	−0.07963	−0.06531	−0.02902	−0.00329
0.6	−0.01569	−0.01544	−0.01384	−0.00990	−0.00614	−0.01093
0.4	0.03530	0.03842	0.04342	0.03860	0.01358	−0.01947
0.2	0.06969	0.07481	0.08225	0.07158	0.02687	−0.02594
0	0.08181	0.08764	0.09596	0.08324	0.03156	−0.02853
η/ξ	0	0.2	0.4	0.6	0.8	1.0

* Maximum computed values.

$-1/2$ and $a/b = 1$, the maximum moment occurs at the center of the plate. For $P/P_E = -1/2$ and $a/b = 1.5$ or 2, the maximum moment acts at the center of the long sides, but for greater values of a/b, the maximum moment moves toward the shorter sides.

BIBLIOGRAPHY

1 "Sur l'équilibre élastique d'une plaque rectangulaire," by M. Levy, Comptes Rendus, vol. 129, 1899, pp. 535–539.

2 "Bending of Rectangular Plates Subjected to a Uniformly Distributed Lateral Load and to Tensile or Compressive Forces in the Plane of the Plate," by H. D. Conway, Trans. ASME, vol. 71, 1949, pp. 301–309.

3 "The Rectangular Plate Subjected to Hydrostatic Tension and to Uniformly Distributed Lateral Load," by R. F. Morse and H. D. Conway, JOURNAL OF APPLIED MECHANICS, Trans. ASME, vol. 73, 1951, pp. 209–210.

4 "Beitrag zur Untersuchung von Behältern mit ebenen Wandungen," by H. Marcus, *Der Bauingenieur*, vol. 17, 1936, pp. 40–44.

5 "La Résistance des Réservoirs à Parois Planes," by H. Marcus, *Annales des Ponts et Chaussées*, vol. 107, 1937, pp. 538–567.

6 "Deflections and Moments of a Rectangular Plate Clamped on All Edges and Under Hydrostatic Pressure," by E. G. Odley, Trans. ASME, vol. 69, 1947, pp. 289–295.

Appendix

NUMERICAL CALCULATIONS FOR $a/b = 4$ AND $P/P_E = -1/2$

($\xi = 2x/a$; $\eta = 2y/b$; $P_E = 4\pi^2 D/b^2$; $\nu = 0.3$)

The following constants are calculated:

$$\frac{Pb^2}{8D} = \frac{P}{P_E} = -\frac{\pi^2}{4} = 2.46740; \quad \frac{Pb^2}{16D} = -1.23370:$$

$$\frac{Pa^2}{8D} = -39.4784; \quad \left(\frac{Pa^2}{8D}\right)^2 = 1558.54485$$

Assuming $X_0 = 1 - 2\xi^2 + \xi^4$, we find

$$C_{x0} = \int_0^1 X_0 d\xi = \frac{8}{15}; \quad A_{x0} = \int_0^1 \frac{d^4X_0}{d\xi^4} d\xi = 24; \quad \frac{A_{x0}}{C_{x0}} = 45$$

Since

$$\left(\frac{Pa^2}{8D}\right)^2 > \frac{A_{x0}}{C_{x0}}$$

Equation [9] is used to determine Y_1. From Equation [15]

$$\phi'_{x0} = 2.2133; \quad \psi'_{x0} = 0.18942$$

and from Equation [19]

$$A' = -0.020244; \quad B' = C' = 0; \quad D' = 1.00587$$

Equation [9] then gives

$$Y_1 = 1 + 0.020244 \cos 2.2133\eta - 1.00587 \cos 0.18942\eta$$

The first approximation to the deflection surface is then

$$\omega_1 = \frac{a^4}{24} \frac{q}{16D} X_0 Y_1$$

Using the foregoing value of Y_1, we find

$$C_{y1} = -\int_0^1 Y_1 d\eta = 0.0075425; \quad A_{y1} = \int_0^1 \frac{d^4Y_1}{d\eta^4} d\eta$$

$$= 0.17443; \quad \frac{A_{y1}}{C_{y1}} = 23.12628$$

Since

$$\left(\frac{Pb^2}{8D}\right)^2 < \frac{A_{y1}}{C_{y1}}$$

Equation [12] is used to determine X_2. From Equation [16]

$$\phi_{y1} = 7.6296; \quad \psi_{y1} = 4.3281$$

and from Equation [20]

$$A'' = 0.022396; \quad B'' = C'' = 0; \quad D'' = 0.020463$$

Equation [12] then gives

$$X_2 = 1 - 0.022396 \sin 7.6296\xi \sinh 4.3281\xi$$
$$-0.020463 \cos 7.6296\xi \cosh 4.3281\xi$$

The second approximation to the deflection surface is then

$$\omega_2 = \frac{b^4}{0.17443} \frac{q}{16D} Y_1 X_2$$

The procedure is then repeated until the successive values of ω converge. In the present case

$$\omega_{10} = \frac{b^4}{2.7812} \frac{q}{16D} [1 + 0.44482 \cos 2.0459\eta$$
$$- 1.22847 \cos 0.86531\eta]$$
$$[1 - 0.020708 \sin 7.7142\xi \sinh 4.4755\xi$$
$$- 0.016254 \cos 7.7142\xi \cosh 4.4755\xi]$$

$$\omega_{11} = \frac{a^4}{712.06} \frac{q}{16D} [1 - 0.020708 \sin 7.7142\xi \sinh 4.4755\xi$$
$$- 0.016254 \cos 7.7142\xi \cosh 4.4755\xi]$$
$$[1 + 0.44479 \cos 2.0459\eta - 1.22842 \cos 0.86530\eta]$$

Since these values are practically the same, a solution to Equation [1] has been obtained, and this solution satisfies the boundary conditions of the problem.

Measurement of Recovery Factors and Friction Coefficients for Supersonic Flow of Air in a Tube

2—Results Based on a Two-Dimensional Flow Model for Entrance Region

By J. KAYE,[1] T. Y. TOONG,[2] AND R. H. SHOULBERG,[3] CAMBRIDGE, MASS.

The first part of a program to obtain reliable data on the rate of heat transfer to air moving at supersonic speeds in a tube has been devoted to measurements made on adiabatic supersonic flow of air in a tube. The details of these measurements have been described in a previous paper. The calculated quantities such as the local apparent friction coefficient, recovery factor, Mach number, and so forth, were obtained from the simple one-dimensional flow model for which the properties of the stream are uniform at any section, and boundary-layer effects are ignored. The analysis of some of the same data given in the previous paper is undertaken here with the aid of a simplified two-dimensional flow model. The supersonic flow in the tube is divided into a supersonic core of variable mass with the fluid remaining in the core undergoing a reversible adiabatic change of state, and a laminar boundary layer of variable mass. The compressible laminar boundary layer increases in thickness in the direction of flow, and then undergoes a transition to a turbulent boundary layer. The two-dimensional flow model is limited here to the region where a laminar boundary layer appears to be present in the entrance region of the tube. The results of the analysis based on the two-dimensional flow model indicate that where the flow in the tube boundary layer appears to be laminar, the measured pressures and temperatures in the tube for adiabatic supersonic flow of air could have been predicted, with sufficient accuracy for engineering problems, from measured data for supersonic flow of air over a flat plate with a laminar boundary layer, and with zero pressure gradient.

Nomenclature

The following nomenclature is used in the paper:

A = cross-sectional area
a = inside radius of pipe
c_p = specific heat at constant pressure
c_v = specific heat at constant volume
c_w = discharge coefficient of nozzle
D = inside diameter of pipe
f = local coefficient of friction, $2g\tau/\rho V^2$
G = flow per unit area, w/A
g = acceleration given to unit mass by unit force
k = ratio of specific heats, c_p/c_v
L = distance from end of curved contour of nozzle
$\mathbf{M}$ = Mach number, $V/\sqrt{gkRT}$
$\mathbf{Pr}$ = Prandtl number, $c_p\mu g/\lambda$
p = static pressure
R = perfect-gas constant
r = recovery factor
s = entropy per unit mass
$\mathbf{Re}_D$ = diameter Reynolds number, $DG/\mu g$
$\mathbf{Re}_L$ = length Reynolds number, $LG/\mu g$
T = temperature, °F abs
t = temperature, °F
V = velocity
w = mass rate of flow
ρ = density
λ = thermal conductivity
μ = viscosity
τ = shear stress at wall
δ = thickness of boundary layer

Superscript * refers to throat of supersonic nozzle where $\mathbf{M} = 1$
Subscripts:

aw = adiabatic wall conditions
b = boundary layer
c = isentropic core
j = station numbers
oi = upstream stagnation conditions
r = atmospheric conditions
s = isentropic conditions

Introduction

Measurements concerned with fluid flow in ducts, with and without heat transfer, have been made for many years. Most of these measurements have been made for subsonic flows in pipes. A simple one-dimensional flow model based on uniform properties at each cross section has been found adequate for calculation and design purposes, provided the entrance region is neglected or fully developed flow is attained. Fortunately, there are many engineering problems where fully developed flow is obtained in a pipe

[1] Associate Professor of Mechanical Engineering, Massachusetts Institute of Technology. Jun. ASME.
[2] Research Assistant in Mechanical Engineering, Massachusetts Institute of Technology.
[3] Assistant in Mechanical Engineering, Massachusetts Institute of Technology.

Contributed by the Applied Mechanics Division and presented at the Annual Meeting, Atlantic City, N. J., November 25–30, 1951, of The American Society of Mechanical Engineers.
Discussion of this paper should be addressed to the Secretary, ASME, 29 West 39th Street, New York, N. Y., and will be accepted until July 10, 1952, for publication at a later date. Discussion received after the closing date will be returned.
Note: Statements and opinions advanced in papers are to be understood as individual expressions of their authors and not those of the Society. Manuscript received by ASME Applied Mechanics Division, May 25, 1951. Paper No. 51—A-29(b)

or where the entrance region is small relative to the total length of flow.

Several types of engineering designs exist where the entrance-region effects have a large influence on the performance of the equipment, such as in ducts in wind tunnels, heat exchangers, ducts in gas-turbine power plants, and other applications where pipes having a relatively small length-diameter ratio are used. For short pipes, the simple one-dimensional flow model has been replaced, in most mathematical treatments of the flow in the entrance region, by two-dimensional flow models or axially symmetrical flow models. These more complicated models have not come into general use for engineering designs and calculations, but are used mainly as a guide in estimation of deviations from the results based on the one-dimensional flow model.

The simple one-dimensional flow model has been used with some degree of success in computation of mean and local friction coefficients for supersonic flow in a tube. It has been shown in a previous paper (1),[4] however, that this simple flow model is not fully adequate in the interpretation of the calculated quantities, and that a more detailed analysis is needed for full comprehension of the phenomena which occur in the entrance length of the tube. This result is not surprising if it is realized that it is usually not possible to maintain supersonic flow in a length of pipe corresponding to that required for fully developed flow. In fact, in many measurements given in the previous paper (1), it has been found that the "entrance" region extends over the entire 42 diameters of length of supersonic flow.

A simplified two-dimensional analysis of supersonic flow in a tube has been examined in detail. The objectives in this analysis have been to analyze quantitatively the experimental data in terms of the laminar boundary layer at tube entrance, to compare quantitatively the calculated friction coefficients and recovery factors with those for supersonic flow over a flat plate, and to predict quantitatively the behavior of supersonic flow in the entrance region of various passages when a laminar boundary layer and an isentropic core are present. It is also evident that the simplified two-dimensional flow model can be used to analyze the supersonic flow of air in a tube with heat transfer in terms of the laminar boundary layer.

Assumptions for Two-Dimensional Flow Model

For the simplified two-dimensional flow model discussed here, the flow in the round tube is arbitrarily divided into two parts as shown in Fig. 1. The first part corresponds to the core which almost fills the tube at the entrance section and decreases in size in the direction of flow. The second part corresponds to the laminar boundary layer which is usually of small size compared with the core at the entrance section and grows in thickness in the direction of flow. As the core diminishes in size, mass is transferred from the core to the boundary layer. The arbitrary thickness of the boundary layer used here corresponds approximately to that thickness at which the local velocity in the boundary layer equals 99 per cent of the mean velocity in the core.

The assumptions of the preceding paragraph are consistent with Prandtl's concept of the boundary layer. His basic assumption was that the flow around an airfoil could be divided into a potential flow region where viscous forces are assumed to be negligible and a boundary-layer region where viscous forces are predominant. For flow in the tube it is assumed here that the effects of viscous forces on the fluid remaining in the core of decreasing mass are negligible and that the viscous forces are concentrated mainly in the boundary layer. Hence it is possible to determine simply and directly the states of the fluid remaining in the core by using isentropic relations.

[4] Numbers in parentheses refer to the Bibliography at the end of the paper.

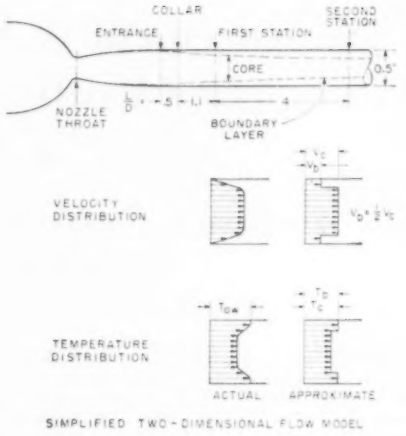

Fig. 1

The following assumptions were made in the analysis of the simplified two-dimensional flow model:

1 A laminar boundary layer exists over the entrance region of the tube.

2 The air remaining in the core undergoes an isentropic change of state from the stagnation pressure to the pressure at a given section.

3 The static pressure is uniform across each section of the tube.

4 Air is a perfect gas with a constant value of the ratio of specific heats ($k = 1.40$) over the range of temperature under consideration.

5 The laminar boundary layer has a linear distribution of velocity which is further approximated by an average velocity in the boundary layer equal to one half the core velocity, as shown in Fig. 1.

6 The stagnation temperature is uniform across each section of the tube where the laminar boundary layer is assumed to exist.

It should be noted that assumption 6 is strictly valid only when the Prandtl number is unity. Since the Prandtl number of air is less than unity a temperature discontinuity appears at the wall, or the temperature gradient (dT/dy) is infinite at the wall. Assumption 6 is not used, however, to calculate the recovery factors but merely to get an approximate value of the air density in the relatively thin boundary layer. The use of assumption 6 in this analysis is similar to the assumption often made that the velocity in the boundary layer varies as some power of the distance from the wall with the understanding that the velocity gradient at the wall (du/dy) is not to be used to find the shear stress at the wall.

Analysis of Simplified Two-Dimensional Flow Model

The following relations hold at each section of the flow in the tube shown in Fig. 1

Continuity: $w = w_b + w_c$ .....[1]

Continuity: $w_b = \rho_b V_b (A - A_c)$ .....[2]

Continuity: $w_c = \rho_c V_c A_c$ .....[3]

Geometry: $A_c = \pi(a - \delta)^2$ .....[4]

Equation of state: $p = \rho_b R T_b$ .....[5]

Equation of state: $p = \rho_c RT_c$ ..... [6]

Definition: $M_c^2 \equiv V_c^2/gkRT_c$ ..... [7]

Assumption: $V_b = V_c/2$ ..... [8]

The following relations hold between the upstream stagnation condition and any tube section shown in Fig. 1

Isentropic: $p_{oi}/p = (\rho_{oi}/\rho_c)^k$ ..... [9]

Isentropic: $T_{oi}/T_c = (p_{oi}/p)^{(k-1)/k}$ ..... [10]

Energy: $wc_pT_{oi} = w_c(c_pT_c + V_c^2/2g) + w_b(c_pT_b + V_b^2/2g)$ ..... [11]

Assumption: $c_pT_{oi} = c_pT_c + V_c^2/2g$ ..... [12]

From Equations [1], [11], and [12], it follows that

$$c_pT_{oi} = c_pT_b + V_b^2/2g \quad \text{.....[13]}$$

Note that T_b is, in reality, defined by Equation [11].

Application of the momentum equation for steady flow to a control volume which encloses the fluid between two adjacent stations of the tube yields

$$(p_j - p_{j+1})A - \tau\pi D(L_{j+1} - L_j) = \left[\frac{(w_cV_c + w_bV_b)}{g}\right]_{j+1} - \left[\frac{(w_cV_c + w_bV_b}{g}\right]_j \quad \text{.....[14]}$$

and the wall shearing stress is given by

$$\tau \equiv f_{j+1/2}\left(\frac{\rho_cV_c^2}{2g}\right)_{j+1/2} \quad \text{.....[15]}$$

where the "true" local friction coefficient $f_{j+1/2}$ is evaluated in terms of the fluid properties midway between the two adjacent stations.

The additional relations used in this analysis are as follows

Definition: $c_w \equiv (w/A^*)/(w/A^*)_s$ ..... [16]

Definition: $r \equiv (T_{aw} - T_c)/(T_{oi} - T_c)$ ..... [17]

Method of Computation. The method of computation is straightforward, using the measured values of pressure and adiabatic wall temperature along the tube. Since a sample calculation is given in the Appendix, it will suffice here merely to indicate the method of computation.

Starting with the measured stagnation pressure and temperature, the states of fluid remaining in the isentropic core can be evaluated at each station from the measured station pressure.[5] The recovery factor in Equation [17] can be evaluated immediately without further calculations of the details of the boundary layer. This method of calculation of recovery factors was used previously (June, 1949), by some of the present authors in presentation of the first report on this work (3), and has been used later by other authors. The details of the laminar boundary layer are then obtained from Equations [1] to [13]. The true local friction coefficient is obtained from Equations [14] and [15].

Results

In a previous paper (1) the measurements for adiabatic supersonic flow of air made in forty runs with three test combinations are presented in detail. It is evident that the use of the simplified two-dimensional flow model to convert all the data in these runs would involve a considerable amount of calculation. Therefore only six runs made with test combination B have been selected for computations made with the various two-dimensional flow models. These six runs correspond to those selected from test combination B for the comparisons made with the earlier test combinations given in the previous paper (1). This selection of the same six runs permits a direct comparison of calculations based on the one-dimensional flow model with those based on the simplified two-dimensional flow model.

One of the objectives of the two-dimensional model is to compare the results quantitatively with the well-known behavior of the development of a laminar boundary layer on a flat plate with zero pressure gradient in the direction of flow. For this reason the characteristics of the boundary layer on a flat plate are used as a basis of comparison on the various charts which will be discussed. It should be noted that this basis of comparison is a temporary expedient to be used until an exact solution for adiabatic supersonic flow in the entrance region of a round tube is available.

The six charts, Figs. 2, 3, 4, 5, 6, and 7, cover the range from laminar flow to turbulent flow in the boundary layer of the tube. None of the data obtained in the original measurements is shown on these charts since all such data are given in the previous paper (1). The calculated quantities based on one flow model are plotted on each chart without reference to the quantities calculated from the other flow model. Thus, in the curve of Mach number versus length Reynolds number, the values of the Mach number and Reynolds number are taken from either the one-dimensional flow model or from the two-dimensional flow model.

Each of the six charts, Figs. 2, 3, 4, 5, 6, and 7, presents the Mach number, mean stream temperature, boundary-layer thickness, recovery factor, and local friction coefficient. For the two-dimensional flow model, the Mach number and mean stream temperature refer to the isentropic core, and the recovery factor is given by Equation [17].

Code. Since the phrases, "two-dimensional flow model" and "one-dimensional flow model," occur frequently in the discussion of results they will be referred to in the abbreviated forms 2-DFM and 1-DFM, respectively.

Laminar Boundary Layer. Figs. 2, 3, and 4 compare the calculations based on the 2-DFM with those based on the 1-DFM for those values of the diameter Reynolds number where all the evidence indicates a laminar boundary layer exists for some distance downstream from the tube entrance.

In Fig. 2, for the smallest value of the Reynolds number, the Mach number based on the 1-DFM decreases from about 2.2 to 1.4 from the tube entrance to exit whereas the Mach number based on the 2-DFM decreases from about 2.6 to 2.2. This same pattern is also found in Figs. 3 and 4 for larger values of the Reynolds number. Thus the 2-DFM results in both a larger velocity in the supersonic core in the tube and a more nearly constant value of this velocity than that based on the 1-DFM.

A similar result is found in the calculation of the mean stream temperature for the 1-DFM and the core temperature for the 2-DFM. The ratio of mean stream temperature to stagnation temperature based on the 1-DFM increases from tube entrance to exit by about 45 per cent in Figs. 2, 3, and 4, whereas the ratio of core temperature to stagnation temperature based on the 2-DFM increases by only about 20 per cent in Figs. 2, 3, and 4. Thus the core temperature based on the 2-DFM is more nearly constant than the mean stream temperature based on the 1-DFM.

The basic hypothesis underlying the 2-DFM is the existence of a laminar boundary layer in the entrance region of the tube. This hypothesis can be tested by computation of the thickness of the laminar boundary layer in the tube. The ratio of this thickness to the tube radius is shown in Figs. 2, 3, and 4. This ratio increases from about 10 to about 45 per cent from the first

[5] By means of table 30 in Reference (2).

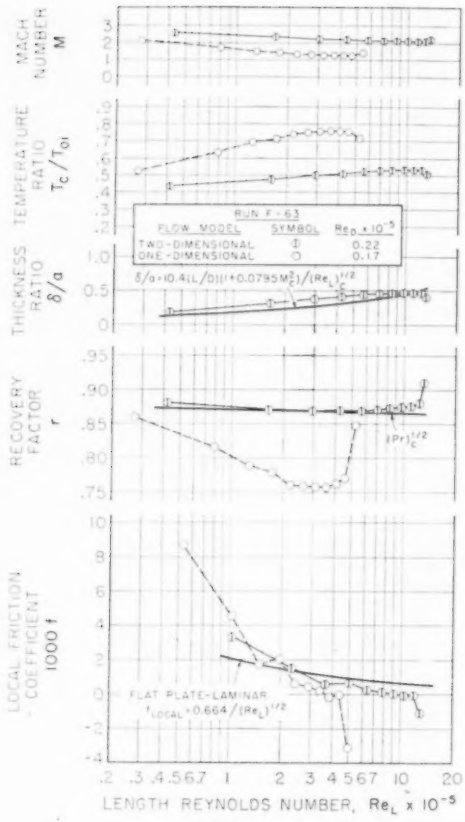

FIG. 2

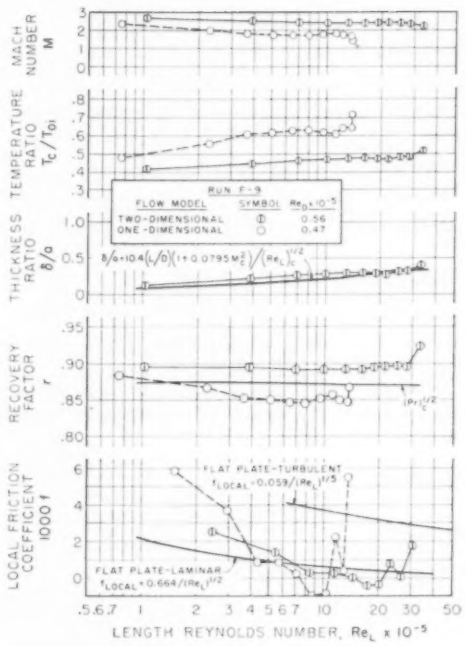

FIG. 3

station to the exit of the tube. Apparently, in Figs. 2, 3, and 4 the entire length of the test section corresponds to an entrance condition for this type of supersonic flow since the laminar boundary layer does not fill the tube at exit and a fully developed flow pattern is not attained.

In addition to computation of the thickness of the laminar boundary layer in the tube on the basis of the 2-DFM, the thickness may be computed from the theoretical predictions for flow over a flat plate with zero pressure gradient in the direction of flow. For incompressible flow, the results of Blasius (4) predict the thickness by the equation

$$(\delta/a) = 10.4(L/D)/\sqrt{(\mathbf{Re}_L)_c} \quad \ldots\ldots\ldots\ldots [18]$$

and those of Howarth (5) for a compressible boundary layer on a flat plate by the equation

$$(\delta/a) = 10.4(L/D)[1 + 0.1987(k-1)M_c^2]/\sqrt{(\mathbf{Re}_L)_c} \quad \ldots\ldots [19]$$

The thickness of the laminar boundary layer calculated from Howarth's work is shown in Figs. 2, 3, and 4. The agreement between the thickness calculated from the 2-DFM and from Howarth's results is very good in view of the fact that the length measurement L, which should be taken as zero at the point of zero boundary-layer thickness, has actually been taken as zero at the end of the curved contour of the nozzle, a point where the boundary-layer thickness is small but not zero. If the point of zero boundary-layer thickness can be determined accurately and used in Howarth's equation, some change in this agreement would result.

In Figs. 2, 3, and 4 the values of the ratio of boundary-layer thickness to tube radius calculated from the 2-DFM change suddenly near the end of the test section. This sudden change, probably caused by the transition from a laminar to a turbulent boundary layer, corresponds to changes in other calculated quantities at about the same length Reynolds numbers.

The original measurements of adiabatic wall temperature, reported in the previous paper (1), could be represented by a horizontal straight line when plotted against tube length with an average deviation of less than 0.4 per cent for all values except those at the first and last stations. It was noted in the previous paper, however, that the recovery factors calculated on the basis of the 1-DFM varied by about 20 per cent. It was concluded that this variation of about 20 per cent was probably a consequence of the inadequacy of the 1-DFM. This conclusion is now confirmed by calculation of the recovery factors based on the 2-DFM.

The recovery factors based on the 2-DFM, shown in Figs. 2 and 3, could be represented by a horizontal straight line with an average deviation of less than 0.4 per cent for all values except at the first and last stations, and by a similar line with a slightly larger value of the average deviation in Fig. 4. Thus the re-

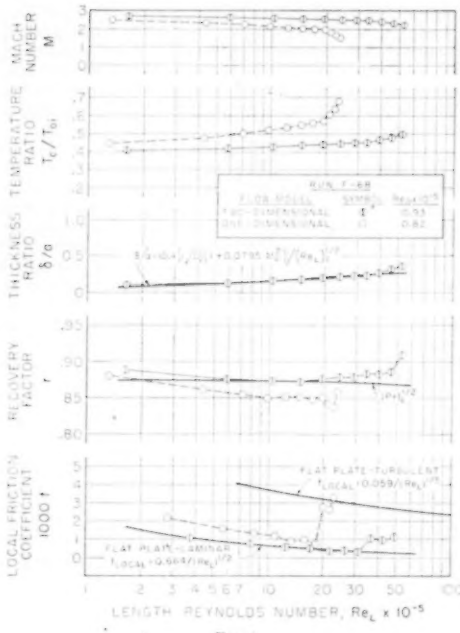

FIG. 4

covery factors based on the 2-DFM exhibit almost exactly the same variation as that shown by the original measured values of the adiabatic wall temperature. This result implies that the recovery factors for supersonic flow in a tube based on the 2-DFM should be directly comparable with those on a flat plate with a free stream condition identical to the core condition in the tube.

The few measurements available on recovery factors for flow around bodies at supersonic speed with a laminar boundary layer are summarized by Stalder, Rubesin, and Tendeland (6) This summary indicates the recovery factor is about 0.86 for a Mach number of about 2.0 for flow about a parabolic body of revolution, even in the presence of a pressure gradient. In addition, their measured recovery factor for a Mach number of 2.4 for flow on a flat plate with a laminar boundary layer is 0.881 over a range of length Reynolds number from 0.2×10^6 to 2×10^6. The recovery factors for the tube flow, based on the 2-DFM, for a Mach number of 2.4, are 0.875, 0.891, and 0.883, as read from Figs. 2, 3, and 4, respectively. The average of these three values is 0.883 ± 0.005. Such agreement should be considered a coincidence until the effect of the pressure gradient on both the tube flow and the plate flow is investigated in greater detail. The effect of Mach number on the recovery factors based on the 2-DFM appears to be small.

The analysis of Emmons and Brainerd (7, 8) for supersonic flow over a flat plate with a compressible laminar boundary layer predicts that the recovery factor should vary as the square root of the Prandtl number. For a compressible boundary layer, some doubt exists as to the temperature to be used in evaluation of the Prandtl number. Figs. 2, 3, and 4 show a curve corresponding to the square root of the Prandtl number evaluated at the core temperature based on the 2-DFM. The recovery factors based on the 2-DFM are in excellent agreement with the theoretical prediction in Figs. 2 and 4, and are about 2 per cent larger than the predicted values in Fig. 3.

The original measurements of static pressure distribution for adiabatic supersonic flow of air in the tube as well as the local apparent friction coefficients based on the 1-DFM are contained in the previous paper (1). It was indicated there that the 1-DFM was inadequate for the entrance region in the tube. The use of the 2-DFM, however, should result in a true local friction coefficient since changes in velocity profile are taken into account approximately. Hence the true local friction coefficients should be in better agreement with those for flow over a flat plate than the "apparent" values based on the 1-DFM.

In Figs. 2, 3, and 4 the true local friction coefficients based on the 2-DFM are compared with the apparent local friction coefficients based on the 1-DFM and with those for incompressible flow over a flat plate with zero pressure gradient. The values for incompressible flow are given by the curve marked "flat plate—laminar." The effect of compressibility in the laminary boundary layer for a Mach number of 2.5 is to reduce the true friction coefficient by about 5 per cent (7, 8). The contrast between the two flow models is immediately apparent in Figs. 2 and 3 where the slope of the friction-coefficient curve for the 2-DFM is greatly reduced compared with the slope of the curve based on the 1-DFM. In addition, the slope of the curve for the 2-DFM is now nearly the same in Figs. 2 and 3 as that for the flat plate.

The extraordinary agreement shown in Fig. 4 between the true local friction coefficients based on the 2-DFM and the flat-plate values could be considered accidental if it were not for the other evidence shown in Fig. 4. There is also nearly perfect agreement between the recovery factors based on the 2-DFM and those for a flat plate with a laminar boundary layer and very good agreement between the values of the corresponding boundary-layer thicknesses. This chart contains the most substantial evidence that comparison with the flat-plate values, a temporary expedient, is an excellent means of interpretation of the phenomena which occur in adiabatic supersonic flow of air in a tube near the entrance region. Furthermore, this chart indicates the possibility of reversing the calculations on the 2-DFM so as to predict the behavior of supersonic flow of air in a tube using the basic data for supersonic flow of air on a flat plate.

The values of the mean true friction coefficient are not shown in Figs. 2, 3, 4, 5, 6, and 7, mainly because of the uncertainty of determining the origin of the laminar boundary layer, or the point where the thickness of this layer is zero. Since the local true friction coefficient for flow over a flat plate approaches infinity as the origin is approached, a considerable error can be introduced in the mean friction coefficient by extrapolation of the local values to an arbitrary origin.

Boundary Layer in Transition and Turbulent Boundary Layer. Figs. 5, 6, and 7 compare the calculations based on the 2-DFM with those based on the 1-DFM for those values of the diameter Reynolds number where the evidence indicates either the presence of a laminar boundary layer for only a short distance downstream from tube entrance, as in Fig. 5, or the presence of only a turbulent boundary layer, as in Figs. 6 and 7. The 2-DFM is based, however, on the existence of a laminar boundary layer in the tube. Hence the results based on the 2-DFM would agree only coincidentally, if at all, with the flat-plate values in the transition region or for the region where a turbulent boundary layer exists.

PREDICTION OF SUPERSONIC FLOW BEHAVIOR IN A TUBE

The good agreement between the values of the laminar-boundary-layer thickness, recovery factor, and local true fricton coefficient, based on the 2-DFM, and the corresponding values for a laminar boundary layer on a flat plate indicates that this simplified and approximate 2-DFM may be used in reverse to

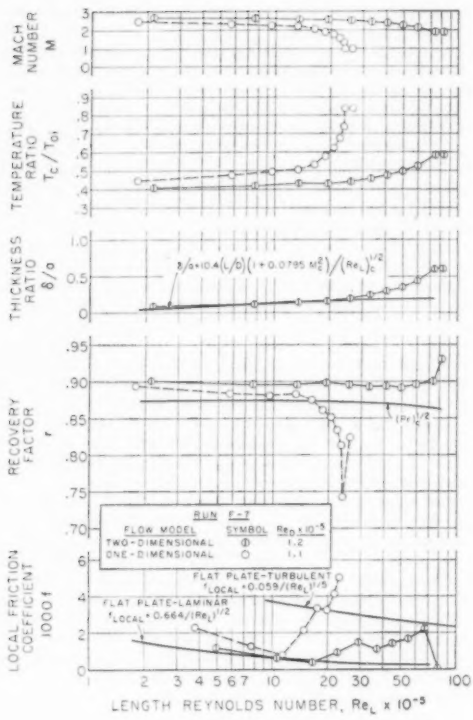

FIG. 5

predict the behavior of supersonic flow of air in a tube, and possibly for other fluids and for other passages. Hence it appears possible to predict for engineering designs the distribution of pressure and adiabatic wall temperature along the length of tube from data based on a laminar boundary layer for supersonic flow on a flat plate with zero pressure gradient.

The analysis to be used for prediction of the distribution of pressure and adiabatic wall temperature is identical with that contained in Equations [1] to [17]. If the stagnation state and discharge coefficient are given, it is necessary to use two new relations to substitute for the measured pressures and temperatures along the tube wall. Equation [20] and either of Equations [19] and [21] for a laminar boundary layer along a flat plate could be used.

$$(\delta/a) = 10.4(L/D)[1 + 0.1987(k-1)M_e^2]/\sqrt{(\mathbf{Re}_L)_c} \quad [19]$$

$$r = (\mathbf{Pr})_c^{1/2} \quad [20]$$

$$f = 0.664/\sqrt{(\mathbf{Re}_L)_c} \quad [21]$$

There would then be a sufficient number of independent relations to specify completely the distribution of pressure and temperature for the supersonic flow in the tube where a laminar boundary layer and an isentropic core were assumed to exist. The prediction method should be used, however, only up to a length Reynolds number of about 10^6, corresponding to the start of the transition to a turbulent boundary layer.

This method of prediction of distribution of pressure and temperature for adiabatic supersonic flow would be sufficiently accurate for many engineering problems. It opens up numerous other possibilities, such as the prediction of pressure and temperature for supersonic flow in a tube with heat transfer. Work is in progress on this phase of the program for obtaining reliable data on supersonic flow in a tube.

Conclusions

Since exact solutions are not available for the adiabatic supersonic flow of air in a round tube with a laminar boundary layer developing from tube entrance, an approximate and simplified two-dimensional flow model is proposed for engineering purposes. The results based on this two-dimensional flow model have been compared with the corresponding quantities for adiabatic supersonic flow of air over a flat plate with zero pressure gradient. The agreement between the corresponding quantities is good for all cases where a laminar boundary layer appears to exist in the tube.

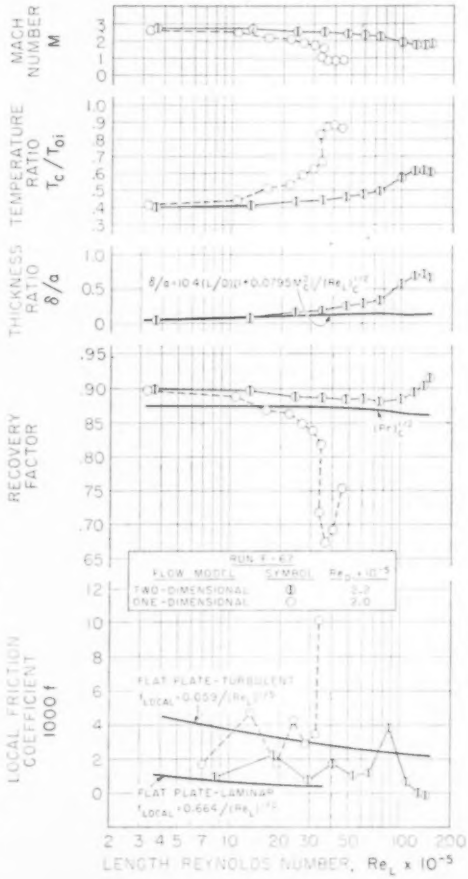

FIG. 6

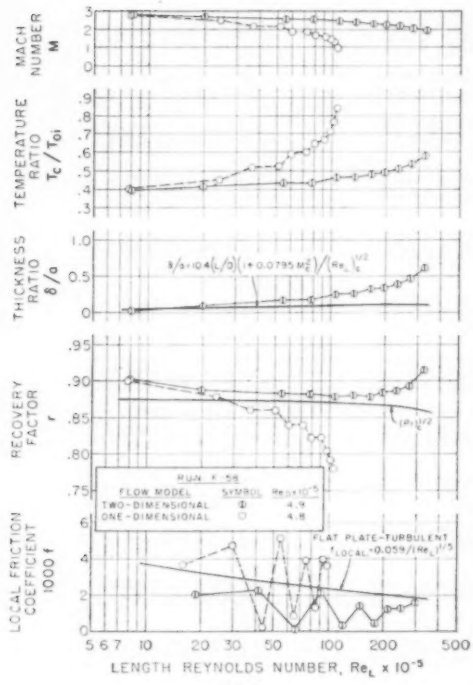
MACH NUMBER M
TEMPERATURE RATIO T_c / T_{0i}
THICKNESS RATIO δ / a
$\delta/a = 10.4 (L/D)(1 + 0.0795 M_L^2) / (Re_L)^{1/2}$
RECOVERY FACTOR r
$r_{(Pr)^{1/2}}$
RUN F-58
FLOW MODEL SYMBOL $Re_L \times 10^{-5}$
TWO-DIMENSIONAL ① 4.9
ONE-DIMENSIONAL ○ 4.8
LOCAL FRICTION COEFFICIENT 1000 f
FLAT PLATE-TURBULENT
$f_{LOCAL} = 0.059 / (Re_L)^{1/5}$
5 6 7 10 20 30 50 100 200 500
LENGTH REYNOLDS NUMBER, $Re_L \times 10^{-5}$

FIG. 7

The results, based on the two-dimensional flow model, compared in detail with those based on the one-dimensional flow model customarily used, yield a much better understanding of the phenomena occurring in supersonic flow of air in a round tube. Some of the inadequacies of the one-dimensional flow model for the entrance region are eliminated by use of the two-dimensional flow model.

The Mach numbers based on the two-dimensional flow model are slightly larger and much more constant along the tube length than those based on the one-dimensional flow model.

The thickness of the laminar boundary layer based on the two-dimensional flow model is in good agreement with that based on Howarth's results for a compressible laminar boundary layer with zero pressure gradient.

Where the flow in the tube boundary layer appears to be laminar, the recovery factors based on the two-dimensional flow model agree within 2 per cent both with the measured and with the theoretical values predicted for supersonic flow over a flat plate with a laminar boundary layer. Where the flow in the tube boundary layer appears to be turbulent, the recovery factors based on the two-dimensional flow model agree, probably by coincidence, within 2 per cent with those for supersonic flow over a flat plate with a laminar boundary layer.

Where the flow in the tube boundary layer appears to be laminar, the local friction coefficients based on the two-dimensional flow model are in good agreement with the experimental values for a compressible boundary layer on a flat plate with zero pressure gradient. Where the flow in the tube boundary layer appears to be turbulent, the local friction coefficients based on the two-dimensional flow model are, roughly, half of the experimental values for a turbulent boundary layer on a flat plate.

The success of the two-dimensional flow model indicates that it may be used in reverse to predict the pressures and temperatures for adiabatic supersonic flow of air in the entrance region of a tube with a laminar boundary layer. In other words, the data for adiabatic supersonic flow of air over a flat plate with a laminar boundary layer may be used to predict the behavior of adiabatic supersonic flow in a tube to a good approximation for engineering problems. In addition, it is probable that a similar method of prediction may be used advantageously for supersonic flow of air in a tube with heat transfer.

ACKNOWLEDGMENTS

The assistance of Robert E. Kendall and George A. Brown in the preparation of this report is gratefully acknowledged.

This investigation is sponsored as Contract Number N5-ori-07805 by the Office of Naval Research of the United States Navy.

BIBLIOGRAPHY

1 "Measurement of Recovery Factors and Friction Coefficients for Supersonic Flow of Air in a Tube," by J. Kaye, J. H. Keenan, K. K. Klingensmith, G. M. Ketchum, and T. Y. Toong, presented at the Annual Meeting, Atlantic City, N. J., November 25–30, 1951, of THE AMERICAN SOCIETY OF MECHANICAL ENGINEERS.

2 "Gas Tables," by J. H. Keenan and J. Kaye, John Wiley & Sons, Inc., New York, N. Y., 1948.

3 "Report of Progress on Measurements of Friction Coefficients Recovery Factors, and Heat Transfer Coefficients for Supersonic Flow of Air in a Pipe," by J. Kaye, J. H. Keenan, and W. H. McAdams, Heat Transfer and Fluid Mechanics Institute, June, 1949, pp. 147–164.

4 "Grenzschichten in Flussigkeiten mit kleiner Reibung," by H. Blasius, *Zeitschrift für Mathematik und Physik*, vol. 56, 1908, pp. 1–37.

5 "Concerning the Effect of Compressibility on Laminar Boundary Layers and Their Separation," by L. Howarth, Proceedings of the Royal Society of London, series A, vol. 194, 1948, pp. 16–42.

6 "A Determination of the Laminar-, Transitional-, and Turbulent-Boundary-Layer Temperature-Recovery Factors on a Flat Plate in Supersonic Flow," by J. R. Stalder, M. W. Rubesin, and T. Tendeland, NACA Technical Note 2077, June, 1950.

7 "Temperature Effects in a Laminar Compressible-Fluid Boundary Layer Along a Flat Plate," by H. W. Emmons and J. G. Brainerd, JOURNAL OF APPLIED MECHANICS, Trans. ASME, vol. 63, 1941, p. A-105.

8 "Effect of Variable Viscosity on Boundary Layers, With a Discussion of Drag Measurements," by J. G. Brainerd and H. W. Emmons, JOURNAL OF APPLIED MECHANICS, Trans. ASME, vol. 64, 1942, p. A-1.

Appendix

CALCULATED RESULTS BASED ON TWO-DIMENSIONAL FLOW MODEL

Calculated Results. This appendix contains the results based on the two-dimensional flow model for six runs made with the adiabatic test section referred to in the previous paper (1) as test combination B. A sample calculation is also included. The original measurements for these six runs, the dimensions of the apparatus, and the other necessary data are given in the previous paper (1). A summary of the calculations based on the two-dimensional flow model is given for six runs in Table 1.

Sample Calculation. The original data for run No. F-9 are taken from Appendix A of the previous paper (1). The method of computation of the nozzle discharge coefficient is identical with that used in the sample calculation of run No. F-9 in the previous paper (1). The values are summarized as follows

$$G_s^* = 28.45 \text{ lbm/(sec ft}^2\text{)}$$
$$(Re_D)_s^* = 5.684 \times 10^4$$

TABLE 1 CALCULATIONS BASED ON TWO-DIMENSIONAL FLOW MODEL

	Station No.	$\frac{L}{D}$	$\frac{p}{p_{oi}}$	$\frac{T_{aw}}{T_{oi}}$	M_c	$\frac{T_c}{T_{oi}}$	r	T_c °Fabs	μ_{c_5} x10^5 $\frac{lbm}{sec\ ft}$	$(Pr)^{\frac{1}{3}}_c$	V_c $\frac{ft}{sec}$	G_c $\frac{lbm}{sec\ ft^2}$	V_b $\frac{ft}{sec}$	T_b °Fabs	G_b $\frac{lbm}{sec\ ft^2}$	w_c x10^2 $\frac{lbm}{sec}$	w_b x10^2 $\frac{lbm}{sec}$	$\frac{\delta}{a}$	$(Re_L)_c$ x10^{-5}	$f_{j+\frac{1}{2}}$ x10^3	
Run No. F-7	oi		1.00000																		
March 14, 1950	1	1.614	0.04279	0.9412	2.70	0.4064	0.901	230.5	0.605	0.875	2011	19.46	1006	483.0	4.643	2.279	0.094	0.0766	2.17		
t_r = 75.0 °F	2	5.600	.04743	.9392	2.64	.4185	.896	237.4	.621	.874	1991	20.73	995.3	484.7	5.076	2.219	.154	.117	7.82	1.15	
p_r = 14.705 psia	3	9.586	.05000	.9400	2.60	.4249	.896	241.0	.630	.874	1980	21.41	989.8	485.6	5.311	2.186	.187	.138	13.6	0.581	
p_{oi} = 19.307 psia	4	13.57	.05168	.9422	2.58	.4289	.899	243.3	.635	.873	1973	21.84	986.3	486.2	5.464	2.164	.209	.151	19.5	0.363	
t_{oi} = 107.5 °F	5	17.56	.05641	.9419	2.52	.4398	.896	249.4	.650	.873	1954	23.03	977.0	487.7	5.889	2.101	.272	.185	26.0	0.939	
	6	21.54	.06418	.9417	2.44	.4548	.893	257.9	.670	.872	1922	24.92	960.8	490.3	6.554	1.998	.375	.236	33.5	1.49	
w_s^* = 0.02441 $\frac{lbm}{sec}$	7	25.53	.07251	.9438	2.36	.4725	.894	268.0	.694	.871	1896	26.74	947.9	492.4	7.276	1.887	.486	.283	41.2	1.10	
	8	29.51	.08448	.9455	2.27	.4936	.892	279.9	.721	.869	1858	29.22	928.8	495.4	8.256	1.727	.646	.344	50.0	1.44	
	9	33.50	.10312	.9508	2.14	.5225	.897	296.4	.758	.867	1804	32.71	901.9	499.5	9.705	1.479	.894	.426	60.4	1.70	
	10	37.49	.14930	.9581	1.90	.5808	.900	329.4	.832	.863	1690	39.93	845.0	507.7	12.95	0.8796	1.493	.599	78.3	2.28	
c_w = 0.972	11	41.47	.15030	.9717	1.90	.5819	.932	330.0	.833	.863	1688	40.07	844.0	507.9	13.02	0.8665	1.506	.603	81.4	0.0300	
w = 0.02373 $\frac{lbm}{sec}$																					
Run No. F-9	oi		1.00000																		
March 14, 1950	1	1.614	0.04731	0.9394	2.64	0.4182	0.896	236.4	0.619	0.874	1988	9.486	993.9	483.1	2.321	1.0000	0.0740	0.124	1.03		
t_r = 74.0 °F	2	5.600	.05993	.9414	2.48	.4474	.894	252.9	.658	.872	1937	10.95	968.6	487.2	2.841	0.9235	.1505	.216	3.89	2.53	
p_r = 14.707 psia	3	9.586	.06887	.9415	2.40	.4656	.891	263.2	.682	.871	1905	11.89	952.6	489.8	3.194	.8688	.2052	.271	6.98	1.41	
p_{oi} = 8.834 psia	4	13.57	.07114	.9427	2.37	.4699	.892	265.7	.688	.871	1897	12.12	948.7	490.4	3.282	.8548	.2192	.283	9.99	0.324	
t_{oi} = 105.6 °F	5	17.56	.07342	.9428	2.35	.4742	.891	268.1	.694	.871	1890	12.34	944.9	491.0	3.369	.8408	.2332	.296	13.1	0.306	
	6	21.54	.07412	.9428	2.35	.4755	.891	268.8	.695	.870	1888	12.41	943.8	491.2	3.396	.8364	.2376	.300	16.1	0.0895	
w_s^* = 0.011187 $\frac{lbm}{sec}$	7	25.53	.07144	.9433	2.37	.4705	.893	266.0	.689	.871	1896	12.15	948.2	490.5	3.294	.8530	.2210	.285	18.8	-0.360	
	8	29.51	.06925	.9439	2.39	.4663	.895	263.6	.683	.871	1904	11.93	951.9	489.9	3.209	.8664	.2076	.273	21.5	-0.306	
c_w = 0.960	9	33.50	.07535	.9454	2.34	.4777	.895	270.0	.698	.870	1883	12.53	941.7	491.5	3.443	.8289	.2451	.306	25.1	0.823	
	10	37.49	.07658	.9450	2.33	.4799	.894	271.3	.701	.870	1879	12.65	939.7	491.8	3.489	.8213	.2527	.312	28.3	0.158	
w = 0.010740 $\frac{lbm}{sec}$	11	41.47	.09445	.9615	2.19	.5096	.922	288.1	.740	.868	1825	14.27	912.5	496.0	4.144	.7116	.3624	.397	33.5	1.88	
Run No. F-58	oi		1.00000																		
July 29, 1950	1	1.614	0.03786	0.9403	2.78	0.3924	0.902	228.6	0.600	0.875	2062	71.53	1031	494.0	16.55	9.534	0.067	0.0148	8.05		
t_r = 84.0 °F	2	5.600	.04518	.9338	2.67	.4128	.887	240.4	.628	.874	2027	79.78	1014	497.0	19.30	9.168	.433	.0852	29.7	2.02	
p_r = 14.576 psia	3	9.586	.05535	.9332	2.54	.4374	.881	254.8	.663	.872	1984	90.26	992.1	500.6	22.97	8.646	.955	.165	54.6	2.25	
p_{oi} = 77.58 psia	4	13.57	.05597	.9333	2.53	.4378	.881	255.6	.665	.872	1982	90.87	990.9	500.8	23.19	8.614	.987	.169	77.6	0.120	
t_{oi} = 122.8 °F	5	17.56	.06836	.9351	2.40	.4646	.879	270.6	.700	.870	1936	102.4	967.8	504.6	27.46	7.966	1.635	.247	107.4	2.10	
	6	21.54	.07060	.9365	2.38	.4689	.880	273.1	.705	.870	1928	104.4	964.0	505.2	28.21	7.847	1.754	.260	133.2	0.328	
w_s^* = 0.09678 $\frac{lbm}{sec}$	7	25.53	.08163	.9385	2.29	.4888	.880	284.7	.732	.869	1892	113.6	945.8	508.1	31.82	7.266	2.335	.317	165.6	1.41	
	8	29.51	.08572	.9415	2.26	.4956	.884	288.7	.741	.868	1879	116.8	939.4	509.1	33.13	7.050	2.551	.337	194.5	0.460	
c_w = 0.992	9	33.50	.09961	.9450	2.16	.5174	.886	301.4	.770	.867	1838	127.2	918.9	512.2	37.42	6.321	3.280	.398	231.5	1.31	
	10	37.49	.11722	.9518	2.06	.5420	.895	315.7	.802	.865	1790	139.2	895.1	515.8	42.60	5.405	4.196	.468	272.2	1.25	
w = 0.09601 $\frac{lbm}{sec}$	11	41.47	.15689	.9656	1.87	.5891	.916	343.1	.861	.862	1696	162.4	847.9	522.7	53.30	3.395	6.206	.610	327.0	1.58	

TABLE 1 (continued) CALCULATIONS BASED ON TWO-DIMENSIONAL FLOW MODEL

Run No. F-63	oi		1.00000																
August 3, 1950	1	1.614	0.05273	0.9330	2.57	0.4314	0.882	244.5	0.638	0.873	1968	4.033	983.9	486.3	1.014	0.3766	0.0446	0.175	0.426	
	2	5.600	.07338	.9326	2.36	.4743	.872	268.8	.695	.870	1892	4.911	946.2	492.3	1.340	.3261	.0951	.305	1.65	3.35
t_r = 75.0 °F	3	9.586	.08701	.9346	2.25	.4978	.870	282.2	.726	.869	1849	5.420	924.7	495.7	1.543	.2926	.1286	.373	2.99	1.56
P_r = 14.689 psia	4	13.57	.09315	.9364	2.20	.5076	.871	287.7	.739	.868	1831	5.635	915.6	497.1	1.631	.2775	.1437	.401	4.33	0.586
P_{oi} = 3.521 psia	5	17.56	.10151	.9379	2.15	.5202	.870	294.9	.755	.867	1808	5.914	903.8	498.9	1.748	.2571	.1641	.437	5.75	0.693
t_{oi} = 107.2 °F	6	21.54	.10458	.9393	2.13	.5246	.872	297.4	.761	.867	1799	6.014	899.6	499.5	1.790	.2497	.1715	.450	7.12	0.229
	7	25.53	.10678	.9406	2.12	.5277	.874	299.1	.765	.867	1793	6.084	896.7	499.9	1.820	.2443	.1769	.459	8.49	0.156
w_s^* = 0.004452 lbm/sec	8	29.51	.10810	.9414	2.11	.5296	.875	300.2	.767	.867	1790	6.125	894.9	500.2	1.838	.2411	.1801	.465	9.85	0.0899
	9	33.50	.10722	.9422	2.11	.5284	.877	299.5	.766	.867	1792	6.097	896.1	500.0	1.826	.2433	.1779	.461	11.2	-0.0600
c_w = 0.946	10	37.49	.10700	.9440	2.11	.5280	.881	299.3	.765	.867	1793	6.091	896.4	500.0	1.823	.2438	.1774	.460	12.5	-0.0156
	11	41.47	.09360	.9565	2.20	.5082	.911	288.1	.740	.868	1830	5.650	915.0	497.2	1.637	.2765	.1447	.403	13.2	-1.05
w = 0.004212 lbm/sec																			

Run No. F-67	oi		1.00000																
August 14, 1950	1	1.614	0.03983	0.9395	2.75	0.3982	0.899	230.4	0.604	0.875	2045	32.60	1023	491.5	7.640	4.101	0.089	0.0429	3.64	
	2	5.600	.04318	.9382	2.70	.4075	.896	235.7	.617	.874	2029	34.27	1015	492.8	8.196	4.027	.163	.0750	13.0	0.914
t_r = 78.7 °F	3	9.586	.05303	.9358	2.56	.4321	.897	250.0	.651	.873	1987	38.86	993.4	496.4	9.784	3.804	.386	.156	23.9	2.28
P_r = 14.768 psia	4	13.57	.05680	.9361	2.52	.4406	.886	254.9	.663	.872	1972	40.50	985.9	497.6	10.37	3.717	.473	.183	34.7	0.741
P_{oi} = 34.15 psia	5	17.56	.06694	.9376	2.41	.4618	.884	267.2	.692	.871	1934	44.67	967.0	500.7	11.92	3.482	.708	.247	47.4	1.72
t_{oi} = 118.8 °F	6	21.54	.07455	.9398	2.34	.4763	.885	275.5	.711	.870	1908	47.59	954.0	502.8	13.04	3.304	.886	.289	60.3	1.07
	7	25.53	.08469	.9400	2.26	.4939	.881	285.7	.734	.868	1875	51.25	937.7	505.3	14.49	3.067	1.123	.340	74.5	1.21
w_s^* = 0.04275 lbm/sec	8	29.51	.14500	.9514	1.92	.5760	.885	333.2	.840	.863	1717	68.87	858.4	517.2	22.19	1.686	2.504	.578	101.2	3.84
	9	33.50	.17882	.9589	1.78	.6115	.894	353.8	.884	.860	1643	76.57	821.6	522.3	25.93	0.9501	3.240	.699	121.4	0.640
c_w = 0.980	10	37.49	.18446	.9629	1.76	.6170	.903	356.9	.891	.860	1632	77.74	815.8	523.1	26.52	0.8310	3.359	.721	136.8	0.0322
	11	41.47	.16980	.9663	1.82	.6025	.915	348.6	.873	.861	1662	74.64	831.0	521.0	24.97	1.143	3.047	.666	148.3	-0.126
w = 0.04190 lbm/sec																			

Run No. F-68	oi		1.00000																
August 14, 1950	1	1.614	0.04303	0.9340	2.70	0.4071	0.889	233.9	0.613	0.874	2023	14.84	1012	489.5	3.545	1.717	0.077	0.0820	1.63	
	2	5.600	.04732	.9279	2.64	.4182	.876	240.3	.628	.874	2004	15.73	1002	491.1	3.849	1.675	.119	.119	5.86	1.06
t_r = 77.1 °F	3	9.586	.05056	.9273	2.59	.4262	.873	244.9	.639	.873	1990	16.38	995.1	492.2	4.075	1.643	.151	.145	10.3	0.727
P_r = 14.768 psia	4	13.57	.05339	.9273	2.56	.4329	.872	248.8	.648	.873	1979	16.93	989.3	493.2	4.270	1.615	.179	.167	14.8	0.589
P_{oi} = 14.768 psia	5	17.56	.05601	.9304	2.53	.4389	.876	252.2	.657	.872	1968	17.43	984.1	494.0	4.448	1.588	.206	.185	19.5	0.513
t_{oi} = 114.9 °F	6	21.54	.05800	.9323	2.51	.4433	.878	254.7	.662	.872	1960	17.80	980.2	494.7	4.582	1.568	.226	.199	24.2	0.370
	7	25.53	.06019	.9327	2.48	.4480	.878	257.4	.669	.872	1952	18.20	976.0	495.3	4.729	1.546	.248	.213	29.0	0.390
w_s^* = 0.01855 lbm/sec	8	29.51	.06197	.9359	2.46	.4518	.883	259.6	.674	.872	1945	18.52	972.7	495.9	4.847	1.528	.266	.225	33.9	0.301
	9	33.50	.06868	.9375	2.40	.4652	.883	267.3	.692	.871	1921	19.68	960.7	497.8	5.284	1.460	.334	.265	39.8	1.05
c_w = 0.967	10	37.49	.07579	.9411	2.33	.4785	.887	275.0	.710	.870	1897	20.85	948.7	499.7	5.736	1.388	.406	.304	46.1	0.966
	11	41.47	.08863	.9544	2.26	.4955	.910	284.7	.732	.869	1866	22.38	933.1	502.2	6.344	1.288	.506	.353	53.0	1.14
w = 0.01794 lbm/sec																			

$$c_w = 0.960$$
$$w_s^* = 0.01119 \text{ lbm/sec}$$
$$w = 0.01074 \text{ lbm/sec}$$
$$A = 0.1978 \text{ in.}^2 = 0.001373 \text{ ft}^2$$

From Table 30 of the "Gas Tables" (2), corresponding to the value of (p/p_{oi}) of 0.04731 for the first station, it is found that

$$M_c = 2.64$$
$$T_c/T_{oi} = 0.4182$$
$$T_c = (T_c/T_{oi})T_{oi} = 0.4182(565.3) = 236.4 \text{ F abs}$$

The recovery factor is found next by

$$r \equiv \frac{\dfrac{T_{ow}}{T_{oi}} - \dfrac{T_c}{T_{oi}}}{1 - \dfrac{T_c}{T_{oi}}} = \frac{0.9394 - 0.4182}{1 - 0.4182} = 0.896$$

For the core

$$\rho_c = \frac{p_{oi}(p/p_{oi})}{RT_c} = \frac{8.834 \times 0.04731 \times 144}{53.342 \times 236.4} = 0.004772 \text{ lbm/ft}^3$$

$$V_c \equiv M_c \sqrt{gkRT_c} = 2.637 \sqrt{32.174 \times 1.400 \times 53.342 \times 236.4} = 1988 \text{ fps}$$

$$G_c \equiv \rho_c V_c = 0.004772 \times 1988 = 9.486 \text{ lbm/(sec ft}^2\text{)}$$

For the boundary layer

$$V_b = V_c/2 = 993.9$$

$$T_b = T_{oi} - V_b^2/(2gc_p) = 565.3 - \frac{(993.9)^2}{2 \times 32.174 \times 778.16 \times 0.2399} = 483.1 \text{ F abs}$$

$$\rho_b = \frac{p_{oi}(p/p_{oi})}{RT_b} = \frac{8.834 \times 0.04731 \times 144}{53.342 \times 483.1} = 0.002336 \text{ lbm/ft}^3$$

$$G_b \equiv \rho_b V_b = 0.002336 \times 993.9 = 2.321 \text{ lbm/(sec ft}^2\text{)}$$

From Equations [1], [2], and [3]

$$\frac{A_c}{A} = \frac{1 - \dfrac{w}{\rho_b V_b A}}{1 - \dfrac{2\rho_c}{\rho_b}} = \frac{1 - \dfrac{0.01074}{2.321 \times 0.001373}}{1 - \dfrac{2 \times 0.004772}{0.002336}} = 0.7676$$

$$A_c = A(A_c/A) = 0.7676 \times 0.001373 = 0.001054 \text{ sq ft}$$
$$A_b = A - A_c = 0.001373 - 0.001054 = 0.000319 \text{ sq ft}$$
$$w_c = G_c A_c = 9.486 \times 0.001054 = 0.010000 \text{ lbm/sec}$$
$$w_b = G_b(A - A_c) = 2.321 \times 0.000319 = 0.000740 \text{ lbm/sec}$$
$$\delta/a = 1 - (1/a)\sqrt{A_c/\pi} = 1 - (24/0.5018)\sqrt{0.001054/\pi} = 0.1239$$

The shear stress at the wall and local true friction coefficient are obtained from the momentum theorem

$$\tau = \left[p_{oi} A \left(\frac{p_j}{p_{oi}} - \frac{p_{j+1}}{p_{oi}}\right) + (1/g)(w_c V_c + w_b V_b)_j - (1/g)(w_c V_c + w_b V_b)_{j+1}\right] \Big/ (\pi D \Delta L)$$

$$= [8.834 \times 0.1978(0.04730 - 0.05993) + (1/32.174)(0.010000 \times 1988 + 0.000740 \times 993.9) - (1/32.174)(0.009235 \times 1937 + 0.001505 \times 968.6)] \Big/ \left(\frac{\pi \times 0.5018 \times 2}{12 \times 12}\right)$$

$$= 0.7889 \text{ lbf/ft}^2$$

$$f_{j+1/2} \equiv \frac{2\tau(2g)}{(\rho_c V_c^2)_j + (\rho_c V_c^2)_{j+1}} = \frac{2 \times 0.7889 \times (2 \times 32.174)}{0.004772(1988)^2 + 0.005650(1937)^2} = 0.00253$$

$$(\mathbf{Re}_L)_c = \frac{G_c D(L/D)}{\mu_c} = \frac{9.486 \times 0.5018 \times 1.614}{12(0.619 \times 10^{-4})} = 1.03 \times 10^5$$

Lateral Vibrations as Related to Structural Stability

By HAROLD LURIE,[1] SANTA MONICA, CALIF.

The apparently different physical problems of lateral vibration and elastic stability are limiting cases of a single phenomenon, the more general expression being the mode of vibration with end thrust. It is shown that the square of the frequency of lateral vibration is approximately linearly related to the end load. The linear relationship is exact if the mode of free vibrations is identical to the buckling mode. In all cases, the load corresponding to zero frequency is the critical buckling load. Experimental tests were conducted on elastically restrained columns in the form of rigid rectangular frames. It was found that the relationship between the square of the frequency and the load is practically linear, and that the extrapolated load corresponding to zero frequency coincides with the buckling load. Rigid-joint trusses also were tested. In some cases the relationship between the square of the frequency and the load deviates considerably from linearity, but the approximate buckling load can be predicted. In the case of thin flat plates, tests showed that the buckling load cannot be predicted from vibration tests in practice. It is indicated that this is probably because the linear plate equations are not valid owing to initial curvatures in the plate.

Nomenclature

The following nomenclature is used in the paper:

P = end thrust
N_x, N_y = edge thrusts per unit length
N_{xy} = edge shears per unit length
$\rho(x)$ = mass per unit length
$p(x)$ = transverse load per unit length
$v(x_i; t)$ = resultant deflection
$w(x_i)$ = synchronous deflection function for free vibrations
$v(x_i)$ = synchronous deflection function with end thrust

$$c^2 = \frac{\rho}{EI}$$

$$\beta^2 = \frac{P}{EI}$$

ω_n = frequency for free vibrations in nth mode
ω_n^* = frequency for vibrations with end thrust in nth mode
h = plate thickness

$$D = \text{plate rigidity} = \frac{Eh^3}{12(1-\nu^2)}$$

$q(x, y)$ = transverse load per unit area
$\mu(x, y)$ = mass per unit area

Introduction

In addition to the mathematical similarity between the simple problem of free vibrations and of elastic stability, some striking analogies occur when certain modifications are introduced. A good example is provided by considering forced vibrations and the stability of an initially curved member. Suppose the static-deflection function of a uniform beam is expanded in a series of functions corresponding to the modes of vibration. Then it is well known that, under a harmonic load, the shape of the deflection curve for a forced vibration with frequency ω is obtained by multiplying every term of the static-deflection function by the "resonance factor"

$$1 \Big/ \left[1 - \left(\frac{\omega}{\omega_0}\right)^2\right]$$

It also can be shown (1)[2] that if the shape of an initially curved column is expanded in a Fourier series, the shape of the deflection curve under an end thrust P is obtained by multiplying every term of the unloaded deflection function by the "magnification factor"

$$1 \Big/ \left[1 - \frac{P}{P_0}\right]$$

It is this similarity between the resonance factor and the magnification factor that might lead one to suspect some connection between P_0 and ω_0^2. The suspicion can be corroborated quite readily in the case of a beam which is pinned at each end. Without any external forces being applied to the system, the equation governing the free harmonic vibrations is

$$EI \frac{d^4w}{dx^4} - \rho w \omega^2 = 0$$

The modes of vibration are given by

$$w = A_n \sin \frac{n\pi x}{l}$$

and the corresponding frequencies of vibration are

$$\omega_n = \frac{n^2\pi^2}{l^2} \sqrt{\frac{EI}{\rho}}$$

Now consider an axial compression P acting along the center line of the beam. The corresponding equation for free vibrations becomes

$$EI \frac{d^4v}{dx^4} + P \frac{d^2v}{dx^2} - \rho v \omega^{*2} = 0$$

The shape of the modes is the same as before, but the frequency is now

---

[1] Lecturer in Aeronautics, California Institute of Technology, Pasadena, Calif. Now with The Rand Corporation.

Presented at the West Coast National Conference of the Applied Mechanics Division, Stanford, Calif., June 22-23, 1951, of The American Society of Mechanical Engineers.

Discussion of this paper should be addressed to the Secretary, ASME, 29 West 39th Street, New York, N. Y., and will be accepted until July 10, 1952, for publication at a later date. Discussion received after the closing date will be returned.

Note: Statements and opinions advanced in papers are to be understood as individual expressions of their authors and not those of the Society. Manuscript received by ASME Applied Mechanics Division, September 17, 1951.

[2] Numbers in parentheses refer to the Bibliography at the end of the paper.

$$\omega_n^2 = \frac{n^2\pi^2}{l^2}\sqrt{\frac{EI}{\rho}\left(1 - \frac{P}{P_n}\right)}$$

where

$$P_n = \frac{n^2\pi^2 EI}{l^2}$$

Hence the effect of the axial compression P is to decrease the natural frequency of vibration. In addition, the variation of the square of the frequency with P is linear; and finally, the frequency falls to zero when P approaches P_n which is the buckling load of the beam.

The question naturally arises as to the generality of this variation, and whether such a behavior can be expected in structures other than simply supported uniform beams. Physical intuition would lead one to believe that if an axial compression does decrease the natural frequency, then the frequency of any structure would fall to zero when buckling is reached.

A review of the literature dealing with this problem reveals the sparseness of information which is available. By far the most extensive work is that by Massonnet (2). The greater portion of his theoretical paper is confined to the solution of a large number of particular cases. He treats uniform beams, plates, rings, and shells, and solves a great number of these with various boundary conditions.

An earlier treatise which was restricted to the vibrations and buckling of rectangular plates was published by Grauers (3). This is an exhaustive study of the vibrations of plates with various boundary conditions, in order to use these modes to find the stability criteria by Ritz's method. No attempt was made to draw any general conclusions between the vibration and stability problems.

A paper somewhat related to the present problem was published by Weinstein and Chien (4), in which the vibrations of a clamped plate under tension were investigated. By using the variational energy approach, they showed that the square of the frequency of vibration increased with increased tension in an approximately linear manner.

Stephens (5*a*) recognized the similarity between the stability and vibration problems, and proposed a method for determining the end-fixity coefficient by a frequency measurement. His analysis, however, is incorrect, as is also his proposed vibration method for determining loads in axially stressed members (5*b*). His paper does contain some useful experimental results on clamped bars.

The only other experimental work which seems to have been conducted is contained in a thesis by Chu (6). Guided by Massonnet's work, Chu tested a simply supported column and also a rectangular frame. His results for the column agreed very closely with theory. However, although he obtained a linear relationship between ω^2 and P for the rectangular frame, the extrapolated value of P_{cr} did not agree with the calculated lowest critical load corresponding to symmetrical buckling, but with a higher critical load which represented the unsymmetrical mode. Chu's work was not sufficiently complete to explain this phenomenon satisfactorily.

From the foregoing discussion it is evident that the problem has by no means been investigated thoroughly. It is particularly desirable to know the restrictions under which the linear relationship holds, and, if the relationship is not linear under certain conditions, the deviation from linearity. In addition, some further experimental work appeared to be necessary. Chu's work needed to be extended in order to understand the technique more fully, and an attempt needed to be made to check further theory.

The practical application of such information is twofold: (*a*) The members of a structure are often subjected to axial loads, and a determination of their natural frequency is of some significance in order to prevent resonance. (*b*) If such a law of variation of natural frequency with end thrust can be established, it would lead to useful practical applications in the form of nondestructive tests for the determination of the static buckling load.

General Equations

Before examining any specific class of elastic bodies, it is possible to study some general expressions which describe the vibrations of continuous systems such as beams and plates. The differential equation for the vibrations of such a system can be written in the general form

$$L[u] + c^2 u_{tt} = f(x_i;t) \qquad [1]$$

where the subscript i takes on as many values as there are space variables. $L[u]$ is a linear differential expression which includes only the unknown deflection function u and its derivatives with respect to the space variables x_i. For example, for the uniform beam

$$L[u] = \frac{\partial^4 u}{\partial x^4} \qquad [2]$$

while for a plate of constant thickness

$$L[u] = \nabla^4 u \qquad [3]$$

In the foregoing general equation, c^2 is a physical constant and $f(x_i;t)$ is proportional to the density of the external force.

In the problem under consideration the case of free vibrations is of primary interest. Mathematically this means that the solution is given by a function u which satisfies the homogeneous differential equation

$$L[u] + c^2 u_{tt} = 0 \qquad [4]$$

together with the initial and boundary conditions of the problem.

Separating variables, harmonic oscillations are obtained together with the eigenvalue equation

$$L[w] - \omega^2 c^2 w = 0 \qquad [5]$$

which determines the admissible values of the parameter ω^2 and hence the natural frequencies of the system. Therefore, in general, the natural frequencies will be given by the equation

$$\omega_n^2 = \frac{L[w_n]}{c^2 w_n} \qquad [6]$$

In the foregoing it was assumed that no external forces were acting on the system. Now suppose that the vibrating system is subjected to an end load P. The only effect of this will be to modify the differential operator L. Denoting this modified operator by L^* and the new deflection function by $v(x_i)$, Equations [2] and [3] now become

$$L^*[v] = \frac{d^4 v}{dx^4} + \frac{P}{EI}\frac{d^2 v}{dx^2} \text{ for beams} \qquad [7]$$

and

$$L^*[v] = \nabla^4 v + \frac{N_x}{D}\frac{\partial^2 v}{\partial x^2} + \frac{N_y}{D}\frac{\partial^2 v}{\partial y^2} - \frac{N_{xy}}{D}\frac{\partial^2 v}{\partial x\,\partial y} \qquad [8]$$

for plates subjected to edge thrusts N_x, N_y, and edge shears N_{xy} per unit length. Equation [6] now becomes

$$\omega_n^{*2} = \frac{L^*[v]}{c^2 v} \qquad [9]$$

Hence from Equations [6] and [9] it can be concluded that

$$\left(\frac{\omega_n^*}{\omega_n}\right)^2 = \frac{wL^*[v]}{vL[w]} \quad \ldots\ldots [10]$$

As L^* is a function of the end load, the right side of this equation will be a function of the end load. Hence Equation [10] will give the general relationship between the square of the frequency and the end load. As w and v are both functions of x, Equation [10] indicates that a necessary condition for $(\omega_n^*/\omega_n)^2$ to be proportional to the end load is that $w(x) = v(x)$, i.e., the mode of free vibration must be unaltered by the application of an end load.

The value of the end load at which the natural frequency is reduced to zero can be deduced from Equation [9]. For ω_n^{*2} to be zero, $L^*[v]$ must vanish. Putting this condition in Equation [7], the natural frequency of a beam will become zero when the end load assumes a value given by

$$\frac{d^4v}{dx^4} + \frac{P}{EI}\frac{d^2v}{dx^2} = 0 \quad \ldots\ldots [11]$$

But the values of P given by this equation correspond to the static buckling loads (7). Hence the natural frequency is always reduced to zero as the end load approaches the critical buckling load.

In precisely the same manner, if $L^*[v]$ vanishes in the case of plates, Equation [8] yields

$$\nabla^4 v + \frac{N_x}{D}\frac{\partial^2 v}{\partial x^2} + \frac{N_y}{D}\frac{\partial^2 v}{\partial y^2} - \frac{N_{xy}}{D}\frac{\partial^2 v}{\partial x\,\partial y} = 0 \quad \ldots\ldots [12]$$

Again the values of N_x, N_y, and N_{xy}, as given by this equation, correspond to the static buckling loads of the plate (1).

Hence the apparently different physical problems of free lateral vibration and elastic stability are limiting cases of a single phenomenon, the more general expression being the mode of vibration with end thrust. The free modes of vibration and the buckling modes correspond to the conditions that $P = 0$ and $\omega_n = 0$, respectively.

Application to Straight Beams

Having derived an expression relating the square of the frequency to the end load in general terms, it is now advantageous to examine in greater detail the form that this equation assumes in the case of straight beams.

The harmonic vibrations of a beam with end thrust P are governed by the equation (1)

$$\frac{d^4v}{dx^4} + \frac{P}{EI}\frac{d^2v}{dx^2} - \frac{\rho}{EI}\omega^{*2}v = 0 \quad \ldots\ldots [13]$$

Therefore, from Equation [10]

$$\left(\frac{\omega_n^*}{\omega_n}\right)^2 = \frac{w\left(\frac{d^4v}{dx^4} + \beta^2\frac{d^2v}{dx^2}\right)}{v\frac{d^4w}{dx^4}} \quad \ldots\ldots [14]$$

where

$$\beta^2 = \frac{P}{EI}$$

The solution of Equation [13] is

$$v = A\cosh\lambda_1 x + B\sinh\lambda_1 x + C\cos\lambda_2 x + D\sin\lambda_2 x \ldots [15]$$

where

$$\lambda_1 = \sqrt{-\frac{\beta^2}{2} + \sqrt{\left(\frac{\beta^2}{2}\right)^2 + c^2\omega^{*2}}}$$

and

$$\lambda_2 = \sqrt{-\frac{\beta^2}{2} - \sqrt{\left(\frac{\beta^2}{2}\right)^2 + c^2\omega^{*2}}}$$

Hence it follows that with no end thrust

$$w = Q\cosh\lambda_1 x + R\sinh\lambda_1 x + S\cos\lambda_2 x + T\sin\lambda_2 x \ldots [16]$$

where

$$\lambda_1 = \sqrt[4]{c^2\omega^2} = \sqrt[4]{\frac{\rho\omega^2}{EI}}$$

An examination of Equations [15] and [16] shows that the two modes can be equal if either the hyperbolic or the trigonometric functions vanish. In addition, for the linear relationship to hold, Equation [14] indicates that

$$\left(\frac{d^4v}{dx^4} + \beta^2\frac{d^2v}{dx^2}\right)$$

must be linearly related to $(d^4w)/(dx^4)$. These two requirements are possible if v and w are either hyperbolic functions or sine functions. No physical boundary conditions will yield purely hyperbolic solutions, hence the sine solutions are the only possible conditions for linearity. These correspond to simply supported ends. In this case Equation [10] becomes

$$\left(\frac{\omega_n^*}{\omega_n}\right)^2 = 1 - \frac{P}{P_n} \quad \ldots\ldots [17]$$

where

$$P_n = \frac{n^2\pi^2 EI}{l^2} = \text{buckling load}$$

corresponding to nth mode of buckling.

This illustrates that the square of the frequency varies linearly with the end thrust. For $P = 0$, the frequency becomes the natural frequency for free vibration; at zero frequency, the end thrust is equal to the buckling load.

The experimental implications of this result are quite considerable. By measuring the natural frequency of free vibration for such a beam, first with no end load and then with an end load which may be well below the buckling load, these two points can be extrapolated by a straight line to intersect the P abscissa for zero ω^2. Then this value of P will correspond to the buckling load. Hence a nondestructive test can be conducted to establish the experimental value of the buckling load.

If $v(x) \neq w(x)$, Equation [14] indicates that the linear relationship between ω^2 and P will no longer be valid. The question then arises as to the magnitude of the deviation from linearity for other end conditions. If the deviation can be shown to be sufficiently small for all practical cases, then the foregoing experimental method could be extended to cases in which the end-fixity coefficients were unknown. It will be indicated later how, in general, energy considerations can be utilized to give an estimation of this deviation.

Thin Plates of Constant Thickness

Proceeding in a similar manner to that for straight beams, it is possible to derive the corresponding equations for a flat plate. If the plate is subjected to compressive end thrusts N_x and N_y per unit length, and end shears N_{xy} per unit length, the dynamic equation becomes (1)

$$\nabla^4 u = \frac{1}{D}\left[N_{xy}\frac{\partial^2 u}{\partial x\,\partial y} - N_x\frac{\partial^2 u}{\partial x^2} - N_y\frac{\partial^2 u}{\partial y^2} - \mu\frac{\partial^2 u}{\partial t^2}\right] \quad [18]$$

where D is the flexural rigidity $= (Eh^3)/[12(1-\nu^2)]$, and μ is the mass per unit area.

Again harmonic oscillations lead to the equation

$$\nabla^4 v + \frac{1}{D}\left[N_x\frac{\partial^2 v}{\partial x^2} + N_y\frac{\partial^2 v}{\partial y^2} - N_{xy}\frac{\partial^2 v}{\partial x\,\partial y}\right] - \frac{\mu}{D}\omega^{*2} v = 0 \quad [19]$$

The frequency relationship, from Equation [10], then becomes

$$\left(\frac{\omega_n^*}{\omega_n}\right)^2 = \frac{w\left\{\nabla^4 v + \frac{1}{D}\left[N_x\frac{\partial^2 v}{\partial x^2} + N_y\frac{\partial^2 v}{\partial y^2} - N_{xy}\frac{\partial^2 v}{\partial x\,\partial y}\right]\right\}}{v\nabla^4 w} \quad [20]$$

If the plate is subjected to a thrust in the x-direction only, Equation [20] reduces to

$$\left(\frac{\omega_n^*}{\omega_n}\right)^2 = \frac{w\left[\nabla^4 v + \frac{N_x}{D}\frac{\partial^2 v}{\partial x^2}\right]}{v\nabla^4 w} \quad [21]$$

It is evident from Equation [19] that for a simply supported rectangular plate uniformly compressed in one direction, the solution can be written as

$$v(x,y) = A_{mn}\sin\frac{m\pi x}{a}\sin\frac{n\pi y}{b}$$

Hence it can be concluded that Equation [21] would yield a linear relationship between ω_n^2 and N_x. However, there are less restrictive conditions under which this linear law is still exact, viz., a rectangular plate uniformly compressed in the x-direction, simply supported along two opposite sides perpendicular to the direction of compression, and having various edge conditions along the other two sides. The equation of motion is obtained from Equation [19]

$$\nabla^4 v = \frac{1}{D}\left(-N_x\frac{\partial^2 v}{\partial x^2} + \mu\omega^{*2} v\right) \quad [22]$$

Assuming a solution of the form

$$v = f(y)\sin\frac{m\pi x}{a} \quad [23]$$

which satisfies the boundary conditions along the simply supported edges $x = 0$ and $x = a$, the $f(y)$ will depend upon the other two boundary conditions. Substituting the value of v from Equation [23] into Equation [22], the differential equation for $f(y)$ is obtained

$$\frac{d^4 f}{dy^4} - \frac{2m^2\pi^2}{a^2}\frac{d^2 f}{dy^2} + \left(\frac{m^4\pi^4}{a^4} - \frac{N_x}{D}\frac{m^2\pi^2}{a^2} - \frac{\mu\omega^{*2}}{D}\right) f = 0 \quad [24]$$

From this equation it can be shown (2) that

$$\left(\frac{\omega_i^*}{\omega_i}\right)^2 = 1 - \frac{N_x}{N_{x^{cr}(i)}} \quad [25]$$

Thus, provided the rectangular plate is simply supported along the two loaded edges, the linear relationship is true for any boundary conditions along the unloaded edges.

It was stated earlier that the condition for the linear relationship to be valid is that the buckling mode of an elastic body should be identical to the mode of free vibration. This is true for all plates of polygonal shape uniformly compressed in their median plane and simply supported along their edges. The normal vibration modes of such a plate are independent of the compression per unit length; they are identical to the normal modes of vibration of a membrane of the same shape and stretched uniformly, in addition to being identical to the buckling modes of the plate. This was proved by Schaefer and Havers (8).

Hence the following general result can be stated: For any thin plate of polygonal shape and uniform thickness which is simply supported along all the edges and subjected to a uniform thrust N per unit length, the frequency ω^* follows the relationship

$$\left(\frac{\omega_n^*}{\omega_n}\right)^2 = 1 - \frac{N}{N_n^{cr}}$$

It is interesting to note that although this relationship is exact for a polygonal plate with an arbitrarily large number of sides, it is not valid in the limit when the number of sides becomes infinite. The boundary would then be curved and the Navier boundary conditions no longer would be applicable. Admittedly, however, the deviation from linearity in the case of a simply supported plate of arbitrary planform would be expected to be very small. This can be seen readily in the case of a circular plate; the normal modes of vibration and of buckling have been investigated fully in classical elasticity, and differ very little. However, it is curious that the exact linear law breaks down in the limit.

Energy Methods

For any boundary conditions, the mode of static buckling does not differ appreciably from the mode of free vibration. This indicates that Rayleigh's principle, which requires only a moderately accurate representation of the amplitudes of vibration in the fundamental mode, can be used to determine the deviation from linearity of the load-frequency^2 relationship.

The amplitudes assumed in Rayleigh's method actually correspond to a slightly constrained mode, the frequency of which can be determined easily by energy calculations. The frequency thus obtained cannot be less than the true fundamental frequency, and so the method gives an upper bound. By using Rayleigh's principle, the approximation to the fundamental frequency will be much closer than the approximation of the assumed amplitudes to the true amplitudes.

The energy method also can be used in a very simple manner to determine the lower bound. This is particularly true where a system is subjected simultaneously to different types of external forces, each of which if acting separately would result in an eigenvalue problem. Then, in general, an inequality can be derived which relates the combined external forces to each of them acting separately (9).

Thus this method is appropriately applicable to the problem of the vibrations of a beam subjected to end thrust. Let a beam of arbitrary mass distribution be subjected to an end thrust P and hence have a lateral vibration frequency ω_n^*. The amounts of work done by the end thrust P and the inertia forces can be represented by PW_1 and $\omega_n^{*2}W_2$, respectively, where W_1 and W_2 depend only upon the deformations. If V represents the strain energy, the exact critical condition is given by

$$V = PW_1 + \omega_n^{*2}W_2 \quad [26]$$

Let P_n be the static buckling load for this beam, and ω_n the natural frequency of free vibration with no end load. The critical relations for these two cases are

$$\left.\begin{aligned} V' &= P_n W_1' \\ \text{and} \quad V'' &= \omega_n^2 W_2'' \end{aligned}\right\} \quad [27]$$

when the primed quantities are calculated from the deformations appropriate to each type of external force. Hence it can be con-

cluded from Rayleigh's principle that

$$V \geq P_n W_1$$

and

$$V \geq \omega_n^2 W_2$$

i.e.

$$W_1 \leq \frac{V}{P_n} \text{ and } W_2 \leq \frac{V}{\omega_n^2}$$

Hence

$$V \leq P \frac{V}{P_n} + \omega_n^{*2} \frac{V}{\omega_n^2}$$

or

$$1 \leq \frac{P}{P_n} + \frac{\omega_n^{*2}}{\omega_n^2} \quad \ldots\ldots\ldots\ldots\ldots\ldots [28]$$

Equation [28] gives a lower limit to the frequency of the axially loaded beam. The equality sign will hold if the modes are identical in all three cases. This checks the previous result obtained for uniform beams which are simply supported.

Now Rayleigh's principle can be made to yield an upper limit to the fundamental frequency by the use of an assumed mode of vibration. Equating the kinetic and total potential energies of a beam

$$\int_0^l EI \left(\frac{d^2v}{dx^2}\right)^2 dx - P \int_0^l \left(\frac{dv}{dx}\right)^2 dx = \omega^{*2} \int_0^l \rho v^2 dx \quad \ldots [29]$$

This relationship is exact if v is the actual deflection function of the vibrating strut, i.e., that which satisfies the differential equation. However, it results in a good approximation if the differential equation is disregarded entirely and v is any function of x which satisfies the boundary conditions and which is a moderately accurate representation of the vibrating mode. By using an approximate function for $v(x)$, the relationship for uniform beams becomes

$$1 \geq c^2 \omega^{*2} \frac{\int_0^l v^2 dx}{\int_0^l \left(\frac{d^2v}{dx^2}\right)^2 dx} + \beta^2 \frac{\int_0^l \left(\frac{dv}{dx}\right)^2 dx}{\int_0^l \left(\frac{d^2v}{dx^2}\right)^2 dx} \quad \ldots [30]$$

Equation [30] gives an upper limit to the frequency of the axially loaded beam. Again the equality sign will hold only if the modes are identical, in which case it checks with Equation [28]. This equation can be used to find the maximum deviation of linearity between P and ω^2 for particular cases. It is obvious that if the buckling mode is used as the approximate deflection function $v(x)$, the coefficient of the P/P_1 term in Equation [30] will be unity. Similarly, the free vibration mode can be used for $v(x)$, in which case the coefficient of the $(\omega^*/\omega)^2$ term will be unity.

As an example of this upper limit in a particular case, consider a beam fixed at each end. The fundamental buckling mode is

$$v = A\left(1 - \cos \frac{2\pi x}{l}\right)$$

Substituting this into Equation [30] the expression becomes

$$1 \geq \frac{3\rho\omega^{*2} l^4}{16\pi^4 EI} + \frac{Pl^2}{4\pi^2 EI} \quad \ldots\ldots\ldots\ldots [31]$$

But for a clamped bar

$$P_1 = \frac{4\pi^2 EI}{l^2}$$

and

$$\omega_1^2 = (22.373)^2 \frac{EI}{\rho l^4}$$

Therefore Equation [31] can be written as

$$1 \geq 0.9635 \left(\frac{\omega_1^*}{\omega_1}\right)^2 + \frac{P}{P_1} \quad \ldots\ldots\ldots\ldots [32]$$

Now let the deflection function be represented by the mode of free vibrations. If the origin be taken at the middle instead of at the ends of a beam clamped at both ends, the value of $v(x)$ takes the form (1)

$$v = A\left(\frac{\cosh mx}{\cosh \frac{1}{2} ml} - \frac{\cos mx}{\cos \frac{1}{2} ml}\right)$$

where $ml = 4.730$. Substituting this into Equation [30] the expression becomes

$$1 \geq \frac{c^2 \omega^{*2}}{\left(\frac{4.730}{l}\right)^4} + \beta^2 \frac{l^2}{40.684}$$

therefore

$$1 \geq \left(\frac{\omega_1^*}{\omega_1}\right)^2 + 0.9704 \frac{P}{P_1} \quad \ldots\ldots\ldots\ldots [33]$$

If Equations [28], [32], and [33] are plotted as in Fig. 1, the true curve of $(\omega_1^*/\omega_1)^2$ against P/P_1 will lie within the triangle bounded by the three straight lines. Hence the shape of the probable curve may be estimated from the figure. It is noticed that the deviation from linearity is extremely small.

For any other boundary conditions, similarly small deviations from linearity would be expected. In all cases Rayleigh's method gives a very close approximation both to the natural frequency if the buckling mode is used, and also to the critical load if the free-vibration mode is used. This method likewise can be

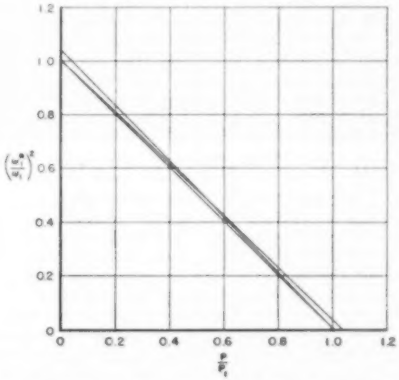

FIG. 1 VARIATION OF FREQUENCY WITH END LOAD BY ENERGY METHODS

applied to flat plates with arbitrary boundary conditions, with similar conclusions.

Experimental Tests on Beams

In order to test elastically restrained columns, Chu (6) had investigated the case of a rectangular frame subjected to end thrusts. Although he obtained a linear relationship between the load and the square of the frequency, the results were not conclusive. Theoretically the frame should buckle in the lowest energy state, which corresponds to a symmetrical mode. However, the buckling load corresponding to the extrapolated value of Chu's curve was approximately equal to the critical load for unsymmetrical buckling, Fig. 2. Owing to local yielding at the

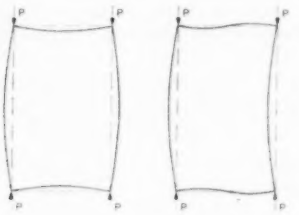

Fig. 2 Symmetrical and Unsymmetrical Modes

knife-edges under application of load, the damping had increased to such an extent that the test could be conducted only up to approximately half the buckling load. Chu remarked that although the measurements indicated that the structure was stable in the unsymmetrical mode of vibration, one could not, however, conclude that the structure would buckle in that mode first.

In view of the foregoing tests, it was decided to carry out further tests on a similar rectangular frame. However, the frame supports would be improved, and a more refined technique of excitation would be developed. It was considered desirable to conduct the tests right up to the physical buckling load in order to correlate the vibration mode with the actual buckling mode.

The frame, made of $^{3}/_{16}$-in. × 1-in. cold-rolled-steel strip brazed together at the four corners, measured approximately 12 in. × 20 in. The load was applied through knife-edges resting in hardened-steel seats. Instead of measuring the free vibrations of the frame, an oscillator was built which would impose an exciting force on the frame. By varying the frequency of the oscillator so as to develop resonance, the natural frequency could be determined at each loading increment. This was arranged by constructing a magnetic circuit with an alternating flux. The arrangement is shown in Fig. 3. Dynamic strain gages were attached to both vertical members of the frame in order to determine whether the vibrations were occurring in the symmetrical or unsymmetrical modes. Measurements were recorded automatically on a two-channel recording oscillograph.

The first test was conducted in order to determine whether Chu's results could be repeated. The first question to be settled was whether the frame, with a stable unsymmetrical vibration mode, would remain stable above the symmetrical buckling load.

Load was applied in increments, and at each load the electromagnet was energized. The frequency of the oscillator was varied until the occurrence of resonance, which was evidenced by maximum amplitude on the oscillograph. It was found that the frame vibrated in the unsymmetrical mode, corroborating Chu's results. The load was increased until it exceeded the theoretical symmetrical buckling load of 7330 lb, and the frame remained

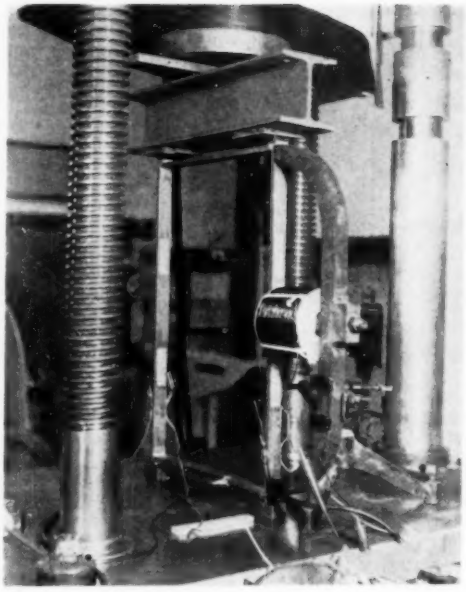

Fig. 3 Rectangular Frame Test Setup

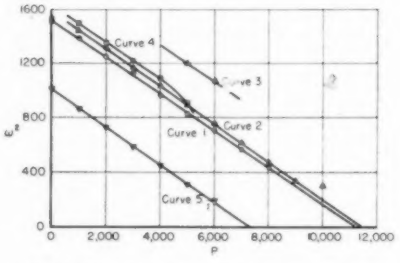

Fig. 4 Test Results for Rectangular Frame

stable. Frequency measurements could be recorded above this load. In order to determine the mode of buckling, the load was increased continuously until instability resulted. It was found that the frame buckled in the unsymmetrical mode. The variation of frequency with load is shown as curve 1, Fig. 4. Extrapolating the curve to zero frequency gives a buckling load of 11,150 lb, as compared to the theoretical unsymmetrical critical load of 11,360 lb for this frame. The test also confirms that the deviation from linearity of the curve for such an elastically restrained strut is so small as to be negligible in comparison with experimental error.

Having established the fact that the mode of buckling is of the same form as the mode of vibration, a second test was conducted on a second frame of the same dimensions. Similar results occurred; the points are plotted as curve 2 in Fig. 4. The actual buckling load was measured as 10,250 lb, as compared with the extrapolated value of 11,450 lb and the theoretical value of 11,360

lb. In this test an endeavor was made to obtain some points representing the symmetrical mode of vibration, but at most frequencies insufficient power was available. However, two points were obtained, and these are plotted as curve 3 in Fig. 4. The fact that this curve lies above that for unsymmetrical vibrations seems to imply that, for some reason, it is a higher-energy state.

The third frame was constructed of similar dimensions, except that the knife-edge seats were arranged eccentrically by moving them 0.2 in. toward the center line of the frame. This would insure symmetrical buckling, and it was desired to determine the corresponding vibration modes. However, the vibrations were still unsymmetrical, and the points are plotted as curve 4 in Fig. 4. The measured buckling load was 5500 lb.

In order to discover this apparent discrepancy with theory, it seemed logical to examine the experimental setup in the light of the theoretical assumptions. The boundary conditions would first come under suspicion. All four knife-edges were firmly supported in V-blocks which would prevent any lateral movement of the four corners. Although this appeared to be a minor point, the support system was modified. The two left-hand knife-edge supports were 90-deg V-blocks as previously, but the right-hand supports were replaced by hardened-steel knife-edge seats. Hence lateral movement of the right-hand supports was now permitted. The modified system is shown in Fig. 5.

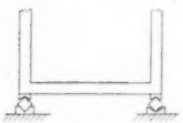

Fig. 5 Modified Arrangement of Knife-Edges

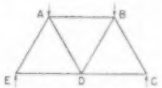

Fig. 6 Rigid-Joint Truss Configuration

The frame tested with the modified boundary conditions was similar to those in the first two tests. This time, however, the symmetrical mode became the stable configuration for all loads. The variation of frequency with load is shown as curve 5, Fig. 4. Linearity is verified to within experimental limits, the extrapolated value of 7330 lb corresponding exactly to the theoretical buckling load. The frame actually failed at 6950 lb in the symmetrical mode.

In view of the results of this test, the reason for the behavior of the frames tested previously now becomes apparent. The effect of maintaining the horizontal distance between the knife-edges is sufficient to cause the unsymmetrical mode to be the stable mode both for vibrations and buckling. These tests thus showed up the very important result that the buckling load of such a frame can be predicted by simply measuring the frequency of vibration under various loads. The correct mode of buckling will be satisfied automatically owing to the fact that the vibrations will also occur in that mode. It is seen now that Chu's extrapolated value would in fact have corresponded to the actual critical load for his boundary conditions had he continued loading up to buckling.

Two important points must be realized in using this experimental method. The first is that the members of the frame must be long enough to fail by elastic instability, i.e., no short column effects. Then the boundary conditions must be such that they will not vary with loading. This second condition is not important in static buckling tests, because the equivalent end fixity at buckling can be computed. However, in the dynamic tests, it is important that the boundary conditions for each vibration test be identical to the boundary conditions which would prevail if buckling were to occur.

Application to Rigid-Joint Trusses

In the previous sections it was pointed out that the approximately linear relationship between the load and the square of the frequency could be expected to apply only to elastic bodies whose boundary conditions did not vary with load. The rectangular frame which was tested complied with this condition as the horizontal members carried no load, and hence the buckling vertical members were restrained by the constant elastic restraints provided by the horizontal members. In the case of a rigid-joint truss, however, the axial force in each member increases with increasing load, and hence the effective rigidity at the end of any particular member does not remain constant. Consequently the deviation from the linear relationship cannot be expected to remain small in such a structure.

In order to ascertain the effect of the change of end restraint with load, it was decided to conduct tests on simple rigid-joint trusses. The truss configuration which was chosen is shown diagrammatically in Fig. 6. The length of all members was 12 in. and the section $^1/_4$ in. square. The material was mild steel, and all joints were brazed to make rigid connections. Hardened-steel knife-edges and seats were used. The knife-edges at A and C were fixed, while those at B and E were allowed to pivot, allowing lateral motion at those points.

The frame was excited by attaching a vibrator to the center of, and normal to, the member AE in the plane of the truss. This vibrator was a modified permanent-magnet speaker. By varying the frequency of energization of the voice coil, the diaphragm of the speaker could be made to vibrate over a considerable range of frequencies. The frequency of vibration was measured by dynamic strain gages attached to the members AB, BC, and BD, and recording the output on an oscillograph. The complete test setup is shown in Fig. 7.

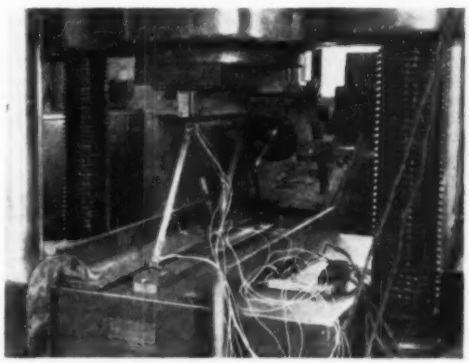

Fig. 7 Rigid-Joint Truss Test Setup

The frame was then loaded in increments, and the lowest resonant frequency recorded at each load. It was found that each of the instrumented members had a different resonant frequency for a particular load on the truss, but in addition there was one frequency at which all the members resonated. This resonant frequency for the complete truss was the one which decreased systematically with load, while the individual frequencies seemed to vary little. The load was increased until, at 1880 lb, the frame suddenly failed by torsional instability out of its plane. This unexpected failure prevented the test from being continued to the desired failure in the plane of the truss. The test results are plotted in Fig. 8 as curve 1.

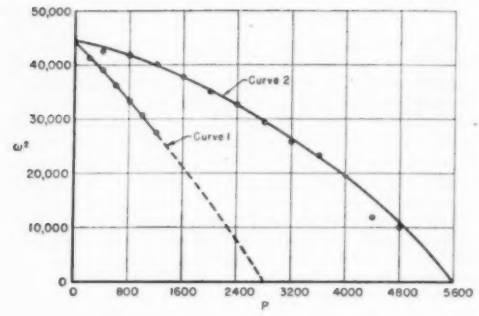

FIG. 8 TEST RESULTS FOR RIGID-JOINT TRUSS

A second frame was then constructed identical to the first, with the exception that the members were twice as wide, viz., $^1/_2$ in. × $^1/_4$ in. In addition, lateral restraint was provided by denying the top loading bar any possible angular rotation. These restraints can be seen in Fig. 7. The frame was loaded and again the lowest resonant frequency for the complete frame was recorded at each load. The frame failed at 4945 lb when the member AE began buckling in the plane of the truss. The test results are plotted in Fig. 8 as curve 2. As would be expected in analyzing the data, it was found that at resonance all the members vibrated either in phase or 180 deg out of phase.

The actual buckling load was lower than the extrapolated value of approximately 5600 lb, and this is apparently due to slight imperfections in the truss. The theoretical buckling load for this truss was computed by a method developed by Winter (10) and extended by Bijlaard (11), and yielded a value of 4150 lb. That the carrying capacity of this truss would exceed this value was again to be expected in view of the fact that the two points A and C were prevented from moving, whereas the theory assumed no restraint. The restraints were necessary in order to prevent undue complication in the test setup.

An examination of Fig. 8 yields some interesting results. As predicted, the relationship is not linear; but more significant is the fact that the deviation from linearity is considerably larger in curve 2. It might seem reasonable to deduce from these tests that the deviation from linearity increases as the section modulus of the members increases. This could be interpreted physically as follows: For a given moment of inertia, as the depth of the members is increased, the change in the end restraints due to axial loads in adjoining members is decreased.

EXPERIMENTAL TESTS ON PLATES

A survey of existing literature failed to yield any experimental data on the vibrations of rectangular plates. It appears that the only tests that have been carried out are on small circular plates for microphone diaphragms. Therefore it was decided to set up a testing program in which both unstiffened and stiffened flat plates could be loaded in compression while frequency measurements were made.

The plates used were made of 24S-T duralumin sheet, 12 in. × 12 in. × 0.040 in. thick. A special ring gage, placed between the specimen and the platform of the testing machine, was used to measure the small increments of load. This gage, mounted above the test specimen, is shown in Fig. 9 which also shows the vibrator (used in the truss tests). The frequencies of the plate were measured by mounting a strain gage on each side of the plate.

The first specimens to be tested were simply supported flat plates. The four supports were V-grooves, and the edges of the plates were fitted with steel knife-edges. The natural frequency decreased only slightly with increase in load, and a typical set of points is plotted in Fig. 10, curve A.

Tests were then conducted on similar plates which, loaded along clamped edges, had the unloaded edges supported on knife-edges. Similar results were obtained, and these are shown in Fig. 10, curve B. The natural frequency for zero load was calculated by the method described in reference (12). In subsequent tests, all four edges were clamped, with similar results.

In order to check the reliability of the experimental setup, the two unloaded edges were allowed to deflect with no restraint, the loaded edges only being clamped. In this case the approximately linear theoretical curve (Fig. 10, curve C) was followed closely, a result to be expected because of the fact that such a plate acts as a wide simple column.

A series of tests were then conducted on a stiffened panel. The plate was of the same dimensions as the unstiffened plate, with the addition of a single channel stiffener riveted longitudinally along the center of the plate. Tests were conducted with various edge conditions, but the results were similar to those for the unstiffened plates.

As a result of the foregoing tests, it appears that thin plates under compression do not follow the linear load-frequency² relation in practice. A possible explanation might be that a thin plate is never perfectly flat, so that initial curvature in the plate has some effect. The tests indicated very clearly that the buckles grow with the beginning of loading, and gradually increase. This fact was also borne out in a paper by Hu, Lundquist, and Batdorf (13) who showed theoretically that the von Kármán large-deflection equations should be used in studying the effect of small deviations from flatness on the buckling of plates in compression.

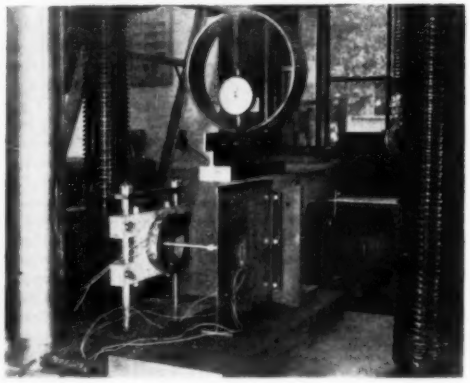

FIG. 9 FLAT-PLATE TEST SETUP

In a recent paper by Massonnet (14) a theoretical relationship between the frequency and end thrust was obtained for the case of circular plates with initial curvature. Using the von Kármán nonlinear plate equations, Massonnet obtained an approximate solution for a clamped circular plate uniformly loaded around the circumference. The load-frequency relationship was computed for various initial deflections of the plate, and his results are plotted in Fig. 11. The curves are plotted for various values of a parameter proportional to the initial deflection δ_0, viz.

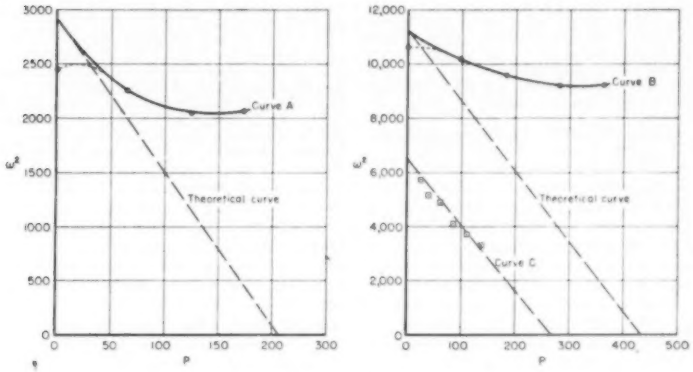

FIG. 10 TEST RESULTS FOR FLAT PLATES

$$\frac{\delta_0 \sqrt{12(1-\nu^2)}}{h}$$

For example, the parameter equal to 1 corresponds to an initial deflection of 0.012 in. for 0.040-in. sheet. Massonnet's results confirm the experimental results as shown in Fig. 10, and lend credence to the conclusion that the initial curvature in the plate caused the considerable deviation from linearity.

Therefore it is inferred that the justification for using the linear equations in such cases is not upheld in practice. The method of using frequency measurements in order to estimate the buckling load cannot be expected to give satisfactory results in the case of plates in compression—at least in the case of aircraft panels, where the deviation from flatness may be of the same order as the thickness of the panel.

A possible way to eliminate the difficulty might be to test the plates in tension, measuring the frequency with each increment of load. In this case any initial curvature will be decreased with increasing load, and the linear equations may be valid. Extrapolation to zero frequency along the negative load axis would thus give the theoretical buckling load.

CONCLUSIONS

For linear systems, the square of the frequency of lateral vibrations is practically linearly related to the end thrust. The relationship is exactly linear if the mode of free vibrations is identical to the buckling mode. This property can be used in practice to determine the buckling load by frequency measurements, provided the boundary conditions do not vary with load. By plotting the square of the frequency against load, a straight-line extrapolation to zero frequency gives a good approximation to the buckling load. The determination of critical load by frequency measurements seems to have the advantage of predicting the load corresponding to the actual boundary conditions which prevail, whereas a theoretical calculation may unjustifiably assume certain conditions which are not realized in practice.

In cases where the boundary conditions do change with load (as in rigid-joint trusses), the method seems to be applicable under restricted conditions. Specialized research in this direction might be valuable in determining these limitations. For example, if the curvature of the load-frequency^2 curve were established as symmetrical, then the buckling load could be predicted from tests up to approximately half that load.

On the other hand, the method does not seem to have a practical application to flat plates, either stiffened or unstiffened. This seems to be due to the fact that the relatively large initial deflections encountered in practice produce nonlinear effects. Tension tests may overcome this difficulty successfully and yield the theoretical buckling load of flat plates.

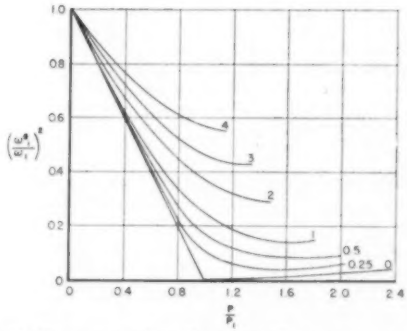

FIG. 11 THEORETICAL LOAD-FREQUENCY RELATIONSHIPS FOR A CLAMPED CIRCULAR PLATE WITH INITIAL CURVATURE

BIBLIOGRAPHY

1 "Theory of Elasticity," by R. V. Southwell, Oxford University Press, London, England, 1941.

2 "Les Relations entre les Modes Normaux de Vibration et la Stabilite des Systems Elastiques," by Ch. Massonnet, Bulletin des Cours et des Laboratories d'Essais des Constructions du Genie Civil et d'Hydraulique Fluviale, Tome I, Nos. 1 and 2, 1940, Brussels, Belgium.

3 "Transversalschwingungen rechteckiger Platten mit besonderer Rucksiekt der Knickung," by Hugo Grauers, *Ingeniorsvetenskapsakadeniens*, Handlinger Nr. 98, Stockholm, Sweden, 1929.

4 "On the Vibrations of a Clamped Plate Under Tension," by A. Weinstein and W. Z. Chien, *Quarterly of Applied Mathematics*, vol. 1, 1943, pp. 61–68.

5(*a*) "Natural Vibration Frequencies of Structural Members as an Indication of End Fixity and Magnitude of Stress," by B. C. Stephens, *Journal of the Aeronautical Sciences*, vol. 4, 1936, pp. 54–60.

5(*b*) "Effective End Restraint of Columns by Frequency Measurements," by Harold Lurie, *Journal of the Aeronautical Sciences*, vol. 18, 1951, pp. 566–567.

6 "Determination of Buckling Loads by Frequency Measurements," by T. H. Chu, thesis at the California Institute of Technology, 1949.

7 "A Note on the Buckling of Struts," by Harold Lurie, *Journal of the Royal Aeronautical Society*, vol. 55, March, 1951, pp. 181–184.

8 "Die Eigenschwingungen der in ihrer Ebene allseitig gleichmässig belasteten gleichseitigen Dreiecksplatte," by H. Schaefer and A. Havers, *Ingenieur-Archiv*, vol. 7, 1936, pp. 83–87.

9 "Rayleigh's Principle," by G. Temple and W. G. Bickley, Oxford University Press, London, England, 1933.

10 "Buckling of Trusses and Rigid Frames," by G. Winter, P. T. Hsu, B. Koo, and M. H. Loh, Bulletin No. 36, Engineering Experiment Station, Cornell University, Ithaca, N. Y., April, 1948.

11 "Investigation on Buckling of Rigid Joint Structures," by P. P. Bijlaard, First Progress Report, Department of Structural Engineering, Cornell University, Ithaca, N. Y., November, 1949 (unpublished).

12 "Vibrations of Rectangular Plates," by Harold Lurie, *Journal of the Aeronautical Sciences*, vol. 18, February, 1951, pp. 139–140.

13 "Effect of Small Deviations From Flatness on Effective Width and Buckling of Plates in Compression," by P. C. Hu, E. E. Lundquist, and S. B. Batdorf, NACA Technical Note No. 1124, 1946.

14 "Le Voilement des Plaques Planes Sollicitees dans leur Plan," by Ch. Massonnet, Final Report of the Third Congress of the International Association for Bridge and Structural Engineering, Liege, Belgium, September, 1948.

Bending Vibrations of a Pipe Line Containing Flowing Fluid

By G. W. HOUSNER,[1] PASADENA, CALIF.

Both free vibrations and forced motions due to cross-winds may create important problems in the design of pipe lines supported above ground. An analytic investigation, based on simple beam theory, shows that the flow of fluid in such a pipe line has no beneficial effect upon the vibrations. The fluid velocity causes a dynamic coupling of the simple modes of vibration so that the normal modes of vibration are of complex shape with 90-deg out-of-phase components. The solution is presented for free vibrations and for steady-state forced vibrations, and it is shown that large amplitudes may be developed if the amount of damping is too small. It is shown that at low fluid velocities there is negligible effect upon the vibration of the pipe line, and at a certain high critical velocity the fluid flow causes a dynamic instability. The present analysis revises the conclusions which appeared in an earlier publication.

Introduction

THE trans-Arabian pipe line is a 30-in-diameter pipe which over a portion of its length is above ground. The pipe is supported at 66-ft intervals and has approximately 20 in. clearance between the bottom of the pipe and the ground as shown in Fig. 1. At certain wind velocities the pipe line has

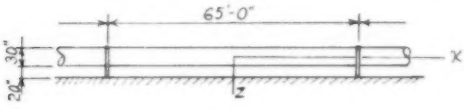

FIG. 1

been observed to vibrate in the following manner: At a wind velocity of approximately 20 mph, the pipe begins to vibrate with a frequency of vibration of approximately 1.2 cycles per second and attains a maximum deflection of $^3/_{16}$ in. at mid-span. After about 20 sec the frequency increases and amplitude decreases so that in approximately 10 sec the pipe has come to rest and the vibration then repeats. During vibration the adjacent spans move in opposite directions with nodes at the supports. The computed natural frequency of vibration of the pipe is 2.5 cps as compared with the observed 1.2 cps. The amplitude of $^3/_{16}$ in. produces bending stresses of the order of 1000 psi.

Differential Equation of Motion

To derive the differential equation consider a pipe full of fluid, whose total mass, pipe plus fluid, per unit length is m, moment of inertia of pipe I, and modulus of elasticity E. Let ρ be the mass per unit length of the fluid and let it have a constant velocity v, relative to the pipe, thus neglecting the effect upon the velocity of the change in length of the pipe during vibration. Let the coordinate measured along the pipe be x, and the vertical displacement of the pipe z. It is desired to derive the differential equation describing the motion of the pipe. As the fluid flows along the curve described by the center line of the pipe, it has a rather complicated motion owing to the fact that each point on the center line has a vertical acceleration, an angular acceleration, and a changing curvature. With a problem of this complexity it is convenient to utilize Hamilton's principle[2] to insure that no part of the motion is overlooked.

As an element of fluid flows along the pipe it has a velocity v tangent to the pipe axis and a velocity $\dot{z} = \partial z/\partial t$ in a vertical direction. Assuming small displacements of the pipe, the x-component of the velocity is v, and the z-component is

$$\dot{z} + vz' = \frac{\partial z}{\partial t} + v\frac{\partial z}{\partial x}$$

The kinetic energy in a length dx of the pipe is that of the pipe plus that of the fluid, which is

$$dT = \left\{\frac{1}{2}(m-\rho)\dot{z}^2 + \frac{1}{2}\rho\left[v^2 + (\dot{z} + vz')^2\right]\right\} dx$$

The first term on the right side represents the kinetic energy of the pipe shell, and the second represents the kinetic energy of the fluid. The strain energy in the length dx is, according to beam theory

$$dV = \frac{1}{2}EI(z'')^2$$

Hamilton's principle states that the variation of $\int_{t_1}^{t_2}(T - V)\,dt$ is equal to zero, which for this problem is

$$\delta\int_{t_1}^{t_2}\int_{x_1}^{x_2}\left\{\frac{1}{2}(m-\rho)\dot{z}^2 + \frac{1}{2}\rho\left[v^2 + (\dot{z} + vz')^2\right] - \frac{1}{2}EI(z'')^2\right\} dx\,dt = 0$$

Performing the variation gives

$$\int_{t_1}^{t_2}\int_{x_1}^{x_2}\left\{(m-\rho)\dot{z}\,\delta\dot{z} + \rho(\dot{z} + vz')(\delta\dot{z} + v\,\delta z') - EIz''\delta z''\right\} dx\,dt = 0$$

Since

$$\delta\dot{z} = \frac{\partial}{\partial t}(\delta z),\ \delta z' = \frac{\partial}{\partial x}(\delta z),\ \delta z'' = \frac{\partial^2}{\partial x^2}(\delta z)$$

---

[1] Division of Engineering, California Institute of Technology.

For presentation at the National Conference of the Applied Mechanics Division, State College, Pa., June 19–21, 1952, of THE AMERICAN SOCIETY OF MECHANICAL ENGINEERS.

Discussion of this paper should be addressed to the Secretary, ASME, 29 West 39th Street, New York, N. Y., and will be accepted until July 10, 1952, for publication at a later date. Discussion received after the closing date will be returned.

NOTE: Statements and opinions advanced in papers are to be understood as individual expressions of their authors and not those of the Society. Manuscript received by ASME Applied Mechanics Division, November 9, 1950. Paper No. 52—APM-3.

[2] See, for instance, "Applied Mechanics-Dynamics," by G. W. Housner and D. Hudson, D. Van Nostrand Co., New York, N. Y., 1950, p. 260.

each term may be integrated by parts so as to eliminate the various derivatives of δz. When this is done, there is obtained

$$\int_{t_1}^{t_2}\int_{x_1}^{x_2}(m\ddot{z} + 2\rho v\,\dot{z}' + \rho v^2 z'' + EIz^{iv})\,\delta z\,dx\,dt = 0$$

where all the integrated terms have disappeared because of the boundary conditions. Since δz is arbitrary, the only way for the integral to be zero is for the expression in square brackets to be identically zero. Equating this to zero gives the differential equation

$$EI\frac{\partial^4 z}{\partial x^4} = -\rho v^2\frac{\partial^2 z}{\partial x^2} - 2\rho v\frac{\partial^2 z}{\partial t\partial x} - m\frac{\partial^2 z}{\partial t^2} \quad \ldots\ldots [1]$$

This equation states that the beam is acted upon by three different inertia forces. The first term on the right represents the inertia force associated with the change in direction of v, enforced by the curvature of the beam; that is, the fluid experiences an acceleration because it travels along a curved path. The second term is the inertia force associated with the Coriolis acceleration which arises because the fluid is flowing with velocity v relative to the pipe, while the pipe itself has an angular velocity $(\partial^2 z)/(\partial t\partial x)$ at any point along its length. The last term represents the inertia force associated with the vertical acceleration of the pipe.

Free Vibrations

Equation [1] differs from the more usual vibration equations in that it contains a mixed derivative $(\partial^2 z)/(\partial x\partial t)$. Although this term contains a first derivative with respect to time, its influence is not the same as a viscous damping term which has the form $\partial z/\partial t$. This can be seen by writing the equation in the form

$$EI\frac{\partial^4 z}{\partial x^4} + \rho v^2\frac{\partial^2 z}{\partial x^2} + m\frac{\partial^2 z}{\partial t^2} = F(x, t) \quad \ldots\ldots [2]$$

where $F(x, t)$ is considered to be an applied force. The free vibrations are then the normal modes which are the solutions of Equation [2] with $F(x, t)$ set equal to zero. For a simply supported beam these are

$$z_n = A_n \sin\frac{n\pi}{l}x\sin\omega_n t \quad \ldots\ldots [3]$$

Assume that the beam is constrained so as to move in the nth mode only. If $F(x, t)$ is $-\partial z/\partial t$ then the applied force is proportional to

$$-A_n\omega_n \sin\frac{n\pi}{l}x\cos\omega_n t \quad \ldots\ldots [4]$$

The intensity of the force is proportional to the displacement and is 180 deg out of phase with the velocity so that the vibrational energy of the beam is dissipated in doing work against the force. However, if $F(x, t) = -(\partial^2 z)/(\partial x\partial t)$ the applied force is proportional to

$$-A_n\omega_n\frac{n\pi}{l}\cos\frac{n\pi}{l}x\cos\omega_n t \quad \ldots\ldots [5]$$

The force is again 90 deg out of phase with the displacement but its intensity in this case is not proportional to the displacement. It is seen that if $\sin(n\pi/l)x$ is symmetrical about the mid-point of the beam then $F(x, t)$ is antisymmetrical and therefore $F(x, t)$ does no work on the mode and is not associated with damping. The significance of $-(\partial^2 z)/(\partial x\partial t)$ is that it represents dynamic coupling, and it is impossible for a symmetrical mode of Equation [2] to exist by itself in a free vibration, for corresponding with this mode there is an antisymmetrical force, 90 deg out of phase, which excites all the antisymmetrical modes, and an antisymmetrical mode produces an $F(x, t)$ which excites all of the symmetrical modes. Thus a normal mode of Equation [1] must be a linear combination of all the normal modes of the homogeneous form of Equation [2] with symmetrical and antisymmetrical modes 90 deg out of phase. A simply supported span thus has normal modes z_i satisfying Equation [1]

$$z_i = \sum_n A_{2n-1}\sin(2n-1)\frac{\pi}{l}x\sin\omega_i t + \sum_k A_{2k}\sin 2k\frac{\pi x}{l}\cos\omega_i t \quad \ldots [6]$$

The normal mode z_i is composed of terms which interact with one another through the mixed derivative term

$$2\rho v\frac{\partial^2 z}{\partial x\partial t}$$

An odd term, say

$$A_{2i-1}\sin(2i-1)\frac{\pi}{l}x$$

must be in dynamic balance with the coupling forces exerted by all the even terms, and an even term must be in balance with the coupling forces exerted by all the odd terms. Each coefficient A_i is coupled with every other coefficient.

The coefficients and the natural frequency ω_i are determined as follows: When Expression [6] for z_i is substituted in Equation [1] the mixed derivative gives rise to terms containing

$$\cos(2n-1)\frac{\pi}{l}x \text{ and } \cos 2k\frac{\pi}{l}x$$

These terms may be expanded in a Fourier series

$$\left.\begin{aligned}\cos(2n-1)\frac{\pi}{l}x &= \sum_k {}_{(2n-1)}C_{2k}\sin 2k\frac{\pi}{l}x\\ \cos 2k\frac{\pi}{l}x &= \sum_n {}_{2k}C_{2n-1}\sin(2n-1)\frac{\pi}{l}x\end{aligned}\right\} \quad \ldots\ldots [7]$$

where

$${}_{2n-1}C_{2k} = \frac{4}{\pi}\frac{(2n-1)}{(2k)^2-(2n-1)^2} \qquad {}_{2k}C_{2n-1} = \frac{4}{\pi}\frac{(2k)}{(2k)^2-(2n-1)^2}$$

With these substitutions, all the terms in Equation [1] can be collected in groups according to whether they contain

$$\sin(2n-1)\frac{\pi}{l}x\sin\omega t$$

or

$$\sin 2k\frac{\pi}{l}x\cos\omega t$$

The coefficients of these terms must then be equated to zero in order to satisfy Equation [1]. This gives the following set of equations, for $n = 1, 2, 3, \ldots$; $k = 1, 2, 3, \ldots$.

$$A_{2n-1}\left[EI(2n-1)^4\left(\frac{\pi}{l}\right)^4 - \rho v^2(2n-1)^2\left(\frac{\pi}{l}\right)^2 - m\omega_i^2\right] = \frac{8\rho v\omega_i}{l}\sum_k A_{2k}\frac{(2k)^2}{(2k)^2-(2n-1)^2}$$

$$A_{2k}\left[EI(2k)^4\left(\frac{\pi}{l}\right)^4 - \rho v^2(2k)^2\left(\frac{\pi}{l}\right)^2 - m\omega_i^2\right] = \frac{8\rho v\omega_i}{l}\sum_n A_{(2n-1)}\frac{(2n-1)^2}{(2n-1)^2-(2k)^2}$$

If the A's are eliminated from these equations, there results the frequency equation whose roots determine the natural frequencies ω_i of the normal modes; then, setting $A_1 = 1$, these equations determine the remaining A for each normal mode. If all the modes are suppressed except the first two, the equations are solved readily. The frequency equation is

$$\frac{32\rho v\omega_i}{3l\left[EI\left(\frac{\pi}{l}\right)^4 - \rho v^2\left(\frac{\pi}{l}\right)^2 - m\omega_i^2\right]} = -\frac{3l}{8}\frac{\left[EI\left(\frac{2\pi}{l}\right)^4 - \rho v^2\left(\frac{2\pi}{l}\right)^2 - m\omega_i^2\right]}{\rho v\omega_i}$$

and the coefficient A_2 is

$$A_2 = -A_1\frac{8\rho v\omega_1}{3l\left[EI\left(\frac{2\pi}{l}\right)^4 - \rho v^2\left(\frac{2\pi}{l}\right)^2 - m\omega_1^2\right]}$$

For the parameters of the trans-Arabian pipe line[3] these give for the fundamental mode

$$A_1 = 1, \quad A_2 = 0.06, \quad \omega_1 = 15.6$$

These values are based on a fluid velocity of 15 fps which is the figure used in the previous paper[3] and which is somewhat larger than the actual velocity in the line. However, it is seen that the 15-fps velocity is not large enough to excite the unsymmetrical A_2 component appreciably, and it has a negligible effect upon the natural frequency which with zero fluid velocity is $\omega_1 = 15.6$ to three significant figures.[4] It may be verified that the strength of the coupling decreases rapidly, so that if A_1, A_2, and A_3 are retained, the magnitude of A_2 is small compared to that of A_2 in the lowest mode of vibration. In general, the dynamic coupling is such that in the ith mode of vibration the coefficient A_i is the largest and the coefficients A_{i+1}, A_{i+2}, ... and A_{i-1}, A_{i-2}, ... decrease in magnitude very rapidly as the subscript goes away from i.

Forced Vibrations

The normal modes of Equation [6] may be used to represent the solution for steady-state forced vibrations. If the aerodynamic forces on the pipe are assumed to be distributed uniformly along the span and to vary sinusoidally with time, the differential equation of motion is

$$EI\frac{\partial^4 z}{\partial x^4} + \rho v^2\frac{\partial^2 z}{\partial x^2} + m\frac{\partial^2 z}{\partial t^2} + 2\rho v\frac{\partial^2 z}{\partial x\partial t} = \frac{4p}{\pi}\sum_n \frac{1}{2n-1}\sin(2n-1)\frac{\pi}{l}x\sin\omega t$$

where the load $p \sin \omega t$ has been expanded in a Fourier series. Substituting the normal modes of Equation [6] leads to the equations

$$A_{2n-1}\left[EI(2n-1)^4\left(\frac{\pi}{l}\right)^4 - \rho v^2(2n-1)^2\left(\frac{\pi}{l}\right)^2 - m\omega^2\right] - 2\rho v\omega\frac{\pi}{l}\sum_k A_{2k}(2k)_{2k}C_{2n-1} = \frac{4p}{\pi}\frac{1}{(2n-1)}$$

$$A_{2k}\left[EI(2k)^4\left(\frac{\pi}{l}\right)^4 - \rho v^2(2k)^2\left(\frac{\pi}{l}\right)^2 - m\omega^2\right] + 2\rho v\omega\frac{\pi}{l}\sum_n A_{2n-1}(2n-1)_{2n-1}C_{2k} = 0$$

These equations determine the coefficients A_{2n-1} and A_{2k}, thus giving the complete solution for the steady-state vibrations. When ω is such that these equations give $A = \infty$ it means that the aerodynamic force is in resonance with a mode and the amplitude becomes increasingly large.

There is a singular case when the amplitudes may become infinite, namely, when the fluid velocity has the critical value

$$v = \sqrt{\frac{EI\pi^2}{\rho l^2}}$$

This may be seen readily from the differential equation for static loading which is

$$EI\frac{\partial^4 z}{\partial x^4} + \rho v^2\frac{\partial^2 z}{\partial x^2} = p$$

This is the same as the equation for the pipe carrying a lateral load p and an axial load $P = \rho v^2$. It follows that the pipe will buckle when P reaches Eulers load, that is

$$\rho v^2 = \frac{\pi^2 EI}{l^2}$$

The term

$$\rho v^2\frac{\partial^2 z}{\partial x^2}$$

which gives rise to the buckling, represents the inertia forces produced by the curvature. The critical velocity is, of course, very large and is not of importance for pipe lines.

The foregoing analysis shows that if the pipe line is undamped, resonance will occur when the frequency of the aerodynamic force coincides with a natural frequency of vibration, and amplitudes of unlimited magnitude will develop. In the actual pipe line there will be, of course, some damping and consequently the amplitude will remain finite. The amplitude attained will depend on the amount of damping present and the magnitude of the exciting force. Thus it is seen that the vibration of the pipe line is a problem of the same sort as the vibration of the Tacoma Narrows Bridge, and if the pipe line is constructed so that it has a very small amount of damping, then it is possible that relatively large amplitudes may be built up.

The values of the parameters for the trans-Arabian pipe line being such that the fluid velocity has only a very small effect, it is of some interest to examine the explicit solution for zero fluid velocity.

Assuming an exciting force $q \sin \omega t$ acting upon a simply supported span and setting $v = 0$ in Equation [1] results in the steady-state forced vibration

$$z = \frac{q}{2m\omega^2}\left(\frac{\cos 2\lambda\frac{x}{l}}{\cos\lambda} + \frac{\cosh 2\lambda\frac{x}{l}}{\cosh\lambda} - 2\right)\sin\omega t \ldots [8]$$

where

$$\lambda = \sqrt[4]{\frac{m\omega^2}{EI}\left(\frac{l}{2}\right)^4}$$

Using the values $m = 11$, $\omega/(2\pi) = 1.2$, $l = 66$, $x = 0$, $z = 1/8$ in., there is obtained $q = 13$ lb per ft. So the reported data im-

[3] "Bending Vibrations of a Pipe Line Containing Flowing Fluid," by H. Ashley and G. Haviland, Journal of Applied Mechanics, Trans. ASME, vol. 72, 1950, pp. 229–232.

[4] This is the frequency using $I = 0.125$ ft^4.

plies an exciting force $F = 13 \sin 2.4\,\pi\,t$ if the differential Equation [1] describes the motion.

A force of 13 lb per ft is too large to be reasonably expected. However, the foregoing analysis does not take into account an axial force which likely is in the pipe. As is well known, the effect of an axial force is to decrease the natural frequency of vibration. The fluid pressure in the pipe is not sufficient to produce an appreciable change in frequency, but if the pipe line is fabricated so that large temperature-expansion stresses exist, the frequency can be changed greatly. For example, if the fluid pressure in the trans-Arabian pipe line is 500 psi and the net axial compressive stresses are 20,000 psi, then the natural frequency is reduced from 2.5 cps to 1.2 cps which coincides with the frequency of the aerodynamic force. It is not unlikely that the axial force in the trans-Arabian pipe line is much larger than it is thought to be, and a relatively small aerodynamic force is approximately in resonance with the pipe. If this is the case, the amplitude of vibration can be controlled by the installation of vibration dampers along the line. However, the essential question yet remaining is "What magnitude of aerodynamic force is possible when air is flowing past a cylinder which is near a plane boundary?" This must be investigated if the problem of pipe-line vibrations is to be solved completely.

Appendix

An investigation of this problem also appeared in an earlier paper[3]. The differential equation studied there was

$$EI\,\frac{\partial^4 z}{\partial x^4} = -\rho v\,\frac{\partial^2 z}{\partial x \partial t} - m\,\frac{\partial^2 z}{\partial t^2} \qquad [9]$$

This equation neglects the inertia forces produced by the curvature of the pipe and includes only one half of the inertia forces due to the Coriolis acceleration, so that it underestimates the influence of the fluid velocity. The solution of this equation is of the same form as that of Equation [1], and for a simply supported beam it is the sum of normal modes

$$z = \sum_i z_i = \sum_i \left[\sum_n A_{2n-1} \sin (2n-1)\,\frac{\pi}{l}\,x \sin \omega_i t + \sum_k A_{2k} \sin 2k\,\frac{\pi}{l}\,x \cos \omega_i t \right] \qquad [10]$$

The coefficients and the natural frequencies ω_i are determined by substituting the ith mode in Equation [9] using the Expansions [7] and collecting terms according to whether they contain

$$\sin (2n-1)\,\frac{\pi}{l}\,x \sin \omega t \text{ or } \sin 2k\,\frac{\pi}{l}\,x \cos \omega t$$

Equating the coefficients to zero gives the equations

$$A_{2n-1}\left[EI(2n-1)^4 \left(\frac{\pi}{l}\right)^4 - m\omega_i^2 \right] - \rho v \omega_i \sum_k A_{2k}\,\frac{\pi}{l}\,(2k)\,{}_{2k}C_{2n-1} = 0$$

$$A_{2k}\left[EI(2k)^4 \left(\frac{\pi}{l}\right)^4 - m\omega_i^2 \right] + \rho v \omega_i \sum_n A_{2n-1}\,\frac{\pi}{l}\,(2n-1)\,{}_{2n-1}C_{2k} = 0$$

These equations determine the frequency ω_i for each normal mode, and setting $A_1 = 1$ they determine the remaining A. It follows that the solution of Equation [9] is the sum of the normal modes z_i of Equation [10]. Since the differential Equation [9] is that of a conservative system, the solution shows, as it should, that there is no energy loss, and the free vibrations once established are permanent. In the previous paper it was concluded "that the flow of fluid in such a pipe line produces marked damping tendencies and thus may reduce the severity of loading." The solution of Equation [9] in the previous paper was based on a power-series approximation and in correspondence with the authors it has been agreed that if the power series contained a sufficient number of terms, the solution would converge to Equation [10]. It also has been agreed that Equation [1] is the correct description of the vibrations.

Heat Conduction in a Compressible Fluid

By J. D. COLE[1] and T. Y. WU,[2] PASADENA, CALIF.

The conduction of heat in a compressible fluid medium is studied in this paper. The compressibility of the fluid has the important effect that an excess of heat is not only carried away by conduction but also causes a pressure wave to move in the fluid. A closely related problem is the effect of heat conduction on the propagation of sound waves in a gas. In both cases the total energy is divided between thermal and pressure waves.

Introduction

IN this study of heat conduction in a compressible fluid the effects of viscosity are omitted. This, of course, is not a realistic assumption since any kinetic theory of matter indicates a close relationship between the coefficients of heat conduction and viscosity. The main justification for the omission is simplification of the equations to be studied. This simplification is in accord with a general viewpoint of trying to isolate the difficulties and of studying certain idealized models of real fluids. A previous work[3] explains this viewpoint and studies the relationship of the real fluid to various idealizations. Further, in that paper, a detailed study is made of the propagation of small disturbances in a viscous, compressible, but nonheat-conducting fluid. (The monograph[3] also contains an extensive bibliography in related topics so that no further references will be given here.) Thus the present work is a natural extension of the previous study.

Another justification for the omission of viscosity is that in many problems the transfer of heat is of main interest and the viscous stresses actually may be quite small. Also, for a certain class of problems, which will be made more precise later, viscous effects do not change the situation at all qualitatively. It also should be pointed out that neglecting viscosity means that dissipation within the fluid is neglected so the analysis cannot be applied directly to any case in which this is of importance.

The subject matter of the paper is as follows: Some exact equations of motion and heat transfer, with the assumptions mentioned in the foregoing, are studied briefly. To make calculations possible it is next assumed that all disturbances are small so that the equations can be linearized, as in the usual theory of sound. For this linear system, which preserves many of the features of the original nonlinear system, the fundamental solutions are found and discussed in some detail.

Basic Equations of Motion and Characteristics

The basic equations are the statements of the laws of conservation of mass, momentum, and energy applied to a continuum. It is assumed that the medium is a perfect gas, so that the perfect gas law

$$P = R\rho T \qquad [1]$$

holds, and viscosity is neglected. The basic equations can then be written as follows:

Conservation of mass

$$\frac{\partial \rho}{\partial t} + \operatorname{div} \rho \vec{Q} = 0 \qquad [2]$$

Conservation of momentum

$$\frac{\partial \vec{Q}}{\partial t} + \vec{Q} \cdot \operatorname{grad} \vec{Q} = \vec{F} - \frac{1}{\rho} \operatorname{grad} P \qquad [3]$$

Conservation of energy

$$\frac{\partial E}{\partial t} + \vec{Q} \cdot \operatorname{grad} E + P\left[\frac{\partial \left(\frac{1}{\rho}\right)}{\partial t} + \vec{Q} \cdot \operatorname{grad} \left(\frac{1}{\rho}\right)\right] = \frac{1}{\rho} \operatorname{div} (k \operatorname{grad} T) + Q \qquad [4]$$

where it is assumed that Fourier's conduction law applies. The heat-flux vector $\vec{H}$ is given by

$$\vec{H} = -k \operatorname{grad} T \qquad [5]$$

We have here a nonlinear system of four equations in the four unknowns P, ρ, T, $\vec{Q}$. The characteristics of the system give some idea about the underlying structure of the system by showing surfaces of propagation of certain disturbances or discontinuities. If we consider only one space variable and let $\psi(x, t) = \text{const}$ denote a characteristic we have[4]

$$\psi_x^2[\psi_t + (Q \pm C_i)\psi_x] = 0 \qquad [6]$$

These characteristics are: (1) $\psi_x^2 = 0$, or $t = \text{const}$. This set indicates propagation of certain disturbances with an infinite speed and are thus associated with the usual conduction of heat. (2) $\psi_t + (Q \pm C_i)\psi_x = 0$ or slope $= Q \pm c_i$. These lines indicate propagation of certain disturbances with the isothermal speed of sound c_i relative to the fluid. It is not yet completely clear what the physical meaning of these characteristics is.

If we consider for a moment a fluid in which the heat conduction $k = 0$, the order and hence the number of characteristics of our system, Equations [1] to [5], is lowered by one. The characteristics are now

$$(\psi_t + Q\psi_x)[\psi_t + (Q \pm C)\psi_x] = 0 \qquad [7]$$

The first bracket indicates the streamlines of the flow, across which temperature and density may now jump (because $k = 0$, $\mu = 0$) and the second bracket indicates propagation of sound waves relative to the fluid with the usual adiabatic speed $C = \sqrt{\gamma RT}$. These characteristic lines which remain undiscovered

[1] Research Fellow, California Institute of Technology.

[2] Graduate Student, California Institute of Technology.

[3] "Problems in the Theory of Viscous Compressible Fluids," by P. A. Lagerstrom, J. D. Cole, and L. Trilling, GALCIT Monograph, March, 1949.

Contributed by the Applied Mechanics Division and presented at the Heat Transfer and Fluid Mechanics Institute, Stanford University, Stanford, Calif., June 20–22, 1951, of The American Society of Mechanical Engineers.

Discussion of this paper should be addressed to the Secretary, ASME, 29 West 39th Street, New York, N. Y., and will be accepted until one month after final publication of the paper itself in the Journal of Applied Mechanics.

Note: Statements and opinions advanced in papers are to be understood as individual expressions of their authors and not those of the Society. Manuscript received by ASME Applied Mechanics Division, November 12, 1951.

[4] See Footnote 3, pp. 18–20.

for $k \neq 0$ must play an important role in the solutions for small values of k. Some light will be shed on this interesting point by the solutions given explicitly later.

Linearization of Equations

The system of Equations [1] to [5] is now linearized by assuming that all velocity components and pressure, density, and temperature perturbation are small, and by neglecting squared terms of small quantities. Equations [1] to [5] now read

$$p = s + \theta \text{ (state)} \quad [8]$$

$$\vec{q}_t = \vec{X} - c_i^2 \operatorname{grad} p \text{ (momentum)} \quad [9]$$

$$s_t + \operatorname{div} \vec{q} = 0 \text{ (continuity)} \quad [10]$$

$$\theta_t - (\gamma - 1)s_t = \kappa\Delta\theta + \Omega \text{ (energy)} \quad [11]$$

The solutions to this system can be applied to the case when there is a large component of velocity in one direction by using a Galilean transformation.[5] It should be remarked here that in linearizing, the dissipation terms drop out in Equation [11] whether or not $\mu = 0$. We are neglecting μ only in the momentum equations.

Before finding solutions of the system, Equations [8] to [11], some general properties of the equations will be discussed. First we show that the flow field described by Equations [8] to [11] are usually irrotational, for if the external forces have a potential

$$\vec{X} = \operatorname{grad} \Xi \quad [12]$$

taking the curl of Equation [9] yields

$$(\operatorname{curl} \vec{q})_t = 0 \quad [13]$$

Thus the vorticity $= \operatorname{curl} \vec{q}$ is independent of time. If the vorticity is initially zero it remains zero. In this case, which will be considered here, it is useful to introduce the velocity potential φ such that

$$\vec{q} = \operatorname{grad} \varphi \quad [14]$$

and then system, Equations [8] to [11], can be reduced to a pair of equations

$$\Delta\varphi - \frac{1}{c_i^2}\varphi_{tt} = \theta_t + \frac{1}{c_i^2}\Xi_t \quad [15]$$

$$\theta_t - \kappa\Delta\theta = \Omega - (\gamma - 1)\Delta\varphi \quad [16]$$

From this system it is easy to see the coupling between the thermal waves and the flow field. Equation [15] appears as a wave equation for the velocity potential with a driving force on the right-hand side provided by the temperature field. The second Equation [16] appears as a heat-conduction equation for the temperature but with a distribution of heat sources on the right-hand side due to the velocity field. It is just this interaction which will be studied shortly.

Several limiting cases which uncouple the Equations [15] and [16] can be indicated briefly. First of all, if the fluid is incompressible we may assume the speed of sound is infinite c, $c_i \to \infty$. Then Equations [15] and [16] become

$$\Delta\varphi = \theta_t + \Upsilon \quad [17]$$

$$\theta_t - \frac{\kappa}{\gamma}\Delta\theta = \frac{\Omega}{\gamma} - \left(1 - \frac{1}{\gamma}\right)\Upsilon \quad [18]$$

(if we assume that some of the force potential remains). Thus the temperature can be found from Equation [18] and the velocity field follows from Equation [17]. As another case we have $\kappa = 0$ and

$$\Delta\varphi - \frac{1}{c^2}\varphi_{tt} = \frac{\Omega}{\gamma} + \frac{1}{c^2}\Xi_t \quad [19]$$

$$\theta_t = \Omega - (\gamma - 1)\Delta\varphi \quad [20]$$

Now the velocity potential can be found from Equation [19] and the temperature follows Equation [20] which now contains the isentropic law.

Fundamental Solutions of the Linearized System

Various fundamental solutions can be defined for linear systems. We consider here only the case of heat addition and assume the force potential Ξ is zero. One fundamental solution can be defined by the response of the system to a certain amount of heat introduced at a point. More specifically, suppose the fluid fills an infinite space and that all perturbations are initially zero. Suppose now that a unit quantity of heat (in suitable dimensionless variables) is introduced instantaneously at the origin of coordinates. The resulting temperature field and potential given by

$$\left.\begin{aligned} \theta &= \Gamma(x_i, t) \\ \varphi &= \Phi(x_i, t) \end{aligned}\right\} \quad [21]$$

is called the fundamental solution of the system (due to a disturbance at the origin). In terms of the equations we can say that Equations [21] are the solution to the system, Equations [15] and [16], in an infinite domain with zero initial conditions when

$$\Omega = \delta(x_i)\delta(t) \quad [22]$$

This fundamental solution thus gives a typical solution and illustrates many features of the system. Furthermore, owing to the linearity of the system, Equations [15] and [16], superpositions can be used. If Ω is an arbitrary function of (x_i, t) the solution, under the same initial conditions and vanishing at infinity, can be represented by

$$\theta(x_i, t) = \int_{-\infty}^{\infty}\int\int\int d\xi_i \int_0^t d\tau \Gamma(x_i - \xi_i, t - \tau)\Omega(\xi_i, \tau) \quad [23]$$

$$\varphi(x_i, t) = \int_{-\infty}^{\infty}\int\int\int d\xi_i \int_0^t d\tau \Phi(x_i - \xi_i, t - \tau)\Omega(\xi_i, \tau) \quad [24]$$

The fact that the fundamental solutions can be taken to depend only on the differences in co-ordinates follows from the homogeneity of Equations [15] and [16] in space and time. These fundamental solutions also can be used to build up the solutions of initial and boundary-value problems. Thus fundamental solutions are an important part of the theory of the system, Equations [15] and [16]. In this paper most of the analytical work is devoted to finding these solutions and studying their properties. Now, when dealing with a system of second-order equations like Equations [15] and [16], which is equivalent to a single equation of higher order, it can be expected that the fundamental solutions are not expressible in terms of well-known functions, but probably themselves define new functions. In order to study the properties of these functions we have to represent the fundamental solutions in terms of elementary solutions to Equations [15] and [16]. In the following paragraphs the Laplace transformation is applied to the system, Equations [15] and [16], and the powerful

[5] See Footnote 3, p. 69.

method of integration in the complex plane is used to obtain integral representations and asymptotic formulas for the fundamental solutions [21].

The Laplace transform with respect to time of a function $f(x_i,t)$ is defined by

$$\bar{f}(x_i,\sigma) = \int_0^\infty e^{-\sigma t} f(x_i,t)\,dt \quad \mathrm{Rl}\,\sigma > 0 \qquad [25]$$

and we also use the complex inversion formula

$$f(x_i,t) = \frac{1}{2\pi i}\int_{\alpha-i\infty}^{\alpha+i\infty} e^{\sigma t}\bar{f}(x_i,\sigma)d\sigma \qquad [26]$$

where the path of integration parallel to the imaginary axis and to the right of all the singularities of $\bar{f}$.[6] Application of the transformation to the system, Equations [15] and [16], with zero initial conditions, yields

$$\Delta\bar{\varphi} - \frac{\gamma\sigma^2}{c^2}\bar{\varphi} = \sigma\bar{\theta} \qquad [27]$$

$$\sigma\bar{\theta} - \kappa\Delta\bar{\theta} = \Omega - (\gamma-1)\Delta\bar{\varphi} \qquad [28]$$

Application of the transformation and convolution theorem to Equations [23] and [24] yields

$$\bar{\theta}(x_i,\sigma) = \int\int\int_{-\infty}^{+\infty} \bar{\Gamma}(x_i-\xi_i,\sigma)\Omega(\xi_i,\sigma)d\xi_i \qquad [29]$$

$$\bar{\varphi}(x_i,\sigma) = \int\int\int_{-\infty}^{\infty} \bar{\Phi}(x_i-\xi_i,\sigma)\Omega(\xi_i,\sigma)d\xi_i \qquad [30]$$

These last equations tell us that the Laplace transforms $\bar{\Gamma}, \bar{\Phi}$ of the fundamental solutions are themselves fundamental solutions to the system, Equations [27] and [28]. The system Equations [27] and [28] can be reduced to a single fourth-order equation for either $\bar{\theta}$ or $\bar{\varphi}$

$$L(\bar{\theta}) = -\frac{1}{\kappa}\left[\Delta - \frac{\gamma\sigma^2}{c^2}\right]\bar{\Omega} \equiv -F(x_i) \qquad [31]$$

$$L(\bar{\varphi}) = -\frac{\sigma}{\kappa}\bar{\Omega} \equiv -G(x_i) \qquad [32]$$

where L is the operator

$$L \equiv \Delta\Delta - \gamma\sigma\left(\frac{1}{\kappa} + \frac{\sigma}{c^2}\right)\Delta + \frac{\gamma\sigma^2}{\kappa c^2} \equiv (\Delta-\lambda_1)(\Delta-\lambda_2) \qquad [33]$$

with

$$\lambda_{1,2} = \frac{\gamma\sigma}{2c^2}\left[\sigma + \frac{c^2}{\kappa} \pm \sqrt{(\sigma-\alpha)(\sigma-\bar{\alpha})}\right] \qquad [34]$$

$$\alpha = \frac{c^2}{\kappa}\left[\left(\frac{2}{\gamma}-1\right) + i\frac{2}{\gamma}\sqrt{\gamma-1}\right] \qquad [35]$$

The factoring of the operator Equation [33] permits us to represent the fundamental solution S of Equation [31], defined by

$$\bar{\theta}(x_i,\sigma) = \int\int\int_{-\infty}^{\infty} S(x_i-\xi_i)F(\xi_i)d\xi_i \qquad [36]$$

as a combination of fundamental solutions of second-order equations. If $S_{1,2}$ are fundamental solutions of

$$(\Delta - \lambda_{1,2})\bar{\theta} = 0 \qquad [37]$$

then

$$S = \frac{1}{\lambda_1-\lambda_2}(S_1 - S_2) \qquad [38]$$

This result easily follows from the definition of fundamental solutions and from Equations [31] and [32]. Also from these equations $\bar{\Gamma}$ and $\bar{\Phi}$ can be simply related to S. Now, S_1 and S_2, as fundamental solutions to second-order equations are known functions in the case of one, two, and three space dimensions. Thus S, $\bar{\Gamma}$, Φ are known, and the desired fundamental solutions Γ, Φ are represented by the complex inversion Equation [26]. The details of this procedure for the one-dimensional case are given in the next section.

Fundamental Solutions in One-Dimensional Case

In the one-dimensional case the Laplacian operator is merely the second derivative with respect to x so that Equation [37] is

$$\left(\frac{d^2}{dx^2} - \lambda_{1,2}\right)\bar{\theta} = 0 \qquad [39]$$

and the fundamental solutions are well known as[7]

$$S_{1,2}(x) = \frac{1}{2\sqrt{\lambda_{1,2}}}e^{-\sqrt{\lambda_{1,2}}\,|x|} \qquad [40]$$

The fundamental solution S of Equation [31] is given by Equation [38] as

$$S(x) = \frac{1}{2(\lambda_1-\lambda_2)}\left\{\frac{1}{\sqrt{\lambda_1}}e^{-\sqrt{\lambda_1}\,|x|} - \frac{1}{\sqrt{\lambda_2}}e^{-\sqrt{\lambda_2}\,|x|}\right\} \qquad [41]$$

By comparing the definitions of fundamental solutions, Equations [29], [30], and [36], and using Equations [31] and [32] we find

$$\bar{\Gamma}(x,\sigma) = \frac{1}{2(\lambda_1-\lambda_2)}\left[\left(\frac{1}{\kappa} - \frac{\lambda_2}{\sigma}\right)\sqrt{\lambda_1}\,e^{-\sqrt{\lambda_1}\,|x|} - \left(\frac{1}{\kappa} - \frac{\lambda_1}{\sigma}\right)\sqrt{\lambda_2}\,e^{-\sqrt{\lambda_2}\,|x|}\right] \qquad [42]$$

$$\bar{\Phi}(x,\sigma) = \frac{\sigma}{2\kappa(\lambda_1-\lambda_2)}\left[\frac{1}{\sqrt{\lambda_1}}e^{-\sqrt{\lambda_1}\,|x|} - \frac{1}{\sqrt{\lambda_2}}e^{-\sqrt{\lambda_2}\,|x|}\right] \qquad [43]$$

The desired fundamental solution Γ, Φ is given by applying the complex inversion Equation [26] to Equations [42] and [43] and it is seen that we have to deal with some rather complicated integrals. The success of the method depends very much on applying conformal transformations of the complex plane to simplify these integrals. If we consider $\bar{\Gamma}$ and successively apply the transformations

$$\sigma = \frac{c^2}{\kappa}\left[\frac{2}{\gamma} - 1 + \frac{\sqrt{\gamma-1}}{\gamma}\left(Z_{1,2} - \frac{1}{Z_{1,2}}\right)\right] \qquad [44]$$

$$Z_i = \frac{1}{\sqrt{\gamma-1}}\,|z^2-1| = -\frac{1}{Z_i} \qquad [45]$$

where $Z_{1,2}$ applies to the term with $e^{-\sqrt{\lambda_{1,2}}\,|x|}$

[6] "Operational Methods in Applied Mathematics," by H. S. Carslaw and J. C. Jaeger, Oxford University Press, 1941.

[7] "Methoden der Mathematische Physik," by R. Courant and D. Hilbert, Interscience Publishers, New York, N. Y., 1937, p. 325.

we obtain the following result

$$\frac{\kappa}{c}\,\Gamma(x,t) = \frac{1}{\sqrt{\gamma}}\,\frac{1}{2\pi i}\int_{\mathfrak{C}_{1,2}} e^{\frac{z}{\gamma}\left(\frac{z^2-\gamma}{z^2-1}\right)\left(z\frac{ct}{\kappa}-\sqrt{\gamma}\,\frac{c|x|}{\kappa}\right)}\,dz \quad \ldots [46]$$

$\mathfrak{C}_1$ for $|x| > c_1 t$

$\mathfrak{C}_2$ for $|x| < c_1 t$

where the contours $\mathfrak{C}_{1,2}$ are shown in Fig. 1. $\mathfrak{C}_1$ is a contour starting at ∞ at an angle of -45 deg with the real axis ending up at ∞ at an angle of $+45$ deg, passing the real axis to the right of the essential singularity at $z = 1$. $\mathfrak{C}_2$ starts and ends in the same place but passes to the left of $z = 1$. Thus we have the important result that there is a discontinuity in the representation of the fundamental solutions across the characteristic of the systems indicated by Equation [6] $x = \pm c_1 t$. For $|x| < c_1 t$, $\mathfrak{C}_2$ can be deformed into the imaginary axis and the fundamental solution represented as a real integral

$$\frac{\kappa}{c}\,\Gamma(x,t) = \frac{1}{\pi\sqrt{\gamma}}\int_0^\infty e^{-\frac{\eta^2}{\gamma}\left(\frac{\eta^2+\gamma}{\eta^2+1}\right)\left(\frac{ct}{\kappa}\right)} \cos\left[\frac{\eta}{\sqrt{\gamma}}\left(\frac{\eta^2+\gamma}{\eta^2+1}\right)\left(\frac{c|x|}{\kappa}\right)\right] d\eta, \quad |x| < c_1 t \quad \ldots [47]$$

which can be asymptotically approximated by

$$\theta = \Gamma(x,t) = \frac{1}{\gamma}\,\frac{1}{2\sqrt{\pi\left(\frac{\kappa}{\gamma}\right)t}}\,e^{-\frac{x^2}{4\left(\frac{\kappa}{\gamma}\right)t}} + O\left(\frac{1}{ct}\right) \quad \ldots [48]$$

For $|x| > c_1 t$ the contour $\mathfrak{C}_1$ can be made to pass through $z = \sqrt{\gamma}$ and it can be shown that most of the contribution comes from the neighborhood of this point on a contour where

$$\mathrm{RI}\left(z\,\frac{z^2-\gamma}{z^2-1}\right) = 0$$

In this case the asymptotic result is

$$\theta = \Gamma(x,t) = \frac{\gamma-1}{2\gamma}\,\frac{1}{\sqrt{4\pi\left(\frac{\gamma-1}{2\gamma}\right)\kappa t}}\,e^{-\frac{(x-ct)^2}{4\left(\frac{\gamma-1}{2\gamma}\right)\kappa t}} + O\left(\frac{1}{ct}\right) \quad |x| > c_1 t \quad \ldots [49]$$

Equations [48] and [49] are good when ct is large. The pressure velocity and density are given by

$$u(x,t) = \begin{cases} -\dfrac{1}{2\gamma}\,\dfrac{x}{\sqrt{4\pi\left(\frac{\kappa}{\gamma}\right)t^3}}\,e^{-\frac{x^2}{4\left(\frac{\kappa}{\gamma}\right)t}} + O\left(\dfrac{1}{t^2}\right), & |x| < c_1 t \\ \dfrac{c}{2\gamma}\,\dfrac{\text{sign } x}{\sqrt{4\pi\left(\frac{\gamma-1}{2\gamma}\right)\kappa t}}\,e^{-\frac{(x-ct)^2}{4\left(\frac{\gamma-1}{2\gamma}\right)\kappa t}} + O\left(\dfrac{1}{t}\right), & |x| > c_1 t \end{cases} \quad \ldots [50]$$

$$s(x,t) = \begin{cases} -\dfrac{1}{\gamma}\,\dfrac{1}{\sqrt{4\pi\left(\frac{\kappa}{\gamma}\right)t}}\,e^{-\frac{x^2}{4\left(\frac{\kappa}{\gamma}\right)t}} + O\left(\dfrac{1}{ct}\right), & |x| < c_1 t \\ \dfrac{1}{2\gamma}\,\dfrac{1}{\sqrt{4\pi\left(\frac{\gamma-1}{2\gamma}\right)\kappa t}}\,e^{-\frac{(|x|-ct)^2}{4\left(\frac{\gamma-1}{2\gamma}\right)\kappa t}} + O\left(\dfrac{1}{ct}\right), & |x| > c_1 t \end{cases} \quad \ldots [51]$$

$$p(x,t) = \begin{cases} \dfrac{\kappa}{c^2}\,\dfrac{1}{2\gamma}\,\dfrac{1}{\sqrt{4\pi\left(\frac{\kappa}{\gamma}\right)t^3}}\left(1-\dfrac{x^2}{2\left(\frac{\kappa}{\gamma}\right)t}\right)e^{-\frac{x^2}{4\left(\frac{\kappa}{\gamma}\right)t}} + O\left(\dfrac{\kappa}{c^2t^2}\right), & |x| < c_1 t \\ \dfrac{1}{2}\,\dfrac{1}{\sqrt{4\pi\left(\frac{\gamma-1}{2\gamma}\right)\kappa t}}\,e^{-\frac{(|x|-ct)^2}{4\left(\frac{\gamma-1}{2\gamma}\right)\kappa t}} + O\left(\dfrac{1}{ct}\right), & |x| > c_1 t \end{cases} \quad \ldots [52]$$

Discussion of Results

The fundamental solution for the temperature given by Equations [48] and [49] illustrates the remarks made in the introduction. Of the unit amount of heat introduced originally some merely diffuses about the origin, Equation [48], as in ordinary heat conduction but some diffuses about the lines $x = \pm ct$, Equation [49], the usual lines of propagation of sound waves. It can be seen by integrating Equations [48] and [49] from $x = -\infty$ to $x = \infty$, and using

$$\frac{1}{2\sqrt{\pi t}}\int_{-\infty}^{\infty} e^{-\frac{x^2}{4t}}\,dx = 1$$

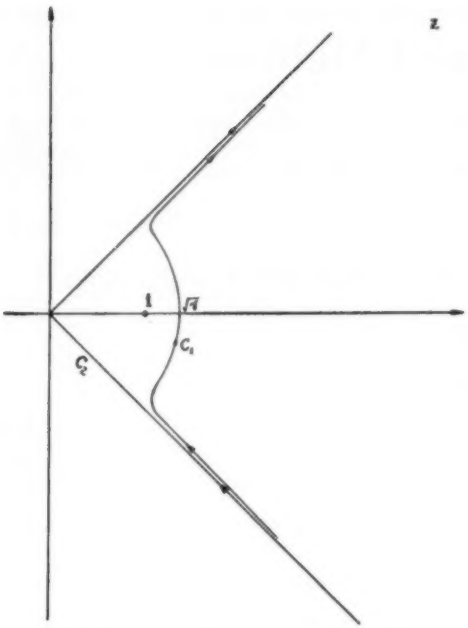

FIG. 1 CONTOURS OF INTEGRATION ON s-PLANE

that $1/\gamma$ of total heat diffuses about the origin, with the coefficient of diffusion κ/γ; $1 - 1/\gamma$ of total heat diffuses about $x = \pm ct$, with the coefficient of diffusion $[(\gamma - 1)/(2\gamma)]\kappa$. As κ becomes smaller all of these disturbances concentrate about their centers and approach δ-functions as $\kappa \to 0$. By examining the formulas for pressure, density, and velocity, Equations [50], [51], and [52], it can be seen that there are appreciable pressure and velocity changes associated with the waves near $x = \pm ct$, but much smaller changes near $x = 0$. Near $x = 0$ the changes are mainly in temperature and density. Thus we see how the introduction of heat at the origin produces both a thermal wave and a pressure wave. It should be mentioned again that the results in the foregoing are asymptotic for t large. For very small values of t pure heat conduction is the dominant process. The pressure waves take some short time to form. From our solution we also can see that heat conduction causes the attenuation of sound waves as $1/\sqrt{\kappa t}$. Thus heat conduction has an effect similar to that of viscosity which causes attenuations like $1/\sqrt{\nu t}$. Thus the picture when both heat conduction and viscosity are considered in this problem should be about the same as here.

The solution for higher dimensional waves also can be worked out, and the results are very similar with the usual geometrical distortions. These cases together with applications to various boundary-value problems will be given in a future paper. For boundary-value problems, where solutions are given by superposition of fundamental solutions, the results are similar to those given here.

ACKNOWLEDGMENT

The authors wish to thank Prof. C. R. dePrima and Mr. R. Talmadge of the California Institute of Technology, for very useful discussions and collaboration. This research was carried out under ONR Contract N6-ONR-244 to VIII.

Design Data and Methods

It is important that the data contained in technical papers be made readily available to designing engineers. In order to satisfy these needs of industry, this section of the Journal includes a concise presentation of data and information drawn chiefly from papers previously published by the Applied Mechanics Division of The American Society of Mechanical Engineers.

The Computation of Flexural–Torsional Buckling Loads

By H. F. MICHIELSEN,[1] DUIVENDRECHT, NETHERLANDS

Solution by ordinary means of the cubic equation for the torsional buckling load, first derived by Kappus, often leads to insufficiently accurate results. A method is presented which avoids the loss of accuracy involved. The procedure is straightforward and no graphical means are involved. However, one formula is to be solved by trial and error.

Introduction

THE problem of primary instability of columns, including flexural and torsional buckling, may be considered as definitely solved with the comprehensive treatise by Kappus.[2] The considerations underlying Kappus' theory, which is an improvement upon Wagner's work[3] were also basically recognized by Lundquist,[4] who, however, did not deal with the general case of unsymmetrical cross sections. Hoff[5] has given a concise strain-energy derivation of the same problem, discussing the several buckling modes that can occur, and using as basic parameters the same cross-sectional properties that appear as the most suitable ones in the present paper.

None of the authors, however, gave full attention to the numerical computation of the buckling load of an unsupported column. Some considerations were given by Kappus[2] to that topic. Formulas and a nomogram were presented, permitting an easy determination of the critical stress. However, this nomogram often leads to an unsatisfactory and in certain cases even insufficient accuracy of the result. This can be seen from the following considerations:

From the nomogram three roots $\omega = K\sigma_D$ (where σ_D is the critical stress) are always read. Only the lowest value is of practical importance. It is obvious, however, that the accuracy deteriorates rapidly when the second lowest root approaches the lowest one.

Now it is well known that a short column will buckle in a basically torsional mode, whereas in a long column the flexural form (Euler-buckling) will prevail. If the cross section is almost symmetrical (with a single axis of symmetry) the range of transition between the two modes is rather limited and in this range the lowest two roots of the equation, which give the critical stress, are nearly equal. This case, therefore, is not exceptional at all. If the cross section is exactly uniaxially symmetrical, the two roots coincide at a certain column length. However, in this case the cubic equation can be decomposed into a quadratic and a linear one, the solution of which does not offer any difficulties.

A direct analytical solution of the cubic equation, for which the nomogram gives the graphical solution, does not obviate the difficulty. After cumbersome computations, it leads in the case mentioned to the determination of an angle φ from $\cos\varphi \approx 1$, whereafter the roots contain a member with the factor $\cos(\varphi/3 \pm \pi/3)$. It is obvious that $\cos\varphi$ being the result of lengthy computations no satisfactory accuracy can be expected.

The relative accuracy of the result, applying Kappus' method, is sometimes unfavorably influenced by the circumstance that both p and q, the quantities laid off along the axes of the nomogram, are determined as algebraic sums of positive and negative numbers. This is so because the warping constant C is related to the centroid of the cross section, whereas the minimum value of C, determining materially the torsional buckling stress, may amount to a small fraction of this value only. This is the case, for instance, with short angle sections. The minimum value of C was used by Hoff[5] as a basic parameter.

In this paper a method is presented which always leads to a satisfactorily accurate result without being too cumbersome. No graphical means are involved but one formula must be solved by trial and error. In most cases no undue difficulties arise from the iteration. It is shown that a satisfactory solution can be found even in extremely unfavorable cases, by using a slide rule only.

---

[1] Royal Aircraft Factory "Fokker," Chief of Structural Research.

[2] "Drillknicken zentrisch gedrückter Stäbe mit offenem Profil im elastischen Bereich," by R. Kappus, *Luftfahrtforschung*, vol. 14, August 20, 1937, p. 444.

"Twisting Failure of Centrally Loaded Open-Section Columns in the Elastic Range," by R. Kappus, NACA Technical Memorandum No. 851, 1938.

[3] "Verdrehung und Knickung von offenen profilen," by H. Wagner, Festschrift 25 Jahre Technische Hochschule Danzig, 1929, p. 329.

"Torsion and Buckling of Open Sections," by H. Wagner, NACA Technical Memorandum No. 807, 1936.

[4] "On the Strength of Columns That Fail by Twisting," by E. E. Lundquist, *Journal of the Aeronautical Sciences*, vol. 4, April, 1937, p. 249.

[5] "A Strain Energy Derivation of the Torsional-Flexural Buckling Loads of Straight Columns of Thin-Walled Open Sections," by N. J. Hoff, *Quarterly of Applied Mathematics*, vol. 1, January, 1944, p. 341.

Discussion of this paper should be addressed to the Secretary, ASME, 29 West 39th Street, New York, N. Y., and will be accepted until July 10, 1952, for publication at a later date. Discussion received after the closing date will be returned.

Note: Statements and opinions advanced in papers are to be understood as individual expressions of their authors and not those of the Society. Manuscript received by ASME Applied Mechanics Division, February 7, 1951.

Method of Computation

The equation to be solved is given by Kappus[6]

$$\sigma_D^3 - \sigma_D^2(\sigma_x + \sigma_z + \sigma_y) + \sigma_D(\sigma_x\sigma_z + \sigma_x\sigma_y + \sigma_z\sigma_y - \rho_{xy}^2 - \rho_z^2 - \rho_y^2) - (\sigma_x\sigma_z\sigma_y + 2\rho_{xy}\rho_z\rho_y - \rho_{xy}^2\sigma_z - \rho_y^2\sigma_x - \rho_z^2\sigma_y) = 0 \quad [1]$$

where

$$\left.\begin{aligned} \sigma_x &= \frac{\pi^2}{l^2}\frac{EI_x}{F} & \sigma_y &= \frac{\pi^2}{l^2}\frac{EI_y}{F} \\ \rho_{xy} &= \frac{\pi^2}{l^2}\frac{EI_{xy}}{F} & & \\ \rho_x &= \frac{\pi^2}{l^2}\frac{ER_x}{\sqrt{FI_p}} & \rho_y &= \frac{\pi^2}{l^2}\frac{ER_y}{\sqrt{FI_p}} \\ \sigma_z &= \frac{GI_T + (\pi^2/l^2)EC}{I_p} & & \end{aligned}\right\} \quad \ldots [2]$$

and

$$\left.\begin{aligned} I_x &= \int y^2 df & I_y &= \int x^2 df \\ I_{xy} &= \int xy df & & \\ I_p &= I_x + I_y & I_T &= \int t^2 df \\ R_x &= \int y w df & R_y &= \int x w df \\ C &= \int w^2 df & & \\ \int y df &= 0 & \int x df &= 0 \\ \int w df &= 0 & & \end{aligned}\right\} \quad \ldots [3]$$

The quantities x, y, w, t, and df are defined according to Fig. 1.

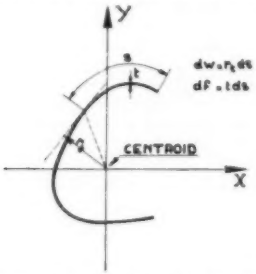

Fig. 1 Definitions in Addition to Equations [2] and [3]

First a transformation to the principal axes of the cross section has to be made. With

$$\left.\begin{aligned} \sigma_{1,2} &= \frac{\sigma_x + \sigma_y}{2} \pm \left[\left(\frac{\sigma_x - \sigma_y}{2}\right)^2 + \rho_{xy}^2\right]^{0.5} \\ \rho_{1,2}^2 &= \frac{\rho_x^2 + \rho_y^2}{2} \pm \left(\rho_{xy}\rho_z\rho_y + \frac{\rho_x^2 - \rho_y^2}{2}\frac{\sigma_x - \sigma_y}{2}\right) \times \left[\left(\frac{\sigma_x - \sigma_y}{2}\right)^2 + \rho_{xy}^2\right]^{-0.5} \end{aligned}\right\} \quad \ldots [4]$$

one finds

$$\left.\begin{aligned} \sigma_1\sigma_2 &= \sigma_x\sigma_y - \rho_{xy}^2 \\ \sigma_1 + \sigma_2 &= \sigma_x + \sigma_y \end{aligned}\right\} \quad \ldots [5]$$

$$\left.\begin{aligned} \rho_1^2 + \rho_2^2 &= \rho_x^2 + \rho_y^2 \\ \rho_1^2\sigma_2 + \rho_2^2\sigma_1 &= \frac{(\rho_x^2 + \rho_y^2)(\sigma_x + \sigma_y)}{2} - 2\rho_{xy}\rho_z\rho_y - \frac{(\rho_x^2 - \rho_y^2)(\sigma_x - \sigma_y)}{2} = \rho_x^2\sigma_y + \rho_y^2\sigma_x - 2\rho_{xz}\rho_z\rho_y \end{aligned}\right\} \quad \ldots [6]$$

[6] Reference 2, equation [84].

Substitution of Equations [5] and [6] into Equation [1] leads to

$$\sigma_D^3 - \sigma_D^2(\sigma_x + \sigma_1 + \sigma_2) + \sigma_D(\sigma_x\sigma_1 + \sigma_x\sigma_2 + \sigma_1\sigma_2 - \rho_1^2 - \rho_2^2) - (\sigma_x\sigma_1\sigma_2 - \rho_1^2\sigma_2 - \rho_2^2\sigma_1) = 0 \quad [7]$$

Now the quantity σ_x^*, defined by

$$\sigma_x^*\sigma_1\sigma_2 = \sigma_x\sigma_1\sigma_2 - \rho_1^2\sigma_2 - \rho_2^2\sigma_1 \quad [8]$$

is introduced. The physical interpretation of σ_x^* is that of a minimum value of σ_x. This will be discussed further in Appendix 1.

Equation [7] can then be written as

$$(\sigma_x^* - \sigma_D)(\sigma_1 - \sigma_D)(\sigma_2 - \sigma_D) = \sigma_D[(\sigma_1 - \sigma_D)\rho_2^2/\sigma_2 + (\sigma_2 - \sigma_D)\rho_1^2/\sigma_1] \quad [9]$$

Equation [9] is essentially identical with Equation [19] of reference 5.

Upon introduction of

$$\left.\begin{aligned} \delta_1 &= \left(\frac{\sigma_x^* + \sigma_1}{2} + \frac{\rho_1^2}{2\sigma_1}\right) + \left[\left(\frac{\sigma_x^* + \sigma_1}{2} + \frac{\rho_1^2}{2\sigma_1}\right)^2 - \sigma_x^*\sigma_1\right]^{0.5} \\ \delta_x^* &= \left(\frac{\sigma_x^* + \sigma_1}{2} + \frac{\rho_1^2}{2\sigma_1}\right) - \left[\left(\frac{\sigma_x^* + \sigma_1}{2} + \frac{\rho_1^2}{2\sigma_1}\right)^2 - \sigma_x^*\sigma_1\right]^{0.5} \end{aligned}\right\} \quad [10]$$

leading to

$$\left.\begin{aligned} \delta_x^*\delta_1 &= \sigma_x^*\sigma_1 \\ \delta_x^* + \delta_1 &= \sigma_x^* + \sigma_1 + \rho_1^2/\sigma_1 \end{aligned}\right\} \quad [11]$$

Equation [9] can be written as

$$(\delta_x^* - \sigma_D)(\delta_1 - \sigma_D)(\sigma_2 - \sigma_D) = \sigma_D(\sigma_1 - \sigma_D)\rho_2^2/\sigma_2 \quad [12]$$

In the same way, with

$$\left.\begin{aligned} \delta_2 &= \left(\frac{\delta_x^* + \sigma_2}{2} + \frac{\rho_2^2}{2\sigma_2}\right) + \left[\left(\frac{\delta_x^* + \sigma_2}{2} + \frac{\rho_2^2}{2\sigma_2}\right)^2 - \delta_x^*\sigma_2\right]^{0.5} \\ \bar{\delta}_x^* &= \left(\frac{\delta_x^* + \sigma_2}{2} + \frac{\rho_2^2}{2\sigma_2}\right) - \left[\left(\frac{\delta_x^* + \sigma_2}{2} + \frac{\rho_2^2}{2\sigma_2}\right)^2 - \delta_x^*\sigma_2\right]^{0.5} \end{aligned}\right\} \quad [13]$$

which leads to

$$\left.\begin{aligned} \bar{\delta}_x^*\delta_2 &= \delta_x^*\sigma_2 \\ \bar{\delta}_x^* + \delta_2 &= \delta_x^* + \sigma_2 + \rho_2^2/\sigma_2 \end{aligned}\right\} \quad [14]$$

Equation [12] can be transformed into

$$(\bar{\delta}_x^* - \sigma_D)(\delta_1 - \sigma_D)(\delta_2 - \sigma_D) = -\sigma_D(\delta_1 - \sigma_1)\rho_2^2/\sigma_2 \quad [15]$$

Either one of Equations [12] or [15] can be used for the final computation of σ_D. From Equation [12] follows

$$\sigma_D = \delta_x^*\left[1 + \frac{(\sigma_1 - \sigma_D)(\rho_2^2/\sigma_2)}{(\delta_1 - \sigma_D)(\sigma_2 - \sigma_D)}\right]^{-1} \quad [16]$$

and from Equation [15]

$$\sigma_D = \bar{\delta}_x^*\left[1 - \frac{(\delta_1 - \sigma_1)(\rho_2^2/\sigma_2)}{(\delta_1 - \sigma_D)(\delta_2 - \sigma_D)}\right]^{-1} \quad [17]$$

The best solution of Equation [16] or [17] can be had by trial and error. It will be shown that a rapid approach is nearly always assured.

First it can be seen from Equation [10] that

$$\bar{\sigma}_1 > \left\{ \begin{matrix} \sigma_1 \\ \sigma_s^* \end{matrix} \right\} > \bar{\sigma}_s^* \quad \ldots\ldots [18]$$

In the case of $\rho_1^2/\sigma_1 = 0$, Equation [18] becomes
$\bar{\sigma}_1 = \sigma_1$ or σ_s^*, whichever has the higher value;
$\bar{\sigma}_s^* = \sigma_s^*$ or σ_1, whichever has the lower value.

From Equation [13] follows

$$\bar{\sigma}_2 > \left\{ \begin{matrix} \sigma_2 \\ \bar{\sigma}_s^* \end{matrix} \right\} > \sigma_s^* \quad \ldots\ldots [19]$$

and from Equations [18], [19], and the first of Equations [4]

$$\left. \begin{matrix} \bar{\sigma}_1 > \sigma_1 \\ \bar{\sigma}_2 \end{matrix} \right\} > \left\{ \begin{matrix} \sigma_2 \\ \bar{\sigma}_s^* \end{matrix} \right\} > \sigma_s^* \quad \ldots\ldots [20]$$

With σ_D increasing from zero, $(\bar{\sigma}_1 - \sigma_D)$ decreases, just like $(\sigma_2 - \sigma_D)/(\sigma_1 - \sigma_D)$. The right-hand member of Equation [16], therefore, decreases from some value below $\bar{\sigma}_s^*$ to zero, which value is reached at $\sigma_D = \sigma_2$. Hence there must be a value σ_D, lower than σ_2 and $\bar{\sigma}_s^*$, satisfying Equation [16].

On the other hand, because of

$$(\bar{\sigma}_1 - \sigma_1) > 0 \quad \ldots\ldots [21]$$

the right-hand member of Equation [17] increases from some value higher than $\bar{\sigma}_s^*$ when σ_D increases from zero.

It follows

$$\left. \begin{matrix} \sigma_2 \\ \bar{\sigma}_s^* \end{matrix} \right\} > \sigma_D > \sigma_s^* \quad \ldots\ldots [22]$$

Equation [16] can be expected to give the better convergence of the iteration. It has, however, the disadvantage of containing three factors with σ_D in the right-hand member, whereas Equation [17] contains only two such factors.

An important feature of the solution just presented can be seen from Fig. 2. The curve in that figure represents the left-hand member of Equation [15]

$$y_l = (\bar{\sigma}^* - \sigma_D)(\bar{\sigma}_1 - \sigma_D)(\bar{\sigma}_2 - \sigma_D) \quad \ldots\ldots [23]$$

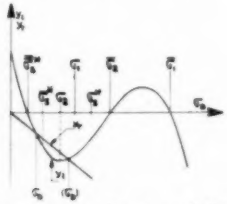

FIG. 2 REPRESENTATION OF EQUATIONS [15], [23], AND [24]

whereas the straight line through the origin corresponds to the right-hand member

$$y_r = -\sigma_D(\bar{\sigma}_1 - \sigma_1)\rho_2^2/\sigma_2 \quad \ldots\ldots [24]$$

Now the co-ordinates y_l for $\sigma_D = \bar{\sigma}_s^*$ and $\sigma_D = \sigma_2$ can be determined

$$y_{l(\sigma_D = \bar{\sigma}_s^*)} = \bar{\sigma}_s^* \bar{\sigma}_1 \bar{\sigma}_2 - (\bar{\sigma}_s^* \bar{\sigma}_1 + \bar{\sigma}_s^* \bar{\sigma}_2 + \bar{\sigma}_1 \bar{\sigma}_2)\bar{\sigma}_s^* + (\bar{\sigma}_s^* + \bar{\sigma}_1 + \bar{\sigma}_2)\bar{\sigma}_s^{*2} - \bar{\sigma}_s^{*3}$$

With the aid of Equations [14] this can be written as

$$y_{l(\sigma_D = \bar{\sigma}_s^*)} = \bar{\sigma}_s^* \bar{\sigma}_1 \sigma_2 - (\bar{\sigma}_s^* \bar{\sigma}_1 + \bar{\sigma}_s^* \sigma_2 + \bar{\sigma}_1 \sigma_2 + \bar{\sigma}_1 \rho_2^2/\sigma_2)\bar{\sigma}_s^* + (\bar{\sigma}_s^* + \bar{\sigma}_1 + \sigma_2 + \rho_2^2/\sigma_2)\bar{\sigma}_s^{*2} - \bar{\sigma}_s^{*3}$$
$$= -\bar{\sigma}_s^*(\bar{\sigma}_1 - \bar{\sigma}_s^*)\rho_2^2/\sigma_2$$

Comparison with Equation [24] leads to

$$\frac{y_{r(\sigma_D = \bar{\sigma}_s^*)}}{y_{l(\sigma_D = \bar{\sigma}_s^*)}} = \frac{\bar{\sigma}_1 - \sigma_1}{\bar{\sigma}_1 - \bar{\sigma}_s^*} \quad \ldots\ldots [25]$$

In the same way it can be shown that

$$\frac{y_{r(\sigma_D = \sigma_2)}}{y_{l(\sigma_D = \sigma_2)}} = \frac{\bar{\sigma}_1 - \sigma_1}{\bar{\sigma}_1 - \sigma_2} \quad \ldots\ldots [26]$$

and because of inequality [20] it is obvious that, no matter how near together the lower roots of σ_D may be, they are separated by $\bar{\sigma}_s^*$ and σ_2.

Furthermore, it is to be expected from Fig. 2 that the most serious difficulties in solving Equation [16] or [17] will occur, if $\sigma_1 \approx \sigma_2 \approx \bar{\sigma}_s^*$ and $\bar{\sigma}_1 \gg \sigma_1$. This implies $\sigma_s^* \gg \sigma_1$ and $\rho_1^2/\sigma_1 \to 0$. In Appendix 2 an example is worked out in which these conditions exist. Two cases, (*a*) and (*b*), with much different values of ρ_2^2/σ_2 are considered. It is seen that in this particular case Equation [17] does not lead to satisfactory results; however, Equation [16] always does.

Another example, (*c*), is given in which only $\sigma_2 \approx \bar{\sigma}_s^*$ and $\rho_2^2/\sigma_2 \to 0$, and thus $\bar{\sigma}_2$ and $\bar{\sigma}_s^*$ differ little from each other. Although in that case, too, the two lower roots of σ_D are relatively near together, no difficulty whatever arises in solving either Equation [17] or [16]. In most cases Equation [17] is to be preferred, since σ_D is usually nearer to $\bar{\sigma}_s^*$ than to $\bar{\sigma}_s^*$ and because Equation [17] contains σ_D only twice in the right-hand member. However, the use of Equation [16] would render the computations of $\bar{\sigma}_2$ and $\bar{\bar{\sigma}}_s^*$ superfluous, although, on the other hand, $\bar{\sigma}_s^*$ gives a valuable indication of the approximate value of σ_D.

It should be noted, furthermore, that in Equation [16], $\bar{\sigma}_s^*$ and σ_2 are interchangeable. Equation [16] is most suitable as long as $\bar{\sigma}_s^* < \sigma_2$. If, however, $\bar{\sigma}_s^* > \sigma_2$ the formula

$$\sigma_D = \sigma_2 \left[1 + \frac{(\sigma_1 - \sigma_D)(\rho_2^2/\sigma_2)}{(\bar{\sigma}_1 - \sigma_D)(\bar{\sigma}_s^* - \sigma_D)} \right]^{-1} \quad \ldots\ldots [27]$$

should be preferred, especially if $\bar{\sigma}_s^* \gg \sigma_2$.

SPECIAL CONDITIONS

The computations according to the Equations [10] and [13] can give rise to difficulties under certain conditions, mentioned later. The procedure recommended in such cases is demonstrated in the examples of Appendix 2.

(*a*) If one of the quantities σ_s^* and σ_1 is very much greater than the other one, $\bar{\sigma}_s^*$ in Equation [10] is found as the difference between two nearly equal numbers. The first Equation [11] then enables one to determine $\bar{\sigma}_s^*$ with a degree of accuracy equal to that of $\bar{\sigma}_1$, σ_s^*, and σ_1. The same consideration applies to Equations [13] and [14].

(*b*) If $\rho_1^2/2\sigma_1$ is very small with respect to σ_s^* and σ_1, while the latter two quantities are nearly equal, the two members under the radical sign in Equations [10] are nearly equal, too. In that case the following transformation is recommended

$$\left[\left(\frac{\sigma_s^* + \sigma_1}{2} + \frac{\rho_1^2}{2\sigma_1} \right)^2 - \sigma_s^* \sigma_1 \right]^{0.5} = \left[\left(\frac{\sigma_s^* - \sigma_1}{2} + \frac{\rho_1^2}{2\sigma_1} \right)^2 + \rho_1^2 \right]^{0.5} \quad \ldots [28]$$

The radical of Equations [13] is written analogously

$$\left[\left(\frac{\sigma_x^* + \sigma_2}{2} + \frac{\rho_2^2}{2\sigma_2}\right)^2 - \sigma_x^*\sigma_2\right]^{0.5} = \left[\left(\frac{\sigma_x^* - \sigma_2}{2} + \frac{\rho_2^2}{2\sigma_2}\right)^2 + \rho_2^2\right]^{0.5} \quad [29]$$

(c) In the last two of Equations [4] the *relative* accuracy of extremely small values of ρ_1^2 or ρ_2^2 can be unsatisfactory, the *absolute* accuracy being of the same order as that of σ_1^2 and σ_2^2. This, however, is of no importance, as long as $(\sigma_x^* - \sigma_1)$ is not of the same order as ρ_1^2/σ_1, or $(\sigma_x^* - \sigma_2)$ of the same order as ρ_2^2/σ_2, respectively.

If, however, $[(\sigma_x^* - \sigma_1)/2 + \rho_1^2/2\sigma_1] \to 0$, the right-hand member of Equation [28] approaches ρ_1. In that case ρ_1 rather than ρ_1^2 should be known with an accuracy comparable with that of $(\sigma_x^* + \sigma_1)$. The same applies to ρ_2^2 in Equation [29].

A sufficiently accurate determination of ρ_1^2 or ρ_2^2, when $(\sigma_x^* - \sigma_1)$ and $(\sigma_x^* - \sigma_2)$ are of the same order as ρ_1^2/σ_1 and ρ_2^2/σ_2, respectively, is made possible through the following transformation:

The last of Equations [4] leads to

$$\rho_1^2\rho_2^2\left[\left(\frac{\sigma x - \sigma y}{2}\right)^2 + \rho_{xy}^2\right] = \left(\frac{\rho_x^2 + \rho_y^2}{2}\right)^2\left[\left(\frac{\sigma_x - \sigma_y}{2}\right)^2 + \rho_{xy}^2\right] - \left[\rho_{xy}\rho_x\rho_y + \left(\frac{\rho_x^2 - \rho_y^2}{2}\right)\left(\frac{\sigma_x - \sigma_y}{2}\right)\right]^2$$
$$= \rho_x^2\rho_y^2\left(\frac{\sigma_x - \sigma_y}{2}\right)^2 - 2\rho_{xy}\rho_x\rho_y\left(\frac{\rho_x^2 - \rho_y^2}{2}\right)\left(\frac{\sigma_x - \sigma_y}{2}\right) + \rho_{xy}^2\left(\frac{\rho_x^2 - \rho_y^2}{2}\right)^2$$

Consequently

$$|\rho_1\rho_2| = \left(\rho_x\rho_y\frac{\sigma_x - \sigma_y}{2} - \rho_{xy}\frac{\rho_x^2 - \rho_y^2}{2}\right) \times \left[\left(\frac{\sigma_x - \sigma_y}{2}\right)^2 + \rho_{xy}^2\right]^{-0.5} \quad [30]$$

With the aid of Equation [30] ρ_1 can be calculated from ρ_2 or vice versa. Since ρ_1 and ρ_2 appear only in quadratic form in the pertinent equations, the sign is of no importance in Equation [30].

Conclusions

A sufficiently accurate computation of the primary buckling loads of unsupported open-section columns can be performed in the following way:

From the properties of the column the parameters σ_x, σ_y, ρ_{xy}, ρ_x, and ρ_y are determined, according to the Equations [2] and [3], and in agreement with Equations [47], [46], [82], [56] and [81] of reference 2. Furthermore, σ_x^* is calculated from the Equations [2], [4], and [8] or directly from

$$\sigma_x^* = \frac{GI_T + (\pi^2/l^2)EC^*}{I_p} \quad [31]$$

Equation [31] is a modification of Equation [48] of reference 2, in so far as the warping constant C with respect to the centroid is replaced by the minimum warping constant C^* with respect to the shear center.

The parameters mentioned are substituted into Equations [4], [10], and [13]. If necessary, the first Equations [11] and [14] as well as Equations [28], [29], and [30] are used to improve the accuracy.

A first approximation to the buckling stress σ_D is then found from Inequality [22]. Solution of Equations [16] or [17] by trial and error leads to the actual value of σ_D. Equation [17] usually is the most efficient one. If it fails to give a satisfactory accuracy, Equation [16] always can serve as a reliable substitute.

If $\sigma_x^* > \sigma_2$, Equation [27] should be used instead of Equation [16].

Appendix 1

Substituting Equations [2] of the present paper into equation [123] of reference 2 one finds

$$\bar{c}_o = \sigma_x + \left(\frac{x_D}{i_p}\right)^2\sigma_x - 2\left(\frac{x_D}{i_p}\right)\left(\frac{y_D}{i_p}\right)\rho_{xy} + \left(\frac{y_D}{i_p}\right)^2\sigma_y - 2\left(\frac{x_D}{i_p}\right)\rho_x + 2\left(\frac{y_D}{i_p}\right)\rho_y = 0 \quad [32]$$

Setting the derivatives with respect to x_D and y_D equal to zero, one has

$$\left.\begin{aligned} +\left(\frac{x_D}{i_p}\right)\sigma_x - \left(\frac{y_D}{i_p}\right)\rho_{xy} - \rho_x = 0 \\ -\left(\frac{x_D}{i_p}\right)\rho_{xy} + \left(\frac{y_D}{i_p}\right)\sigma_y + \rho_y = 0 \end{aligned}\right\} \quad [33]$$

The values of x_D and y_D, for which $\bar{\sigma}_x$ is a minimum, are then found as

$$\left.\begin{aligned} \frac{x_D}{i_p} = \frac{\rho_x\sigma_y - \rho_y\rho_{xy}}{\sigma_x\sigma_y - \rho_{xy}^2} \\ \frac{y_D}{i_p} = \frac{\rho_x\rho_{xy} - \rho_y\sigma_x}{\sigma_x\sigma_y - \rho_{xy}^2} \end{aligned}\right\} \quad [34]$$

Substitution of (x_D/i_p) times the first of Equations [33] and (y_D/i_p) times the second of Equations [33] into Equation [32] leads to

$$\bar{\sigma}_{x\min} = \sigma_x - \left(\frac{x_D}{i_p}\right)\rho_x + \left(\frac{y_D}{i_p}\right)\rho_y$$

From Equations [34]

$$\bar{\sigma}_{x\min}(\sigma_x\sigma_y - \rho_{xy}^2) = \sigma_x(\sigma_x\sigma_y - \rho_{xy}^2) - \sigma_y\rho_x^2 + 2\rho_{xy}\rho_x\rho_y - \sigma_x\rho_y^2 \quad [35]$$

Setting $\rho_{xy} = 0$ and replacing accordingly the subscripts x and y by 1 and 2, respectively, one can transform Equation [35] into

$$\bar{\sigma}_{x\min}\sigma_1\sigma_2 = \sigma_x\sigma_1\sigma_2 - \sigma_2\rho_1^2 - \sigma_1\rho_2^2 \quad [36]$$

Comparison with Equation [7] shows

$$\sigma_x^* = \bar{\sigma}_{x\min} \quad [37]$$

If x_p and y_p are introduced to denote the co-ordinates of the shear center with respect to the principal axes through the centroid of the cross section, Equation [34] leads to

$$\frac{x_p}{i_p} = +\frac{\rho_1}{\sigma_1} \qquad \frac{y_p}{i_p} = -\frac{\rho_2}{\sigma_2} \quad [38]$$

Through Equations [38] a physical interpretation of ρ_1 and ρ_2 is found, in addition to that of σ_x^*.

Appendix 2

Example (a):

Let it be assumed that

$$\sigma_1 = \underline{14.8} \quad \sigma_2 = \underline{14.7} \quad \sigma_x^* = \underline{637} \quad \frac{\rho_1^2}{\sigma_1} = \underline{4.7}$$

According to Equation [10]

$$\vartheta_1 = (325.9 + 2.35) + \sqrt{328.25^2 - 9430}$$
$$= 328.25 + 313.5 = 641.75$$
$$\vartheta_s^* = 328.25 - 313.5 = 14.75$$

From Equation [11]

$$\sigma_s^* = \frac{14.8 \times 637}{641.75} = 14.8 - \frac{14.8 \times 4.75}{641.75} = 14.8 - 0.11$$
$$= 14.69 = 328.25 - 313.56$$
$$\vartheta_1 = 328.25 + 313.56 = 641.8$$

With the assumption

$$\frac{\rho_2^2}{\sigma_2} = 76.2$$

Equation [13] yields

$$\vartheta_2 = (14.695 + 38.1) + \sqrt{52.795^2 - 216}$$
$$= 52.795 + 50.8 = 103.6$$
$$\sigma_s^* = 52.795 - 50.8 = 2.0$$

With the aid of Equation [14] one obtains

$$\sigma_s^* = \frac{14.7 \times 14.69}{103.6} = 2.085 = 52.795 - 50.71$$
$$\vartheta_2 = 52.795 + 50.71 = 103.5$$

Application of Equation [17] results in

$$\sigma_D = \frac{2.085}{1 - \dfrac{627.0 \times 76.2}{(641.8 - \sigma_D)(103.5 - \sigma_D)}}$$

Substitution of	leads to
$\sigma_D = 12$	$\sigma_D = \dfrac{2.085}{1 - \dfrac{47{,}800}{629.8 \times 91.5}} = \dfrac{2.085}{1 - 0.828} = 12.1$
$\sigma_D = 13$	$\sigma_D = \dfrac{2.085}{1 - \dfrac{47{,}800}{628.8 \times 90.5}} = \dfrac{2.085}{1 - 0.839} = 12.95$
$\sigma_D = 14$	$\sigma_D = \dfrac{2.085}{1 - \dfrac{47{,}800}{627.8 \times 89.5}} = \dfrac{2.085}{1 - 0.850} = 13.9$

No reliable result obtainable. Equation [16] is tried now

$$\sigma_D = \frac{14.69}{1 + \dfrac{(14.8 - \sigma_D) \times 76.2}{(641.8 - \sigma_D)(14.7 - \sigma_D)}}$$

Substitution of	leads to
$\sigma_D = 12$	$\sigma_D = \dfrac{14.69}{1 + \dfrac{2.8 \times 76.2}{629.8 \times 2.7}} = \dfrac{14.69}{1 + 0.126} = 13.05$
$\sigma_D = 13$	$\sigma_D = \dfrac{14.69}{1 + \dfrac{1.8 \times 76.2}{628.8 \times 1.7}} = \dfrac{14.69}{1 + 0.128} = 13.02$
$\sigma_D = 14$	$\sigma_D = \dfrac{14.69}{1 + \dfrac{0.8 \times 76.2}{627.8 \times 0.7}} = \dfrac{14.69}{1 + 0.139} = 12.90$

Therefore: $\sigma_D = 13.02$

Example (*b*):

Let it be assumed that

$$\sigma_1 = 14.8 \quad \sigma_2 = 14.7 \quad \sigma_s^* = 637 \quad \frac{\rho_1^2}{\sigma_1} = 4.7$$

According to example (*a*)

$$\vartheta_s^* = 14.69 \quad \vartheta_1 = 641.8$$

With the assumption

$$\frac{\rho_2^2}{\sigma_2} = 0.08$$

Equation [13] yields

$$\vartheta_2 = (14.695 + 0.04) + \sqrt{14.735^2 - 216}$$
$$= 14.735 + \backsimeq 1$$

Application of Equation [29] results in

$$\vartheta_2 = (14.695 + 0.04) + \sqrt{(-0.005 + 0.04)^2 + 0.08 \times 14.7}$$
$$= 14.735 + \sqrt{0.0012 + 1.176}$$
$$= 14.735 + 1.085 = 15.82$$
$$\bar{\sigma}_s^* = 14.735 - 1.085 = 13.65$$

From Equation [17]

$$\sigma_D = \frac{13.65}{1 - \dfrac{627.0 \times 0.08}{(641.8 - \sigma_D)(15.82 - \sigma_D)}}$$

Substitution of	leads to
$\sigma_D = 14.5$	$\sigma_D = \dfrac{13.65}{1 - \dfrac{50.15}{627.3 \times 1.32}} = \dfrac{13.65}{1 - 0.0605} = 14.53$
$\sigma_D = 14.6$	$\sigma_D = \dfrac{13.65}{1 - \dfrac{50.15}{627.2 + 1.22}} = \dfrac{13.65}{1 - 0.0655} = 14.61$
$\sigma_D = 14.7$	$\sigma_D = \dfrac{13.65}{1 - \dfrac{50.15}{627.1 \times 1.12}} = \dfrac{13.65}{1 - 0.0715} = 14.70$

No reliable result obtainable. Equation [16] is tried now

$$\frac{14.69}{1 + \dfrac{(14.8 - \sigma_D) \times 0.08}{(641.8 - \sigma_D)(14.7 - \sigma_D)}}$$

Substitution of	leads to
$\sigma_D = 14.60$	$\sigma_D = \dfrac{14.69}{1 - \dfrac{0.20 \times 0.08}{627.2 \times 0.10}} = \dfrac{14.69}{1 - 0.000255} = 14.69$
$\sigma_D = 14.68$	$\sigma_D = \dfrac{14.69}{1 - \dfrac{0.12 \times 0.08}{627.1 \times 0.02}} = \dfrac{14.69}{1 - 0.00076} = 14.68$

Therefore, $\sigma_D = 14.68$

Example (*c*):

Let it be assumed that

$$\sigma_x = 41.5 \quad \sigma_y = 18.4 \quad \sigma_s^* = 27.1$$
$$\rho_x = -26.8 \quad \rho_y = +8.6 \quad \rho_{xy} = -7.4$$

According to Equations [4]

$$\sigma_1 = 29.95 + \sqrt{11.55^2 + 54.75} = 29.95 + 13.72 = 43.67$$
$$\sigma_2 = 29.95 - 13.72 = 16.23$$
$$\rho_1^2 = \frac{718 + 74}{2} + \left[(7.4 \times 26.8 \times 8.6) + \left(\frac{718 - 74}{2} \times 11.55\right)\right] \times \frac{1}{13.72}$$
$$= 396 + (1705 + 3720) \times \frac{1}{13.72} = 396 + 395 = 791$$
$$\rho_2^2 = 396 - 395 \approx 1$$

From Equation [30]

$$|\rho_1\rho_2| = \frac{(-26.8 \times 8.6 \times 11.55) + (7.4 \times 322)}{13.72} = \frac{-2660 + 2385}{13.72} = 20$$

$$\rho_1 = \sqrt{791} = 28.15 \quad \rho_2 = 0.71 \quad \rho_2^2 = 0.50$$
$$\frac{\rho_1^2}{\sigma_1} = 18.1 \qquad \frac{\rho_2^2}{\sigma_2} = 0.031$$

According to Equation [10]

$$\delta_1 = (35.385 + 9.05) + \sqrt{44.435^2 - 1185} = 44.435 + 28.1 = 72.5$$
$$\delta_x^* = 44.435 - 28.1 = 16.3$$

With the aid of Equation [11] one obtains

$$\delta_s^* = \frac{43.67 \times 27.1}{72.5} = 16.32$$

From Equation [13] and Equation [29]

$$\delta_2 = (16.275 + 0.015) + \sqrt{(+0.045 + 0.015)^2 + 0.50} = 16.29 + 0.71 = 17.00$$
$$\bar{\sigma}_2^* = 16.29 - 0.71 = 15.58$$

Application of Equation [17] results in

$$\sigma_D = \frac{15.58}{1 - \frac{28.8 \times 0.031}{(72.5 - \sigma_D)(17.00 - \sigma_D)}}$$

Substitution of	leads to
$\sigma_D = 15.7$	$\frac{15.58}{1 - \frac{0.89}{56.8 \times 1.30}} = \frac{15.58}{1 - 0.01205} = 15.77$
$\sigma_D = 15.8$	$\frac{15.58}{1 - \frac{0.89}{56.7 \times 1.20}} = \frac{15.58}{1 - 0.01305} = 15.78$

Therefore, $\sigma_D = 15.78$

From Equation [16]

$$\sigma_D = \frac{16.32}{1 - \frac{(43.7 - \sigma_D) \times 0.031}{(72.5 - \sigma_D)(16.23 - \sigma_D)}}$$

Substitution of	leads to
$\sigma_D = 15.7$	$\sigma_D = \frac{16.32}{1 - \frac{28.0 \times 0.031}{56.8 \times 0.53}} = \frac{16.32}{1 + 0.0288} = 15.86$
$\sigma_D = 15.8$	$\sigma_D = \frac{16.32}{1 - \frac{27.9 \times 0.031}{56.7 \times 0.43}} = \frac{16.32}{1 + 0.0355} = 15.76$

Therefore, $\sigma_D = 15.78$

If Equation [27] is used

$$\sigma_D = \frac{16.23}{1 - \frac{(43.7 - \sigma_D) \times 0.031}{(72.5 - \sigma_D)(16.32 - \sigma_D)}}$$

Substitution of	leads to
$\sigma_D = 15.7$	$\sigma_D = \frac{16.23}{1 - \frac{28.0 \times 0.031}{56.8 \times 0.62}} = \frac{16.23}{1 + 0.0246} = 15.84$
$\sigma_D = 15.8$	$\sigma_D = \frac{16.23}{1 - \frac{27.9 \times 0.031}{56.7 \times 0.52}} = \frac{16.23}{1 + 0.0293} = 15.77$

Therefore, $\sigma_D = 15.78$

Torsional Vibration Modes of Tapered Bars

By H. E. FETTIS,[1] DAYTON, OHIO

The author offers a solution for the differential equation which governs the torsional vibration modes of a shaft or bar, these modes being simple harmonic functions of time.

THE torsional vibration modes of a shaft or bar which are simple harmonic functions of time are governed by the differential equation

$$\frac{d}{ds}\,GJ\,\frac{d\theta}{ds} = -\omega^2 I\theta \qquad [1]$$

where

s = spanwise co-ordinate, ft
ω = frequency, radians per sec
θ = angular displacement, radians
I = cross-sectional mass moment of inertia, in-lb sec^2
GJ = torsional rigidity, lb-ft^2

The paper is concerned with the solution of Equation [1] for cantilever bars in the case where I and GJ are proportional to the fourth power of the spanwise co-ordinate. It is seen that this last assumption holds exactly for solid linearly tapered bars of uniform, isotropic material,[2] and also may be used with a good degree of approximation even in cases where these conditions do not hold exactly (e.g., in aircraft wings with torque-box-type construction).

On the basis of the fourth-power law, Equation [1] may be replaced by the following equation

$$\frac{d}{ds}\,s^4\,\frac{d\theta}{ds} + \beta^2 s^4\theta = 0 \qquad [2]$$

where the constant β is defined by the relation

$$\beta^2 = \frac{I\omega^2}{GJ} \qquad [3]$$

I and GJ and the values of I and GJ at some convenient reference point, and s is assumed to be measured from the projected tip of the tapered bar, Fig. 1.

The "taper ratio," λ, will be defined as the ratio of the dimension at the fixed end of the bar to that at the free end. Thus the co-ordinates of the two ends are taken to be, respectively, $s = \lambda a$ and $s = a$, the length of the bar being $L = a(1 - \lambda)$. Thus Equation [2] must be solved subject to the conditions

$$\left.\begin{aligned}\theta(\lambda a) &= 0\\ \theta'(a) &= 0\end{aligned}\right\} \qquad [4]$$

corresponding to the conditions of zero amplitude at the fixed end and zero torque at the free end.

FIG. 1 CO-ORDINATE SYSTEM FOR TAPERED BAR

The general solution of Equation [2] can be shown to be

$$\theta = s^{-2}\left\{A_1\left[\frac{\sin(\beta s)}{\beta s} - \cos(\beta s)\right] - A_2\left[\sin(\beta s) + \frac{\cos(\beta s)}{\beta s}\right]\right\} \qquad [5][3]$$

where A_1 and A_2 are arbitrary constants. Also, by differentiation

$$\theta' = \beta(s^{-2})\left\{-A_1\left[\left(\frac{3}{\beta s^2} - 1\right)\sin(\beta s) - \frac{3}{\beta s}\cos(\beta s)\right] + A_2\left[\frac{3}{\beta s}\sin\beta s + \left(\frac{3}{\beta s^2} - 1\right)\cos\beta s\right]\right\} \qquad [6]$$

Inserting the end conditions, Equations [4], it is found that the resulting equations for A_1 and A_2, namely

$$\left.\begin{aligned}A_1\left[\frac{\sin(\lambda\beta a)}{\lambda\beta a} - \cos(\lambda\beta a)\right] - A_2\left[\sin(\lambda\beta a) + \frac{\cos(\lambda\beta a)}{\lambda\beta a}\right] &= 0\\ A_1\left[\left(\frac{3}{\beta a^2} - 1\right)\sin(\beta a) - \frac{3}{\beta a}\cos\beta a\right] - A_2\left[\frac{3}{\beta a}\sin\beta a + \left(\frac{3}{\beta a^2} - 1\right)\cos\beta a\right] &= 0\end{aligned}\right\} \qquad [7]$$

can only have a nontrivial solution if the quantity βL is a root of the transcendental equation

$$\frac{\operatorname{Tan}\beta L}{\beta L} = \frac{3(\lambda-1)^3 - \lambda\beta L^2}{3(\lambda-1)^3 + (\lambda-1)(3\lambda-1)\beta L^2} \qquad [8]$$

Since β is proportional to the frequency ω, according to Equation [3], Equation [8] is the "characteristic equation" which determines the natural frequencies of the bar. With each root βL of Equation [8] there is associated (except for a constant factor) a corresponding solution of Equation [5], determining the natural mode shape. The undetermined factor may be chosen so as to make the amplitude at the free end unity.

Equation [8] has been solved for the cases $\lambda = 1/2, 2/3, 8, \infty$, the first five roots being given in Table 1. The corresponding

[1] Mathematician, Flight Research Laboratory, Wright-Patterson Air Force Base.

[2] "A Treatise on the Mathematical Theory of Elasticity," by A. E. H. Love, Dover Publications, New York, N. Y., 1944, art. 216, equation 9.

Discussion of this paper should be addressed to the Secretary, ASME, 29 West 39th Street, New York, N. Y., and will be accepted until July 10, 1952, for publication at a later date. Discussion received after the closing date will be returned.

NOTE: Statements and opinions advanced in papers are to be understood as individual expressions of their authors, and not those of the Society. Manuscript received by ASME Applied Mechanics Division on April 30, 1951.

[3] This also may be expressed in terms of Bessel functions[4]

$$\theta = s^{-3/2}[A_1 J_{3/2}(\beta s) + A_2 N_{3/2}(\beta s)]$$

[4] "Tables of Functions," by E. Janke and F. Emde, Dover Publications, New York, N. Y., 1944, art. viii, sec. 7.

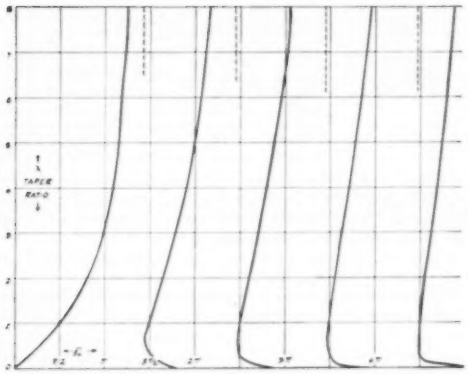

FIG. 2(a) FIRST FIVE CHARACTERISTIC NUMBERS $\overline{\beta L}_i$ FOR A LINEARLY TAPERED, UNIFORM, SOLID CANTILEVER BAR, AS FUNCTIONS OF THE TAPER RATIO, λ; $\overline{\beta L}_i = \omega \sqrt{\frac{IL^2}{GJ}}$

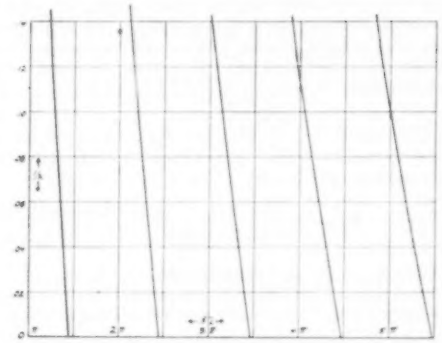

FIG. 2(b) FIRST FIVE CHARACTERISTIC NUMBERS $\overline{\beta L}_i$ FOR A LINEARLY TAPERED, UNIFORM, SOLID CANTILEVER BAR, AS FUNCTIONS OF THE INVERSE TAPER RATIO, $1/\lambda$

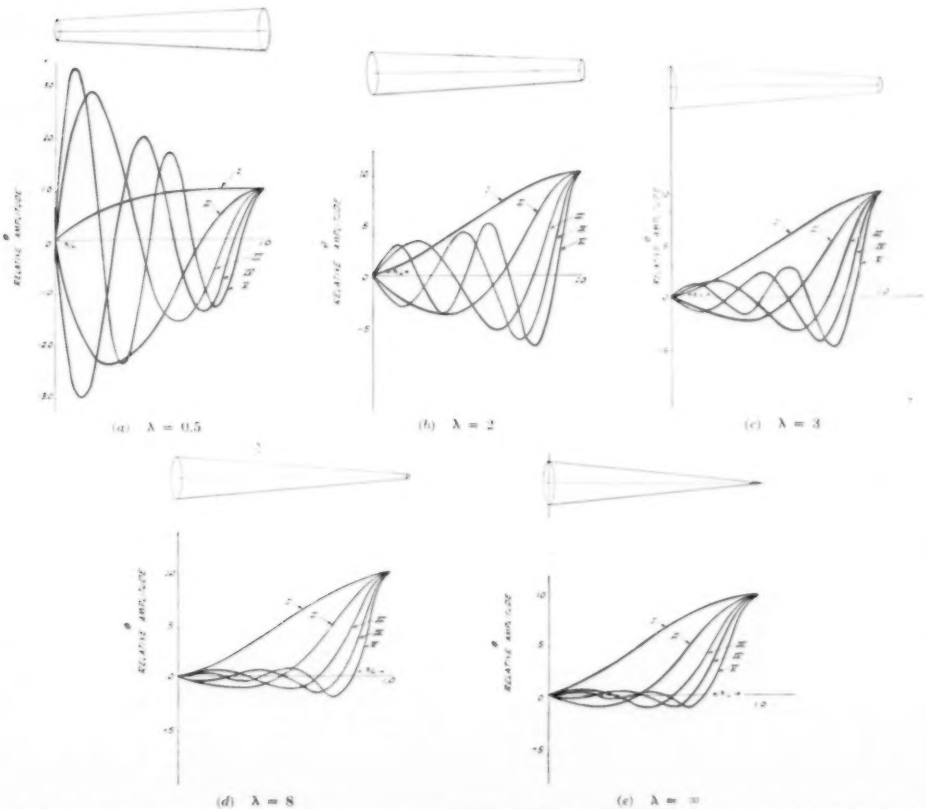

(a) $\lambda = 0.5$ (b) $\lambda = 2$ (c) $\lambda = 3$

(d) $\lambda = 8$ (e) $\lambda = \infty$

FIG. 3 SHAPES OF FIRST FIVE NORMAL MODES OF VIBRATION OF A LINEARLY TAPERED, UNIFORM, SOLID CANTILEVER BAR FOR VARIOUS TAPER RATIOS

mode shapes are shown in Fig. 3 (*a*) and (*e*). In Fig. 2 (*a*) and (*b*), the variation of the first five characteristic numbers $\beta\bar{L}_i$ with taper ratio is shown. In Fig. 3 (*a*) and (*e*), the origin has been shifted from the projected tip to the fixed end by means of the transformation

$$x = \frac{\lambda}{\lambda - 1} - \frac{s}{L} \quad \ldots\ldots\ldots\ldots\ldots\ldots [9]$$

The mode shapes in terms of the new co-ordinate x, are defined by the equation

$$\theta_i(x) = \frac{1}{[\lambda - (\lambda - 1)x]^3} \frac{\left\{(\lambda-1)^2 + \lambda\overline{\beta L_i}^2[\lambda - (\lambda-1)x]\right\} \sin \beta\bar{L}_i(x) - (\lambda-1)^2 \beta\bar{L}_i\left[x \cos \beta\bar{L}_i x\right]}{\left[(\lambda-1)^2 + \lambda\beta\bar{L}_i^2\right] \sin \beta\bar{L}_i - (\lambda-1)^2 \beta\bar{L}_i \cos \beta\bar{L}_i} \quad \ldots\ldots [10]$$

in which $\beta\bar{L}_i$ is any root of the characteristic Equation [8].

The author also has derived the characteristic equation for the case where a concentrated load is attached to either or both ends of the bar. Lack of space prohibits the inclusion of these results in the present paper.

TABLE 1 VALUES OF THE FIRST FIVE CHARACTERISTIC NUMBERS $\beta\bar{L}_i$ FOR A LINEARLY TAPERED, UNIFORM SOLID CANTILEVER BAR, FOR VARIOUS TAPER RATIOS

Taper ratio λ	$\beta\bar{L}_1$	$\beta\bar{L}_2$	$\beta\bar{L}_3$	$\beta\bar{L}_4$	$\beta\bar{L}_5$
0.5	0.82500	4.60044	7.79087	10.94966	14.10159
1	1.57080	4.71239	7.85398	10.99557	14.13717
2	2.52610	5.19280	8.16025	11.21842	14.31185
3	3.06743	5.63645	8.47964	11.46680	14.50463
8	3.93278	6.77280	9.59953	12.46435	15.38063
∞	4.49341	7.72524	10.90412	14.06619	17.22079

Analysis of Elastic Two and Three-Section Short Columns

By C. M. TYLER, JR.,[1] AND F. Z. LEE,[2] PITTSBURGH, PA.

Short columns subjected to repeated loading or in which permanent deformation is not permissible should be designed on the basis of maximum fiber stress. This stress may vary considerably in apparently identical columns owing to small inaccuracies of shape and application of load. The effects of all probable deviations of both column and load can be represented by an "equivalent eccentricity of loading" or by an "equivalent curvature of the column" (1, 2).[3] These equivalents are so chosen that calculated fiber stresses will equal the maximum probable stress encountered in the actual column. In the paper, analytical formulas in terms of equivalent eccentricity are developed for two and three-section short columns. These may be considered as extensions of the secant column formula (3) to more complicated shapes. Specific numerical examples of sectional short columns may be analyzed by a relaxation method (4). Sectional long columns have been treated by Thompson (5) and Radomski (6).

Nomenclature

The following nomenclature is used in the paper:

P	=	axial load on column
e	=	eccentricity of load
M_0	=	eccentric end moment; equals Pe
M_a, M_b	=	bending moments at a and b
δ_a	=	deflection at a, normal to axis of column
x	=	length co-ordinate of column or of a section
$M(x)$	=	bending moment
$m(x, a)$	=	bending moment at x due to a unit dummy load at a applied normal to axis of column
L	=	length of column
L_i	=	length of section of column
$E(x)$	=	modulus of elasticity
$I(x)$	=	moment of inertia
J	=	load stiffness parameter; equals $\sqrt{EI/P}$
1, 2, 3	=	subscripts referring to sections of column

Analysis of Problem

A sectional column subject to an end moment can be analyzed completely if the bending moments at the ends of the sections are known. Each section can be treated as a beam-column with different moments at each end.

The moment at the end of any section, say, M_a, will equal the moment M_0 due to eccentricity of loading plus the product of the axial load and the deflection at the end of the section

$$M_a = M_0 + P\delta_a$$

The deflection may be expressed by elastic energy theory (7) as

$$\delta_a = \int_0^L \frac{M(x)m(x, a)}{E(x)I(x)}\,dx$$

Then

$$M_a = M_0 + P\int_0^L \frac{M(x)m(x, a)}{E(x)I(x)}\,dx \quad \ldots\ldots [1]$$

The bending moment at any point along the length of a section of a column, Fig. 1, with end moments M_i and M_j is given by

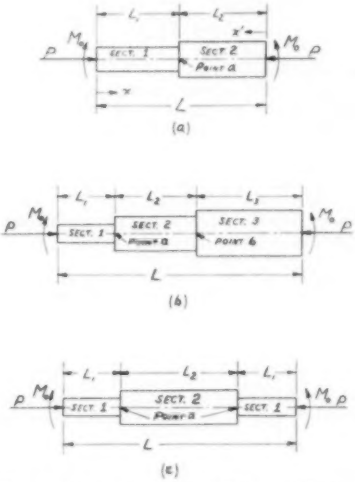

Fig. 1 Nomenclature for General Two and Three-Section Columns and for Symmetrical Three-Section Column

Equation [2] (8). In this expression L_i and J_i are the length and load stiffness of the section, and x is measured from the end of the section

$$M(x) = \frac{M_j - M_i\cos\dfrac{L_i}{J_i}}{\sin\dfrac{L_i}{J_i}}\sin\frac{x}{J_i} + M_i\cos\frac{x}{J_i} \quad \ldots\ldots [2]$$

A sectional column with end moment M_0 will determine an expression like Equation [2] for each section. These expressions can be substituted in Equation [1] and integrated to yield simultaneous equations in terms of moments at the ends of the sections. With these moments known the bending moment on any cross section can be found from Equation [2].

---

[1] Assistant Professor of Mechanical Engineering, Carnegie Institute of Technology. Jun. ASME.

[2] Graduate Student, Department of Mechanical Engineering, Carnegie Institute of Technology.

[3] Numbers in parentheses refer to the Bibliography at the end of the paper.

Discussion of this paper should be addressed to the Secretary, ASME, 29 West 39th Street, New York, N. Y., and will be accepted until July 10, 1952, for publication at a later date. Discussion received afer the closing date will be returned.

Note: Statements and opinions advanced in papers are to be understood as individual expressions of their authors, and not those of the Society. Manuscript received by ASME Applied Mechanics Division, July 5, 1951.

For the two-section column, Fig. 1(*a*), with load P and end moment M_0, Equation [1] can be written as

$$M_a = M_0 + P\int_0^{L_1} \frac{M(x)}{E_1 I_1}\frac{L_2}{L}\,x\,dx + P\int_{L_1}^{L} \frac{M(x)}{E_2 I_2}\left(L_1 - \frac{L_1 x}{L}\right)dx$$

The second integral may be put in the same form as the first by making the transformation $x' = L - x$. Then letting $J^2 = EI/P$

$$M_a = M_0 + \frac{L_2}{LJ_1^2}\int_0^{L_1} M(x)x\,dx + \frac{L_1}{LJ_2^2}\int_0^{L_2} M(x')x'dx'. \quad [3]$$

When expressions for $M(x)$ and $M(x')$ are obtained from Equation [2] and integrated in Equation [3], the ratio of M_a to M_0 is found to be

$$\frac{M_a}{M_0} = \frac{\dfrac{L_2}{L}\dfrac{L_1}{J_1}\csc\dfrac{L_1}{J_1} + \dfrac{L_2}{J_2}\csc\dfrac{L_2}{J_2}}{\dfrac{L_2}{L}\dfrac{L_1}{J_1}\cot\dfrac{L_1}{J_1} + \dfrac{L_2}{J_2}\cot\dfrac{L_2}{J_2}} \quad [4]$$

The case of the three-section column, Fig. 1(*b*) can be solved in a similar manner. Two applications of Equation [1] yield two simultaneous equations in terms of M_a, M_b, and M_0. Solution of these equations yields the ratios of M_a to M_0 and M_b to M_0.

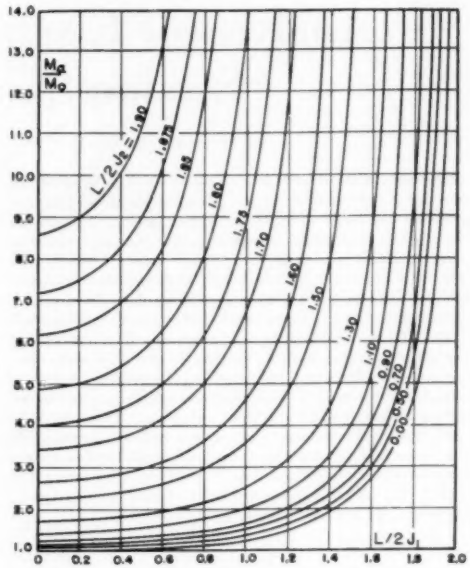

FIG. 2 CHART FOR DETERMINING BENDING MOMENT AT CENTER OF TWO-SECTION COLUMNS WITH SECTIONS OF EQUAL LENGTH

$$\frac{M_a}{M_0} = \frac{\left(\frac{L_1}{J_1}\csc\frac{L_1}{J_1}\right)\left(\frac{L_2}{J_2}\cot\frac{L_2}{J_2}\right) + \frac{L_1}{L_3}\left(\frac{L_2}{J_2}\csc\frac{L_2}{J_2}\right)\left(\frac{L_3}{J_3}\csc\frac{L_3}{J_3}\right) + \frac{L_2}{L_3}\left(\frac{L_3}{J_2}\cot\frac{L_3}{J_3}\right)\left(\frac{L_1}{J_1}\csc\frac{L_1}{J_1}\right)}{\left(\frac{L_1}{J_1}\cot\frac{L_1}{J_1}\right)\left(\frac{L_2}{J_2}\cot\frac{L_2}{J_2}\right) + \frac{L_1}{L_3}\left(\frac{L_2}{J_2}\cot\frac{L_2}{J_2}\right)\left(\frac{L_3}{J_3}\cot\frac{L_3}{J_3}\right) + \frac{L_2}{L_3}\left(\frac{L_3}{J_2}\cot\frac{L_3}{J_3}\right)\left(\frac{L_1}{J_1}\cot\frac{L_1}{J_1}\right) - \frac{L_1}{L_3}\frac{L_2^2}{J_2^2}} \quad [5]$$

$$\frac{M_b}{M_0} = \frac{\left(\frac{L_1}{J_1}\csc\frac{L_1}{J_1}\right)\left(\frac{L_2}{J_2}\cot\frac{L_2}{J_2}\right) + \frac{L_3}{L_1}\left(\frac{L_2}{J_2}\csc\frac{L_2}{J_2}\right)\left(\frac{L_1}{J_1}\csc\frac{L_1}{J_1}\right) + \frac{L_2}{L_1}\left(\frac{L_1}{J_1}\cot\frac{L_1}{J_1}\right)\left(\frac{L_3}{J_3}\csc\frac{L_3}{J_3}\right)}{\left(\frac{L_1}{J_1}\cot\frac{L_1}{J_1}\right)\left(\frac{L_2}{J_2}\cot\frac{L_2}{J_2}\right) + \frac{L_3}{L_1}\left(\frac{L_2}{J_2}\csc\frac{L_2}{J_2}\right)\left(\frac{L_1}{J_1}\cot\frac{L_1}{J_1}\right) + \frac{L_2}{L_1}\left(\frac{L_1}{J_1}\cot\frac{L_1}{J_1}\right)\left(\frac{L_3}{J_3}\cot\frac{L_3}{J_3}\right) - \frac{L_3}{L_1}\frac{L_2^2}{J_2^2}} \quad [6]$$

When a three-section column, Fig. 1(*c*), is symmetrical about its center $M_a = M_b$ and $L_1 = L_3$, Equations [5] and [6] then simplify to

$$\frac{M_a}{M_0} = \frac{\dfrac{L_1}{J_1}\csc\dfrac{L_1}{J_1}}{\left(\dfrac{L_1}{J_1}\cot\dfrac{L_1}{J_1}\right) - \left(\dfrac{L_1}{L_2}\right)\left(\dfrac{L_2}{J_2}\tan\dfrac{L_2}{2J_2}\right)} \quad [7]$$

NUMERICAL APPLICATIONS

For numerical calculations the designer must decide upon the probable equivalent eccentricity of the load on the column. The end moment M_0 is equal to the product of the load P and its eccentricity e. With M_0 known the bending moments at the ends of the sections can be calculated by Equations [4], [5], [6], and [7]. The results of these equations may be presented graphically. As an example, Fig. 2 is a chart for two-section short columns with sections of equal length. As an aid in using the equations Table 1 contains values of

$$\frac{x}{J}\cot\frac{x}{J},\ \frac{x}{J}\csc\frac{x}{J},\ \text{and}\ \ \frac{x}{J}\tan\frac{x}{2J}$$

derived from related functions (9).

The maximum bending moment of a section may not be at its ends. The location of the maximum bending moment of a section of length L_i with end moments M_0 and M_i is given by the expression (8)

$$\tan\frac{x}{J_i} = \frac{M_i}{M_0}\csc\frac{L_i}{J_i} - \cot\frac{L_i}{J_i},\quad 0 \le x \le L_i$$

and its magnitude by

$$M_{max} = M_0/\cos\frac{x}{J_i},\quad 0 \le x \le L_i$$

These equations are inconvenient to use. Their results are presented graphically in Fig. 3. For cases which are outside the range of this graph, the following approximate equation can be used

$$\frac{M_{max}}{M_0} = \frac{M_i}{M_0}\csc\frac{L_i}{J_i} + \left(0.10 - \cot\frac{L_i}{J_i}\right);\ \frac{L_i}{J_i} > 1.40 \quad [8]$$

TABLE 1 TRIGONOMETRIC FUNCTIONS FOR NUMERICAL CALCULATIONS

$\frac{x}{j}$, radians	$\frac{x}{j}\cot\frac{x}{j}$	$\frac{x}{j}\csc\frac{x}{j}$	$\frac{x}{j}\tan\frac{x}{2j}$	$\frac{x}{j}$, radians	$\frac{x}{j}\cot\frac{x}{j}$	$\frac{x}{j}\csc\frac{x}{j}$	$\frac{x}{j}\tan\frac{x}{2j}$
0.00	1.0000	1.0000	0.0000	1.60	— 0.0467	1.6008	1.6474
0.04	0.9995	1.0003	0.0008	1.64	— 0.1137	1.6439	1.7576
0.08	0.9979	1.0011	0.0032	1.68	— 0.1842	1.6900	1.8742
0.12	0.9952	1.0024	0.0072	1.72	— 0.2585	1.7394	1.9979
0.16	0.9915	1.0043	0.0128	1.76	— 0.3370	1.7921	2.1291
0.20	0.9866	1.0067	0.0201	1.80	— 0.4200	1.8484	2.2683
0.24	0.9807	1.0097	0.0289	1.84	— 0.5076	1.9088	2.4165
0.28	0.9737	1.0132	0.0395	1.88	— 0.6006	1.9736	2.5741
0.32	0.9656	1.0173	0.0516	1.92	— 0.6991	2.0433	2.7425
0.36	0.9564	1.0220	0.0655	1.96	— 0.8039	2.1186	2.9223
0.40	0.9461	1.0272	0.0811	2.00	— 0.9153	2.1997	3.1148
0.44	0.9346	1.0331	0.0984	2.04	— 1.0342	2.2873	3.3213
0.48	0.9220	1.0395	0.1175	2.08	— 1.1613	2.3821	3.5435
0.52	0.9082	1.0466	0.1383	2.12	— 1.2975	2.4857	3.7829
0.56	0.8932	1.0543	0.1610	2.16	— 1.4438	2.5981	4.0418
0.60	0.8770	1.0626	0.1856	2.20	— 1.6013	2.7211	4.3226
0.64	0.8596	1.0717	0.2121	2.24	— 1.7718	2.8563	4.6278
0.68	0.8409	1.0814	0.2405	2.28	— 1.9566	3.0048	4.9611
0.72	0.8209	1.0920	0.2710	2.32	— 2.1580	3.1686	5.3263
0.76	0.7996	1.1031	0.3036	2.36	— 2.3781	3.3501	5.7284
0.80	0.7770	1.1152	0.3382	2.40	— 2.6199	3.5537	6.1733
0.84	0.7530	1.1280	0.3752	2.44	— 2.8877	3.7807	6.6680
0.88	0.7275	1.1418	0.4142	2.48	— 3.1847	4.0371	7.2218
0.92	0.7005	1.1563	0.4559	2.52	— 3.5174	4.3271	7.8455
0.96	0.6721	1.1719	0.4998	2.56	— 3.8941	4.6599	8.5545
1.00	0.6421	1.1884	0.5463	2.60	— 4.3215	5.0429	9.3655
1.04	0.6105	1.2060	0.5955	2.64	— 4.8146	5.4915	10.3050
1.08	0.5772	1.2246	0.6474	2.68	— 5.3879	6.0176	11.4050
1.12	0.5420	1.2442	0.7022	2.72	— 6.0650	6.6467	12.7116
1.16	0.5053	1.2653	0.7600	2.76	— 6.8785	7.4113	14.2896
1.20	0.4666	1.2875	0.8209	2.80	— 7.8759	8.3584	16.2341
1.24	0.4259	1.3111	0.8852	2.84	— 9.1291	9.5611	18.6335
1.28	0.3831	1.3362	0.9530	2.88	—10.7573	11.1359	21.8932
1.32	0.3382	1.3626	1.0245	2.92	—12.9618	13.2855	26.2467
1.36	0.2910	1.3908	1.0998	2.96	—16.1212	16.3908	32.4517
1.40	0.2415	1.4207	1.1792	3.00	—21.0438	21.2585	42.3042
1.44	0.1894	1.4524	1.2630	3.04	—29.8240	29.9760	59.7956
1.48	0.1348	1.4861	1.3514	3.08	—49.9500	50.0501	99.9808
1.52	0.0773	1.5220	1.4447				
1.56	0.0168	1.5601	1.5433				

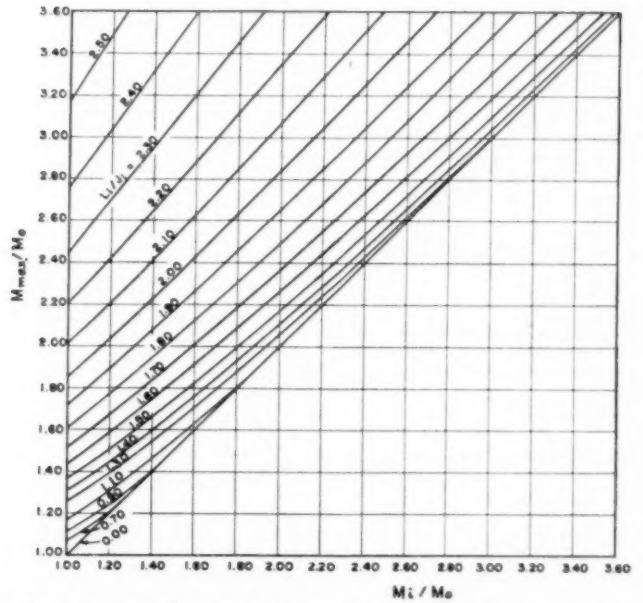

FIG. 3 CHART FOR DETERMINING MAXIMUM BENDING MOMENT ON A SECTION OF A COLUMN

The results obtained by using Equation [8] outside of the range of Fig. 3 will always be accurate within 1.3 per cent. When

$$\frac{M_i}{M_0} > 3.6 \quad \text{and} \quad \frac{L_i}{J_i} < 1.40$$

the maximum bending moment will be at or near the end of the section. Then M_{max} may be taken as equal to M_i.

BIBLIOGRAPHY

1 "Dimensionless Coefficients Applied to the Solution of Column Problems," by K. G. Merriam, *Journal of the Aeronautical Sciences*, vol. 7, September, 1950, pp. 478–480.

2 "Rational Design of Steel Columns," by D. H. Young, Trans. ASCE, vol. 101, 1936, pp. 422–500.

3 "A New Relationship for Use in the Design of Machine Columns," by W. H. Clapp, JOURNAL OF APPLIED MECHANICS, Trans. ASME, vol. 60, 1938, p. A-52.

4 "Analysis of Straight and Curved Beam-Columns," by C. M. Tyler, Jr., and J. G. Christiano, JOURNAL OF APPLIED MECHANICS, Trans. ASME, vol. 73, 1951, pp. 283–284.

5 "Critical Load of Columns of Varying Cross Section," by W. T. Thompson, JOURNAL OF APPLIED MECHANICS, Trans. ASME, vol. 72, 1950, pp. 132–134.

6 "Knickstabe mit Sprungweise Veranderlichem Tragheitsmoment," by B. Radomski, *Luftfahrtforschung*, vol. 14, August 20, 1937, pp. 438–443. Translated as "Compression Struts With Nonprogressively Variable Moment of Inertia," NACA, TM-861.

7 "Elastic Energy Theory," by J. A. Van Den Broek, second edition, John Wiley and Sons, Inc., New York, N. Y., 1942, pp. 41–46.

8 "Airplane Structures," by A. S. Niles and J. S. Newell, vol. II, third edition, John Wiley and Sons, Inc., New York, N. Y., 1943, chapter 14.

9 "Tables of Functions With Formulae and Curves," by E. Jahnke and F. Emde, fourth revised edition, Dover Publications, Inc., New York, N. Y., 1943, addenda, pp. 32–35.

Brief Notes

On the recommendations of the Executive Committee of the ASME Applied Mechanics Division, it has been decided to initiate a section devoted to brief notes on technical matters in mechanics. These notes must not be longer than 750 words (about 2½ double-spaced typewritten pages, including figures) and will be subject to the usual review procedure prior to publication. After approval such notes will be published in the next issue of the Journal. The notes should be submitted to the Secretary of the ASME Applied Mechanics Division.

Bending of Orthotropic Beams

By H. D. CONWAY,[1] ITHACA, N. Y.

PROBLEMS in orthotropic plane stress resolve themselves into the solution of the differential equation

$$\left(\frac{\partial^2}{\partial x^2} + k^2\frac{\partial^2}{\partial y^2}\right)\left(\frac{\partial^2\phi}{\partial x^2} + \frac{\partial^2\phi}{\partial y^2}\right) = 0;\ k^2 = \frac{E_y}{E_x} \quad \ldots\ldots [1]$$

subject to the boundary conditions. The stresses are given by

$$\sigma_x = \frac{\partial^2\phi}{\partial y^2},\ \sigma_y = \frac{\partial^2\phi}{\partial x^2},\ \tau_{xy} = -\frac{\partial^2\phi}{\partial x\partial y} \quad \ldots\ldots [2]$$

A number of orthotropic problems have been solved in a recent paper.[2] Use of polynomial stress functions will be made here for two practically important problems of orthotropic beams, such as those made from wood. The corresponding isotropic solutions are well known.[3]

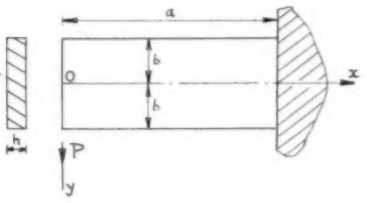

FIG. 1

The appropriate stress function for the isotropic beam in Fig. 1 is

$$\phi = \frac{P}{6I}(3b^2xy - xy^3) \quad \ldots\ldots [3]$$

Since this function satisfies Equation [1] as well as the biharmonic equation $\nabla^4\phi = 0$, the stresses

$$\sigma_x = -\frac{Pxy}{I},\ \sigma_y = 0,\ \tau_{xy} = -\frac{P}{2I}(b^2 - y^2) \quad \ldots\ldots [4]$$

are appropriate for orthotropic as well as isotropic beams.

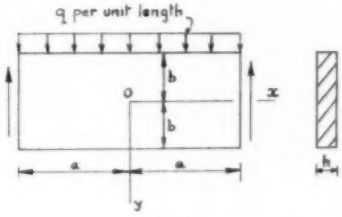

FIG. 2

For the isotropic beam shown in Fig. 2, the stress function is

$$\phi = \frac{q}{60I}[y^3(y^2 - 2b^2 + 5a^2) - 5x^2(y^3 - 3yb^2 - 2b^3)] \quad \ldots\ldots [5]$$

All terms except x^2y^3 and y^5 satisfy Equation [1], and, for the orthotropic case, we write

$$\phi = \frac{q}{60I}[y^3(Ay^2 - 2b^2 + 5a^2) - 5x^2(y^3 - 3yb^2 - 2b^3)] \quad \ldots\ldots [6]$$

From Equation [1]

$$A = \frac{k^2 + 1}{2k^2}$$

and the bending stress is

$$\sigma_x' = \frac{q}{2I}(a^2 - x^2)y + \frac{q}{2I}\left(\frac{k^2 + 1}{3k^2}y^3 - \frac{2}{5}b^2y\right) \quad \ldots\ldots [7]$$

The boundary conditions on $y = \pm b$ are satisfied. On $x = \pm a$, the force and moment are, respectively

$$\int_{-b}^{b}\sigma_x h\,dy = 0,\ \int_{-b}^{b}\sigma_x hy\,dy = -\frac{qb^2}{10}\frac{k^2 - 1}{k^2}$$

Therefore we must apply moments

$$\frac{qb^2}{10}\frac{k^2 - 1}{k^2}$$

to the ends of the beam and make use of Saint Venant's principle. This requires only the addition of a stress function of the form By^3 to Equation [6] and this produces stresses

$$\sigma_x'' = \frac{3qy}{20hb}\frac{k^2 - 1}{k^2},\ \sigma_y'' = 0,\ \tau_{xy}'' = 0$$

The final stresses for the orthotropic version in Fig. 2 are then

$$\sigma_x = \frac{q}{2I}(a^2 - x^2)y + \frac{q}{2I}\frac{k^2 + 1}{k^2}\left(\frac{y^3}{3} - \frac{b^2y}{5}\right)$$

$$\sigma_y = -\frac{q}{2I}\left(\frac{y^3}{3} - b^2y + \frac{2b^3}{3}\right)$$

$$\tau_{xy} = -\frac{qx}{2I}(b^2 - y^2) \quad \ldots\ldots [8]$$

[1] Professor of Mechanics, Cornell University. Jun. ASME.

[2] "Some Problems of Orthotropic Plane Stress," by H. D. Conway, submitted for publication in the JOURNAL OF APPLIED MECHANICS.

[3] "Theory of Elasticity," by S. Timoshenko and J. N. Goodier, McGraw-Hill Book Company, Inc., New York, N. Y., 1951, pp. 35–44.

Discussion of this paper should be addressed to the Secretary, ASME, 29 West 39th Street, New York, N. Y., and will be accepted until one month after final publication of the paper itself in the JOURNAL OF APPLIED MECHANICS.

NOTE: Statements and opinions advanced in papers are to be understood as individual expressions of their authors and not those of the Society. Manuscript received by ASME Applied Mechanics Division, February 18, 1952.

Note on Energy of Bending of Plates

By H. L. LANGHAAR,[1] URBANA, ILL.

THE differential equation for small deflections of a flat isotropic elastic plate ($\nabla^4 w = q/D$) does not contain Poisson's ratio explicitly, because the expression $2(1-\nu)(w_{xx}w_{yy} - w^2_{xy})$ which occurs in the formula for the total potential energy of the plate satisfies Euler's equation of the calculus of variations identically. This circumstance reflects the fact that the surface integral of the foregoing expression may be transformed into a line integral on the boundary by means of the Gauss-Bonnet theorem of differential geometry. Cases for which the line integral cancels from the natural boundary conditions of the plate have been discussed in the literature, but seemingly not from the most general point of view.

There is no need to limit the discussion to small deflections. Regardless of the magnitudes of the deflections, the expression for the strain energy of bending of a flat isotropic elastic plate of constant thickness is

$$U_b = \frac{1}{2} D \int\int_A \left[\frac{1}{r_1^2} + \frac{1}{r_2^2} + \frac{2\nu}{r_1 r_2} \right] dA \quad \ldots\ldots [1]$$

in which r_1 and r_2 are the principal radii of curvature of the deformed middle surface of the plate. The derivation of Equation [1] employs the assumptions that plane stress exists in any lamina that is parallel to the middle plane of the plate, and that shearing stresses on planes parallel to the middle plane of the plate are zero. Furthermore, the strains must be so small that the differential area dA may be considered to be invariant, but still the deflections may be large, if the plate is thin.

Equation [1] may be written alternatively

$$U_b = D \int\int_A [2M^2 - (1-\nu)K]\, dA \quad \ldots\ldots [2]$$

where

$$M = \frac{1}{2}\left(\frac{1}{r_1} + \frac{1}{r_2} \right), \quad K = \frac{1}{r_1}\frac{1}{r_2} \quad \ldots\ldots [3]$$

The quantities M and K are known as the "mean curvature" and the "Gaussian curvature" of the deformed middle surface of the plate.

Let the middle surface of the plate be simply connected, and let the bounding curve of the deformed middle surface be C. Let the curve C be composed of several smooth arcs that form exterior angles $\theta_1, \theta_2, \ldots\ldots$ at their vertexes; then

$$\int\int_A K\, dA = 2\pi - \Sigma\theta_i - \int_C \kappa_g\, ds \quad \ldots\ldots [4]$$

where κ_g is the geodesic curvature of the curve C on the deformed middle surface of the plate. Equation [4] is known as the "Gauss-Bonnet theorem."[2]

Since an additive constant in the strain energy is of no interest, Equations [2] and [4] yield

$$U_b = 2D \int\int_A M^2\, dA + D(1-\nu) \int_C \kappa_g\, ds \quad \ldots\ldots [5]$$

provided that the angles θ_i are constants.

The absolute value of the geodesic curvature κ_g of the curve C at the point P is the magnitude of the orthogonal projection of the curvature vector $\mathbf{K}$ of the curve C on the plane that is tangent to the deformed middle surface of the plate at the point P. The vector $\mathbf{K}$ is directed along the principal normal to the curve C. It is equal in magnitude to the curvature $1/R$ of the curve C. By definition, the geodesic curvature of a geodesic is zero. The curvature vector $\mathbf{K}$ of a geodesic is normal to the deformed middle surface, or else it is zero. Consequently, if the curve C is composed of arcs of geodesics, Equation [5] reduces to

$$U_b = 2D \int\int_A M^2\, dA \quad \ldots\ldots [6]$$

Two special cases of Equation [6] are noteworthy:

(*a*) If the plate is polygonal, and if the deflection w vanishes at the boundary, the edges remain straight. Consequently, the edges are geodesics, and Equation [6] is valid. This case has been mentioned by Nadai.[3]

(*b*) If a continuous plate or slab is supported by a gridwork of flexible beams, and if all panels have the same size and the same deformation, the deflection curves of the beams are geodesics, since they are plane curves whose principal normals are normal to the deformed plate. Consequently, Equation [6] applies for any panel. This case was pointed out to the writer by Prof. L. E. Goodman.

If the deflection is zero at the edge of the plate, C is a plane curve, and its curvature vector $\mathbf{K}$ is independent of the deformation. Then

$$\kappa_g = \frac{1/R}{\sqrt{1 + (dw/dn)^2}} \quad \ldots\ldots [7]$$

where dw/dn is the normal derivative of the deflection at the boundary of the plate.

An important case of Equation [7] arises, if the plate is clamped at its boundary. Then $dw/dn = 0$. Consequently, Equation [7] shows that the line integral of κ_g is independent of the deflection. Since an additive constant in the strain energy is irrelevant, Equation [6] is accordingly valid for any type of deformation of a simply connected plate that is clamped at its boundary. This conclusion has been derived previously by Stodola.[4]

A multiply connected plate may be reduced to a simply connected one by means of cross cuts. This device is well known in the integration theory of complex functions. If the widths of the gaps between pairs of cuts approach zero, the integrals of geodesic curvature along the cuts cancel each other. Consequently, Equation [4] remains valid for a multiply connected plate, if the curve C is interpreted to be the entire boundary of the deformed middle surface of the plate, and the inner parts of the boundary are described in the opposite sense to the outer boundary. It follows that Equation [6] is valid for a multiply connected plate with straight edges, provided that the edges remain straight and the angles between consecutive edges remain constant. Likewise, Equation [6] is valid for any multiply connected plate with clamped edges.

---

[1] Professor, Theoretical and Applied Mechanics Department, University of Illinois. Mem. ASME.

[2] "Differential Geometry," by D. Struik, Addison-Wesley Press, Inc., Cambridge, Mass., 1950, p. 155.

Discussion of this paper should be addressed to the Secretary, ASME, 29 West 39th Street, New York, N. Y., and will be accepted until one month after final publication of the paper itself in the JOURNAL OF APPLIED MECHANICS.

NOTE: Statements and opinions advanced in papers are to be understood as individual expressions of their authors and not those of the Society. Manuscript received by ASME Applied Mechanics Divison, February 6, 1952.

[3] "Elastische Platten," by A. Nadai, Julius Springer, Berlin, Germany, 1922, p. 275.

[4] "Ueber die Schwingungen von Dampfturbinen-Laufrädern," by A. Stodola, *Schweizerische Bauzeitung*, 1914, p. 251.

Discussion

Stresses in Pipe Bundles[1]

E. H. Lee.[2] The following points were not made clear to the writer in the presentation of the paper:

1 The interaction between tubes has been considered as a reaction force acting through the welds. Is it clear from the symmetry of the problem that no couple is required in addition to this point force reaction? In general, one would expect such a couple to arise, but it would be zero if there were no tendency for relative rotation between the tubes at the welds.

2 It was stated that the equivalent elastic constants in two directions at right angles were almost the same. Since there are three directions of symmetry at 120 deg to each other, it seems that this might imply complete symmetry, by analogy with the similar case of the moment of inertia of an isosceles triangle, where the three axes of symmetry determine the ellipse of gyration to be a circle. If such general symmetry applies in this case, it would provide a check on the numerical analysis.

Authors' Closure

The authors wish to thank Dr. Lee for the interesting questions raised by him.

In reply to the first question, it is quite true that the possibility of moment reactions at the contact points was not considered in the paper, and this point should be settled before the solution used in the calculation of the equivalent elastic constants can be considered to be complete. The truth of the matter is that under the action of the force reactions the angular deflection of the contact points is the same for adjacent pipes and hence there is no need for moment reactions.

To see this, consider the tube assembly, say, for tension p_x along the x-axis, as shown in Fig. 6 of the paper, or in Fig. 1 of this closure. Tube I, subject to the forces F_2, F_4, distorts from its circular shape to some other shape. Clearly there is no rotation at point A, hence no moment arises there. There is, however, slope change at point B. But the tube II deforms to precisely the same shape as tube I, since it is subjected to the same pattern of forces; hence no relative rotation occurs at the contact point B either. Thus the moment that might arise at B is zero. Note that this argument, which is also valid for the p_y-loading in Fig. 5 of the paper, is based on our fundamental assumption of slowly changing stresses in the equivalent solid, which underlies the calculation of the elastic constants E_x, E_y, μ_x, μ_y, G. We assume that the state of stress is nearly uniform so that variations in these stresses over distances of one tube diameter can be considered as insignificant.

The authors are much indebted to Dr. Lee for raising the second question, and for suggesting isotropy of the structure in the x, y-plane. This is an important attribute of structures with equilateral triangle symmetry; the calculation of E_x, E_y, etc., in the original paper was carried out by analogous but quite dissimilar procedures which did not suggest the relations $E_x = E_y$, $\mu_x = \mu_y$, $G = E_x/2(1 + \mu_x)$.

To prove these relations, consider the structure in Fig. 2 of this closure, loaded by an applied tension p in the $\alpha = \pi/3$ direction.

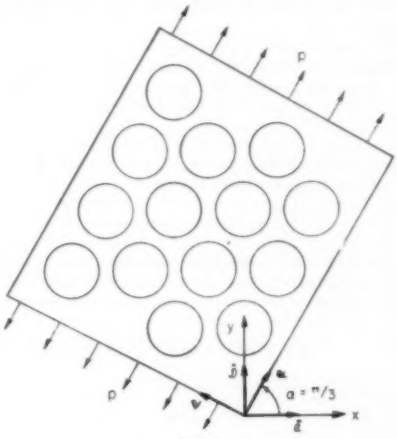

Fig. 2

In this direction the E_x, μ_x constants hold; hence, writing

$$\left.\begin{aligned} \mathbf{u} &= \mathbf{i}\cos\pi/3 + \mathbf{j}\sin\pi/3 = \mathbf{i}/2 + \mathbf{j}\sqrt{3}/4 \\ \mathbf{v} &= -\mathbf{i}\sin\pi/3 + \mathbf{j}\cos\pi/3 = -\mathbf{i}\sqrt{3}/4 + \mathbf{j}/2 \end{aligned}\right\} \quad \ldots[1]$$

the strain dyadic becomes

$$\frac{p}{E_x}\,\mathbf{uu} - \frac{\mu_x p}{E_x}\,\mathbf{vv} = \frac{p}{4E_x}\{[\mathbf{ii} + \sqrt{3}(\mathbf{ij} + \mathbf{ji}) + 3\mathbf{jj}] - \mu_x[3\mathbf{ii} - \sqrt{3}(\mathbf{ij} + \mathbf{ji}) + \mathbf{jj}]\} \quad \ldots[2]$$

There result therefore the strains

$$\left.\begin{aligned} \epsilon_x &= \frac{p}{4E_x}(1 - 3\mu_x) \\ \epsilon_y &= \frac{p}{4E_x}(3 - \mu_x) \\ \gamma_{xy} &= \frac{\sqrt{3}}{2}\frac{p}{E_x}(1 + \mu_x) \end{aligned}\right\} \quad \ldots[3]$$

[1] By H. Poritsky and G. Horvay, published in the September, 1951, issue of the Journal of Applied Mechanics, Trans. ASME, vol. 73, pp. 241–250.

[2] Associate Professor of Applied Mathematics, Brown University, Providence, R. I. Mem. ASME.

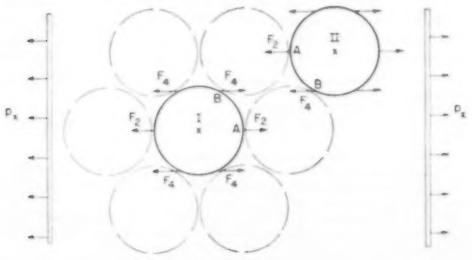

Fig. 1

On the other hand, the stress dyadic is

$$p\mathbf{uu} = p\left[\frac{1}{4}\,\mathbf{ii} + \frac{\sqrt{3}}{4}\,(\mathbf{ij} + \mathbf{ji}) + 3/4\,\mathbf{jj}\right] \ldots\ldots [4]$$

and is equivalent to the stresses

$$\sigma_x = \frac{p}{E'},\quad \sigma_y = \frac{3p}{4},\quad \tau_{xy} = \frac{\sqrt{3}}{4}\,p \ldots\ldots [5]$$

These stresses give rise to the strains

$$\left.\begin{aligned} \epsilon_x = \frac{p}{4}\left(\frac{1}{E_x} - 3\,\frac{\mu_y}{E_y}\right),\quad \epsilon_y = \frac{p}{4}\left(\frac{3}{E_y} - \frac{\mu_x}{E_x}\right) \\ \gamma_{xy} = \sqrt{3}\,p/4G \end{aligned}\right\} \ldots [6]$$

Comparison of Equations [3], [6] yields the desired relations

$$E_x = E_y,\ \mu_x = \mu_y,\ G = E_x/2(1 + \mu_x) \ldots\ldots [7]$$

From the proof it is also obvious that the particular value, $\alpha = \pi/3$, of the $\mathbf{u}$-direction in which the properties E_x, μ_x of the $\mathbf{i}$-direction repeat is inconsequential; once the existence of the second direction $\mathbf{u}$ is established, isotropy of the structure in the x, y-plane is insured.

A third question raised at the time of the presentation of the paper concerned the S_2 stress system in an isotropic cylinder for axially symmetric loading. We plan to treat this problem at greater length elsewhere, but a brief outline of it here will be of interest.

The problem is the determination of the stress system arising when a self-equilibrating system, $\sigma_z(r, z)$, of normal tractions acts on an end face, $z = 0$, of a long cylinder

$$\int_0^R \sigma_z r dr = 0 \quad \text{for} \quad z = 0 \ldots\ldots [8]$$

The treatment of this problem differs slightly from the one outlined at the end of the paper for a nonisotropic body. For the isotropic cylinder one assumes a Love stress function φ in the form

$$\varphi = e^{-\beta z}[\beta r J_1(\beta r) + \kappa J_0(\beta r)] \ldots\ldots [9]$$

This satisfies the biharmonic equation

$$\nabla^4\varphi = 0 \ldots\ldots [10]$$

and leads to stresses σ_r, σ_θ, σ_z, τ_{rz} that can be expressed as third derivatives of φ.[3] The conditions

$$\sigma_r(R) = 0,\ \tau_{rz}(R) = 0 \ldots\ldots [11]$$

at the lateral surface of the cylinder impose the conditions on κ and $\mu\,(\mu \equiv \beta R)$

$$\left.\begin{aligned} (1 - 2\mu)J_0(\mu) - \mu J_1(\mu) + \kappa[-J_1(\mu) + J_1(\mu)/\mu] = 0 \\ -\mu J_0(\mu) - 2(1 - \mu)J_1(\mu) + \kappa J_1(\mu) = 0 \end{aligned}\right\} \ldots [12]$$

These equations are consistent when μ is a root μ_j, of the eigenvalue equation

$$J_0^2(\mu)/J_1^2(\mu) = -1 + 2(1 - \mu)/\mu^2 \ldots\ldots [13]$$

We denote the values of κ corresponding to μ_j by κ_j. The roots μ_j are all complex. (The smallest root is $\mu = 3.05\exp(0.15\,\pi\,i)$.) If μ_j is a root, then so are $-\mu_j$, $\bar{\mu}_j$, and $-\bar{\mu}_j$. Hence one can write, denoting $\rho = r/R$

$$\varphi = \sum_j (A_j\Re + B_j\Im)\,[\mu_j\rho J_1(\mu_j\rho) + \kappa_j J_0(\mu_j\rho)] \ldots [14]$$

where $\Re$, $\Im$ denote real and imaginary parts. The coefficients A_j, B_j are determined from the two conditions that apply at the end face, $z = 0$

$$\tau_{rz} = 0,\ \sigma_z = \text{prescribed function of } r \ldots\ldots [15]$$

If the cylinder is rather short then, in place of Equation [9], solutions of the form

$$\varphi = (\cosh \beta z, \sinh \beta z)\,[\beta r J_1(\beta r) + \kappa J_0(\beta r)] \ldots [16]$$

must be used.

[3] As shown in "Theory of Elasticity," by A. E. H. Love, Cambridge University Press, London, England, fourth edition, 1927, p. 276; or "Theory of Elasticity," by S. Timoshenko and J. N. Goodier, McGraw-Hill Book Company, Inc., New York, N. Y., 1951, p. 343.

On the Extrusion of a Very Viscous Liquid[1]

P. G. Lund.[2] The author's attention is invited to a paper by A. Thom.[3] The type of problem treated in this paper is one of three-dimensional flow with axial symmetry, and the specific problem that of sudden enlargement of a circular pipe by a diametral factor of 4. The results are used to give the end correction in capillary-tube measurements of viscosity.

Plastic-Wave Propagation Effects in High-Speed Testing[1]

D. S. Wood.[2] The authors have presented a most useful method for determining whether plastic-wave propagation effects may be neglected or not in any given experimental arrangement for longitudinal impact testing. In the case of impact experiments in which plastic-wave propagation in the specimen must be considered, it might be well to emphasize that it may be necessary to consider the waves in the hammer and anvil of the testing arrangement as well as those in the specimen. Unfortunately, an infinitely rigid material which could be used to eliminate this complication does not exist.

The authors' example of how plastic strain-wave effects in the specimen can lead to an apparent but false increase in energy absorption per unit volume illustrates an error which has been made by several investigators, including the writer, in their interpretation of the results of impact tests.

Authors' Closure

We wish to thank Dr. Wood for his useful comments. In certain cases it will certainly be necessary to consider elastic waves in the anvil and testing arrangement. In the case of longitudinal waves, this can be readily handled by the method of characteristics, but the analysis will be more complicated. For the test arrangement discussed in the paper, strains, large compared with elastic strains, were under consideration so that relative displacements of the order 0.1 in. occurred in the specimen. Since the give of the anvil is expected to have been of the order of 0.001 in., its motion was negligible in comparison with that of

[1] By Herschel Weil, published in the September, 1951, issue of the Journal of Applied Mechanics, Trans. ASME, vol. 73, pp. 267–272.

[2] Engineering Laboratory, Oxford, England.

[3] "Arithmetical Solution of Problems in Steady Viscous Flow," by A. Thom, published as Aeronautical Research Committee Reports and Memoranda, No. 1475, May, 1932.

[1] By E. H. Lee and H. Wolf, published in the December, 1951, issue of the Journal of Applied Mechanics, Trans. ASME, vol. 35, pp. 379-386.

[2] Assistant Professor of Mechanical Engineering, California Institute of Technology, Pasadena, Calif. Jun. ASME.

other parts of the system, and so it is permissible to consider the anvil to have been rigid and at rest. This assumption is compatible with that of a plastic-rigid material which is used to approximate the actual elastic-plastic body. For a satisfactory analysis at small strain magnitudes it would be necessary to remove these assumptions and accept the added complexity. This was, in fact, done in one case for the elastic component of strain, which was found to have a negligible influence under the circumstance treated of total strain large compared with elastic strain.

On the Inextensional Theory of Deformation of a Right Circular Cylindrical Shell[1]

N. J. Hoff.[2] For loads symmetric to the plane which is perpendicular to the axis of the cylinder and divides the cylinder in two equal halves, the inextensional shell theory discussed in the paper reduces essentially to a ring theory. Timoshenko's[3] formula becomes the well-known expression for the shortening of the diameter of a circular ring subjected to equal and opposite radial loads applied at the end points of the same diameter if $2DL$ is replaced by EI. As $2L$ is the length of the shell and $D = Eh^3/12(1 - \nu^2)$, the difference between the two formulas is only the factor $(1 - \nu^2)$, that is, about 9 per cent. For very short cylinders, therefore, the shortening of the diameter of the shell calculated from the shell theory may be about 9 per cent too small in consequence of the assumption that the anticlastic curvature is suppressed.

For very long cylinders, however, the inextensional theory must be incorrect, as can be seen from the following argument: If Δ is the shortening of the diameter of a cylinder whose length to diameter ratio is 50, the shortening of a cylinder twice as long and having the same diameter is $\Delta/2$ from the inextensional shell theory. On the other hand, any material added beyond a distance of 25 times the diameter cannot change the state of deformations in view of Saint Venant's theorem. The formula mentioned yields a shortening of the diameter which decreases to zero as the length of the cylinder increases indefinitely while in reality the diameter must shorten a finite amount even when the cylinder is infinitely long. This is borne out by Yuan's[4] investigation.

This argument naturally holds only for concentrated loads, and the inextensional theory gives good results when the cylinder is loaded uniformly along generators.

F. K. G. Odqvist.[5] The writer does not agree with author's introductory statement as to the application of the general theory of bending of cylindrical shells, if this is intended to include the type of loading covered by Figs. 1 to 3 of the paper. The author himself quotes Yuan who treats Fig. 1 from the point of view of the general theory for a pipe of infinite length. For pipes of finite length and closed ends, corresponding and even more general problems have been treated by the writer in a series of publications:

[1] Covering the case of Fig. 1, as well as the case of a simply supported cylindrical tube with a single concentrated load (theory and experiment) and general symmetric load along a generatrix.[6]

[2] Giving formulas for more general load distribution along generatrix of the cylinder.[7]

[3] Giving a table for the numerical values of the transcendental functions concerned.[8]

Author's Closure

The foregoing comments by Professor Hoff will lead to a better understanding of the interrelationship between the physical phenomenon involved in the system which is under consideration and the mathematics whereby we choose to analyze this physical phenomenon. It is indeed fortunate that the discussion of the printed papers offers an opportunity for this interrelationship to be pointed out since the original paper, whose object was solely to report on the result of some experimental investigations, did not admit the inclusion of such a discussion.

The additional bibliography supplied by Professor Odqvist is welcome. It might be well to re-emphasize, however, that the papers cited deal with cylinders with closed ends rather than those, namely, cylinders with open ends, which constituted the topic of the original paper.

A New Method of Calculation of Repeat Factors for Turbines and Compressors[1]

D. J. Bloomberg.[2] In steam-turbine design practice the reheat factor represents an important item in the flow-path and performance calculations. With pressure ratios of 1000 or more this reheat factor can account for 20 or more per cent of the adiabatic available energy. Each design group has its own way of deriving these reheat values—mostly by taking step-by-step energy values from a "state line" drawn on the entropy chart.

In actual turbine-flow paths, the first stage derives no benefit at all from reheat. The remaining stages will have varying amounts of expansion and efficiencies. For precise calculations the step-by-step method is required.

In turbines utilizing air or other gases, there usually are few stages. Also, the over-all pressure ratios are comparatively small. In these cases the reheat factor is usually neglected because its relative magnitude is inconsequential. Any gain in energy resulting from reheat is usually offset by radiation and other heat losses.

The proposed method of calculation (which of necessity is limited to the situation in which we have an infinite number of stages operating at constant efficiency) will be useful mainly in preparing comparison graphs involving different gases.

A. J. Stepanoff.[3] While the use of reheat factor is rather general among the steam-turbine designers and further refine-

[1] By R. M. Hermes, published in the December, 1951, issue of the Journal of Applied Mechanics, Trans. ASME, vol. 73, pp. 341–344.

[2] Head of Department of Aeronautical Engineering and Applied Mechanics, Polytechnic Institute of Brooklyn, Brooklyn, N. Y. Mem. ASME.

[3] "Theory of Plates and Shells," by S. Timoshenko, McGraw-Hill Book Company, New York, N. Y., 1940, p. 432.

[4] "Thin Cylindrical Shells Subjected to Concentrated Loads," by S. W. Yuan, *Quarterly of Applied Mathematics*, vol. 4, 1946, p. 13.

[5] Professor vid Kungl. Tekniska Högskolan, Stockholm, Sweden.

[6] "The Load Carrying Action of Thin Cylindrical Shells" (written in Swedish with summary in English), The Royal Swedish Academy of Engineering Sciences, Proceedings No. 164, 1942, pp. 53.

[7] "Action of Forces and Moments Symmetrically Distributed Along a Generatrix of a Thin Cylindrical Shell," Journal of Applied Mechanics, Trans. ASME, vol. 68, 1946, p. A-106.

[8] "Hållfasthetslära" (Strength of Materials, written in Swedish), *Natur o. Kultur Editors*, Stockholm, Sweden, 1948, pp. 792–795.

[1] By Joseph Kaye and K. R. Wadleigh, published in the December, 1951, issue of The Journal of Applied Mechanics, Trans. ASME, vol. 73, pp. 387–392.

[2] Engineer, Aircraft Gas Turbine Engineering Division, General Electric Company, Schenectady, N.Y. Mem. ASME.

[3] Engineer, Cameron Engineering Department, Ingersoll-Rand Company, Phillipsburg, N. J. Mem. ASME.

ments are introduced in the method of calculation of the reheat factor, very well exemplified by the present paper, there is a definite trend in thinking, putting a somewhat different aspect upon the physical meaning and use of the reheat factor.

In the field of turbocompressors, need for a reheat factor never has existed for reasons that follow. It should be realized that efficiency of a turbomachine (turbine or compressor) is a fixed definite quantity depending entirely upon the degree of hydrodynamic and mechanical perfection. Like that for any machinery it is equal to

$$\text{Efficiency} = \text{output/input}$$

The output of a turbine can be measured easily but the input cannot be ascertained directly. This led to the introduction of "adiabatic" efficiency based on the isentropic enthalpy drop for the input. However, the true input of the available energy is lower than the enthalpy drop; hence the true output/input efficiency is higher than the "adiabatic" conventional efficiency, the difference increasing with the expansion ratio. Therefore a "correction factor" became necessary to connect the actual output with the isentropic input and known adiabatic stage efficiency.

It has been shown that the true input to a turbine is represented by the change of available energy across the turbine, or what became known as change in "availability." The latter is Keenan's term for a special case of Gibbs "zeta" function, widely used in thermodynamics of chemical processes under different names. Efficiency of a multistage turbine based on availability is a true output/input efficiency, called by Keenan "effectiveness" and remains constant for the same individual stage efficiency, thus requiring no reheat-factor correction.

Statements that efficiency of a multistage turbine improves due to "recovery" of heat resulting from hydraulic losses is most misleading and has all the marks of infringement on the second law of thermodynamics.

With turbocompressors the input can be measured directly but the output (foot-pounds per pound, or head in feet) is calculated from the observed pressure and temperature rise by using theoretical adiabatic formulas, for uncooled compressors. The adiabatic conventional efficiency is lower than the true output/input efficiency, because the true output (head in feet corresponding to a given pressure) is higher as a result of temperature rise caused by hydraulic losses. The true output/input efficiency, sometimes referred to as "internal hydraulic" is closely approached by using "polytropic" formulas for the output calculation. The polytropic exponent n for gases obeying the state law $pv = RT$ is easily calculated from the observed pressures and temperatures. For new machines the polytropic exponent is determined from an estimated polytropic efficiency using known relationships from thermodynamics. The polytropic efficiency of a multistage compressor (centrifugal) is lower than that of the individual stages but for hydraulic rather than thermodynamic reasons. The multiplier for the adiabatic efficiency to obtain the true output/input (polytropic) efficiency is greater than unity and not less than unity as the "reheat factor reasoning in reverse" would indicate. This is easily calculated with available formulas in terms of polytropic efficiency and the known gas properties.

Polytropic efficiency as a best approach to the output/input efficiency applies with equal accuracy to gas turbines; thus in this field use of reheat factor is hardly justified.

It is not expected that new trends in theoretical thermodynamics will change the design methods now in use for steam turbines, but it is important to bring the theoretical reasoning behind them up to date.

Authors' Closure

Mr. Bloomberg's comments are appreciated by the authors. It should be noted that the paper was intended to review the laborious step-by-step methods of computation of reheat factors for steam, as noted by Mr. Bloomberg. It was also intended to present a simple method of computation of reheat factors for all gases for which the equation of state, $pv = RT$, is valid, without the additional requirement of constant specific heat.

Mr. Bloomberg indicates that the proposed method of calculation is limited to the case of an infinite number of stages in the turbine. In the paper we have shown, however, how to handle the case of a finite number of stages in the turbine. In fact, the proposed method has demonstrated the customary rule-of-thumb used as an approximation by the turbine designer, namely, that the ratio of the reheat gain for a finite number of stages to the reheat gain for an infinite number of stages is approximately equal to one minus the reciprocal of the number of stages, or

$$\frac{\rho_{in.\ i-a}}{\rho_{i\infty.\ i-a}} \simeq 1 - \frac{1}{n}$$

Although we agree with Mr. Bloomberg's opinion that the design of present-day gas turbines may not justify the refinement of the reheat factor, it is probable that future gas-turbine designs may find it highly useful.

Dr. Stepanoff's remarks on reheat factors applied to turbocompressors are interesting. It is evident that the utility of reheat factors for design of turbocompressors depends on the particular definition of "efficiency" which is selected. The authors agree with Dr. Stepanoff that the phrases "gain in energy due to reheat" and "recovery of heat due to hydraulic losses" are completely misleading and should never be used. Here again we feel that terms should be carefully defined to avoid the pitfalls of ambiguous reasoning.

The Safety Factor of an Elastic-Plastic Body in Plane Strain[1]

F. S. Shaw.[2] To the structural engineer one of the classes of problems of considerable interest related to the behavior of metal structures is the so-called elastoplastic stress distribution. At present, however, to solve such problems is generally impossible. Accordingly, the authors have provided the next best piece of information, namely, bounds on the "failing load."

The authors' work is a further extension of information in the field of limit design which is now receiving practical application in structural work. In this instance, however, it is necessary to keep in mind the severe restrictions imposed by the initial assumptions concerning the idealized material discussed: First (and this point is now well know) the assumption of "ideal plasticity" behavior is, at best, a poor approximation to the behavior of most structural metals in use. Then too, and of considerable importance, is the fact that for a load a little smaller in magnitude than the ultimate load that can be carried by the component, no information other than a ratio is available showing how close to failure the component may be. Thus imperfections and variations in material properties, and so on, cannot readily be taken into account. For design purposes, then, the theory should be used with considerable care, and supplemented by experimental information.

---

[1] By D. C. Drucker, H. J. Greenberg, and W. Prager, published in the December, 1951, issue of the Journal of Applied Mechanics, Trans. ASME, vol. 73, pp. 371–378.

[2] Department of Aeronautical Engineering and Applied Mechanics, Polytechnic Institute of Brooklyn, Brooklyn, N. Y.

Authors' Closure

As Professor Shaw explains, idealizations always impose restrictions on the practical use of theoretical results. However, the engineering limitations of a perfectly plastic solution are no more severe than those of a perfectly elastic solution and are often less. In particular, any imperfections in the material in the sense of local regions of low-yield strength can be handled relatively easily because the theorems of the paper still apply.[3] Also, initial stresses, which may completely nullify an elastic solution, have no influence on the plastic solution. The major difficulty in limit analysis involves the question of whether or not the ductility of the material is sufficient for the solution to be valid. Much experimental work is needed on this problem but the answer will certainly be as clear as is the significance of elastic solutions in fatigue problems.

A Statistical Distribution Function of Wide Applicability[1]

T. C. Tsu.[2] The author should be congratulated for having devised a distribution function of truly wide applicability, as evidenced by the seven examples presented in his paper.

Since the writer is currently concerned with the problems of particle-size distribution in aerosols, he is interested in the possible utilization of the author's method to reduce the necessary amount of experimental work. In this connection he would like to ask the following questions.

1 In applying the author's distribution function it is necessary to determine the parameters x_u, x_0, and m. If the distribution function is a true representation of the observed data, then any three sets of the values of P and x would be sufficient to evaluate these three parameters. In the author's examples he did not specify how his parameters were obtained. Would he care to discuss this point briefly?

2 When the function is applied to an unknown distribution, how many observed data are necessary to yield the parameters reliably? Considerable practical value would be added to the author's function if its application could result in a saving of experimental work.

3 The relations shown in Figs. 1, 2, and 3 in the paper, appear to represent the equation

$$P = 1 - e^{-\left(\frac{x - x_u}{x_0}\right)^m}$$

rather than

$$P = 1 - e^{-\frac{(x - x_u)^m}{x_0}}$$

Could that be a misprint? The values for $\log (x - x_u)$ in Fig. 2 do not correspond to the given values of x and x_u in the second example (size distribution of fly ash), the discrepancy being appreciable when x is small. Could there be some numerical errors? If so, would the author kindly show a corrected figure?

R. A. Mugele.[3] The author's treatment is definitely a contribution to the literature on distribution functions. The range of fields treated in his examples is also impressive.

However, the reason for introducing the minimum value x_u, and ignoring the maximum x_m is not entirely clear. Probably it relates to the original applications, which may have been the Cystoidea or the yield strengths and fatigue-life data of steels.

Now, for such a case as Fig. 2 of the paper, one would expect the maximum particle to be more tangible, and also more significant practically, than the minimum.

Incorporation of both a maximum and a minimum value of x will bring Equation [5] into the form

$$F(x) = 1 - e^{-k\left(\frac{x - x_u}{x_m - x}\right)^m}$$

which will again reduce to Equation [5] as x_m becomes infinite, and to the Rosin-Rammler type of equation[4] as x_u vanishes.

Of course one may start with any distribution function where the argument has infinite range, and convert it to one where the range is finite. This has been illustrated in the case of the log-normal distribution by Van Uven[5] and more recently by Mugele and Evans.[6] The latter reference also gives a critical review of the Rosin-Rammler and other distribution functions.

A word of warning also should be added in regard to the examples in the paper: They contain some arithmetical and dimensional errors. However, when these are corrected, the examples illustrate excellently the general statements of the text.

F. A. McClintock.[7] The distribution function suggested by the author is attractive because of its simplicity, the ease with which it can be applied to studying the size effect, and its implication of a lower limit to a distribution. In order to apply the distribution impartially, however, some systematic means of fitting it to experimental data should be used. For a simple distribution the following procedure appears useful.

The parameters, x_0, x_u, and m can be chosen so that the first three moments of the distribution function coincide with those of the data. The nth moment of the theoretical distribution is first calculated from the cumulative distribution

$$F = 1 - \exp\left[-\left(\frac{x - x_u}{x_0}\right)^m\right] \quad \ldots\ldots\ldots\ldots [1]$$

Differentiation gives the frequency distribution

$$f = \frac{dF}{dx} = \frac{m}{x_0}\left(\frac{x - x_u}{x_0}\right)^{m-1} \exp\left[-\left(\frac{x - x_u}{x_0}\right)^m\right] \quad \ldots [2]$$

The nth moment about x_u is

$$\mu_n' = \int_{x_u}^{\infty} (x - x_u)^n f\, dx = \int_{x_u}^{\infty} (x - x_u)^n \frac{m}{x_0}\left(\frac{x - x_u}{x_0}\right)^{m-1} \exp\left[-\left(\frac{x - x_u}{x_0}\right)^m\right] dx \quad \ldots\ldots [3]$$

On changing the variable of integration to

$$\left(\frac{x - x_u}{x_0}\right)^m \equiv \eta$$

---

[3] "Extended Limit Design Criteria for Continuous Media," by D. C. Drucker, W. Prager, and H. J. Greenberg, *Quarterly of Applied Mathematics*, vol. 9, no. 4, January, 1952, pp. 381–389.

[1] By Waloddi Weibull, published in the September, 1951, issue of the Journal of Applied Mechanics, Trans. ASME, vol. 73, pp. 293–297.

[2] Associate Professor of Engineering Research, The Pennsylvania State College, State College, Pa. Mem. ASME.

[3] Oakland, Calif.

[4] "Feinheit und Struktur des Kohlenstaubs," by P. Rosin and E. Rammler, *Zeitschrift des Vereines deutscher Ingenieure*, vol. 71, 1927, pp. 1–7.

[5] "Skew Frequency Curves," by M. J. Van Uven, Proc. Kon. Akad. v. Wetens, vol. 19, 1917, p. 670.

[6] "Droplet Size Distribution in Sprays," by R. A. Mugele and H. D. Evans, *Industrial and Engineering Chemistry*, vol. 43, 1951, pp. 1317–1324.

[7] Assistant Professor of Mechanical Engineering, Massachusetts Institute of Technology, Cambridge, Mass. Jun. ASME.

this becomes

$$\mu_n' = x_o^n \int_0^\infty \eta^{n/m} \exp(-\eta) d\eta \quad [4]$$

This integral can be expressed in terms of the Gamma function

$$\mu_n' = x_o^n \Gamma(1 + n/m) \quad [5]$$

The second and third moments about the mean are

$$\mu_2 = x_o^2[\Gamma(1 + 2/m) - \Gamma^2(1 + 1/m)]$$

and

$$\mu_3 = x_o^3[\Gamma(1 + 3/m) - 3\Gamma(1 + 2/m)\Gamma(1 + 1/m) + 2\Gamma^3(1 + 1/m)] \quad [6]$$

From these a measure of the skewness can be obtained

$$\alpha_3 \equiv \mu_3/\mu_2^{3/2} \quad [7]$$

Since α_3 is a function of m only, the value of m can be chosen so that the values of α_3 for the theoretical distribution and the experimental data coincide. Then since the second moment about the mean, that is, the square of the standard deviation, of the experimental data is known, the relation

$$\mu_1/x_o^2 = \Gamma(1 + 2/m) - \Gamma^2(1 + 1/m) \quad [8]$$

can be solved for x_o. Finally, the relation

$$\mu_1'/x_o = (\bar{x} - x_u)/x_o = \Gamma(1 + 1/m) \quad [9]$$

can be solved for x_u, since the mean of the experimental data is known. Plots of the quantities α_3, μ_2/x_o^2, and μ_1'/x_o are given in Figs. 1 and 2 of this discussion.

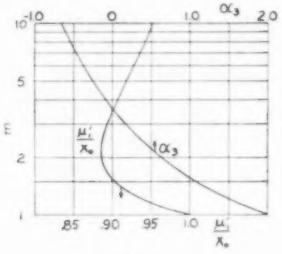

FIG. 1

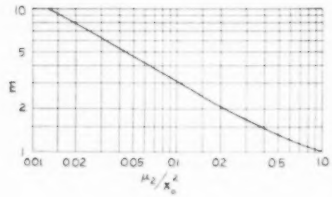

FIG. 2

The writer would like to ask what procedure, preferably systematic, should be followed in the case of a "complex" distribution. An extension of the foregoing procedure looks impractical, and yet the writer would like to try applying the distribution in other cases. For example, it would be interesting to see whether the other data on the ST-37 steel reported by Müller-Stock would result in the same division of the population as found from Figs. 6 and 7 of the paper.

AUTHOR'S CLOSURE

The author appreciates the comments made by the discussers. The proposal of Professor Tsu to take any three sets of the values P and x is quite correct but does not use the data efficiently. This method may be improved by taking the set from a smoothed curve. Up to the past year the author's usual method has been to plot the data as shown in the paper and to choose the value x_u to give the best straight line. In this way it is easy to decide if the distribution is simple or complex, but the procedure is not entirely free of subjectiveness.

About a year ago the author decided that it would be better to start by standardizing the variable x, i.e., by putting $z = (x - \bar{x})/\sigma$, where $\bar{x}$ is the mean and σ the standard deviation and eliminating two of the parameters, for instance, x_u and x_0. The distribution function then takes the form

$$P = 1 - \exp\{-[z\sqrt{\pi(2\alpha) - \pi^2(\alpha)} + \pi(\alpha)]^{1/\alpha}\}$$

where $\alpha = 1/m$.

A curve paper for different values of α, also including the standardized Gaussian distribution, may be prepared. By plotting the points (P, z) on this paper, it is easy to decide whether the distribution is simple or complex and to estimate, with a good approximation, the value of α.

As to the third question, the parentheses are an awkward misprint. The values for $\log(x - x_u)$ in Fig. 2 do not correspond to the given value $x_u = 1.5 \times 20\mu$ but to $x_u = 1 \times 20\,\mu$. It should be mentioned that the x-values are mid-point values and should correctly have been increased by $\frac{1}{2}$. Thus the value $x_u = 30\,\mu$ is the correct one.

The introduction of a maximum value x_m proposed by Mr. Mugele is a valuable extension of the function. It was not found necessary to introduce this new parameter in the field of strength of materials, probably because the theoretical strength may be perhaps a hundred times higher than the technical strength. But in other fields conditions may be quite different.

The method proposed by Professor McClintock to use the first three moments is quite good if the distribution is simple and the population not too small. The author has been aware of this possibility of computing the parameters and has mentioned it (with some different notation for the gamma function) in an earlier paper.[6] Actually, however, he has never applied this method, but admits that it may sometimes have its advantages.

As to the question of a systematic procedure when the distribution is complex, the author is sorry to admit that so far he has found no better method than to cut and try. This is, of course, not very satisfactory, but a simple electronic computing machine, recently completed, facilitates the otherwise tedious computations.

The Theory of Plasticity Applied to a Problem of Machining[1]

B. T. CHAO[2] AND K. J. TRIGGER.[3] In applying the new method of analyzing stress and strain distributions during chip formation, the authors assume that in commercial high-speed machining operations the metal behaves like an ideally plastic

[6] "The Phenomenon of Rupture in Solids," by Waloddi Weibull, IVA Handling, No. 153, p. 23.

[1] By E. H. Lee and B. W. Shaffer, published in the December, 1951, issue of the JOURNAL OF APPLIED MECHANICS, Trans. ASME, vol. 73, pp. 405–413.

[2] Assistant Professor of Mechanical Engineering, University of Illinois, Urbana, Ill.

[3] Professor of Mechanical Engineering, University of Illinois. Mem. ASME.

material that does not work-harden. Experience obtained by the writers in the actual cutting of three kinds of steel and one type of electrolytic copper fully justifies such an assumption. In fact, this constitutes one of the major conclusions reached by one of the writers 4 years ago after conducting research in metal cutting in the Machine Tool Laboratory of the University of Manchester.[4] A ductile material undergoing high-speed chip formation acts as if no work-hardening occurred during the time that deformation takes place along the shear surface as indicated by line AC in Fig. 1 of the paper. However, this does not mean that the deformed metal (chip) is not strain-hardened. It was first shown by E. G. Herbert that the hardness of the chip may be several times that of the undeformed chip material. That such a paradox can be explained by the dislocation theory for the plastic deformation of crystalline solids has been given in a recent paper.[5]

It should be pointed out that the yield stress k referred to by the authors is the dynamic yield stress. It differs appreciably in magnitude from either Tresca's yield limit or von Mises' quadratic limit. Both these quantities refer to quasi-static loading conditions. For structural steels, it has been found that the dynamic yield stress is in the neighborhood of the static ultimate tensile strength.

The authors indicate that the influence of the compressive stress on the dynamic yield stress is much less than that assumed by Merchant. Recently this has been brought out in the cutting investigation of spheroidized SAE 52100 steel using a wide range of speeds, feeds, and three different tool-rake angles. No correlation has been found to exist between the so-called machining constant and the "assumed" slope of yield stress-compressive stress curve. However, Merchant's plasticity equation does agree with experimental data to a good degree of approximation

$$2\,(\text{shear angle}) + \begin{pmatrix}\text{friction angle at}\\ \text{tool chip interface}\end{pmatrix} - \text{tool rake} = \text{const}$$

The authors' speculation of the existence of a tiny built-up edge which arises naturally as a consequence of the mathematical analysis may serve as an explanation for the foregoing controversy and should be explored fully by future experimentation.

Except for the small percentage which is retained as latent heat in the deformed chip, nearly all of the energy expended in metal-machining operations transforms into sensible heat, resulting in a large temperature rise. The effect of such temperature rise on the mechanism of chip formation has been reported recently.[5,6] In distinction to what the authors have stated, the dynamic yield stress is practically unaffected, if shearing takes place in a narrow zone, since the heating effect does not actually occur until after the shear energy has been imparted to cause plastic deformation. On the other hand, such heating due to deformation and that produced due to tool-chip rubbing do have an appreciable effect on the mechanism of chip formation through their influence on interface friction.

With a slip-line field configuration as shown in Fig. 6 of the paper, the deformation process is greatly complicated. Shearing takes place over a fan-shaped region AFC. Both temperature and strain-hardening may exhibit their influence, depending not only on the magnitude of temperature and strain involved but also upon the effective time of heating. It is difficult to analyze this aspect of the built-up nose solution without further experimentation.

Quantitative verification of the authors' new theory needs an accurate determination of the tool-chip friction angle λ_t which is not the same as that determined under the condition when shear occurs over a narrow band. It cannot readily be calculated from tool-force dynamometer data and chip thickness measurements. Examination of the nature of tool-chip contact under a magnification of $\times 30$ to $\times 50$ after the tool has been in use for a short time reveals the existence of two distinct regions of contact on the active tool face. This may serve as a clue for the experimental determination of the angle θ by actually measuring the length EC in Fig. 6. Once θ is known, together with the tool-force and chip-thickness data, the combined Mohr circle diagram, Fig. 8 of the paper, can be drawn without difficulty.

It is hoped that the authors will continue their work in the future.

R. S. Hahn.[7] This paper presents an interesting analysis of the metal-cutting process and seems to be the first to give an analysis involving the built-up edge. Previously it has been considered that the type 2 chip was formed without a built-up edge. The writer, in tests where the chip appeared to be of type 2, has found a very small built-up edge in all cases—indeed a few thousandth of an inch in size. (Chips that are produced by an abrupt ending caused by the tool entering an interruption often carry at their end a very small built-up edge which can be seen under the microscope.) Such chips, even though their back side is very smooth and highly burnished, have been formed with a built-up edge. The region BC in Fig. 6 of the paper serves to burnish the chip so highly that all roughness caused by the flow along FC is eradicated, and generally it has been believed that such chips were produced without a built-up edge. Consequently, it appears that there is considerable truth in the authors' conclusion that a built-up edge always exists.

The analysis presented considers flow to take place in the x-direction only, Fig. 6. That this is not strictly true is evidenced by the curvature of the chip. The authors state that the curva-

[4] "On Elements in Metal Machining-Dynamic Factors in Orthogonal Cutting, by B. T. Chao, 1947, PhD Dissertation, Library of the College of Technology, University of Manchester.

[5] "Thermophysical Aspects of Metal Cutting," by B. T. Chao, K. J. Trigger, and L. B. Zylstra, presented at the Annual Meeting, Atlantic City, Nov. 25–30, 1951, of The American Society of Mechanical Engineers.

[6] "Cutting Temperatures and Metal-Cutting Phenomena," by B. T. Chao and K. J. Trigger, Trans. ASME, vol. 73, 1951, pp. 777–793.

[7] Research Engineer, The Heald Machine Company, Worcester, Mass. Mem. ASME.

Fig. 1 Photomicrograph of Chip Showing Curved Elongated Grains Found in Chips of Small Radius; $\times 200$

ture of the chip is due to residual stress and thermal strain conditions. The fact that curved chips may be heated to incandescence without changing curvature tends to disprove the foregoing. Also, they will be found to retain their curvature to the last as they are dissolved in acid. It appears from experiments that the chip curvature is a result of flow along the u-slip lines as well as the v-slip lines. In certain cases the chip velocity of the metal adjacent the tool face has been observed to be as much as 30 per cent higher than the velocity of the metal forming the outside face of the chip. We may consider the grains in the uncut metal to be essentially equiaxed so that after deformation they become elongated showing the directions of principal strains. It will be evident from Fig. 1 of this discussion that a nonhomogeneous state of strain exists and that the authors' analysis will not apply accurately in such cases.

M. EUGENE MERCHANT.[9] This paper marks another important step forward in the development of the science of metal cutting. However, while the present-day plasticity theory used by the authors is sound and well established, it appears that the practical assumptions made in applying it to the metal-cutting problem are open to some question. The result is that while the qualitative findings of the resulting limiting chip-stress solution agree well with observed facts and in some cases offer a better explanation of these facts than had previously existed, nevertheless the quantitative predictions of that solution do not agree as well with experimental data as do the predictions of the more approximate minimum-energy solution.

The first case which the authors consider is that of machining without a built-up edge. In applying the theory to this case they assume that the yield stress is a constant, yet it is known that this stress is affected by a number of factors. Among the more important of these is that of normal stress (hydrostatic pressure), the effect of which has been demonstrated by Bridgman[3] and Rotner[10] (the writer is indebted to Prof. M. C. Shaw of M.I.T. for his kindness in bringing the latter reference to his attention). Measurements made in our own laboratory by Kemeny[11] and by Krabacher and Whisler[12] on a Bridgman-type apparatus confirm this same effect. Data obtained in these investigations, as presented by Ernst[13] are shown in Fig. 2 of this discussion. Introduction of this effect of normal stress on yield stress into the minimum-energy solution has a profound effect upon that solution, making it a much better approximation to reality. Therefore is it not likely that the introduction of this same effect into the authors' limiting chip-stress solution would also have a profound effect on the quantitative results?

The authors consider next the case of machining with a built-up edge. The fact that the authors' limiting chip-stress solution predicts the presence of a built-up edge marks a real step forward in the mechanics of cutting. Little progress has been made in developing the mechanics of this case previously. However, the quantitative predictions of the theory as to the size of the built-up edge, the values of friction at which it comes into existence, and so on, are questionable because of the assumptions made. Primarily, yield stress again is assumed to be a constant and independent of the several factors which are known to influence it. This assumption alone could have a profound effect on the quantitative results of the theory as already indicated. Then, too, the authors assume that the bottom of the built-up edge is in frictional contact with the work surface, whereas photomicrographs of chip formation have shown that the built-up edge actually is continuous with the work material at this point. Continuous plastic flow takes place in this region in the same manner as it does on the shear plane and strain-hardening also occurs. As a result the bottom portion of the built-up edge gradually builds downward, increasing in size, until it becomes so large as to be unstable and is then carried away with the machined surface, after which the cycle begins again. (It is this process of the building up and sloughing off of fragments of built-up edge on the machined surface which accounts for the roughness of such surfaces when produced under condition where a built-up edge exists.)

In the composite solution, resulting from the consideration of the two cases already discussed, the authors have presented a comparison of the quantitative predictions of the limiting chip-stress solution with experiment in Fig. 12 of the paper. They indicate that the reason the experimental data extend beyond the theoretical boundary determined by $\mu_t = 1$ in the figure is that elastic deformation modifies the solution at the tool-chip interface. If this is so, then it would appear that the data should show at least some downward trend toward point F in Fig. 12 beyond the boundary, in keeping with the downward trend of the boundary. However, no such downward trend is observed in these data nor even in other data obtained at higher values of λ-γ than those shown experimentally in Fig. 12 of the paper. On the other hand, the minimum-energy solution, though more approximate from a theoretical point of view, actually gives a better approximation to the experimental results than that shown for the limiting chip-stress solution in Fig. 12. The degree of approximation given by the minimum energy solution is illustrated in Fig. 3 of this discussion. (The symbols used are those originally proposed by the writer,[14] but the ordinate and abscissa are the same as those of the authors' Fig. 12.)

It can be seen that the degree of approximation of the experimental data to the line labeled $2\phi + \tau - \alpha = 77$ deg predicted by the minimum-energy solution, is rather better than the approximation predicted by the limiting chip-stress solution in Fig. 12. However, the authors object to this agreement since it involves the conclusion that the proportionality constant relating yield stress to normal stress must be of the order of 0.23 (cot 77 deg), since according to the minimum-energy solution the sum $2\phi + \tau - \alpha$ should equal approximately the complement of the slope angle of the yield stress versus normal stress line in a plot such as that shown in Fig. 2 of this discussion. Nevertheless, Bridgman,[3] Rotner,[10] Kemeny,[11] and Krabacher and Whisler[12] all obtain values of this order for the proportionality constant for a variety of metals. For example, a comparison between the values of $2\phi + \tau - \alpha$, obtained from metal-cutting tests, and values of the complement of the slope angle of the yield-stress plot, obtained from torsion-compression tests made in this laboratory on four different steels, is given in Table 1. It can be seen that the degree of correlation between the data obtained from the two quite different types of tests is relatively good. It would appear therefore that for the values of strain common in metal cutting the influence of hydrostatic pressure on yield stress is of a large enough magnitude to be significant in the theory of machining.

Since the authors' limiting chip-stress solution based on plasticity theory actually results in a poorer approximation to experiment than does the simple and approximate minimum-energy

[9] Assistant Director of Research, The Cincinnati Milling Machine Company, Cincinnati, Ohio. Mem. ASME.

[3] See Authors' Bibliography, reference (19).

[10] "Change of Mechanical Properties of Metals Under Hydrostatic Pressure," by S. I. Rotner, *Journal of Technical Physics*, USSR, vol. 19, 3rd edition, March, 1949, p. 408.

[11] "Torsion and Compression Testing," by J. Kemeny, University of Cincinnati thesis, 1947.

[12] "Torsion and Compression Testing" by E. J. Krabacher and K. W. Whisler, University of Cincinnati thesis, 1949.

[13] "Fundamental Aspects of Metal Cutting and Cutting Fluid Action," by Hans Ernst, Annals of the New York Academy of Sciences, series II, vol. 53, 1951, pp. 805–823.

[14] See Authors' Bibliography, reference (18).

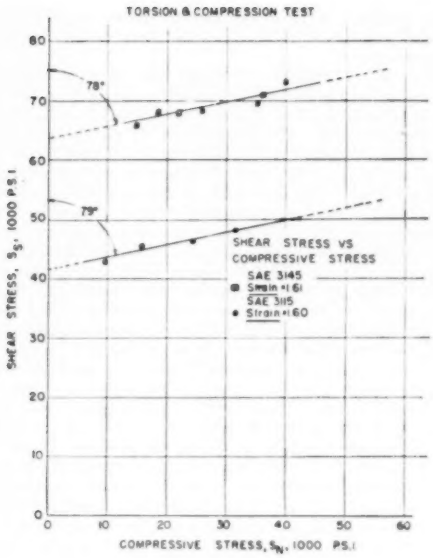

FIG. 2

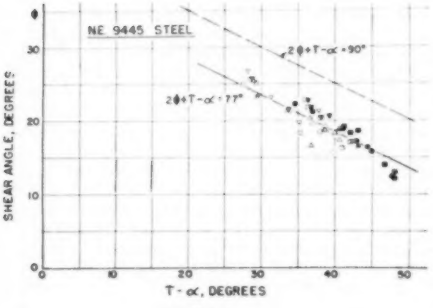

FIG. 3

TABLE 1 COMPARATIVE RESULTS OF METAL-CUTTING AND TORSION-COMPRESSION TEST DATA

Steel	Shearing strain	$2\phi + \gamma - \alpha$ from metal-cutting tests	Complement of slope angle of yield-stress plot from torsion-compression tests
SAE 3115	2.87	76	78
SAE 3150, spheroidized	3.11	76	84
SAE 3150, pearlitic	3.15	71	74
SAE 3450	2.96	78	83

solution, even though on a theoretical basis it should be expected to be more exact, it would seem that the next desirable step for the authors to take would be the introduction of improved assumptions into their solution to determine the extent to which these help to bring it into line with experimental findings. Furthermore, it would appear that the authors would benefit by carrying out a few critical experiments to test certain points in their theory as a guide in choosing the assumptions to be used.

It is the writer's feeling that if these things are done a useful and practical theory can be developed from this approach which will mark a major advance in the science of machining.

E. K. HENRIKSEN.[15] Metal-cutting operations have been investigated more or less continuously since the 1870's and, therefore, it is not surprising that it is hard to find basically new thoughts in the constant flow of contemporary publications on this subject. The present, paper, however, is a very pleasant exception to this rule. The authors have approached the problem by original methods, and they have laid a new cornerstone to the foundation of a great, yet unfinished building.

However, many engineers and other workers in the metal-cutting field will fail to visualize the value and importance of this paper, simply because they do not feel themselves prepared to follow the mathematical methods used. For this reason the writer would like to present a simplified development, leading up to the principal equation.

Referring to Fig. 4 of this discussion, AC is assumed to be the

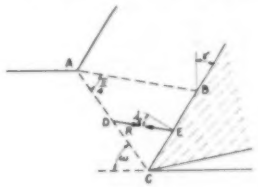

FIG. 4

plane where the shearing deformation occurs, and it follows that it is the plane of maximum shearing stress. B is the upper limit for contact between chip and tool and, therefore, the upper limit for transmission of force between the two bodies. It follows then:

There is no load on AB.
There is no stress on AB.
Specifically there is no shearing stress on AB.
Hence AB is a plane of principal stress.

From the general rule that the maximum shear occurs under 45 deg with the planes of principal stress, it follows that

$$\sphericalangle BAC = 45 \text{ deg}$$

With the shearing stress k and the normal stress p, it can be shown elementarily by means of a triangular free-body diagram $p = k$.

Now the shear stress is contant, equal to k, over AC; it is reasonable to assume that also the normal stress is constant, and equal to p. But then the resultant R will go through the middle of AC, under an angle of 45 deg and therefore, be parallel to AB and its point of intersection E with BC will be the middle of BC. Equilibrium of the body ABC requires that the resultant of the forces on BC will fall in the same line, that is, pass through E, but as E is the middle of BC it is reasonable (so far, at least, see later) to assume that the load on BC is contant.

Now

$$\sphericalangle DEC = \frac{\pi}{2} - \lambda_t$$

where λ_t is the friction angle between chip and tool, hence (from the triangles ABC and DEC)

$$\frac{\pi}{2} + \gamma - \omega + \frac{\pi}{2} - \lambda_t + \frac{\pi}{4} = \pi$$

[15] Professor in Charge, Head of Department of Materials Processing, Cornell University, Ithaca, N. Y. Mem. ASME.

and

$$\omega = \frac{\pi}{4} - \lambda_t + \gamma$$

which is the basic Equation [2] of the paper. The rest is elementary.

As to the subject itself, the authors have based their analysis upon the assumption of no load beyond point B, that is, ignoring elastic stresses in the chip. For analysis of this character such an assumption is natural and justified, the consequences of this assumption being that AB is a straight line, and constant pressure over BC.

The writer would like to show the effect of omitting this limiting assumption.

FIG. 5

As shown before,[16] there will be a region FB, Fig. 5 of this discussion, with elastic stresses in the chip and there will be a sharp rise in pressure from F to B. The plastic deformation begins at B and beyond B the rate of increase in pressure will be less, the pressure will reach a maximum and will then decrease somewhat toward C.

The boundary AB between the elastic and the plastic region in the chip itself no longer will be a straight line, but will be curved with the concave side in the direction of the flow of the chip.

AUTHORS' CLOSURE

The authors first wish to express their thanks for the interest shown by the discussers of this paper.

They appreciate the comments of Professors Chao and Trigger confirming the use of an ideally plastic stress-strain relation, and emphasizing the smaller influence of hydrostatic pressure than had been assumed in earlier work. The discussion of the influence of temperature distribution will be important in the future development of the theory; in the analysis under discussion such influences were merely averaged and results compared which would not be expected to be sensitive to such averaging.

We appreciate the comments of Dr. Hahn concerning the experimental observation of a built-up edge as predicted in the paper. We agree that a more detailed study of chip strains including bending effects is called for. In this connection B. W. Shaffer[17] has developed a theory of the turning process with relative rotation between the tool and the work, in contrast to the planing-type theory under discussion. In this solution varying shear through the chip thickness occurs.

Dr. Merchant's discussion is concerned mainly with the influence of hydrostatic pressure on the yield stress in shear. In contrast to the references cited by Dr. Merchant, the discussion below indicates that the consensus of opinion on this controversial issue appears to be against an appreciable hydrostatic-pressure effect.

The study of plasticity of metals has led to the general conclusion that while fracture conditions are highly influenced by hydrostatic pressure, this does not affect plastic-flow conditions appreciably. This is emphasised by the general acceptance of the Mises or Tresca yield conditions, both for initial yield, and as a basis for a generalized stress-strain relation over a range of strain. Both these limits are independent of the average hydrostatic pressure, depending only on the stress deviator. The insensitiveness of the flow stress in tension to hydrostatic pressure up to large strains has been checked directly by Bridgeman.[18] This is in agreement with the concept of plastic potential (see Hill[19]) which has recently received both experimental[20] and theoretical[21] justification. Thus we must answer the question: In metal forming theory why is it generally accepted that hydrostatic pressure affects fracture but not plastic flow, and yet in machining theory an appreciable influence on plastic flow has been commonly accepted? A recent discussion of this question in connection with a paper by Chao and Bisacre[22] shows that many workers in the field of metal-cutting theory do not accept an appreciable influence of hydrostatic pressure. Discussers J. M. Lickley, M. C. Shaw, and E. H. Lee independently emphasize this point. Shaw states: "Calculations based upon atomic structure and inter-ionic forces revealed that normal stresses of about the magnitude that were found in metal cutting should have no influence upon flow stress. That the yield stress for ductile metals was found to be the same in tension and compression was further evidence that normal stress did not influence the ductile properties of metals. Schmidt and Boas had demonstrated that normal stress did not affect the flow stress of ductile single crystals." In the closure Chao and Bisacre agreed with Shaw's comments and mentioned an independent check of Bridgeman's compression-torsion-type test with α brass[23] which gave a zero hydrostatic-pressure effect. In view of these comments, what then is the significance of the papers quoted by Dr. Merchant? In the report,[24] of which the paper under discussion is a shortened version, the shortcomings of the notched torsion-compression tests were discussed. While this test serves admirably to demonstrate the influence of hydrostatic pressure to inhibit fracture, the complex stress and strain distribution makes interpretation in terms of flow stress extremely difficult. This test does not produce shear under hydrostatic pressure, but appreciable longitudinal and lateral strain also which may have an appreciable influence on the results. In machining, such strains are inhibited by the constraint of elastic material, indicating superposed hydrostatic pressure in contrast to the axial compression occurring in the test. It seems therefore that Bridgeman's results for tension quoted above should take

[16] "Stress Distribution in a Continuous Chip—A Solution of the Paradox of Chip Curl," by E. K. Henriksen, Trans. ASME, vol. 73, 1951, pp. 461–466.

[17] "Analysis of Chip Formation in the Turning Operation," by B. W. Shaffer. Brown University Technical Report A11-56, 1951.

[18] "Studies in Large Plastic Flow and Fracture," by P. W. Bridgeman, McGraw-Hill Co., Inc., 1952, p. 64 ff.

[19] "A Variational Principle of Maximum Plastic Work in Classical Plasticity," by R. Hill, *Quarterly Journal of Mechanics and Applied Mathematics*, 1. 1. March, 1948, p. 21.

[20] "A Connexion Between the Criterion of Yield and the Strain Ratio Relationship in Plastic Solids," by G. I. Taylor, Proceedings of the Royal Society, series A, vol. 191, 1947 p. 441.

[21] "Some Implications of Work-Hardening and Ideal Plasticity," by D. C. Drucker, *Quarterly of Applied Mathematics*, 7, 9, 1950, p. 411.

[22] "The Effect of Feed and Speed on the Mechanics of Metal Cutting," by B. T. Chao and G. H. Bisacre. Proceedings of The Institute of Mechanical Engineers, 65(W.E.P. No. 63), 1951.

[23] Report MF/MS 37 to the Mechanical Engineering Research Board of the Department of Scientific and Industrial Research G. H. Bisacre, 1950.

[24] "The Theory of Plasticity Applied to a Problem in Machining," by E. H. Lee and B. W. Shaffer. Brown University Technical Report A11-43, 1949.

precedence over his results in this test. Because of the language difficulty we were unable to examine Rotner's work in detail in the short time available.

Thus it seems that the agreement of experimental results with Merchant's theory including a pressure effect calls for explanation on other grounds. This point was made by J. M. Lickley in the discussion mentioned previously. The limiting chip stress solutions given in the paper under discussion offer such an explanation.

The discussion of built-up edge development given by Dr. Merchant corresponds to a large intermittent nose usually classed as a type-3 chip. Perhaps the small built-up nose discussed in the paper behaves differently according to its connection with the base material. However, it would be of interest to study the influence of material shear under the nose base on the present theory. We do not appreciate the need for a tendency toward the point F in Fig. 12 of the paper, as suggested by Dr. Merchant. It would seem that elastic effects might very well merely involve smooth extension of the curves μ_n = constant beyond the boundary $\mu_t = 1$.

We agree that the simple derivation given by Professor Henriksen may have greater appeal to some engineers. In the case of the built-up nose solution it seems that it may not be possible to avoid the mathematical considerations in this way. We agree with the importance of considering the bending effect in a more detailed analysis.

The Calculated Performance of Dynamically Loaded Sleeve Bearings—III[1]

G. B. Du Bois.[2] We have some experimental data which is related to this paper, as it tends to support the short-bearing approximate method of solution for the steady-load case. The theoretical part of our project by Professor Ocvirk is listed in the author's Bibliography as reference (12).

Prof. F. W. Ocvirk and the writer are associated with a research project at Cornell University being sponsored and financed by the National Advisory Committee for Aeronautics. This research project was begun in 1948, and at the present time is engaged in an experimental investigation of eccentricity ratio, friction, and oil flow to obtain actual data on this subject for the steady-load case. The short-bearing approximation theory for the steady-load case was extended recently by Professor Ocvirk and is being used as a convenient vehicle for plotting the experimental results. Both Professor Ocvirk and the writer would like to offer some brief comments.

We are using a $1^3/_8$-in. shaft, at speeds up to 6000 rpm, loads on projected area up to 900 psi, with SAE 10 oil. The eccentricity of the shaft in the bearing is being measured by a system of levers and dial gages, and we also are obtaining friction and oil-flow data in both directions of rotation. At the present time the data cover length-diameter ratios of $^1/_4$, $^1/_2$, and 1.

Using the short-bearing approximate method, theoretical lines can be plotted to represent the eccentricity ratio, n versus the Sommerfeld number S, and we obtain a group of fan curves, on which the lines for l/d of 1, $^1/_2$, and $^1/_4$ can be labeled. On such a plot these lines are far enough apart for the l/d mentioned so that experimental data should show a trend quite readily. It is significant that our data for l/d of $^1/_4$, $^1/_2$, and 1 are in general agreement with the short-bearing approximation. The points show a moderate spread with the center slightly above the theoretical line. We expect that these data for the steady-load case will be available in an NACA technical note within a few months.

According to the short-bearing approximate method, we theoretically can plot the eccentricity ratio, n versus S $(l/d)^2$, making use of a new capacity number C_a, and obtain a single line. The experimental points of all of our tests again fall in a moderate spread slightly above this line. This capacity number, originated by our project, is mentioned by the author just above his Equation [12]. We believe that this capacity number may turn out to be of more practical value than the well-known Sommerfeld number for bearings of a short l/d ratio, up to 1 or a little more.

These theoretical curves are approximate in that they include the side flow which can be illustrated by a parabolic velocity profile, and they include the part of the circumferential flow which can be illustrated by a triangular velocity profile. However, they neglect the parabola superimposed on the triangle. The Sommerfeld solution, on the other hand, neglects the side flow and includes both parts of the circumferential flow. Thus it seems that the Sommerfeld theory and the short-bearing theory should be considered as the two halves of the same type of solution, rather than as being competitive. Each has a range of l/d in which it is the more useful. In our opinion, this short-bearing theory deserves wide recognition for its ability to include oil flow and give a useful approximation for short-bearing lengths commonly used.

The author also points out that some of the solutions assume the oil film for load purposes to have an extent of 360 deg, while others take 180 deg, neglecting the negative-pressure region. He also points out that the attitude angle is 90 deg for the 360-deg or 2π case, and approximates a semicircle for the 180-deg or π case. Our experimental data for unit loading up to 900 psi tend to follow the semicircle result.

In general, the experimental work reveals a number of practical considerations such as shaft deflection, variations in clearance, and in oil-inlet pressure which considerably affect the results, and tend to minimize the importance of minor error in the short-bearing approximation. This will be one of the most interesting phases of our report.

Referring to Fig. 9 (a) of the paper, the author states that at $n = 0.8$, the error in 1/S is about 20 per cent for an l/d of $^1/_4$, which is correct. If we use the same figure and enter with a value of S = $^1/_4$ or 1/S = 4, the two curves give values of n of about 79 per cent and 81 per cent—a difference of about 2 per cent.

On a plot of n versus S, the two theories in question give two lines close together, and the distance between them in the direction of the n-axis is small. On the other hand, intercepts in the direction of the S-axis are farther apart.

B. L. Newkirk.[3] Fig. 2 of the paper, with the theory pertaining to it, throws light on the question of stability of a journal in its equilibrium position. In the course of an experimental study of the oil-film whirl[4] it was found that an unloaded journal would whirl at a whirl frequency of one half its rotation frequency when running at low speed. At higher speed this whirl disappeared, but when the bearing was free to oscillate it did so, and at a frequency equal to one half the shaft rotation speed.

[1] By J. T. Burwell, published in the December, 1951, issue of the Journal of Applied Mechanics, Trans. ASME, vol. 73, pp. 393–404.

[2] Professor of Mechanical Engineering, Cornell University, Ithaca, N. Y.

[3] Consultant, 17 Ross Road, Schenectady, N. Y. Mem. ASME.

[4] "Shaft Whipping Due to Oil Action in Journal Bearings," *General Electric Review*, vol. 28, August, 1925, pp. 559–568.

Hagg[6] found a similar result using a relatively large bearing and a light shaft.

This motion does not appear generally at higher speeds or at heavier bearing loads. In one case[6] in which the unit load was very small (of the order of 1 psi), the shaft ran steadily up to the top speed of 30,000 rpm. It might have occurred, and escaped notice, at low speeds. In one commercial machine having a 7-in. journal with a cap load, the half-frequency whirl was a disturbing factor.

That a half-running-frequency stimulus is present at all speeds may be inferred from the fact that rotors running on journal bearings develop a whirl at their resonant frequency when running at twice that frequency. The internal damping of rotors is generally low, and a minute stimulus of the natural frequency calls forth a response. It would seem, however, that journals, in general, do not follow such paths as the larger orbits shown in Fig. 2 of the paper. Motions of this magnitude could hardly have escaped detection in the studies reported in references mentioned.[4,5] Hummel[7] in his study of the theory of the half-bearing concluded that all journals running with eccentricities less than 0.7 are unstable. His experiments confirmed a mild instability (restlessness) in this region; however, his clearances were abnormally large (for example, 0.006 in. per in.), and his bearing was substantially without an upper half. He states that with "small" journal clearances (less than 0.004 in. per in.) smooth operation is possible.

The effect of this phenomenon on behavior of the rotating-plug viscometer ought to be studied. It is possible that with very small clearance the plug runs essentially in a centered position. With normal bearing clearance an unloaded journal certainly moves out of the center and moves around.

The writer cannot subscribe fully to the statement just above Equation [25*a*] of the paper. "This is the origin of the oil film-excited shaft whirl." It is perhaps a matter of personal preference in the present state of knowledge whether one will agree that a whirl at, say, 1000 whirls per min when the shaft runs at 5000 rpm, is due to a tendency of the journal to whirl at 2500 whirls per min, slowed down by end leakage or other causes, or to ascribe the whirl in such cases to a different instability characteristic of the oil film. We are now studying a rotor that runs without any severe whirl up to 5 times its critical speed and then breaks into a vigorous whirl with the whirl frequency equal numerically to the critical speed.

F. W. Ocvirk.[8] This paper compares bearing-load capacities as given by various analytical expressions both approximate and exact. From these comparisons it may be seen that in so far as the bearing of useful width is concerned, most of the analyses are approximate ones with the exception of the results obtained by Cameron and Wood. Although the Sommerfeld solution is exact for the infinitely wide bearing, it too is approximate in the realm of real bearings.

Of the equations giving an approximate solution for load capacity, it appears to us of the NACA—Cornell bearing project, that Equations [21*a*] and [21*b*] of the paper are the most realistic for short bearings under constant load. Experimental data for l/d of 1, $^1/_2$, and $^1/_4$ as obtained by the project show good agreement with these equations as well as with the curves of Cameron and Wood as might be expected from the comparison in Fig. 9 of the paper.

Experimental oil-film pressure distributions for bearings of l/d of 1 as obtained by this project and by McKee and McKee are also in good agreement with the pressure-distribution function of Michell and Cardullo from which Equations [21*a*] and [21*b*] are derived.

The author's illustration of the overlapping of load-capacity curves given by Equations [18*a*] and [19*a*] is extremely interesting. He shows that the load-capacity curve given by Sommerfeld for the infinitely wide bearing intersects the curves given by the approximate solution for short bearings. At these intersections either of these equations may be used to predict bearing-load capacity. The length-to-diameter ratios of short bearings at which the intersections occur is given by

$$l/d = \left[\frac{6(1 - n^2)}{(2 + n^2)}\right]^{\frac{1}{2}} \quad \ldots\ldots\ldots\ldots\ldots [1]$$

A similar consideration of Equations [19*a*] and [21*a*] of the paper gives the following

$$l/d = \left[\frac{3\pi(1 - n^2)^{3/2}}{(2 + n^2)\left[n^2 + \frac{\pi^2}{16}(1 - n^2)\right]^{1/2}}\right]^{\frac{1}{2}} \quad \ldots\ldots [2]$$

As indicated by the author, the plotting of l/d against n results in a curve which is an aid in determining the length-to-diameter range over which approximate solutions will predict conservative load capacities. The area under the curve gives the region in which the short-bearing approximate solutions should be used; the area outside of the curve is one in which the Sommerfeld equations give the more realistic results. The curve itself may be looked upon as defining the region of bearings of intermediate width. The maximum value of l/d, given at $n = 0$, is 1.73 for Equation [1] of this discussion and 2.50 for Equation [2] indicating that the short-bearing approximate solution given by Equations [21*a*] and [21*b*] of the paper is applicable to a slightly greater range of l/d than Equations [18*a*] and [18*b*]. It is interesting to note that the Cameron and Wood curves give intersections with the Sommerfeld curve to show that they are applicable to a much greater range of l/d than that given by Equations [1] and [2], herewith, and that they reach well into the region of intermediate-width bearings.

E. M. Simons.[9] As the author points out, the idea of dropping the $\partial p/\partial x$ term instead of the $\partial p/\partial z$ term in the Reynolds equation is not new. He is to be commended on his ingenious and comprehensive application of this narrow-bearing theory to the case of dynamically loaded bearings. Also, his comparisons with existing theories for steady unidirectional loads demonstrate that this treatment provides results which are sufficiently accurate to be of practical use to bearing designers for bearings with l/d up to $^1/_4$.

One question which naturally comes to mind is, "How do the results of this study compare with experimental observations on real bearings?" The writer has conducted laboratory studies[10] on a bearing with $l/d = ^1/_2$. Apparently, there was sufficient damping in the machine used for these tests to prevent orbital motion of the journal center in all experiments with steady unidirectional loads. This means that comparisons can be drawn

[5] "The Influence of Oil-Film Journal Bearings on the Stability of Rotating Machines," by A. C. Hagg, Journal of Applied Mechanics, Trans. ASME, vol. 68, 1946, pp. A-211–220.

[6] "Oil-Film Whirl—A Nonwhirling Bearing," by B. L. Newkirk and Lloyd P. Grobel, Trans. ASME, vol. 56, 1934, pp. 607–615.

[7] "Kritische Drehzahlen als Folge der Nachgiebigkeit des Schmiermittels im Lager," by Charles Hummel, *VDI, Forschungsarbeiten auf dem Gebiete des Ingenieurwesens*, Berlin, Germany, Heft 287, 1926.

[8] Associate Professor of Mechanical Engineering, Cornell University, Ithaca, N. Y.

[9] Research Engineer, Battelle Memorial Institute, Columbus, Ohio. Mem. ASME.

[10] Reference (16), author's bibliography.

only with the poles of families of orbits given by the author's Equation [16] for this loading condition.

Fig. 1 of this discussion is analogous to the author's Fig. 8 (*a*), with the addition of an experimental curve for steady loads with an unbroken oil film. Unfortunately, the theories predict load capacities which are higher than those found by test. Furthermore, the discrepancies are greatest at high values of η, making it risky to use this work for design purposes when l/d is as large as $^1/_2$. This same situation exists in the case of ruptured films, although, as may be seen from Fig. 2, herewith, the agreement is somewhat better, especially at the higher values of η.

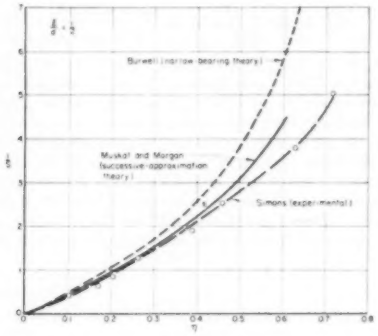

FIG. 1 COMPARISON OF THEORETICAL AND EXPERIMENTAL PERFORMANCE OF BEARING OPERATING WITH CONTINUOUS OIL FILM

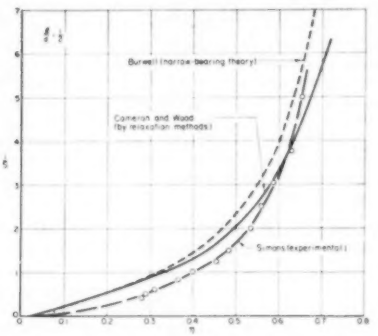

FIG. 2 COMPARISON OF THEORETICAL AND EXPERIMENTAL PERFORMANCE OF BEARING OPERATING WITH RUPTURED OIL FILM

The writer has found experimentally[10] that when the film is ruptured under a steady load, the eccentricity ratio for a given S can vary over a sizable range, depending on the oil-feed pressure. The limiting curve, shown in Fig. 2, was obtained with flood lubrication. Presumably, however, if the ambient and oil-feed pressures were below atmospheric, a new limiting curve would result. Such observations lead to the conclusion that the eccentricity in a real bearing, operating under a constant unidirectional load with a given Sommerfeld number, is not uniquely determined when the oil film is discontinuous. In real bearings, incipient film rupture occurs in a highly localized region of peak negative pressure. If the external load is increased or the lubricant-feed pressure decreased, the area over which the film is ruptured increases correspondingly in both the axial and circumferential directions. Any realistic theory for discontinuous films must take into account this concept of varying degrees of film rupture.

Since a given S can produce a range of η when the film is incomplete, it seems logical that there also would be a range of possible locations of the line of centers for each S. Fig. 3 of this discussion illustrates that this is indeed the case. Although the author's approximation agrees fairly well with the curve of Cameron and Wood[11] in Fig. 3, neither theory explains the broad range in the experimental values of φ for a given S.

When the test bearing was subjected to a constant rotating load, the journal-center orbits were circular when N_p/N_j was greater than about $^1/_4$. For speed ratios less than $^1/_4$, the orbits were more complicated. Unfortunately, there was not sufficient time to carry out the integration of the author's Equations [11*a*] and [11*b*] to obtain $\eta(t)$ and $\varphi(t)$ for comparison purposes with these latter orbits. When the orbits were circular, φ was not $\pi/2$,

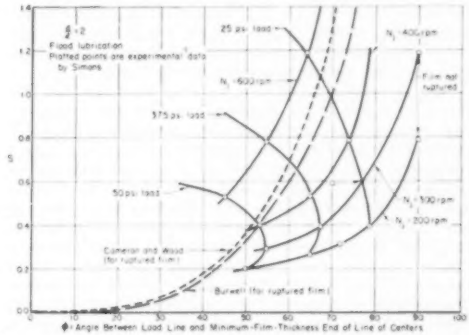
Flood lubrication
Plotted points are experimental data by Simons
25 psi load
375 psi load
50 psi load
Film not ruptured
Cameron and Wood (for ruptured film)
Burwell (for ruptured film)
φ = Angle Between Load Line and Minimum-Film-Thickness End of Line of Centers

FIG. 3 COMPARISON OF THEORETICAL AND OBSERVED PHASE ANGLES FOR BEARING OPERATING WITH RUPTURED OIL FILM

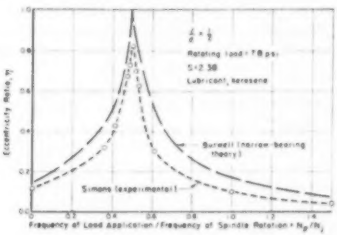
Rotating load = 7.8 psi
Lubricant, kerosene
Burwell (narrow-bearing theory)
Simons (experimental)
Eccentricity Ratio, η
Frequency of Load Application / Frequency of Spindle Rotation = Np/Nj

FIG. 4 EFFECT OF RELATIVE FREQUENCY OF LOAD APPLICATION ON ECCENTRICITY RATIO FOR CONSTANT LOAD OF 7.8 PSI ROTATING AT CONSTANT SPEED

as predicted by Equation [24*b*]. However, experimental curves of η versus N_p/N_j had the shape predicted by Equation [24*a*]. For example, Fig. 4, herewith, shows that the equation predicts values of η which are about 20 per cent higher than the test results.

In the tests, the predicted eccentricity ratio of unity when $N_p/N_j = ^1/_3$ was approached when such nonideal conditions as tiny misalignments and extraneous loads were reduced or eliminated. However, such changes affected the curve only in the immediate vicinity of $N_p/N_j = ^1/_2$.

[11] Reference (4), author's bibliography.

Author's Closure

The foregoing discussions have been particularly valuable for the reason that they all report on experimental observations on bearings under conditions like those considered in the present theory and this, of course, is the proof of any theory. From these discussions one would conclude that there is a fairly good agreement, particularly for the case of a constant load, and that the theory can be used reasonably safely for calculating the performance of bearings under this type of loading having l/d ratios as large as unity. This should be useful in simplifying bearing-performance calculations since the application of a side-leakage factor to the result calculated or read from charts for the infinitely wide bearing has always been required in the past. Here, one single calculation using a relatively simple equation gives the final answer.

However, the agreement even in the constant-load case is not as good as one would like and definitely suggests that one or more of the factors omitted from the theory for purposes of mathematical simplicity is having a significant effect in an actual case. In particular, Messrs. du Bois, Ocvirk, and Simons all observe that the assumption of a continuous oil film gives definitely poorer agreement than the assumption of a ruptured film.

That journal-bearing oil films are often incomplete has been known for a long time. Recent experiments providing direct visual observation of the film have been conducted in the M.I.T. Lubrication Laboratory which substantiate this point. In these experiments a glass bearing having $l/d = 1$ was used and the oil film was rendered visible by adding a fluorescent dye to the oil and then viewing the bearing with ultraviolet light. The ruptured portion of the oil film was plainly visible and its behavior was found to very clearly substantiate Mr. Simons' statement that the lubricant feed pressure, among other factors, should change the extent of the ruptured portion. The oil film was found to be entirely continuous if the supply pressure was sufficiently high. As this pressure was decreased keeping the speed and load constant, a point was reached where a very small ruptured or cavitated region appeared, located on the center line of the bearing and in the diverging region approximately where the continuous-film theory would predict the minimum absolute pressure. With further decrease in feed pressure, this ruptured region increased in extent both axially and circumferentially.[12]

[12] In this respect it disagrees with the present narrow bearing theory which requires the ruptured region to extend from $\theta = \pi$ to $\theta = 2\pi$ for all loads and speeds.

Obviously then, as Mr. Simons concludes, the location of the shaft will be different for different supply pressures, as a result of each of these different film dispositions.

Mr. Simons is quite correct in concluding that "the eccentricity in a real bearing, operating under a constant unidirectional load with a given Sommerfeld number, is not uniquely determined when the oil film is discontinuous." This can be demonstrated analytically. It is seen most easily in the case of the infinitely wide bearing where the expression for the pressure gradient, resulting from the first integration of the Reynolds equation, can be written

$$\frac{dp}{d\theta} = 12\pi \left(\frac{r}{c}\right)^2 \mu N \eta \cdot \frac{\cos\theta - \cos\theta_m}{(1 + \eta\cos)^3} \quad \ldots\ldots [1]$$

where θ_m is the integration constant. From the equation it is seen that θ_m and θ_{-m} correspond to the angular positions where the pressure gradient is zero. Furthermore, as stated on p. 395, the correct boundary conditions for an incomplete film are that both the pressure and the pressure gradient must be zero at the trailing edge. Hence the position of the trailing edge is determined by the value of θ_m; specifically, it is located at the angular position $-\theta_m$. Therefore the boundary conditions for determining the two integration constants in the expression for the pressure resulting from integration of Equation [1] above may be expressed analytically:

$$\left.\begin{aligned} p &= O^{[13]} \\ \frac{dp}{d\theta} &= O \end{aligned}\right\} \text{ at } \theta = -\theta_m$$

From this it is clearly seen that the limits of the oil film are not uniquely determined but must be expressed in terms of the unknown constant θ_m. Further integration of the pressure over the film to obtain the total load yields an expression still containing θ_m so that the load is not uniquely determined either, as Mr. Simons concludes. Obviously, another boundary condition is needed and it is fixed very simply by the requirement that at the position of the oil inlet the pressure in the oil film must equal the oil-inlet pressure. Applying this condition, it becomes possible to express θ_m in terms of this pressure. The same argument applies in the general case where side leakage is considered although it is more complicated since the edge of the oil film will depend on Z as well as θ.

[13] Strictly speaking, p equals the oil vapor pressure in the cavitated region but this is substantially zero under most conditions.

Book Reviews

Vibration and Shock Isolation

VIBRATION AND SHOCK ISOLATION. By Charles E. Crede. John Wiley & Sons, Inc., New York, N. Y., 1951. Cloth, 6 × 9 in., xvii and 328 pp., illus., bibliography, tables, index, $6.50.

REVIEWED BY G. HORVAY[1]

THIS timely and up-to-date book on a subject which acquired prominence only in recent years, by a man who actively participated in its development, is a welcome addition to any design engineer's bookshelf. One finds it hard to realize today that only 30 years have passed since S. Timoshenko's arrival in our country. The inspiration exercised by him, first on a handful of engineers at Westinghouse, and later, through his teaching and books, on nearly every student of mechanical engineering, set off a tremendous upsurge in applied mechanics. Vibration analysis became an important subject, both in school and in industry. Two dates seem to me particularly outstanding; the early date, 1928, when J. Ormondroyd and J. P. Den Hartog, two young associates of Timoshenko, wrote their important paper on the "vibration absorber," an idea that exercised profound influence on the development of the subject, and the recent date, 1945, when R. D. Mindlin has, in another important paper, established a permanent pattern for many of the approaches used today in the study of vibration and shock. Crede's book deals with a branch of vibration analysis, that of vibration and shock isolation. The book is evidently not intended as a textbook; the subject is too specialized for that purpose. Rather, it is intended as a guide or handbook to the practical engineer whose job is to properly design or install equipment that is exposed to vibration or shock.

In addressing himself to a practicing engineer, Crede faces a delicate question. Does the engineer, in the field, know more or does he know less than his more studious counterpart in classroom? Has he, on the job, forgotten part of his fundamental mathematics, or has he progressed well beyond his student days? Crede, on page 8 of his book, thinks for a moment that the relation $\sin(\varphi_1 + \varphi_2) = \sin\varphi_1 \cos\varphi_2 + \cos\varphi_1 \sin\varphi_2$ may cause difficulty to the reader, and provides a reference where the subject might be reviewed. Fortunately this is the only lapse of this kind in the book. The text is on the level of the average book on vibrations, and to some extent also overlaps in content. But the subject of vibration and shock isolation is explored thoroughly, in a manner not available elsewhere in book form. Most of the important formulas are presented in convenient charts; a detailed discussion is given of the mechanical properties of rubber, felt, and cork.

After an introductory chapter on basic notions and the calculation of stiffnesses in nonprincipal directions Crede treats in chapter 2 the vibrations of the one-degree-of-freedom and multi-degree-of-freedom systems due to excitation by applied periodic forces or by prescribed oscillations of the support. The notions of force and displacement transmissibilities are introduced. [I have found the notation on page 44, using the same letter both for length (positive quantity) and for co-ordinate (positive or negative quantity) somewhat confusing.] The method of decoupling modes is explained in great detail and with great clarity. In the next chapter isolation of shock motion and shock force is considered both for the cases of excessive and for intermediate deflections of the isolator. The roles of damping and of nonlinearity, and the support of excessive static loads form the subject of the following chapter. There is also a brief section on sound isolation. Properties of materials, design of isolators are treated in chapter 5. The last chapter discusses a variety of industrial equipment in regard to particular vibration or shock considerations that may be appropriate.

The reviewer feels that in a parallel development of vibration and shock an emphasis on contrasts, rather than on similarities, may more readily penetrate a tired engineer's mind; he would have also preferred a somewhat more extensive treatment of advanced topics, particularly sound isolation, at the expense of the more elementary considerations in the early chapters. The almost complete lack of foreign references was also somewhat of a surprise. Last, but not least, he wished the author had gone into greater detail in the description of shock stand characteristics, practice in military designs, and similar subjects, the development of which Mr. Crede was so intimately connected with. Evidently, security considerations did not permit more details. These are, however, minor complaints. The book is well written and bound to acquire widespread use because it is informative, authoritative, and replete with practical information. It will greatly facilitate the design engineer's task. It also fills an important gap in the literature.

[1] Engineering Division, Knolls Atomic Power Laboratory, General Electric Company, Schenectady, New York.

Aircraft Vibration and Flutter

INTRODUCTION TO THE STUDY OF AIRCRAFT VIBRATION AND FLUTTER. By Robert H. Scanlan and Robert Rosenbaum. The Macmillan Company, New York, N. Y., 1951. Cloth, 6 × 9 in., illus., x and 428 pp., $7.50.

REVIEWED BY PAUL A. LIBBY[2]

THAT problems of aeroelasticity have occupied the interest of aeronautical engineers for the past 30 years is attested by the considerable volume of technical literature treating such problems during this time. However, there has never been a text which could be considered satisfactory for the teaching of a graduate course treating these problems or which presented succinctly the state of development in the aeroelastic field at any given time. The recent book by Professor Scanlan and Mr. Rosenbaum admirably fills these needs; it will be found by many professors a useful teaching aid and by many practical dynamics engineers a convenient source of much useful information.

The first two chapters of this book present the mathematical techniques which are exploited subsequently. Thus one finds a discussion of the solution of ordinary linear differential equations with constant coefficients, the solution of some elementary partial differential equations, elements of determinant and matrix theory, and the use of the Lagrangean equations to establish the equations of motion for dynamic systems.

The third and fourth chapters may be considered to be a short but clear treatment of the material usually presented in undergraduate vibration courses, that is, the free and forced vibration of one and two degree of freedom systems.

The remaining twelve chapters of the book are concerned with aeroelastic or related problems and methods of their solution.

[2] Associate Professor of Aeronautical Engineering, Polytechnic Institute of Brooklyn, Brooklyn, N. Y.

Thus several practically important methods of obtaining the uncoupled natural modes of bending and torsion oscillation of beams are presented. The modes so obtained are then applied to the three-dimensional wing and tail-empennage flutter problems. The use of coupled modes of vibration, as may be obtained by vibration test, is then discussed. The various methods of solving the stability determinant whose vanishing determines the critical flutter velocity and frequency are presented. The aeroelastic problems of wing reversal and aileron reversal and reduction in aileron rolling effectiveness are discussed. The book closes with a discussion of instrumentation and testing and a preliminary treatment of the flutter of sweep wings. The treatment of the aerodynamic forces for the flutter problem is presented in detail in an appendix; only the coefficient representation is, therefore, given in the main body of the text.

In their preface the authors point out that the topics and presentation reflect their own experience and point of view. This is quite natural; it must be expected, however, that people using this text will, for the same reason, prefer in certain sections their own points of view. Thus, for example, the reviewer feels that the presentation of the various methods of modal analysis of dynamic problems, both steady state and transient, as an expansion in terms of various complete orthonormal sets, that is, the uncoupled or coupled, free body or cantilever modes of vibration, brings considerable clarity and unity to the various techniques which are presented in this text and in the technical literature. The possibility of other points of view does not detract from the book; the authors must be congratulated in so successfully filling a void in the textbook literature.

Differential Geometry

LECTURES ON CLASSICAL DIFFERENTIAL GEOMETRY. By Dirk J. Struik. Addison-Wesley Press, Inc. (Mathematics Series), Cambridge, Mass., 1951. Cloth, 6 × 8 in., viii and 221 pp., illus. $6.

REVIEWED BY H. L. LANGHAAR[3]

THIS is an authoritative textbook on the classical differential geometry of curves and surfaces in three-dimensional Euclidean space. Emphasis is placed on the historical development of the science, as it stemmed from the works of Monge and Gauss.

In addition to the standard basic theory, the author has included a surprising amount of supplementary material; the general theory of order of contact, theory of integration of natural equations of curves, theory of curves of constant slope, evolutes and involutes, imaginary curves, a few theorems of differential geometry in the large, triply orthogonal systems of surfaces, theory of curvilinear co-ordinates in space, geodesic co-ordinates, variational theorems on geodesics, surfaces of constant Gaussian curvature, the Gauss-Bonnet theorem, interpretation of the non-Euclidean geometry of Lobachevsky and Bolyai, theory of envelopes of families of surfaces, conformal mapping of surfaces, isometric and geodesic mapping of surfaces, theory of minimal surfaces, theories of ruled surfaces and developable surfaces, and imaginaries in surface theory.

The author's style is direct, but concise. Needless to say, the reader requires an understanding of the fundamentals of mathematical analysis. Some knowledge of Gibbs's vector analysis is also advisable, since the brief explanation of this theory in the book is scarcely adequate. Gibbs's vector notation is used throughout, but tensor notation is not employed.

The text contains many drawings, including some notable ones from other books. Also, there are some illustrative photographs of plaster models. Numerous examples are worked out, and many problems for students are given. Biographical sketches of the lives of the principal contributors to classical differential geometry are an attractive novel feature of the book. In all, the requirements for an instructive and teachable graduate mathematics text are fulfilled.

[3] Professor, Theoretical and Applied Mechanics Department, University of Illinois, Urbana, Ill. Mem. ASME.

Algebra of Vectors and Matrices

THE ALGEBRA OF VECTORS AND MATRICES. By Thomas L. Wade. Addison-Wesley Press, Inc. (Mathematics Series), Cambridge, Mass., 1951. Cloth, 5½ × 8½ in., ix and 189 pp., illus., bibliography. $4.50.

REVIEWED BY R. F. TINEHART[4]

THERE has existed a serious lack, cited by the author in this book's preface, of a good textbook for a first course in the theory and application of matrices. There still does. This book seems likely to find favor with neither the mathematician nor the physical scientist or engineer.

The stated aim of the book is to present "an elementary exposition of the algebra of vectors and matrices, that exposition being articulated with the basic concepts of modern algebra ..." The author achieves his purpose to the extent that the exposition is lucid in most of the places where his mathematics is correct.

The book opens with a brief exposition of the concepts of group, ring, integral domain and field, followed by an elementary treatment of the algebra and geometry of two and three-dimensional vectors. A chapter on the algebra of n-dimensional vectors completes the stage setting for a treatment of matrices from the vector standpoint. After the fundamental properties of matrices have been established, linear transformation theory, the characteristic equation, rank, systems of linear equations, and bilinear and quadratic forms are treated. The exercises are not very numerous or meaty.

In contrast to the mathematical accuracy, the selection of material and the order of its presentation can be subject to only minor criticism, if one remembers that the book is designed for a beginning course only. No nongeometric applications are given. The reviewer believes that the "law of nullity" is important and elementary enough to have been included. The principal defect with regard to order of material is the presentation of the characteristic equation before systems of linear equations have been discussed. This robs the characteristic equation of motivation and makes the discussion of characteristic vectors somewhat awkward and barren.

A number of theorems in the book are stated without proof, with references to proofs provided. Proofs of some of these could have readily been included without violating the elementary spirit of the book and without perceptible extension of the text.

On the other hand, some of the theorems which are proved might better have been stated without proof in view of the errors therein. "Proofs" containing major errors occur in: the theorem on the equality of the row rank, column rank, and determinant rank of a matrix (page 140); in the implied (false) theorem (page 154) regarding a fundamental set of solutions of a system of nonhomogeneous linear equations; in the theorem on transformation of a symmetric bilinear form (page 165).

Other mathematical errors and confusions are plentiful and many are of such a nature as to perplex any but the best students. For example:

1 Page 10—"As a consequence of these two theorems ...a set of two or more elements (numbers) is called a *field F*, when p and q, ($q \neq 0$) are any elements whatever of S, then $p + q$,

[4] Professor of Mathematics, Case Institute of Technology, Cleveland, Ohio.

$p - q$, $p \cdot q$, p / q are also elements of S." (No associative or distributive laws are apparently needed.)

2 An effort is made (page 56) to motivate the sum of two matrices by a sum of "points." This seems meaningless and confusing.

3 After defining a matrix, addition of matrices, multiplication of a matrix by a scalar, and proving the theorems (sic): $A + B = B + A$, $(A + B) + C = A + (B + C)$, $rA + sA = (r + s)A$, $(rs)A = r(sA)$, $r(A + B) = rA + rB$, (r and s scalars), the author then decides it is time to discuss equality of matrices!

4 Having defined a scalar as an element of a field, the author summarizes the last four theorems mentioned in the startling Theorem VII: "Linear combinations of matrices with scalar coefficients obey the laws of ordinary scalar algebra."

5 On page 70 the author defines a diagonal matrix as "a square matrix in which all the elements are zero except those along the principal diagonal." This leads to confusion later when it becomes clear that he intends to permit zero elements on the diagonal.

6 On page 84 the author alludes to a right inverse as "the inverse" of a matrix, then subsequently shows that a right inverse is also a left inverse and that it is unique.

7 On page 168, having established the theorem on the reducibility of a quadratic form to a diagonal form for an arbitrary field of characteristic zero, the author then restates the theorem for the real field after supplying the three additional sentences of proof he regards as required in this case.

In several instances the necessary nonsingularity of a matrix is not stated (e.g., Exercise 2, page 96, page 164). In other instances the necessary "squareness" is not stated (e.g., page 43). The phrase "the necessary and sufficient condition" abounds through the book.

The reviewer has just used the book as a text in a course for graduate engineers, having chosen the book sight unseen, because of belated publication, on the basis of its table of contents. Strangely enough, the book did not work badly. The errors in the book have the healthy effect of stimulating the good student to read the text with great care. All in all, it was good fun.

Applied Mechanics

APPLIED MECHANICS FOR ENGINEERS. By Sir Charles Inglis. Cambridge University Press, London, England, and New York, N. Y., 1951. Cloth, 6½ × 9¼ in., xii and 404 pp., 437 figs., $7.50.

REVIEWED BY E. STERNBERG[5]

THIS book is based on lectures given by the author to students working toward an honor's degree in engineering at Cambridge University. The level of the book is intermediate; its scope defies the course classification traditional in this country.

The first two chapters are devoted primarily to an analytical and graphical treatment of plane rigid-body statics. The author's interest in structures is made apparent quite early by excursions into questions related to bridge design. There follow a discussion of cable and catenary problems, and two chapters on the stresses and deformations in ideal trusses, including some statically indeterminate cases. A chapter on dry friction concludes the treatment of statics.

The remainder of the book deals with dynamics, and includes several chapters on the kinematics and kinetics of particle motion as well as a discussion of plane rigid-body motion. Mechanical vibrations are given considerable prominence and constitute the subject matter of five chapters. Systems of one and two degrees of freedom, as well as simple examples of one-dimensional continuous systems, are covered. A separate chapter on nonlinear restoring forces, pressure waves, and self-excited oscillations is particularly noteworthy. The book ends with a discussion of gyroscopic motions.

It is clear from the beginning that the author is anxious to reach techniques of solving problems, and specific applications, with a minimum of delay. This desire is probably responsible for the occasionally hurried treatment accorded to basic principles. Thus this reader wonders whether the statement on page 3, that ". . .in a two-dimensional system a number of forces can always be balanced by a single force. . .," might not be misinterpreted. The author, however, has succeeded admirably in accomplishing his primary objective. The book abounds with genuine applications even at an elementary level; it contains a host of illustrative examples which are presented with unusual care, and an uncommon attention to numerical detail. Teachers of mechanics are apt to find the large supply of exercises most helpful.

The emphasis on approximate methods is a novel feature. Numerical and graphical integration of differential equations, as well as harmonic analysis, are used, at a relatively early stage, to bring within the scope of the book stimulating problems of engineering significance. It is refreshing to note the conspicuous absence of the myriads of unhappy pulleys which have long populated the pages of traditional texts on mechanics.

The point of view adopted by the author is reflected in his resolution to "employ the simplest mathematical methods in preference to those which may be more elegant but less obvious." This attitude has led the author to place a great deal of emphasis on intuitive insight into the mathematical methods used and upon physical interpretation of the results obtained. On the other hand, it has induced him to stay clear of vector methods, to dismiss Lagrange's equations with a reference to the "mysticism of an ingenious mathematical technique," and to allude to the "red herring of convergency" in connection with his treatment of Fourier series. More generally, he announces his ideal in the preface, "to make mathematics a servant, and not allow it to become a master." Remarks of this kind are likely to appeal to many readers; however, they are also apt to create an impression which was not intended. For, as the author has often demonstrated, one way of escaping mastery by mathematics is to learn to master it.

This is not just another text on mechanics; it is a very personal and eloquent account of the subject matter which throughout bears the mark of its author's long and rich experience.

Finite Deformation of an Elastic Solid

FINITE DEFORMATION OF AN ELASTIC SOLID. By Francis D. Murnaghan. John Wiley and Sons, Inc., New York, N. Y.; Chapman and Hall, Ltd., London, England, Applied Mathematics Series, 1951. Cloth, 5⅛ × 9 in., exercises, tables, index, 140 pp., $4.

REVIEWED BY C. W. MACGREGOR[6]

THIS book forms a part of the Wiley Applied Mathematics Series under the editorship of I. S. Sokolnikoff, and treats elastic solids where the assumption is not made that deformation magnitudes are sufficiently small such that the squares and products of the strain components are negligible. It is a subject on which the author has published frequently and with widespread acceptance.

[5] Professor of Mechanics, Illinois Institute of Technology, Chicago, Ill. Mem. ASME.

[6] Vice-President in charge of engineering and scientific studies, University of Pennsylvania, Philadelphia, Pa. Mem. ASME.

Effective use of the theory of matrices has been made throughout the book. As in the modern treatment of many other engineering problems, matrix theory is so useful here as to be beyond contention. An examination of the general proofs and developments in the text will substantiate this. For those wishing a review of matrix theory or even confronting it for the first time, chapter 1 provides adequate treatment for the material which follows.

Chapters 2 and 3 are devoted to the geometries of strain and stress and the relationships between them. In the treatment of isotropic elastic media in chapter 4, the influence of initial states of stress on isotropy are considered. The increased number of elastic constants for isotropic bodies under higher-order strain effects are also outlined. Compressibility relations are developed between hydrostatic pressure and volume, both for the linear and the finite high-elastic-strain theories. Comparisons are made of these with Bridgman's experimental results.

Nonisotropic elastic media are treated briefly in chapter 5. The elastic sensitivity of the medium to special rotations is discussed.

The separate problems of simple shear and tension are developed in chapter 6 where both the elementary linear theory and the second-order corrections are determined. The last chapter contains solutions of three problems, namely, the effect of internal and external pressure on a spherical shell, on a circular tube, and the torsion of a circular cylinder. In each case the solutions based on elementary considerations are compared with those considering finite elastic strains.

The reviewer found this book to be a stimulating treatment of a subject too long neglected. While clearly written, the use of more subheadings and a few figures would have added greatly to the presentation. The notations for stress, strain, and other variables do not follow current practice in this country, and especially for this reason the inclusion of a table of nomenclature would prove effective. The latter are more or less minor criticisms and should not be construed as detracting in any appreciable manner from the value of this book. The reviewer hopes that the author will continue his effective work in this field and that further volumes will follow.

Linear Computations

LINEAR COMPUTATIONS. By Paul S. Dwyer. John Wiley & Sons, Inc., New York, N. Y., 1951. Cloth, 6 × 9 in., xi and 344 pp., approximately 160 tables, references, name and subject indexes, $6.50.

REVIEWED BY GEORGE E. FORSYTHE[7]

BY "linear computations" the author means the solution of a system of linear algebraic equations, the inversion of a matrix, the evaluation of a determinant, and similar calculations. Most of the book is devoted to the exposition of refined Gaussian pivotal methods of performing these linear computations on desk calculators. These are all basically the elimination method taught in high school, but few casual computers are aware of the great efficiencies made possible by over a century of development. Techniques worked out by Doolittle, Cholesky, Banachiewicz, Crout, Dwyer, and others take full advantage of the ability of desk machines to accumulate products easily, and reduce the slow and error-producing recordings to a minimum.

The author is a professor of statistics at the University of Michigan. In the problems of experimental statistics he is convinced that iterative methods are less successful than pivotal methods in carrying out linear computations. I gather from the work of Hardy Cross and Southwell's school that the conclusion does not carry over to all engineering calculations. Even so, elimination methods are important, and the present book must surely be a standard reference on these techniques. There is nothing comparable in the literature.

Four or five chapters are devoted to calculating machines and to the principles of designing a computation for them. One chapter deals with computation with approximate numbers as such. This material is drawn upon in determining the errors in linear computations. A number of chapters deal with such problems as obtaining the characteristic polynomial of a matrix, evaluating a linear form whose variables are solutions of a linear system, and getting an inverse matrix.

Professor Dwyer's book is written at an unusually elementary level. Nothing but easy high-school algebra is needed to follow the development of the efficient elimination schemes for solving linear equations. Then determinants and matrices are introduced, and their elementary properties are described and used thereafter. The book will therefore be a useful reference to computers with little mathematical background. The elementary level is partly a result of presenting techniques more than tools of numerical analysis. The reader who desires to develop analytical tools would do better to start with a good grounding in elementary matrix theory, including the triangular decomposition and the use of various norms.

The numerous carefully prepared tables include layouts and one or more numerical examples of almost all the methods discussed. The lists of references are unusually complete in the English language, rather modest on European work, and quite devoid of Russian entries. The book is well printed, with few misprints or other errors.

The chapter titles are: (1) Introductory remarks, (2) Computation with approximate numbers, (3) The principles of computational design, (4) The solution of simultaneous equations with the method of multiplication and subtraction, (5) The method of multiplication and subtraction with (exact) division—method of determinants, (6) The solution of equations with approximate methods, (7) Relations between the coefficients, (8) The solution of related and associated equations, (9) Introduction to determinants, (10) The evaluation of determinants and determinantal ratios, (11) The evaluation of linear forms, (12) An introduction to the algebra of matrices, (13) The inverse matrix and its calculation with approximate methods, (14) The calculation of the adjoint and inverse with the method of determinants, (15) Problems involving the characteristic equation, (16) Other methods, (17) The errors of linear computations, (18) Application to statistics, (19) Application to nonlinear problems—concluding remarks.

Introduction to Acoustics

AN INTRODUCTION TO ACOUSTICS. By Robert H. Randall. Addison-Wesley Press, Inc., Cambridge, Mass., 1951. Cloth 6 × 9 in., illus., tables, references, index, problems, xii and 340 pp., $6.

REVIEWED BY SAMUEL LEVY[8]

FOR students for physics and engineering who plan to specialize in communications, this book will form a valuable basic text. It presents, in easily understandable form, the physical principles underlying acoustic phenomena and the methods of applying these principles to engineering problems. Thus one finds both the development of the wave equation for the propagation of sound in a gas and the engineering equations applicable to the transmission of sound in pipes and to the design of horns.

[7] Mathematician, National Bureau of Standards, Los Angeles, Calif.

[8] Chief, Aircraft Structures Group, National Bureau of Standards, Washington, D. C. Mem. ASME.

The author has emphasized, wherever possible, the analogy between the equations of acoustics and those of other branches of physics. His book is thus of added value in giving the student a broad view of physics. Examples of his use of analogies are found in his comparison of acoustic with electromagnetic waves and of the electrical transmission line with an air conduit. The use of complex notation in discussing acoustic impedance is presented with frequent comparison to the analogous use of complex notation for impedance of electrical circuits.

The mechanics of vibrating strings, plates, and bars is presented in detail. This is followed by a discussion of musical instruments. The author takes advantage of this discussion to point out to the student the great difficulty of setting down the boundary conditions of most actual acoustical problems in precise mathematical form and the need, in many cases, of making approximations to obtain an answer at all. He wisely feels that the student must be impressed at an early stage in his learning with the practical importance of approximate methods. A review is given of the available knowledge regarding speech and hearing both from the subjective and mechanical points of view. The methods of designing loudspeakers are given and the advantages and disadvantages of the different types are compared. Numerous other examples of the application of acoustic theory are presented.

The large number of problems included in the text for solution by the student have been carefully selected to emphasize the principles presented. The many illustrations have been well prepared and add to an understanding of the subject matter.

This book will be welcome to the teacher of acoustics, to undergraduate students in physics, and communications engineering.

Fundamentals of Acoustics

FUNDAMENTALS OF ACOUSTICS. By Lawrence E. Kinsler and Austin R. Frey. John Wiley and Sons, Inc., New York, N. Y., 1950. Cloth, 5½ × 8½ in., vii and 516 pp., 166 figs., 17 tables, 213 problems, index, glossary, $6.

REVIEWED BY SAMUEL LEVY[9]

THIS is a book on advanced acoustics written primarily for graduate students in either physics or engineering electronics. The book is intended as a textbook for classroom use. It should also, however, find wide use as a reference for practicing engineers because of the broad coverage, the detailed consideration of the basic assumptions, and the derivation of each important equation from the fundamental laws of physics. The comprehensive set of excellent problems should afford a good check on the student's grasp of the subject.

The first nine chapters, comprising 264 pages, present clearly and concisely the fundamentals of theoretical acoustics in the form of analyses of the various types of vibration of solid bodies and of the propagation of sound waves through fluid media. The presentation of this material is illuminated by the mention of practical applications for the equations that are derived. The use of vectors to express harmonic variation with time, as is commonly done in electrical engineering, is presented logically in discussing the motion of a simple oscillator. The definitions of motional impedance and transfer admittance proceed from a discussion of the dynamic loudspeaker. The concept of wave impedance is presented in connection with the motion of strings. The presentation of vibration theory includes discussions of the axial and transverse vibrations of bars, the transverse vibration of membranes, and the transverse vibrations of plates. The treatment of sound transmission starts with the derivation of the general wave equation and proceeds logically with discussion of spherical acoustic waves, directivity of waves, radiation impedance, resonators, filters, reflection at interfaces, and absorption.

The remaining seven chapters, comprising 235 pages, are concerned with applications. The topics considered include the design of dynamic loudspeakers, cabinets, baffles, horn-type loudspeakers, and microphones of all kinds. A chapter on psychoacoustics describes the behavior of the ear, the subjective characteristics of loudness, pitch and timbre, and binaural localization. A chapter on architectural acoustics provides design information on reverberation time and the damping of standing waves. Underwater acoustics is covered in unusual detail with the presentation of much valuable information regarding attenuation, refraction, and temperature-gradient effects in sea water as well as design information for sonar, and discussions of echo ranging and underwater communication. The last chapter, dealing with ultrasonics, discusses the generation of ultrasonic waves, the detection of flaws and cracks in solids, and propagation phenomena in gases, liquids, and solids.

In the opinion of the reviewer, this book is well balanced as to content between theoretical and applied acoustics. Its clear and rigorous style puts it in the forefront among graduate textbooks on acoustics. This text should also be of considerable value as a reference work for designers and engineers.

[9] Chief, Aircraft Structures Group, National Bureau of Standards, U. S. Department of Commerce, Washington, D. C. Mem. ASME.

Fourier Transforms

FOURIER TRANSFORMS. By Ian N. Sneddon. McGraw-Hill Book Company, New York, N. Y., International Series in Pure and Applied Mathematics, 1951. Cloth, 6 × 9 in., xii and 542 pp., illustrated, $10.

REVIEWED BY ERIC REISSNER[10]

THE present book is concerned with the theory and applications of trigonometric series, Bessel function series, Fourier integrals, Bessel integrals, Mellin integrals, and Laplace transforms. In three chapters of some ninety pages the author discusses the theory of the various procedures. The remainder of the book is devoted to various applications which in general are preceded by a brief introduction to the fields from which these applications are taken. We find problems of vibrating strings, membranes and plates, problems from the theory of heat conduction, from hydrodynamics, from elasticity in two dimensions and with axial symmetry. Separate chapters deal with such timely subjects as the slowing down of neutrons in matter and with applications to atomic and nuclear physics.

Some sixty pages of the book are devoted to problems of hydrodynamics. Incompressible potential flow is illustrated by the problems of flow through an aperture (without free boundaries) and linearized problems of gravity waves. This is followed by the solution of some linearized problems in incompressible viscous flow. There is one nonlinear problem, concerning plane viscous flow, where the Fourier technique can be used, since the differential equation is of second degree, to reduce the problem to a nonlinear integrodifferential equation for the Fourier transform of the stream function. In the main the author has contented himself with discussing classical results of the type found in Lamb's Treatise. One regrets the omission of present-day applications of the Fourier technique to the fields of steady and nonsteady linearized supersonic flow and to the field of turbulence and, in this connection, of the subject of generalized harmonic analysis.

In elasticity the treatment is primarily concerned with boundary value problems for the half space, the infinite plate, and the

[10] Professor of Mathematics, Massachusetts Institute of Technology, Cambridge, Mass.

infinite circular cylinder. A departure from the usual treatments in this field concerns the solution of mixed boundary-value problems, such as the problem of the rigid punch on the surface of a half space, by Fourier methods. Such problems can be reduced by the use of the Fourier or Bessel integral to so-called dual integral equations. The author shows examples where these dual integral equations can be solved in closed form. However, the problems in question have previously been solved by other more direct techniques and where these more direct techniques break down the dual integral-equation technique likewise does not seem to supply a solution.

Perhaps not enough stress is laid by the author on the problem of evaluating a Fourier transform solution once it has been obtained. In this connection one thinks of such problems as the forced oscillations of an elastic half space as treated by Lamb in a classical paper or of the problem of transient beam vibrations with transverse shear deformation taken into account which recently was found to be of considerable technical importance.

Aside from limitations such as these the book is very well written and represents a useful addition to the literature on applied mathematics.

Boundary-Layer Theory

GRENZSCHICHT-THEORIE. By Hermann Schlichting. Verlag und Druck G. Braun, Karlsruhe, Baden, Germany. 1951. Cloth, $6^{5}/_{8} \times 9^{1}/_{2}$ in., xv and 483 pp., figs., tables, bibliography, author and subject indexes, $12.50 U.S.A.

REVIEWED BY ASCHER H. SHAPIRO[11]

HERE is a book which is indispensable to advanced designers, research workers, and students dealing with problems of fluid motion in the fields of aeronautical engineering, mechanical engineering, chemical engineering, and applied physics.

The appreciation of the value of the boundary-layer concept and of the place of boundary-layer theory in fluid dynamics has grown during the past 20 years from a point where comparatively few understood its implications to the present condition where it is matter-of-factly accepted as an indispensable tool. Yet the principal treatises (Prandtl's article in volume 3 of Durand's *Aerodynamic Theory;* and Goldstein's *Modern Developments in Fluid Dynamics*) prior to Dr. Schlichting's book are now 15 years old. The present book, besides incorporating recent developments in the theory of compressible boundary layers, in the theory of transition from laminar to turbulent flow, and in the turbulent boundary layer, is in the reviewer's opinion superior to Prandtl's and Goldstein's treatises in respect to choice, presentation, and organization of subject matter.

In his foreword, Dr. Schlichting points out that the book is written primarily for engineers. This aim, together with the title of the book, seems to have guided the author in his choice of material. Those theoretical aspects of boundary-layer theory which are relevant to and useful in engineering design form the main subject matter of the book. Experimental data are introduced mainly to illustrate the accuracy or range of validity of the theoretical considerations. Of course not all the topics treated are of direct applicability to the quantitative solution of engineering problems—many give rather a general understanding of the mode of boundary-layer behavior in typical situations and provide some basis for qualitative decisions on the part of the designer. In accordance with the practical aims of the book, there are numerous charts and tables which help to eliminate lengthy computations.

The book is divided into four main parts. In Part A are set forth the fundamental concepts and laws for dealing with the motion of viscous fluids: The concepts of viscosity, dynamic similitude, and of the boundary layer; the formulation of the Navier-Stokes equations and the assumptions implied therein; the general behavior of viscous fluids as indicated by the Navier-Stokes equation; some exact solutions of the Navier-Stokes equation; and creeping flow. Part B covers the laminar boundary layer: The development of the boundary-layer equations; the general behavior of laminar boundary layers; some exact solutions for laminar boundary layers; unsteady flows; integral methods of solution; boundary-layer control; the thermal boundary layer, and the compressible boundary layer. Part C deals with the transition from laminar to turbulent flow, and covers mainly the stability of laminar boundary layers to disturbances of very small amplitude. Part D is concerned with turbulent boundary layers: The "apparent" turbulent stresses owing to momentum exchange; the semiempirical mixing-length theory of Prandtl, vorticity-transport theory of Taylor, and similarity theory of von Kármán; turbulent flow in pipes; turbulent boundary layers on flat plates and rotating disks; effects of pressure gradients on turbulent boundary layers; problems of free turbulence; and some miscellaneous information relating to profile drag.

The format, typography, and illustrations live up to the magnificent prewar standards of German technical books, and set an example for American publishers.

It is to be hoped that some American or British publisher will take the initiative of having this valuable book translated and published in an English text.

Theory of Control

AN INTRODUCTION TO THE THEORY OF CONTROL IN MECHANICAL ENGINEERING. By R. H. Macmillan. Cambridge University Press, London, England, and New York, N. Y., 1951. Cloth, $7 \times 10^{1}/_{2}$ in., xiii and 195 pp., illus., examples, tables, bibliography, appendixes, author and subject indexes, $6.

REVIEWED BY JOHN A. HRONES[12]

THIS book of less than two-hundred pages is one of the first devoted to the theory of automatic control and written from the viewpoint of a mechanical engineer. The chapter titles indicate the nature of the ground covered by the author, namely, the principles of control, control-system elements, servo-system operation, servo-system performance, general servo analysis, analytical methods, and graphical methods.

Also included are brief appendixes dealing with complex numbers and the Laplace transform method.

The book is well written; is adequately illustrated with clear sketches and diagrams; and is supplemented with numerous problems. It should prove to be more easily read by novices in the field than most existing texts.

The transient and steady-state behavior of simple single loop systems in response to square wave and sinusoidal disturbances is discussed. Graphical and analytical methods for determining such responses are presented. Certain simple nonlinear systems are briefly covered. The book, although limited in scope, will be of considerable interest to those who wish a brief but competent introduction to the subject.

[11] Associate Professor of Mechanical Engineering, Massachusetts Institute of Technology, Cambridge, Mass. Mem. ASME.

[12] Professor of Mechanical Engineering, Massachusetts Institute of Technology, Cambridge, Mass. Mem. ASME.